LA-UR-16-27630
Approved for public release; distribution is unlimited.

Title: FINAL REPORT OF THE PEÑA BLANCA NATURAL ANALOGUE PROJECT

Author(s): Goldstein, Steven Joel; Levy, Schon S.; Abdel-Fattah, Amr I.; Amato, Ronald S.; Anthony, Elizabeth; Cook, Paul; Dobson, Patrick F.; Fayek, Mostafa; French, Diana; Garza, Rodrigo de la; Ghezzehei, Teamrat; Goodell, Philip C.; Harder, Steven H.; Ku, Teh-Lung; Luo, Shangde; Murrell, Michael Tildon; Norman, Deborah E.; Nunn, Andrew J.; Oliver, Ronald; Pekar-Carpenter, Katrina; Rearick, Michael Sean; et al.

Intended for: Report

Issued: 2016-10-04

FINAL REPORT OF THE PEÑA BLANCA NATURAL ANALOGUE PROJECT

September 27, 2016

Compiler: Schön S. Levy

Authors:

Amr I. Abdel-Fattah
Ronald S. Amato
Elizabeth Anthony
Paul Cook
Patrick F. Dobson
Mostafa Fayek
Diana French
Rodrigo de la Garza
Teamrat Ghezzehei
Steven J. Goldstein
Philip C. Goodell
Steven H. Harder
Teh-Lung Ku
Schön S. Levy
Shangde Luo
Michael T. Murrell
Deborah E. Norman
Andrew J. Nunn
Ronald Oliver
Katrina Pekar-Carpenter
José Alfredo Rodríguez Pineda
Michael Rearick
Minghua Ren
Ignacio Reyes-Cortés
George Saulnier
Sowmitri Tarimala
John Walton

FINAL REPORT OF THE PEÑA BLANCA NATURAL ANALOGUE PROJECT

TABLE OF CONTENTS

EXECUTIVE SUMMARY

FOUNDATIONS OF THE CONCEPTUAL MODEL FOR URANIUM TRANSPORT AT THE NOPAL I NATURAL ANALOGUE SITE

Schön S. Levy, Steven J. Goldstein, Patrick F. Dobson, Philip C. Goodell, Teh-Lung Ku, Shangde Luo, Katrina Pekar-Carpenter, Diana French, Michael T. Murrell, Mostafa Fayek, José Alfredo Rodríguez Pineda, Ronald Oliver, Teamrat Ghezzehei, Ignacio Reyes-Cortés, Paul Cook, Elizabeth Anthony, Minghua Ren, and Rodrigo de la Garza

REGIONAL HYDROLOGY AND URANIUM OCCURRENCES AROUND NOPAL I

Philip C. Goodell, José Alfredo Rodríguez Pineda, Patrick F. Dobson, Steven H. Harder, and Schön S. Levy

URANIUM-SERIES CONSTRAINTS ON RADIONUCLIDE TRANSPORT AND GROUNDWATER FLOW AT THE NOPAL I URANIUM DEPOSIT, SIERRA PEÑA BLANCA, MEXICO

Steven J. Goldstein, Amr I. Abdel-Fattah, Michael T. Murrell, Patrick F. Dobson, Deborah E. Norman, Ronald S. Amato and Andrew J. Nunn

NATURAL ANALOGUE STUDIES AT PEÑA BLANCA, MÉXICO: URANIUM-SERIES RADIOISOTOPE MEASUREMENTS

Teh-Lung Ku and Shangde Luo

GROUNDWATER COLLOIDS AT NOPAL I

Amr I. Abdel-Fattah, Sowmitri Tarimala, Steven J. Goldstein, and Schön S. Levy

GROUNDWATER ANALYSES FOR NOPAL I AND THE PEÑA BLANCA REGION, CHIHUAHUA, MÉXICO

Michael Rearick, Patrick F. Dobson, Steven J. Goldstein, José Alfredo Rodríguez Pineda, and Schön S. Levy

EXECUTIVE SUMMARY

The Peña Blanca region, 50 km north of Chihuahua City, Chihuahua, México, was a target of uranium exploration and mining by the Mexican government. After mining ceased in 1981, researchers became interested in this region as a study area for subsurface uranium migration with relevance to geologic disposal of nuclear waste. Many studies related to this concept were conducted at the Nopal I mine site located on a cuesta (hill) of the Sierra Peña Blanca. This site has geologic, tectonic, hydrologic, and geochemical similarities to Yucca Mountain, Nevada, a formerly proposed site for a high-level nuclear-waste repository in the unsaturated zone.

The U.S. Department of Energy (U.S. DOE), Office of Civilian Radioactive Waste Management (OCRWM), sponsored studies at Nopal I in the 1990s and supported the drilling of three research wells – PB1, PB2, and PB3 – at the site in 2003. Beginning in 2004, the Peña Blanca Natural Analogue Project was undertaken by U.S. DOE, OCRWM to develop a three-dimensional conceptual model of the transport of uranium and its radiogenic daughter products at the Nopal I site.

SITE STRATIGRAPHY AND DEPOSITIONAL HISTORY

Four main stratigraphic units were penetrated by the continuously cored PB1 well. These units comprise all of the unsaturated zone and about 25 m of the saturated zone. The lowest unit is Cretaceous limestone that represents carbonate deposits east (basinward) of the Cretaceous reef complex bordering the Chihuahua Trough. The Pozos Formation above the limestone is a continental molasse deposited on the margins of terrane uplifted during early to mid-Tertiary time. The age of the unit is constrained between 54 and 44.8 million years (Ma). The tuffaceous Coloradas Formation unconformably overlies the Pozos Formation. Constraints on the age of this unit are the same as for the Pozos Formation. The 44.8-Ma Nopal Formation, also a tuff, is the uppermost preserved stratigraphic unit of the cuesta.

URANIUM DISTRIBUTION IN THE NOPAL WELLS

The most complete information about uranium distribution in the subsurface rock comes from borehole natural gamma logs and hand-held scintillometer survey of the continuous core from PB1. Both surveys measured gross gamma counts. High gamma counts predominantly reflect the presence of uranium.

High gamma counts associated with the main ore deposit are strongest in PB1, where values between 500 and 100,000 counts per second (cps) were recorded from the surface to about 113-m depth. The corresponding interval in PB2 is from the surface to 86-m depth ($\leq$ 3,000 cps) and in PB3 from 17 to 119-m depth ($\leq$ 4,500 cps). Deeper gamma anomalies (beneath the Nopal I ore body) are mostly within the Pozos conglomerate. The strongest anomalies are in the lower Pozos and, only in PB3, in Cretaceous limestone. Natural gamma values in the 125-m-deep well PB4, within limestone 1.3 km SE of Nopal I, do not exceed 175 cps. The hand-held gamma survey of PB1 drill core detected “hot

spots" associated with iron oxide-oxyhydroxide mineralization. The iron-mineralized fractures with uranium have approximately the same vertical distribution as the ore body.

URANIUM ENRICHMENT AND MINERALIZATION HISTORY

Rock units at the Nopal cuesta have a complex and incompletely understood alteration history. This section highlights selected alteration processes that contributed to uranium transport or sequestration.

Early Silicification and Uranium Enrichment in the Pozos Formation

Various types of silicification are present in sediments throughout the Pozos Formation in PB1 core. The green ultraviolet-stimulated fluorescence of the secondary silica attests to a significant uranium content. Clasts of silicified limestone in the conglomerates preserve evidence of the earliest silicification, likely inherited from the parent limestone because many calcareous clasts are not altered. Silica-altered volcanic clasts also are common. Microquartz cement is present in clasts and as *in situ* cement. Uraniferous silica enrichment occurred through processes of erosion and redeposition of silicified rock and through alteration and silica cementation of volcanogenic sediment. One sample of silica-cemented sediment contains 475 parts per million (ppm) uranium.

Uranium Mineralization in the Nopal and Coloradas Formations

Initial Stage 1 uraninite precipitated in the Nopal and Coloradas Formations from 45-55°C fluids that interacted with the welded tuffs. Mineralization occurred at 32±8 Ma under reducing conditions within a vertical breccia zone at the intersection of two faults. Within the uncertainty of the uraninite age, mineralization was approximately contemporary with the earliest phase of Basin and Range extension at no more than about 29 Ma. Primary uraninite was preserved only within a strongly silicified breccia.

The alteration of Stage 1 minerals resulted in the precipitation of Stage 2 uranium minerals. Uranophane, schoepite/dehydrate schoepite, and weeksite are the dominant Stage 2 uranium minerals, with minor amounts of colloform uraninite. Ages of these minerals include 3.1±0.5 Ma for uranophane (oxidizing event), 1.6±0.5 Ma for colloform uraninite (reducing event), and 85±8 thousand years (ka) for schoepite/dehydrated schoepite. Weeksite/boltwoodite from near the margins of the deposit gives an age of 41±5 ka. The two most recent mineral precipitation events occurred under oxidizing conditions.

Uranium Mineralization in the Pozos Formation

Uraninite is present in a uranium-rich portion of tuffaceous Pozos conglomerate located nearly 100 m below the main ore body and 30 m above the water table. The silicified rock described above contains disseminate grains of TiO_2 and TiO_2 replacements of highly altered sphene, as well as pyrite. Some of the titaniferous material is the TiO_2 polymorph anatase with rims of uraninite. The U-Pb age of the uraninite is <1 Ma. The

depositional temperature is estimated to have been 10° to 20°C. Anatase is actively sequestering uranium from fluids that have interacted with the conglomerate.

Aqueous Uranium Transport in the Shallow Unsaturated Zone

A water-collection system, consisting of 240 separate 30-cm^2 compartments that were each connected to a 125-mL bottle, was installed in April 2005 within the +00 m (arbitrary vertical reference datum) adit of the mine to collect water that had infiltrated from the +10 level (surface) and seeped into the adit. The seepage pathway from the ground surface to the collection system, assuming vertical fluid flow through fractures, is about eight meters. Analyses of seepage samples provide information about uranium-dissolution rates and uranium-isotopic compositions of the seepage water, described below.

Seepage analyses confirm that uranium-dissolution inputs for fractures with water-rock interaction times of ~0.5 days are ~1 part per billion (ppb) dissolved uranium per day under present conditions. Evidence of Quaternary-age uranium and uranium-daughter mobilization, transport, and sequestration has been observed in fractures exposed on the +10 surface of the mine. The uranium is associated with iron oxides-oxyhydroxides probably derived from sulfide alteration.

Samples of iron oxide-oxyhydroxide fracture fillings were collected from the PB1 drill core to extend previous uranium-series investigations into three dimensions. High uranium concentrations in the fracture-fill materials (12-7700 ppm) indicate uranium mobility and transport from the deposit in the past. Uranium concentrations generally decease with horizontal distance way from the ore deposit. The number of PB1 parent core samples analyzed (3) is insufficient to draw conclusions about trends in uranium concentrations with depth. Isotopic activity ratios indicate a complicated geochemical evolution in terms of the timing and extent of actinide mobility. Uranium shows both open- and closed-system behavior, depending on both sample and time scale. $^{234}U/^{238}U$ activity ratios generally are distinct from secular equilibrium and indicate some degree of open-system uranium behavior during the past 1.2 Ma. However, calculated closed-system ^{230}Th-^{238}U-^{234}U model ages generally are >183 ka for the drill core samples, suggesting closed-system behavior for uranium and thorium over this most recent time period. Whole-rock isochrons drawn for the drill-core samples show that at two of the three depths (8.5 m and 191.0 m), the fractures have remained closed with respect to uranium and thorium mobility for > 200 ka. However, open-system behavior for uranium in the last 350 ka is suggested by the sample from 67-m depth.

SITE GEOHYDROLOGY

Regional groundwater flow is from west to east, with the highest present-day water-table levels (>1500 meters above sea level [masl]) to the west and lower levels (~1200 masl) to the east.

Previous studies of the Nopal I ore deposit postulated that the ore body formed in the saturated zone and that oxidative mineralogic alteration and mobilization of uranium began when the deposit was uplifted into the unsaturated zone. Paleohydrology and present-day geohydrology of the site have not been systematically studied, but some inferences can be made from existing information.

The existing topography around the cuesta hosting the Nopal I deposit places bounds on possible high stands of the regional static water level at this location. As a result of uplift, mass wasting, and stream incision, the cuesta is bounded on the north, east, and south by erosional features at elevations of no more than about 1380 to 1400 masl. A channel in the alluvium on the west side of the west-dipping cuesta occupies elevations of about 1420 to 1440 masl. The regional static water level below the cuesta, measured in borehole PB1, is at an elevation of about 1240 masl.

At the PB1 drill site, the uneroded remnant of the uranium deposit extends from the ground surface at 1463 masl to about 1350 masl. Thus, the present-day static water level is about 110 m below the base of the deposit. The existing state of erosion around most of the cuesta would preclude the static water level from reaching a position higher than about 1380 to 1400 masl, just above the level of the base of the ore deposit.

A general inference from the Cenozoic-Quaternary history of more thoroughly studied sections of the Basin and Range Province is that the present topography and drainages of the Sierra Peña Blanca, including the Nopal I cuesta, began to develop 9-13 Ma and are likely to be at least several million years old. The maturity of the dissected landscape around the Nopal cuesta implies that all or most of the Nopal I ore body has been in the unsaturated zone for at least the last several million years.

EVIDENCE OF CHANGING REDOX CONDITIONS

The groundwater beneath the Nopal cuesta contains dissolved oxygen, an indication of present oxidizing conditions in the shallow saturated zone and, presumably, the unsaturated zone. The evolution of redox conditions beginning at the time of initial uranium mineralization is inferred from the record of uranium-mineral deposition and alteration and from the distribution of sulfide minerals.

As described above, the uranium minerals of Nopal I record a long history of varying redox conditions. Initial ore-body uraninite precipitated at 32±8 Ma under reducing conditions. A major oxidation event involving uranophane deposition occurred at about 3.1 Ma. This event was followed by a reducing event at about 1.6 Ma in which a second generation of uraninite was formed. The ages of schoepite (about 85 ka) and weeksite/boltwoodite (about 41 ka) document more recent oxidizing conditions in the ore deposit. Uraninite within Pozos conglomerate is less than one million years old. Anatase is actively sequestering uranium as uraninite from fluids that have interacted with the conglomerate under reducing conditions.

Sulfides formerly existed throughout the stratigraphic section penetrated by borehole PB1. The shallowest surviving sulfides include pyrite associated with uraninite (not intersected by PB1) and protected by silicification in the Nopal Formation and sulfides primarily within lithic inclusions in the Coloradas Formation. Sulfides are common only below a depth of about 180 m in the Pozos conglomerate and Cretaceous limestone. Pseudomorphous iron oxide-oxyhydroxide replacements of sulfides are present in the Nopal and Coloradas Formations. The downward transition from rare to common sulfide preservation at the 180-m depth in the Pozos conglomerate may mark the stable position of a former water table. The depth also corresponds to a downward transition to lower-permeability rocks. Both factors could have restricted the interaction of rock sulfides with oxygenated water in what is now the deep unsaturated zone.

URANIUM SERIES GEOCHEMISTRY OF NOPAL I GROUNDWATERS

Groundwaters at Nopal I and nearby regional wells were analyzed for uranium-series disequilibria. Unsaturated-zone seepage waters were collected between 2000 and late 2006. The waters were analyzed for chemical and isotopic suites including total uranium, $^{234}U/^{238}U$, total thorium, ^{230}Th, ^{226}Ra, and ^{239}Pu.

Seepage waters from the front of the +00 m adit, where the ore body is located, generally have $^{234}U/^{238}U$ activity ratios near unity (0.9 to 1.5) and uranium concentrations between 0.7 and 422 ppb. These attributes result from dissolution of rock with a preponderance of uranium in secular equilibrium, as well as longer water-rock interaction times and interaction of water with uranium-rich rock. Analyses of high-grade uranium ore from Nopal I confirm that uranium-series radionuclides high in the decay chain are close to secular equilibrium. Waters from the rear of the adit, away from the ore body, have higher $^{234}U/^{238}U$ activity ratios ranging from 2.6 to 5.2 and mostly lower uranium concentrations (0.1 to 14.9 ppb). These differences reflect preferential dissolution of recoil-related ^{234}U and uranium concentrations affected by varying fluid flux and/or water-rock interaction times. Seepage-water samples from the middle of the adit have $^{234}U/^{238}U$ activity ratios and uranium concentrations overlapping the values for the front and back of the adit. Stable-isotope data for seepage samples show evidence of evaporation during the dry season that would have increased the concentrations of solutions. The effects on uranium-isotopic systematics are described below.

Uranium concentrations and isotopic ratios were measured for shallow saturated-zone waters from Nopal I and regional wells. For most wells, samples were collected from 2003 to 2006. Uranium concentrations in the Nopal wells have decreased over time as the local effects of drilling contamination have diminished. During the last year of sampling (2005-2006), concentrations were between 23 and 61 ppb in PB1 and between 370 and 1077 ppb in PB3. Concentrations in the smaller sample set for PB2 are between 11.9 and 137.2 ppb. From 2003 to 2006, uranium varied between 0.1 and 15 ppb in PB4 and between 5.0 and 5.8 ppb at the Pozos Ranch well (~1.3 km ESE of PB1). Uranium in the Peña Blanca Ranch well (~4.4 km NW of PB1) varied from 9.5 to 10.0 ppb between 2003 and 2005.

Activity ratios of $^{234}U/^{238}U$ for all analyzed PB1 and PB2 water samples are between 1.005 and 1.102. Ratios for PB3 are between 1.363 and 1.974. The activity-ratio data, uranium-concentration data, and hydrologic-testing results for the three wells all indicate good connectivity between PB1 and PB2 and poor connectivity between these wells and PB3. Hydraulic testing also revealed that PB3 has higher permeability than the other two wells, as it experienced almost no drawdown during pumping. Activity ratios for the regional wells are mostly >2.

The near-unity $^{234}U/^{238}U$ activity ratios and uranium concentrations less than 100 ppb in the PB1 and PB2 groundwaters presumably were acquired by percolating water, like the front-adit seepage, that interacted with bedrock containing abundant uranium in secular equilibrium. Waters of this composition could have traveled unmodified from the uraniferous source rock to the shallow saturated zone. However, considerable mixing could occur with minimal effect on the near-unity $^{234}U/^{238}U$ activity ratios if high-uranium waters (e.g., >100 ppb) mix with low-uranium water (e.g., <10 ppb) of any observed activity ratio.

Percolation in the shallow unsaturated zone is highly variable with regard to uranium content and $^{234}U/^{238}U$ activity ratios. For the cuesta as a whole, shallow percolation is likely to have relatively low uranium concentrations and activity ratios in the range of about two to five, like seepage from the back of the adit, because the ore body occupies only a small part of the cuesta.

Groundwaters in the Nopal wells have higher colloid contents (~0.4 to 2 mg/L) than regional well waters (~0.001 to 0.09 mg/L). Differences may reflect both the recent drilling and more intense host-rock alteration of the Nopal wells. Uranium-concentration measurements of unfiltered and ultrafiltered water from PB1 and PB4 indicate that ~93 to 97% of uranium present is truly dissolved.

Uranium-Series Constraints on Radionuclide Mobility

The retardation factor, $R_f(^{238}U)$, was estimated to vary between ~30 and 7200 in the saturated zone, with a mean value of 1300, by combining long-lived and short-lived nuclide data. ^{239}Pu values below a well defined detection limit, combined with measured uranium systematics for the Nopal and PB4 waters, were used to estimate that plutonium mobility is at least three orders of magnitude lower than uranium mobility in the saturated zone. Average values of saturated-zone retardation factors range from 10^3 to 10^7, and decrease in the order $^{239}Pu \approx {}^{210}Po \approx {}^{230}Th > {}^{210}Pb > {}^{238}U \approx {}^{226}Ra$. Using the mean value for $R_f(^{238}U)$ in the saturated zone, estimated retardation factors for U-series daughter nuclides in the unsaturated zone range from ~10 to 230 for ^{226}Ra and from ~1300 to 260,000 for ^{230}Th.

Modeling Uranium-Isotopic Systematics of Seepage Water

An analytical model was constructed based on the concept that intermittent seasonal infiltration and percolation in the shallow unsaturated zone leads to a linear relationship between reciprocal uranium concentration and $^{234}U/^{238}U$ ratio in percolating waters. Seepage waters from various locations in the adit define distinct linear trends based on wet-versus-dry-season collection time. The underlying cause of this difference is the accumulation of recoil-produced ^{234}U on rock-pore and fracture surfaces during the dry season, followed by preferential uptake of the surficial ^{234}U by percolating water during the wet season. Other factors contributing to the trends include rock-water interaction (or water-transit) time, uranium-dissolution rate, and the rate of recoil that supplies ^{234}U to the rock surfaces. Longer periods of low infiltration and lower uranium-dissolution rates lead to high $^{234}U/^{238}U$ ratios in the percolating water.

RADIONUCLIDE TRANSPORT IN SOIL AT THE NOPAL CUESTA

Surficial weathering of the uranium ore body exposed at the surface of the Nopal cuesta has potential importance as a source of uranium transported into the unsaturated zone. Aspects of this process could be relevant analogues to extreme nuclear-waste release scenarios involving exposure or deposition of contaminated material on the ground surface.

At Nopal I, the natural soil was removed during the mining operation. A site with natural soil was studied close to where blocks of uranium ore were stockpiled in the 1980s. One residual ore block was selected to study the migration of uranium and its daughters into the underlying soil over a period of about twenty-five years. Samples from the ore block and underlying soil profile were analyzed by gamma spectroscopy to identify radionuclide peaks from the ^{238}U-decay series.

Gross-gamma counts on two incomplete soil-sample suites show the radioactivity generally decreasing with depth to low levels below six to seven centimeters. These findings are consistent with similar studies elsewhere. The ore-block sample was relatively close to secular equilibrium for daughter/parent pairs $^{230}Th/^{234}U$ and $^{226}Ra/^{230}Th$, with activity ratios of 1.222 and 1.206, respectively. A majority of the soil samples have non-equilibrium $^{230}Th/^{234}U$ activity ratios in the range of 1.80 to 2.18. The two shallowest samples from two soil suites have activity ratios between 1.18 and 1.50, probably due to incorporation of ore-block fragments into the soil. All soil samples had non-equilibrium $^{226}Ra/^{230}Th$ activity ratios in the range of 1.70 to 2.71. Data for a complete eight-interval suite from below the ore block show that background radiation levels are reached at depths of about 10 to 15 cm.

PERFORMANCE ASSESSMENT MODELING

The simulation of radionuclide transport at Nopal I was conducted by the Yucca Mountain Project, a former repository program. A numerical model was used to analyze the mobilization and groundwater transport of radionuclides released from the ore

deposit. The goal of the investigation was to estimate whether further investigations at the Nopal I site would provide a credible natural-analogue comparison with the expected performance of the Yucca Mountain site.

The numerical analysis used as input a combination of Yucca Mountain process models and Nopal I site-specific data such as the vertical section of rock units in the unsaturated zone, porosity and permeability data, the inferred eastward direction of regional groundwater flow, and the dimensions of the ore body. Estimates of the uranium content of the original ore deposit and the inventory of uranium species and daughter products were based on published studies. The model assumed that uranium oxide (uraninite) is analogous to spent nuclear fuel.

The model simulated meteoric-water infiltration into the unsaturated zone, downward water percolation and dissolution of the uraninite, fluid mixing in the unsaturated and saturated zones, and eastward transport in the saturated zone. Radionuclide concentrations were captured for the saturated zone 150, 600, and 1,300 m downgradient from the ore body. The only corroborating data available were water analyses for well PB4, 1,300 m SE of Nopal I.

A base-case analysis was run, along with sensitivity analyses, to investigate the effects of reduced infiltration, variations in the solubility of the ore body, and variations in sorption coefficients. The study concluded that, even with strong sorption, uranium could be transported from the vicinity of Nopal I in amounts that would be detectable in PB4 water. The simulations projected concentrations of ^{99}Tc in the groundwater derived predominantly from natural fission of ^{238}U . The pertechnetate anion behaves as a conservative non-sorbing species in water, unlike uranium. Model results suggested that ^{99}Tc concentrations would be very low, but detectable (~10^{-8} mg/L or ~10^{-5} ppb).

The numerical model was updated as the Peña Blanca Natural Analogue Model (PBNAM). The results were calibrated to uranium concentrations reported for 2003 water samples from the shallow saturated zone in boreholes PB1, PB2, and PB3. Examples of model results include a base-case simulation for ^{238}U transport for 100 realizations of the uncertain dissolution parameters, but not including sorption. The observed uranium concentrations in Nopal well waters are bracketed by the range of results obtained in the simulations and within the uncertainty of the source-dissolution parameters. This result remains generally valid even with the trend of gradually diminishing uranium content shown by more recent water samples. The updated PBNAM predicted a ^{99}Tc concentration of 2.8×10^{-2} ppb in groundwater directly beneath the ore body. However, analytical results of Nopal well waters from two laboratories determined that no ^{99}Tc was observed above a detection limit of about 6×10^{-5} ppb.

After the PB wells were drilled at Nopal I, elevated uranium concentrations in the wells might have provided an opportunity for an informal saturated-zone tracer test in which higher uranium concentrations might be detected in well PB4. The three-year record of water chemistry for PB4 contains no clear evidence of water with elevated uranium

content. The record of decreasing uranium concentrations and the concentrations of short-lived uranium-series daughters in the Nopal wells were used to estimate upper-limit groundwater velocities of 5 to 15 m/y, so that any tracer plume could take hundreds of years to reach PB4.

CONCLUSIONS

The Peña Blanca Natural Analogue Project studies reported here will support the development of hypotheses regarding unsaturated-zone and saturated-zone uranium transport away from the Nopal I ore body as an analogue for a nuclear waste repository in the unsaturated zone. The drilling of three boreholes, one continuously cored, at Nopal I provided core samples for stratigraphic, mineralogic, and radiometric analyses. Borehole geophysical logs documented vertical and lateral variations in bedrock radioactivity. Analyses of the multiyear sample sets of saturated-zone waters from the Nopal wells, along with samples from regional wells, supported estimates of groundwater travel time, water mixing, saturated-zone retardation factors, and the relative contributions of various uranium reservoirs to the groundwater. These data also contributed to conceptual models of uranium dissolution and transport.

Percolating waters collected from a shallow adit below ground surface generally show differences in uranium content and $^{234}U/^{238}U$ ratios between waters traversing the ore body and waters moving through fractures in unmineralized rock. Waters from the ore body tend to have higher uranium contents and $^{234}U/^{238}U$ ratios close to unity. Percolation from the unmineralized rock has lower uranium content and higher $^{234}U/^{238}U$ ratios.

The first radiometric dating of uranium minerals established an age of 32 ± 8 Ma for the primary uranium mineralization. Alteration and secondary-uranium-mineral deposition at 3.1 ± 0.5 Ma may mark the beginning of a transition from a reducing environment under saturated conditions to an oxidizing environment under unsaturated conditions. Local reducing environments have survived, indicating that after three million years, the rock units have not fully equilibrated with the mostly oxidizing environment.

Initial uranium enrichment in the Pozos conglomerate may date from a period of early diagenesis. Authigenic uraninite less than one million years old in the Pozos documents recent water-rock interaction involving the redistribution of uranium. Most of the uranium redistribution in the unsaturated zone appears to have diminished prior to about 200 ka.

The updated numerical transport model, dubbed the Peña Blanca Natural Analogue Model, included results calibrated to uranium concentrations for 2005 Nopal waters. Within the uncertainty of the source-dissolution parameters, the results are generally valid even with the trend of diminishing uranium content shown by more recent samples. A ^{99}Tc concentration of 2.8×10^{-2} ppb predicted by the model in groundwater directly beneath the ore body was not confirmed: no ^{99}Tc was observed above a detection limit of about 6×10^{-5} ppb.

FOUNDATIONS OF THE CONCEPTUAL MODEL FOR URANIUM TRANSPORT AT THE NOPAL I NATURAL ANALOGUE SITE

Schön S. Levy, Steven J. Goldstein, Patrick F. Dobson, Philip C. Goodell, Teh-Lung Ku, Shangde Luo, Katrina Pekar-Carpenter, Diana French, Michael T. Murrell, Mostafa Fayek, José Alfredo Rodríguez Pineda, Ronald Oliver, Teamrat Ghezzehei, Amr Abdel-Fattah, Ignacio Reyes-Cortés, Paul Cook, George Saulnier, Elizabeth Anthony, Minghua Ren, Rodrigo de la Garza, and John Walton

INTRODUCTION

The Peña Blanca region, approximately 50 km north of Chihuahua City, Chihuahua, México, was a major target of uranium exploration and mining by the Mexican government because the region contains numerous uranium deposits. After mining ceased in 1981, researchers became interested in this region as a study area for subsurface uranium migration with relevance to geologic disposal of nuclear waste. Many studies related to this concept were conducted at the Nopal I mine site located on a cuesta (hill) of the Sierra Peña Blanca; a description of early studies is given by Dobson et al. (2008). This site has many geologic, hydrologic, and climatic similarities to Yucca Mountain, Nevada, the former proposed site for a high-level nuclear-waste repository. Among them are 1) both are located in arid to semi-arid regions, 2) both are horst structures within the Basin-and-Range province of North America, 3) both sites consist of Tertiary rhyolitic tuffs overlying carbonate rock, and 4) both are located in a chemically oxidizing environment within an unsaturated zone at least 200 m above the water table, and have generally similar water chemistries. The Peña Blanca Natural Analogue Project was undertaken by the U.S. Department of Energy (U.S. DOE), Office of Civilian Radioactive Waste Management, to develop a three-dimensional conceptual model of the transport of uranium and its radiogenic daughter products at the Nopal I uranium mine site. The project was intended as an expansion of the natural analogue concept from earlier site work in which the natural mineral uraninite and its alteration products were studied as analogues for the degradation of spent nuclear fuel (Pearcy et al., 1994). Analogue studies at Nopal I also have the potential to support a site study addressing the construction of an underground facility for Mexican radioactive waste in the same geologic province (García Ramírez, 2006, p. 157).

The unique advantage of natural-analogue studies for nuclear-waste disposal is the opportunity to document relevant processes over very long periods of time. Natural processes relevant to uranium transport have operated at Nopal I over time periods of decades to millions of years. The upper bound on the time period of interest for this natural analogue is the age of original uranium mineralization. When the Peña Blanca Natural Analogue Project began, the ages of primary and secondary mineralization were not known but were thought to be in the range of about six to ten million years (e.g., Muller, Ildefonse, and Calas, 1990, p. 601; Pearcy, Prikryl, and Leslie, 1995, p. 695).

Study results of the natural analogue project included the first direct dating of uranium minerals. The age of 32 ± 8 million years (ma) for primary uraninite (Fayek et al., 2006) defines the beginning of the time period in which this analogue for spent nuclear fuel has interacted with the changing environment. The value of the Nopal I site as a natural analogue for uranium transport derives from the development of a conceptual alteration model incorporating all processes that have affected transport throughout the history of the ore deposit. While it is true that performance requirements for nuclear-waste repositories generally focus on geologic conditions of the Quaternary Period and the next million years, there is an understanding that many site attributes reflect the cumulative effects of processes active at various periods of time. Also, processes that affected a natural analogue site in the more distant past may be valuable for predicting the effects of potential future changes. Therefore, it is appropriate that the alteration history of the uranium ore deposit at the Nopal I site be considered in its entirety in this report. The Peña Blanca Natural Analogue Project was not intended to establish the origin of the ore deposit, but it is essential to place the uranium mineralization and subsequent remobilization within the context of the local geologic history.

The uranium-transport system has had time to develop greater complexity than was originally anticipated by natural-analogue researchers. This makes it more challenging to reconstruct the earliest processes of uraninite alteration and uranium mobilization most comparable to nuclear-waste degradation. It does, however, present opportunities to investigate the effects of long-term processes such as evolving tectonic regimes, fluctuating water table, changing groundwater redox conditions, and extreme erosion.

This synthesis of information used to build the conceptual model of uranium transport at Nopal I begins with summaries of basic information about the site. The stratigraphy is briefly described, based on studies of drill core from well PB1 that was drilled as part of this project (Dobson et al., 2008). The depositional history of geologic units encountered in the drill core is drawn from a number of previous studies. The tectonic history is taken from regional studies with additional site data. Early and concurrent studies of the Peña Blanca uranium-mining district by the U.S. Nuclear Regulatory Commission and the Center for Nuclear Waste Regulatory Analyses were summarized by Pickett et al. (2011). We have used some of their results in developing our interpretations, but have not attempted a full integration of all data.

The field-scale subsurface distribution of uranium at the site is based on natural gamma surveys of the three wells – PB1, PB2, and PB3 (identified in some publications as PB-1, PB-2, and PB-3) – drilled at Nopal I. Additional petrographic studies examine the distribution of sulfide minerals and ultraviolet fluorescence in core samples to document evidence of early uranium deposition and later oxidation. The environment and geochronology of rock alteration and uranium mineralization, to the extent that they are known, are described. Evidence of uranium transport in the shallow unsaturated zone is presented with emphasis on the analysis of waters from a seepage-collection system. The description of site geohydrology includes the evolution from saturated to unsaturated conditions and inferences about fluid pathways and changing redox conditions. The uranium-series geochemistry of groundwater supports the exploration of fluid mixing in

the unsaturated zone. Studies of uranium-series radionuclide migration into the soil were conducted in an area where high-grade uranium ore blocks were stored for about two decades. A numerical simulation of subsurface radionuclide transport at the Nopal cuesta was performed as a scoping study.

Companion reports describe the regional hydrology and nearby uranium occurrences, aqueous uranium-isotope and uranium-series geochemistry, colloid characteristics, and general groundwater chemistry in greater detail. The report, *Uranium-Series Constraints on Radionuclide Transport and Groundwater Flow at the Nopal I Uranium Deposit, Sierra Peña Blanca, México* (Goldstein et al., 2016, also published as Goldstein et al., 2010), contains groundwater analyses for total uranium, ^{238}U, and its long-lived daughters. These data are used to place bounds on groundwater-flow velocities, mixing, and radionuclide mobility in the saturated zone and to investigate uranium dissolution in the unsaturated zone. The report, *Natural Analogue Studies at Peña Blanca, Mexico: Uranium-Series Radioisotope Measurements* (Ku and Luo, 2016), describes the abundances of short-lived uranium-series daughters in Nopal ground waters. The report, *Regional Hydrology and Uranium Occurrences Around Nopal I* (Goodell et al., 2016), contains water-level measurements for regional wells used to document the regional hydrologic gradient and a summary of regional surficial uranium occurrences above background. Chemical analyses of saturated-zone and unsaturated-zone waters are presented in the report, *Groundwater Analyses for Nopal I and the Peña Blanca Region, Chihuahua, México* (Rearick et al., 2016). Abdel-Fattah et al. (2016) describe colloid-size distributions and colloid concentrations in saturated-zone ground waters and a seepage sample from Nopal I.

Site-scale natural-analogue studies like this one typically are less detailed than site characterization conducted for an actual nuclear-waste repository site. The lower level of resource investment in the characterization of Nopal I inevitably left gaps in our knowledge of site attributes and processes. We relied upon data from other locations, expert knowledge, and conjecture to bridge these gaps as well as possible. For example, the stratigraphic, tectonic, and paleohydrologic reconstructions presented here are based on project data and published information from other studies. In the absence of existing studies devoted to local paleohydrology, general inferences have been synthesized from information about pyroclastic deposition, erosion and sedimentation, tectonism, and rock alteration. The interpretations of these data rely in part on studies of paleohydrology and rock alteration at Yucca Mountain.

SITE STRATIGRAPHY AND DEPOSITIONAL HISTORY

The geologic history of the Sierra Peña Blanca from Early Cretaceous through Tertiary time and the resulting sedimentary and pyroclastic depositional units have been described by Rodriguez Torres et al. (1976), Goodell (1981), and Reyes-Cortés (1997, 2002). Geochronology of the pyroclastic units is based on Alba and Chavez (1974), with ages recalculated according to decay constants of Steiger and Jäger (1977) by Dobson et al. (2008). The local stratigraphy, based on core from borehole PB1, is summarized from Dobson et al. (2008).

Four main stratigraphic units were penetrated by the PB1 well (Figure 1). In ascending order, these units are the Cretaceous limestone, the Pozos Formation, the Coloradas Formation, and the Nopal Formation (Dobson et al., 2008). These units comprise the uppermost 250 m of the local stratigraphy, including all of the unsaturated zone and

Figure 1. Stratigraphic column and selected geophysical logs for well PB1. Borehole gamma and core gamma values are given in counts per second (plotted on a log scale), neutron measurements are in API units, and temperature values are in degrees Celsius (Dobson et al., 2008).

about 25 m of the saturated zone. Depths and elevations (meters above sea level, masl) of contacts and the water table for all three Nopal wells are shown in Table 1.

Cretaceous limestone was encountered from a depth of 244.40 m to the bottom of the cored borehole at 250.00 m. The limestone contains marine microfossils in a recrystallized micritic matrix. This rock represents basin carbonate deposits of the uppermost Tamaulipas Formation or the Cuesta del Cura Formation, east (basinward) of the Cretaceous reef complex (Stege et al., 1981, p. 270-271) bordering the Chihuahua Trough. Reyes-Cortés (1997, p. 209) considers some of the limestone to be part of the Glen Rose Formation defined in Texas.

The Pozos Formation is present at depths of 136.38 to 244.40 m in PB1. This unit is described by Goodell (1981) as a continental molasse deposited on the margins of terrane uplifted during early to mid-Tertiary time. The age of the unit is constrained by the 54 million year age of the underlying Cuervo Formation (not present at Nopal I) and the 44.8 million year age of the Nopal Formation capping the Nopal cuesta (Reyes-Cortés, 1997, p. 215). Conglomerate is the dominant lithology, with lesser sandstone. Clasts are mostly volcanic rock, limestone, and chert formed by replacement of limestone. Three intercalated pumiceous tuffs may be correlative with portions of the Corrales Formation, a volcanic unit of problematic age and distribution. Portions of the Pozos Formation have been affected by intense silicification that formed a hard, low-permeability rock (Goodell, 1981, p. 277).

The Coloradas Formation, extending from 22.30 to 136.38-m depth in PB1, unconformably overlies the Pozos Formation (Reyes-Cortés, 1997, p. 217). It is composed of welded, lithic-rich rhyolitic ash-flow tuffs. This formation has not been dated, and constraints on its age are the same as for the Pozos Formation.

The 44.8 million year old Nopal Formation, with a minimum residual thickness of 131 m (Goodell, 1981, Table 1), is the uppermost preserved stratigraphic unit of the cuesta. Younger volcanic and alluvial units overlying the Nopal Formation have been eroded away. Borehole PB1 penetrated 22.30 m from the lower part of the formation. The recovered core is a densely welded, crystal-rich rhyolitic ash-flow tuff.

The petrologic characteristics of the pyroclastic units preserved at the Nopal cuesta, at least those above the Pozos Formation, are consistent with subaerial deposition and cooling. Chief among these characteristics is the presence of densely welded tuffs in both the Nopal and Coloradas Formations. Secondary quartz in pumice lapilli of the Coloradas Formation retains the wedge-shaped morphology of high-temperature vapor-phase tridymite, an additional indication of terrestrial deposition.

Table 1. Depths and Elevations of Contacts and Water Table in Nopal I Boreholes

	PB1 (core)	PB2 (cuttings)	PB3 (cuttings)
Ground elevation (masl)	1463	1463	1452
Depth/elevation of Nopal-Coloradas contact (m/masl)	22.3/1440.7	22/1441	17/1435
Depth/elevation of Coloradas-Pozos contact (m/masl)	136.38/1326.3	142/1321	130/1322
Depth/elevation of Pozos-limestone contact (m/masl)	244.4/1218.6	242/1221	227/1225
Depth/elevation of water table (m/masl)	222.6/1240.4	228.6/1234.4	214.1/1238
Total depth of well (m)	255.0	253.7	243.0

Sources: CRWMS M&O (2004), Table 10.4-5 for water-table depth, Figures I-1, I-4, and I-5 for contacts in PB2 and PB3, and total depths of wells; Dobson et al. (2008) for contacts in PB1; Harder (2006) and Goodell et al. (2016) for ground elevations, adjusted for casing height.

TECTONIC HISTORY

The tectonic history is important for understanding the environment of uranium mineralization and subsequent alteration because tectonism has controlled or influenced magmatism, faulting, and fracturing, as well as the development of topography, drainage, and ground-water flow. Changes in the nature of tectonism affecting the Peña Blanca region during the 32 million years following primary uranium mineralization therefore must be taken into account. The information below identifies tectonic effects pertinent to the study of long-term aqueous uranium transport. A similar description in a more regional context, accompanied by schematic figures, is given by Goodell (1985).

Pre-Basin and Range compressional deformation – folding and thrust faulting associated with the Eocene-age Hidalgoan Orogeny (equivalent to Laramide Orogeny) – affected the sediments and volcanic rocks of the Cuervo Formation (Reyes-Cortés, 2002, p. 322, 326-7). This unit, whose age is in the range of 52-54 ma, is present in the Sierra Peña Blanca but not at the Nopal cuesta. It is not considered further here except to note that the orientations of some much younger fracturing and faulting may be related to reactivation of Hidalgoan-age structures (Reyes-Cortés, 1997, p. 227).

The Sierra Peña Blanca horst is the first range east of the larger Sierra del Nido block. A significant elevation decrease takes place from the high volcanic plateau of the Sierra del Nido to the Chihuahua trough east of the Sierra Peña Blanca and other horsts. The Sierra Peña Blanca probably is a tectonic fragment that was originally part of the Sierra del Nido tectonic block. There are several faults to the west and northwest of the Nopal cuesta that were recurrently active during the period of deposition of the volcanic units

younger than the Nopal Formation (Goodell, 1981, p. 282). These faults had surface expressions as drainages or drainage barriers, as shown by their influence on the thicknesses of 36 to 37 million-year-old pyroclastic and alluvial deposits (Goodell, 1981, p. 280).

McDowell and Mauger (1994, p. 130) postulate that the increased volcanic activity from 46 to 27.5 Ma in central Chihuahua (including the Nopal Formation and probably the Coloradas Formation) was related to a reduction in the magnitude of compressional stress following Laramide contraction. The change at 46 Ma is earlier than any documented estimate for the initiation of tensional stress, but is later than contractional deformation. The age of the graben separating the Sierra Peña Blanca from the Sierra del Nido is less than 29 million years, based on the age of the youngest offset volcanic unit (Goodell, 1981, p. 277). McDowell and Mauger (1994, p. 130) suggest that regional-scale normal faulting did not appear before 24 million years ago. However, McDowell (2007) speculates that the 29-million-year-old volcanism itself may have been a localized response to intensification of tensional stress. Therefore, extensional deformation in the Peña Blanca area may have begun as long ago as 29 million years.

Basin and Range extensional faulting during middle to late Miocene time is poorly documented in Chihuahua, including the Sierra Peña Blanca area, due to the absence of volcanic units younger than about 27.5 million years. A timing of maximum extension during the period of 13 to 9 million years ago is inferred from geologic studies reported by Henry and Aranda-Gomez (2000, pp. 16-17), although maximum extension in Chihuahua probably occurred during a more restricted time period. They conclude that the same episode of extension affected a wide area from southern Arizona and New Mexico southward to the northern edge of the Trans-Mexican Volcanic Belt and eastward to the eastern edge of the Basin and Range Province.

It is uncertain whether the Rio Grande Rift of Colorado, New Mexico, and Texas extends southward into Chihuahua. Reyes-Cortés (2002, p. 327) identified range-bounding listric and normal faults in the Sierra del Cuervo south of Sierra Peña Blanca as Rio Grande Rift features. Perhaps more important to this study are the timing and intensity of the faulting. Handschy and Dyer (1987, p. 629) noted that the faults in the Sierra del Cuervo have not noticeably cut the basin fill or alluvial fans whose ages are not known. Reyes-Cortés (1997, p. 176) observed no offsets in talus and alluvial material in a study area located about three kilometers northwest of the Nopal cuesta.

Data mostly from New Mexico indicate the most recent pulse of extensional tectonism along the Rio Grande Rift occurred during late Miocene to early Pliocene time, with smaller-scale deformation continuing to the present (Machette et al., 2000, pp. 6-7). Rates of slip on normal faults generally have been less than 0.1 mm/year during the last few million years (Connell et al., 2005, p. 129). A reasonable inference from the available information would be that the youngest major extension in the vicinity of Sierra Peña Blanca occurred during late Miocene to early Pliocene time, followed by little or no subsequent deformation.

EVIDENCE OF ALTERATION: SURVEYS OF PB BOREHOLES AND CORE

Basic visual observations of lithology and variations in alteration with depth in drill core from PB1, accompanied by photographs, are given by Goodell et al. (2003). That report also summarizes gross gamma emissions along the core, based on a hand-held scintillometer survey. Preliminary petrographic descriptions of PB1 thin sections by Melchor Pérez (2004) provided corroborative information to support the data presented in this section.

This section contains tabulated data about gross natural gamma intensity in the three Nopal boreholes, lithology and sulfide-mineral distribution in rock samples and thin sections from PB1, and ultraviolet fluorescence in rock samples from PB1. These data were collected or summarized specifically to support interpretations of alteration history, site geohydrology, and uranium transport for the conceptual model.

Natural Gamma Variations in the Nopal Wells

The most complete information about uranium distribution in the subsurface of the Nopal cuesta comes from the borehole natural gamma logs and the hand-held scintillometer survey of the continuous core from PB1. Both surveys measured gross gamma counts. Borehole gamma logs are described in detail below. The results of the hand-held PB1core survey are plotted at the same scale as the borehole gamma survey in Figure 3 of Dobson et al. (2008).

Borehole natural gross gamma logs were recorded for the PB1, PB2, PB3, and PB4 wells by the Comision Federal de Electricidad (Garay Jiménez, 2003). Given that the Nopal cuesta is an area of known uranium mineralization, it is a reasonable assumption that high gamma counts predominantly reflect the presence of uranium. As noted by Dobson et al. (2008), the gamma log records radioactive decay derived from the rock mass beyond the wellbore. For this reason, the gamma log anomalies do not necessarily correlate with areas of high gamma counts measured in recovered drill core or other evidence of uranium mineralization in core.

Gamma anomalies associated with the main ore deposit manifest most strongly in PB1. Elevated values between 500 and 100,000 counts per second (cps) were recorded from the surface to about 113-m depth. The approximate corresponding interval in PB2 is from the surface to about 86-m depth (≤ 3,000 cps) and in PB3 from about 17- to 119-m depth (≤ 4,500 cps), with the highest values in the 90- to 119-m depth interval.

Natural gamma values in well PB4, located 1.3 km SE of Nopal I, did not exceed 175 cps. This well is situated entirely within Cretaceous limestone. Based on the low gamma counts, there is no uranium mineralization present within the 124.75-m section penetrated by the well.

Deeper gamma anomalies are located predominantly within the Pozos conglomerate (Table 2). The strongest anomalies were recorded in the lower Pozos and, only in PB3, in the upper sixteen meters of the Cretaceous limestone penetrated by that hole. This anomaly is much stronger in PB3 than in the other two Nopal wells. The presence of the deep gamma anomaly in all three Nopal boreholes suggests the existence of a mineralized zone of greater lateral continuity and extent than the Nopal I ore deposit, though with lower uranium concentrations. The location and geometry of this anomaly may indicate a genetic relationship with the water table. In PB1 and PB3, the anomaly includes a narrow zone with the highest values that brackets the present-day water table (see Table 1 for water-table locations). The narrow zone is about 9 to 15 m thick and is located at about the same elevations in both PB1 and PB3. The gamma record of this anomaly in PB2 is different, with high vertical variability but no narrow zone of consistently higher values.

There is little additional geologic information pertinent to the nature of the stronger deep anomaly in PB3. The continuation of the anomaly into the Cretaceous limestone below the Pozos conglomerate may be an indication of enhanced local interformational permeability. A small offset of the Pozos/limestone contact at or near PB3, noted in Table 1, could be associated with local fault displacement and fracturing that increased the permeability. The anomaly does not extend into the limestone in PB1, the only cored Nopal borehole; however, the presence of sulfides associated with fractures in the limestone (Table 3) at least hints that reducing fluids penetrated the upper part of the limestone through fractures.

The substantially higher gamma values associated with the deep anomaly in PB3 relative to PB1 and PB2 seem to correlate with the higher uranium content of the groundwater sampled in that well (Goldstein et al., 2016, Table 2). If the higher uranium content of rock and water are related, it implies that the uranium content of groundwater samples from the shallow saturated zone at the Nopal cuesta is most strongly influenced by rock-water interaction in the vicinity of the water table. Drilling-related effects could account for the higher uranium content of PB3 water, but drilling residua should not have seriously affected the gamma response.

Table 2. Borehole Gamma Anomalies below the Nopal I Main Ore Deposit (base of deposit ~113 m depth)

Well PB1			Well PB2			Well PB3		
Depth interval (m)	Gamma counts/second	Stratigraphic interval	Depth interval (m)	Gamma counts/second	Stratigraphic interval	Depth interval (m)	Gamma counts/second	Stratigraphic interval
144.1-151.7	500-1,000		163.1-165.4	500-2,000		130.0-204	500-3,000	Pozos
166.1-179.1	500-2,000	All Pozos	173.6-177.6	500-1,000	All Pozos			
			180.1-184.3	500-2,000				
189.1-226.7*	500-5,000		194.5-199.3	500-2,000		204-242.8‡	500-32,300	Pozos and Cretaceous limestone
			211.5-235.5†	500-11,000				

*Highest values are in the 216- to 225-m interval. †Well was not surveyed below 235.5 m. ‡Highest values are in the 204- to 219-m interval.
Source: Garay Jiménez (2003).

Lithology and Sulfide-Mineral Distribution

Sulfide minerals are important for this natural-analogue study because, like uranium minerals such as uraninite, they form under reducing conditions. In some circumstances, they are abundant enough to influence the redox potential of ground water. Occurrences of pyrite within the Nopal I ore body were described by Pearcy et al. (1994, pp. 717, 724), who made detailed petrographic studies of the ore and its associated minerals. The sulfide observations for PB1 drill core samples (Table 3) underrepresent occurrences of sulfides in the upper part of the rock section because the borehole did not penetrate the main ore body. Table 3 identifies samples from portions of the core with gamma counts above background based on information from Goodell et al. (2003) and Dobson et al. (2008, Figure 3). The significance of evidence relating to sulfide-mineral occurrences is further discussed in the alteration history section.

Table 3. Lithology and Sulfide-Mineral Distribution in PB1 Drill Core

Sample number	Sample depth (m)	Sample type	Formation: lithology (* denotes gamma count above background)	Sulfide observations
PB 1023772	7.54	thin section	Nopal: devitrified, densely welded tuff	no sulfides; possible iron oxyhydroxide replacement of sulfides in lithic inclusions
PB1023775	8.95	core	Nopal: high-angle cm-scale fracture/ breccia zone in tuff*	no sulfides or sulfide pseudomorphs; Iron oxyhydroxide fracture fillings
PB1023782	17.45	thin section	Nopal: devitrified and altered vitrophyre	no sulfides or sulfide pseudomorphs
PB1023783	18.10	thin section	Nopal: devitrified, densely welded vitrophyre	no sulfides or sulfide pseudomorphs
PB1023783	18.10	core	Nopal: devitrified, densely welded tuff	no sulfides; red spots ≤ 0.5 mm may be altered sulfides
PB1023791	25.87	thin section	Coloradas: devitrified, densely welded tuff*	no sulfides or sulfide pseudomorphs
PB1023798	29.78	thin section	Coloradas: high-angle cm-scale fracture/breccia zone in welded tuff*	iron oxyhydroxide deposits in fractures include ≤ 0.05-mm cubic pseudomorphs probably of pyrite
PB1023798	29.78	core	Coloradas: high-angle cm-scale fracture/breccia zone in welded tuff*	≤ 1 mm cubic cavities in iron oxide-oxyhydroxide deposits may be altered sulfides
PB1023812	37.75	core	Coloradas: welded tuff	no sulfides or sulfide pseudomorphs; iron oxyhydroxide fracture coatings
PB1023830	52.06	thin section	Coloradas: devitrified, densely welded tuff with recrystallized breccia zone*	no sulfides or sulfide pseudomorphs
PB1023849	66.5	core	Coloradas: brecciated tuff	no sulfides or sulfide pseudomorphs
PB1023860	76.57	thin section	Coloradas: devitrified, densely welded tuff	no sulfides or sulfide pseudomorphs
PB1023862	78.2	thin section	Coloradas: devitrified, densely welded tuff, finely fractured*	no sulfides or sulfide pseudomorphs; iron oxyhydroxide along fractures
PB1023865	79.77	thin section	Coloradas: devitrified, densely welded tuff*	no sulfides; possible iron oxyhydroxide replacement of sulfides in lithic inclusions
PB1023886	100.75	thin section	Coloradas: devitrified, welded tuff	no sulfides or sulfide pseudomorphs
PB1023890	104.35	thin section	Coloradas: welded tuff*	no sulfides or sulfide pseudomorphs

PB1023898	109.62	core	Coloradas: welded tuff	trace quantities of yellow sulfides ≤ 0.01 mm, some with reddish haloes, mostly in lithic inclusions; possible iron oxyhydroxide pseudomorphs of sulfides in altered pumice lapilli, on fracture surfaces, and locally in matrix
PB1023912	118.91	core	Coloradas: welded tuff	no sulfides or sulfide pseudomorphs
PB1023912	118.91	thin section	Coloradas: welded tuff	no sulfides or sulfide pseudomorphs
PB1023917	123.16	core	Coloradas: welded tuff	no sulfides or sulfide pseudomorphs
PB1023917	123.16	thin section	Coloradas: welded tuff with mineralized fracture zone	no sulfides or sulfide pseudomorphs; iron oxyhydroxide in fracture zone
PB1023935	135.90	core	Coloradas: welded lithic tuff	no sulfides or sulfide pseudomorphs; iron oxyhydroxide in breccia zone
PB1023935	135.90	thin section	Coloradas: welded lithic tuff with 3-mm-wide breccia zone	no sulfides or sulfide pseudomorphs; iron oxyhydroxide in breccia zone
PB1023938	138.44	core	Pozos: brecciated conglomerate with clay-altered, silicified, and silica-cemented clasts	no sulfides or sulfide pseudomorphs; iron oxyhydroxide fracture filling fragmented in breccia zone
PB1023938	138.44	thin section	Pozos: silicified limestone clast in conglomerate	no sulfides or sulfide pseudomorphs; cm-scale clots of iron oxyhydroxide
PB1023950	148.65	thin section	Pozos: calcite-cemented conglomerate with pebbles of limestone, partially silicified limestone, and altered volcanic rock in sandy matrix of quartz-rich recrystallized volcanic fragments and limestone	no sulfides or sulfide pseudomorphs; iron oxyhydroxide staining of rock matrix
PB1023963	157.80	core	Pozos: conglomerate with clasts of silica-cemented sandstone, chert, and clay-altered volcanic rock, sparry calcite cement	no sulfides or sulfide pseudomorphs
PB1023974	166.21	core	Pozos: brecciated conglomerate*	no sulfides or sulfide pseudomorphs
PB1023974	166.21	thin section	Pozos: brecciated conglomerate of mostly quartz-rich recrystallized volcanic fragments and clay-rich altered volcanic fragments*	no sulfides or sulfide pseudomorphs
PB1023985	174.65	thin section	Pozos: crystal-lithic tuff*	no sulfides or sulfide pseudomorphs; iron oxyhydroxide in fracture zone
PB1023995	181.25	core	Pozos: fine-grained tuffaceous conglomerate	possible grayish metallic sulfides
PB1024004	187.05	thin section, core	Pozos: pumiceous tuff	no sulfides; spots of iron oxyhydroxide alteration could be sulfide pseudomorphs
PB1024009	190.8	core	Pozos: tuffaceous conglomerate*	dispersed pale yellow metallic sulfides ≤ 0.05 mm
PB1024018	198.15	thin section	Pozos: conglomerate of clay- and quartz-altered volcanic rocks, micritic and fossiliferous pelletal mudstones deformed by compaction and partially silicified	no sulfides or sulfide pseudomorphs
PB1024024	202.51	thin section	Pozos: volcanic sandstone with calcite-, clay-, and quartz-altered grains	no sulfides or sulfide pseudomorphs

PB1024028	205.60	thin section	Pozos: conglomerate with mostly volcanic clasts	no sulfides or sulfide pseudomorphs
PB1024035	210.29	thin section	Pozos: silicified pebbly micritic siltstone*	oxidized/reduced boundary between rock with 2% disseminated cubic pyrite euhedra ≤ 0.05 mm and oxidized portion with sulfide grains replaced by iron oxyhydroxide pseudomorphs
PB1024049	219.50	thin section	Pozos: silicified conglomerate matrix*	sulfides present in one area of thin section with concentration of calcite-altered volcanic clasts
PB1024052	221.14	core	Pozos: slightly brecciated, quartz-cemented conglomerate*	1% overall abundance, with local concentrations, of yellow and iridescent metallic sulfide minerals in ≤ 1-mm crystals and aggregates, mostly within volcanic clasts but also in voids and fractures in silica cement
PB1024052	221.14	thin section	Pozos: slightly brecciated conglomerate cemented by microquartz with local ≤ 0.2-mm quartz spherulites*	2 to 3% ≤ 1-mm aggregates of silvery sulfides(?), also in veinlets, with lesser amounts of yellow metallic sulfides ≤ 0.1 mm disseminated or associated with silvery minerals.
PB1024068	234.00	thin section	Pozos: conglomerate with clasts of volcanic rocks and silicified limestone	no sulfides or sulfide pseudomorphs
PB1024082	243.20	thin section	Pozos: tuff or tuff breccia	disseminated yellow metallic sulfide in cubic grains ≤ 0.1 mm and polycrystalline aggregates ≤ 0.5 mm that transgress pyroclast boundaries
PB1024085	245.59	thin section	Limestone: biomicrite	no sulfides or sulfide pseudomorphs
PB1024088	247.72	thin section	Limestone: biomicrite	≤ 1% very pale yellow metallic sulfide crystals ≤ 0.3 mm in one sparry calcite vein and in matrix adjacent to an intersecting vein

Ultraviolet Fluorescence in PB1 Core

Visible fluorescence of uranium compounds under ultraviolet illumination is well known and has been used for prospecting and analytical purposes. The typical green and yellow-green fluorescence is produced by hexavalent uranium (uranyl) compounds and mixed hexavalent-tetravalent compounds, but compounds containing only tetravalent uranium do not fluoresce (Booman and Rein, 1962). Secondary silica is one of the most common geologic materials that may exhibit this fluorescence. Zielinski (1980, 1982) studied many aspects of the incorporation of uranium into silica.

Table 4 summarizes the ultraviolet fluorescence of core samples from PB1. The most common is the greenish fluorescence of secondary silica, including detrital clasts, in the Pozos Formation. Most occurrences of faint greenish fluorescence are associated with areas of altered feldspar whose mineralogy probably is a microscopic mixture of kaolinite and secondary silica. The reddish fluorescence of vein calcite in the Pozos Formation may be activated by a combination of Pb and Mn impurities (Fluorescent Mineral Society, 1992-2004). The source of the faint whitish fluorescence in the Coloradas Formation has not been identified.

Table 4 Ultraviolet Fluorescence of PB1 Core Samples

Sample Number	Sample Depth (m)	Formation	Fluorescence observations
PB1023775	8.95	Nopal	no fluorescence
PB1023783	18.10	Nopal	no fluorescence
PB1023798	29.78	Coloradas	no fluorescence
PB1023802	37.75	Coloradas	1% patches of faint greenish-white fluorescence in sw associated with kaolinite patches and fracture coatings
PB1023849	66.5	Coloradas	no fluorescence
PB1023898	109.62	Coloradas	no fluorescence
PB1023912	118.91	Coloradas	no fluorescence
PB1023917	123.16	Coloradas	1% faint greenish fluorescence in mm-scale patches, sw stronger
PB1023935	135.90	Coloradas	faint whitish fluorescence in lw around a fracture and a few mm-scale secondary cavities, fainter in sw
PB1023938	138.44	Pozos	2-3% moderate greenish fluorescence in brecciated conglomerate clasts, including broken pieces of silica cement that fluoresce in lw and sw; 10% faint greenish fluorescence in brecciated margin of silicified limestone clast
PB1023963	157.80	Pozos	2-3% local areas of silica cement fluoresce greenish in sw, whitish in lw
PB1023974	166.21	Pozos	2-3 % faint greenish fluorescence of broken silica cement in brecciated conglomerate
PB1023995	181.25	Pozos	calcite in 3-4-mm wide vein fluoresces red in sw
PB1024004	187.05	Pozos	very faint greenish fluorescence of kaolinized pumice, stronger in lw
PB1024009	190.8	Pozos	red and yellow-orange fluorescence in 2-mm-wide calcite veinlet, stronger in lw; very faint to moderate greenish fluorescence in altered feldspar, 30% of rock
PB1024052	221.14	Pozos	20-30% greenish fluorescing areas in sw, associated with silica cement in conglomerate, including detrital cement

Notes: Lithology is included in Table 3. “sw” = short-wave ultraviolet, “lw” = long-wave ultraviolet.

The greenish secondary-silica uranyl fluorescence in sample PB1024052 (221.14-m depth) from the Pozos Formation is of particular interest because the sample location lies within the interval of highest borehole gamma response (Table 2). As noted in Table 4, fluorescence was observed in the silica cement of the conglomerate and in detrital clasts containing silica cement. Zielinski (1980, 1982) concluded that secondary silica concentrates uranyl from solution when it precipitates and that the uranyl thereafter remains immobile within the silica. More recent work (e.g., Michard et al., 1996) has shown that aqueous uranyl ions can be sorbed by amorphous silica gel. This process must have been in effect at Peña Blanca over long periods of time. The Pozos Conglomerate received an initial input of uranium-enriched silica derived from erosion of a pre-existing silica-cemented sediment. Clastic input of silicified limestone also would have added uranium-enriched material. Cementation of the Pozos sediments by

uraniferous silica was an early diagenetic process contributing to uranium enrichment. Petrogeraphic studies supporting this interpretation are reported in the following section. Figure 2 shows the resulting macroscopic variation in flourescence.

The uranium in silica cement probably was derived in part from leaching and diagenesis of pyroclastic material within the Pozos Formation. Uranium concentrations in the Pozos silica have not been measured, but concentrations in uranyl-fluorescent opal occurrences in Wyoming contain at least 50 ppm (Zielinski, 1980, p. 594). Maximum uranium contents of fluorescing opal for sites not associated with uranium ore bodies are location-specific, with about 200 ppm in the Wyoming site (Zielinski, 1980, p. 595), about 780 ppm at Yucca Mountain, Nevada (Neymark et al., 2002, Table 1; Paces et al., 2001, Appendix 2b),and about 800 ppm at Virgin Valley, Nevada (Zielinski, 1982, p. 205). Crystalline silica (quartz and chalcedony) tends to have lower uranium content than opal, but a threshold uranium content for fluorescence has not been established. An occurrence of weakly fluorescing quartz from Nevada has a uranium content of 5.3 parts per million (Cowan, Priest, and Levy, 1993, p. 1037). This value may be taken as an estimate of the minimum uranium content of fluorescing silica.

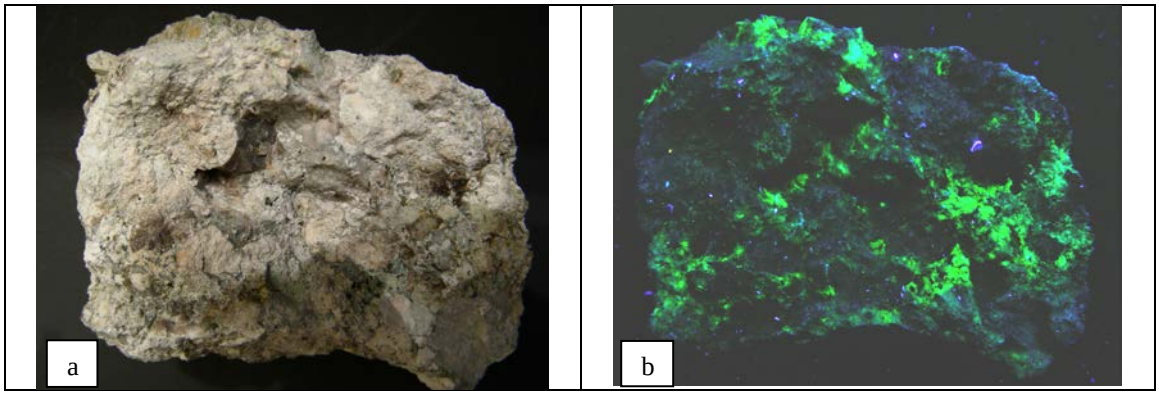

Figure 2. Pozos Conglomerate sample PB1024052 (221.14-m depth) under incandescent light (a) and short-wave ultraviolet light (b). Long dimension of sample is 4.5 cm.

ALTERATION HISTORY

The rock units at Nopal cuesta have a very complex alteration history that has received little attention apart from studies of uranium mineralization. A general description of alteration in the pyroclastic units is given by Reyes-Cortés (1997, p. 267-269). The only dated materials are some of the pyroclastic units, uranium minerals, and uraniferous fracture fillings. Therefore, the synopsis of alteration history presented here is preliminary and incomplete. An attempt has been made to highlight alteration processes that may have contributed to uranium transport or sequestration.

Silicification in the Pozos Formation

Evidence of silicification in the Pozos Formation may represent some of the earliest Tertiary alteration episodes. Goodell (1981, p. 277) noted that portions of the Pozos Formation near the contact with the overlying Coloradas Formation (then considered part of the Nopal Formation) were intensely altered. Limestone fragments were partially replaced, and cobbles cemented, by red chalcedony. The alteration was attributed by Goodell to degassing and vapor-phase activity during the deposition of the overlying Coloradas Formation or, alternatively, to diagenetic alteration of that unit.

The possible contribution of alteration in the Coloradas Formation to the silicification of the Pozos Formation remains untested. Various types of silicification are present in sediments throughout the 108-m thickness of the Pozos in PB1 core, and at least some of them probably predate emplacement of the Coloradas Formation.

Clasts of silicified limestone in the conglomerates preserve evidence of the earliest silicification. In some cases, the only indications of original lithology are preserved ghosts of fossils or of stylolitic sutures (a distinctive type of fracture unique to carbonate rocks). This silicification most likely is inherited from alteration of a parent limestone because of the intermixture of altered and unaltered calcareous clasts in the conglomerate. In thin section, the silicification appears as more or less continuous patches of microquartz.

Silica-altered volcanic clasts are common constituents of the Pozos sediments. Most of these were altered prior to erosion of the parent bedrock, again because of the heterogeneity in degree of alteration. Some clasts with indistinct margins may have undergone *in situ* recrystallization or deposition of overgrowths.

Microquartz cement is present in clasts of sedimentary rocks incorporated into the Pozos conglomerates and as *in situ* cement. The recycled quartz cement is locally distinguishable from *in situ* cement where there is a difference in intensity of ultraviolet fluorescence, but there is no consistent difference. Conglomerate sample PB1024052

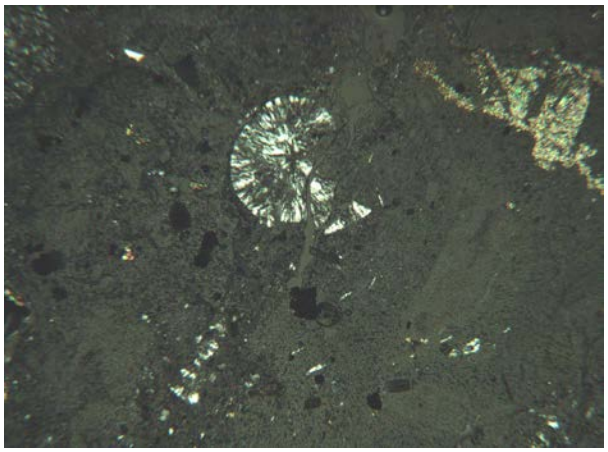

Figure 3. Pozos Conglomerate sample PB1024052 (221.14-m depth) thin section, slightly uncrossed polarizers. This view shows a quartz spherulite, width approximately 0.2 mm, from the vicinity of a fluorescing portion of the rock.

(221.14-m depth) contains well-developed microquartz cement with local formation of ≤ 0.2-mm quartz spherulites (Figure 3). Additional information about early uranium accumulation in siliceous Pozos sediments is contained in the section on ultraviolet fluorescence of PB1 core.

Uranium Mineralization

Uranium enrichment in the rocks of the Nopal area occurred principally as the result of two very different processes. An early enrichment period included the incorporation of silicified limestone clasts, diagenesis, and hydrothermal alteration of the Pozos Conglomerate, and the end product was uraniferous silicified rock. The second process was the hydrothermal uranium mineralization that produced the Nopal I ore body in the Nopal and Coloradas Formations. The Nopal I ore body and surrounding rocks have experienced subsequent hydrothermal modification and low-temperature alteration and weathering accompanying redistribution of uranium. The Pozos Formation also has experienced recent uranium transport and deposition.

Uranium Enrichment in the Pozos Formation

Silicification of portions of the Pozos Formation, attributed to hydrothermal alteration, diagenesis, or both, was described above. The green fluorescence of the secondary silica attests to a significant uranium content, but there is little quantitative information on uranium concentrations in this rock unit. Fayek et al. (2006, p. 57) reported a uranium content of about 475 parts per million for the uranium-rich portion of the Pozos conglomerate about 25 m above the water table. This is a reasonable value for a rock in which the uranium predominantly resides in secondary silica. Additional uraniferous secondary phase may include kaolinite, sulfides, and titanium minerals. One example of uraninite associated with titanium minerals is described below.

Uraninite is present in a uranium-rich portion of tuffaceous Pozos conglomerate located nearly 100 m below the main ore body and 30 m above the water table (Fayek et al., 2006, p. 57-58). A sample of PB1 core from the 190.8-m depth contains disseminated grains of TiO_2 and TiO_2 replacements of highly altered sphene, as well as pyrite. Some of the titaniferous material is the TiO_2 polymorph anatase with rims of uraninite. The U-Pb age of the uraninite is < 1 Ma. The depositional temperature is estimated to have been 10º to 20ºC. This preliminary result suggests that anatase is actively sequestering uranium from fluids that have interacted with the conglomerate.

The alteration history of the Pozos Formation as it relates to possible uranium mobilization remains largely unknown. General mineralogic trends over time toward increasing silica crystallinity through dissolution and reprecipitation would suggest that at least some of the uranium originally present in the clasts and cement has been released

and redistributed. However, uranium-lead systematics of the older uraniferous secondary silica from the unsaturated zone at Yucca Mountain indicate that the silica has retained uranium for at least the last eight million years (Neymark et al., 2002). The host rock did not experience pervasive hydrothermal alteration during that time.

The Pozos Formation most likely has experienced multiple episodes of hydrothermal and geochemical alteration after initial silicification. Possible alteration events include alteration related to emplacement of the Coloradas tuffs, the mineralizing event that produced the uranium ore body in the Coloradas and Nopal tuffs, kaolinization and sulfide-mineral deposition, uranium redistribution in the tuffs, and the transition to a more oxidizing environment as the unit emerged from the saturated zone. Most of these events are described in greater detail below. The evidence from Yucca Mountain suggests that uranium mobilization involving secondary silica may have been a minor or insignificant process at least since the Pozos Formation was uplifted into the unsaturated zone. Titanium minerals are loci of uranium accumulation as uraninite. Kaolinite and other clay minerals presumably have both accumulated and released uranium, based on studies by Muller, Ildefonse, and Calas (1990) and Allard and Muller (1998). Sulfide minerals were preferred sites of uranium deposition, but the gradual oxidation of sulfides during the transition to unsaturated conditions may have resulted in the release of uranium.

Uranium Mineralization in the Nopal and Coloradas Formations

The conditions under which the original uranium mineralization occurred at Nopal I have not been fully determined. Many studies have been done at Nopal I, and not all of them agree as to the timing or conditions of mineralization. The present study builds upon detailed petrographic studies of the ore by Pearcy et al. (1993) that document the basic paragenesis of uranium minerals and their associates without an absolute time scale. Descriptions of uranium mineralization presented here highlight the results of U-Pb, U-series, and oxygen-isotopic analyses of primary and secondary uranium phases by secondary ion mass spectrometry (Fayek et al., 2006).

The initial Stage 1 uraninite precipitated in the Nopal and Coloradas Formations from 45-55ºC fluids that interacted with constituents of the welded tuffs. The uraninite occurs in association with quartz and also along cleavages of feldspar grains. Mineralization occurred at 32±8 million years ago under reducing conditions, based on preliminary U-Pb dating of uraninite from mineralized Nopal tuff (Fayek et al., 2006, pp. 57-58). Very little of the primary uraninite escaped subsequent alteration. Uraninite was preserved only within a portion of the deposit consisting of a strongly silicified breccia. Textural relations suggest that silicification of the tuff occurred during the primary mineralizing event (Pearcy et al., 1993, p. 3-1 to 3-2).

The alteration of Stage 1 minerals resulted in the precipitation of Stage 2 uranium minerals, also concentrated along fractures in the tuff. Uranophane, schoepite/dehydrated schoepite, and weeksite are the dominant Stage 2 uranium minerals, with minor amounts of colloform uraninite. Uranium-series analyses of these minerals give a range of ages:

3.1±0.5 Ma for uranophane (oxidizing event), 1.6±0.5 Ma for colloform uraninite (reducing event), and 85±8 ka for schoepite/dehydrated schoepite. Weeksite/boltwoodite

from near the margins of the deposit gives an age of 41±5 ka. The two most recent mineral-precipitation events occurred under oxidizing conditions (Fayek et al., 2006, p. 57, 59).

Primary uranium mineralization in the Nopal and Coloradas Formations occurred within a vertical breccia zone at the intersection of two step faults with several meters of offset (Goodell, 1981, p. 284). More detailed renditions of the fractures and faults that define the breccia zone are given by Pearcy, Prikryl, and Leslie (1995, p. 686-693), Reyes-Cortés (1997, p. 222-243), and Fayek et al. (2006, p. 57, 60). Within the uncertainty of the primary uraninite age, the timing of mineralization is approximately contemporary with the earliest phase of Basin and Range extension. As described above, the earliest recognized extension in the vicinity of the Nopal cuesta may have been no more than about 29 million years ago, which is the maximum age of the graben separating the Sierra Peña Blanca from the Sierra del Nido to the west (Goodell, 1981, page 277). The faults and fractures produced by extensional deformation would have provided access to hydrothermal fluids.

Clay Alteration

Clay alteration has not been systematically studied throughout the Nopal cuesta, although several specialized studies focused on clays associated with uranium mineralization. Kaolinite is the most abundant and widespread clay mineral in the altered volcanic rocks of the Nopal Formation (Muller, Ildefonse, and Calas, 1990, p. 601-602). The degree of kaolinization is highest in the breccia zone that hosts the uranium deposit and decreases with distance from this zone. Kaolinite occurs as pseudomorphs of feldspar and as fracture fillings. Textural relations were interpreted to indicate that kaolinization was contemporaneous with primary hydrothermal uranium mineralization. Some kaolinite deposits are crosscut or overlain by secondary uranium minerals. The preceding information is based on studies of clays exposed on the open-pit mine faces of the Nopal and Coloradas Formations.

Reconnaissance studies of the PB1 drill core suggest that kaolinite is a very common constituent of the Nopal, Coloradas, and Pozos Formations (Goodell et al., 2003). The white clay occurs as a replacement of feldspars and as fracture fillings. An example of kaolinite fillings in tectonic fractures is described in a subsequent section.

Oxygen-isotopic studies of the kaolinite associated with reduced-uranium mineralization on the open-pit faces were interpreted by Calas et al. (2008, p. 211) to indicate formation at 50 to 75ºC in equilibrium with meteoric water. This temperature range is similar to the 45-to-55ºC range calculated by Fayek et al. (2006) from oxygen-isotope geothermometry of primary Stage I uraninite, supporting the interpretation that uranium mineralization and kaolinization were contemporaneous.

Muller, Ildefonse, and Calas (1990) and Allard and Muller (1998) studied paramagnetic defect centers in kaolinite from the open-pit faces. They found that defect-center concentrations correlate in a general way with uranium abundance in the associated

whole-rock samples, confirming that irradiation by uranium and its daughters generated the defect centers. The authors saw in these observations a potential to use kaolinite as a paleodosimeter to help reconstruct the history of uranium-decay-series mobility. Measured uranium concentrations in kaolinite samples from the ore body and the surrounding rock were compared with calculated concentrations based on two different uranium-mobilization scenarios. The first scenario postulated that all kaolinite, both feldspar replacements and fracture fillings, is 44 million years old (a presumed maximum age of primary uranium mineralization). The second scenario postulated that feldspar-replacing kaolinite is 44 million years old and fracture-filling kaolinite is seven million years old (a presumed age of secondary-uranium mineralization). Neither scenario led to close matches of all measured and calculated data pairs, but the calculated values for a multistage mobilization history more closely approximate the distribution of measured values (Allard and Muller, 1998, p. 761-763).

Pearcy (1994, p. 4-1) stated that tuff in the SE portion of the +00 mined surface is heavily weathered mainly to smectite with minor kaolinite. This is inferred to be a result of surficial weathering that was associated with aqueous transport of uranium away from the primary deposit. Reyes-Cortés (1997, p. 267-268) reported that the clay minerals nontronite, saponite, and montmorillonite have been identified in altered vitrophyres, presumably of the Nopal and Coloradas Formations. At least some of the smectite coats kaolinite deposits and therefore is younger than the kaolinite (Calas et al., 2008, Figure 3). Calas et al. (2008, p. 210) suggest that formation of smectites outside the uranium-mineralized zone occurred at around 40ºC in equilibrium with meteoric water.

Sulfide Deposition and Alteration

Table 3 contains basic visual observations about the distribution of sulfide minerals in the PB1 core. The exact identities of sulfide minerals were not determined in the course of this study. These observations suggest that sulfide minerals previously were present in all rock units of the core. The shallowest observed occurrence of surviving sulfide in the core is in the Coloradas Formation at a depth of 109.62 m. Apart from that occurrence, sulfides are common but not abundant in the Pozos Formation below a depth of about 180 m and in the underlying Cretaceous limestone.

A few occurrences of sulfides or possible former sulfides in the Coloradas Formation (Table 3, 79.77-m and 109.62-m depths) mostly are restricted to lithic inclusions. These are probable examples of sulfides derived from altered volcanic rock incorporated into the Coloradas eruptive unit. The sulfide-bearing lithic inclusions are relatively uncommon in the PB1 Coloradas section and only in trace quantities where present.

Various pertinent observations and interpretations have been made about sulfide deposition at Nopal I. Pearcy et al. (1994, p. 717) reported that granular uraninite that replaces phenocrysts within silicified breccia fragments commonly is intergrown with syngenetic, euhedral pyrite in the main ore body (not intersected by PB1). This paragenesis, representing the initial uranium mineralization, was preserved by the

silicification that protected it from later alteration. Calas et al. (2008, p. 211) interpreted the presence of carbonates in the uranium ore deposit as an indication of transport from the underlying limestone that provided sedimentary sulfides and organic matter favoring reducing conditions and uraninite/pyrite precipitation.

Prikryl et al. (1995, p. 2-6 to 2-9) studied iron oxy-hydroxide deposits in a prominent E-W fracture system that cuts the original ore deposit. Microscopic textures of the fracture fillings suggest there are iron oxy-hydroxide pseudomorphs after pyrite. Jarosite, an iron sulfate, also is part of the alteration mineral assemblage. This was interpreted as evidence that pyrite, unaccompanied by uranium minerals, was deposited in the fractures by hydrothermal solutions some time after primary mineral deposition and later altered to iron oxy-hydroxides. Textural indications of cubic sulfide replacement by iron oxy-hydroxide are moderately common in tuffs of the Nopal and Coloradas Formations (Table 3). Pseudomorphs of altered sulfides are present in the matrix, lithic inclusions, pumice lapilli, and fractures or breccia zones. Iron oxy-hydroxide fracture fillings and breccia cements without recognizable sulfide-pseudomorph textures also may have been derived from sulfide alteration.

Fayek et al. (2006, Figure 3) observed a textural association of uraninite with titanium-rich minerals and pyrite in a PB1 core sample from the 190.8-m depth in the Pozos conglomerate. The uraninite is less than one million years old (Fayek et al., 2006, p. 57), but this provides no constraint on the age of the pyrite. The complexity of sulfide mineralogy in the Pozos conglomerate probably indicates an equally complex depositional history. At least some of the sulfide in the Pozos Formation has been replaced by iron oxy-hydroxide.

Uranium Transport in the Shallow Unsaturated Zone

Recent research for the natural analogue project includes monitoring, collection, and analysis of seepage water from an adit located about eight meters below the +10 surface. The objective of the research is to provide the basic information required to evaluate rock-water interaction and flow and transport processes where percolating water first encounters uranium-rich rock in the unsaturated zone. Preliminary modeling of the hydrologic processes of infiltration and seepage through the fractured welded tuff was done by Ghezzehei et al. (2006).

Collection and Analysis of Seepage Water

A water-collection system, consisting of 240 separate 30 cm × 30 cm compartments that are each connected to a 125-mL bottle, was installed in April 2005 within the +00 m adit of the mine to collect water that had infiltrated from the +10 level (surface) and seeped into the adit (Dobson et al., 2012; Goldstein et al., 2016). The seepage pathway from the ground surface to the collection system, assuming vertical fluid flow, is about eight meters. The system was upgraded in November 2005 with the addition of

instrumentation to six collector sites to measure seepage rates continuously. Analyses of seepage-water samples from the adit provide information about the variability of uranium-dissolution rates and uranium-isotopic compositions of the seepage water.

Modeling Uranium-Isotopic Systematics of Seepage Water

Ku et al. (2009) constructed an analytical model based on the concept that intermittent seasonal infiltration and percolation in the shallow unsaturated zone leads to a linear relationship between reciprocal uranium concentration and $^{234}U/^{238}U$ ratio in percolating waters. They showed that seepage waters from various locations in the adit define distinct linear trends based on wet-versus-dry-season collection time. The underlying cause of this difference is the accumulation of recoil-produced ^{234}U on rock-pore and fracture surfaces during the dry season, followed by preferential uptake of the surficial ^{234}U by percolating water during the wet season. Other factors contributing to the trends include rock-water interaction (or water-transit) time, uranium-dissolution rate, and the rate of recoil that supplies ^{234}U to the exposed rock surfaces. Longer periods of little or no infiltration and lower uranium-dissolution rates lead to high $^{234}U/^{238}U$ ratios in the percolating water.

Seepage waters with $^{234}U/^{238}U$ ratios close to unity and relatively high dissolved uranium content were collected from the front of the adit where the water interacted with uranium-mineralized rock (Goldstein et al., 2016). Ku et al. (2009) suggest that the dissolution of abundant uranium close to secular equilibrium masks the effects of processes that otherwise would produce waters with higher $^{234}U/^{238}U$ ratios. Additional details and interpretations of the uranium-isotopic data for UZ waters as they relate to aqueous transport to the saturated zone are given in a subsequent section.

Uranium in Fracture Fillings

Researchers from the Center for Nuclear Waste Regulatory Analyses have studied evidence of uranium mobilization, transport, and sequestration, especially within an E-W fracture system exposed on the +10 surface of the mine at Nopal I (e.g., Pearcy et al., 1995; Pickett et al., 1996). Eight sampling traverses were performed, most of which crossed the boundary of the ore body. Samples of host rock and fracture fillings were analyzed for contents and activity ratios of ^{238}U decay-series radionuclides to detect evidence of recent element mobility indicated by disequilibrium within the decay chain. Additional analyses included X-ray diffraction mineralogical determination and selective extraction of ^{238}U, ^{234}U, ^{232}Th, and ^{230}Th to understand the intrasample distribution of these four radionuclides.

Quaternary-age uranium transport documented by the fracture fillings would have occurred in the shallow vadose zone at depths of as much as 40 m. This estimate of depth is based on residual topography that documents the amount of overburden removed during open-pit mining (Pickett et al., 1996, Figure 2-1). The evidence of uranium migration away from the ore body, studied on the horizontal +00 and +10 surfaces, represents unknown combinations of vertical and lateral transport.

The uranium-concentration data document patterns of diminishing uranium content with distance from the ore body within the fractures. Apparent lateral uranium-transport distances of at least 20 m within long-trace, high-angle fractures of >1-mm aperture appear typical (Pickett et al., 1996, p. 2-9). The uraniferous fracture fillings in the major fracture set at 13.5 m N beyond the edge of visible uranium mineralization consist of quartz, amorphous iron oxyhydroxide, hematite, jarosite, goethite, and kaolinite (Prikryl, Pickett, and Pearcy, 1995, p. 2-6, 2-16). Constituents of the iron oxide-oxyhydroxides and iron sulfate minerals probably were derived from in-situ alteration of pyrite originally deposited by hydrothermal solutions not associated with the primary uranium deposit (Prikryl, Pickett, and Pearcy, 1995, p. 2-18). Selective leaching experiments suggested that most of the uranium is associated with the crystalline iron oxide-oxyhydroxide phases (Pickett et al., 1996, p. 2-9). Prikryl et al. (1997, p. 64) interpreted the absence of uranium minerals to indicate that uranium was incorporated into the iron oxide-oxyhydroxide phases by coprecipitation during secondary-mineral growth and by sorption.

Several researchers have measured the uranium-series systematics of iron oxide-oxyhydroxide fracture fillings from the major fracture set. In all cases, bulk fracture-filling materials were analyzed for uranium-series isotopes. The methodologies included alpha spectrometry (Prikryl, Pickett, and Pearcy, 1995), gamma spectrometry (Wong, Goodell, and Anthony, 1999), and mass spectrometry (Murrell, Goldstein, and Dixon, 2002). Mass-spectrometric results generally were necessary to detect small differences in U-Th disequilibria with the required precision.

Prikryl, Pickett, and Pearcy (1995, p. 2-21) found $^{234}U/^{238}U$ ratios greater than unity in bulk fracture-filling samples from the 13.5 m N fracture set and interpret these data to indicate uranium mobilization within the last million years. ^{238}U-^{234}U-^{230}Th data obtained by Murrell, Goldstein, and Dixon (2002, p. 339) confirm the $^{234}U/^{238}U$ disequilibria results but lie on a whole-rock isochron that requires closed-system behavior for the last 400 ka. $^{231}Pa/^{230}U$ activity ratios within error of unity suggest closed-system behavior for U and Pa for at least the past 100 ka. $^{226}Ra/^{230}Th$ activity ratios range from 0.76 to 0.99 (i.e., <1), which suggests recent radium loss and mobility due to ongoing fluid flow in the fractures. Gamma-spectroscopy isotopic analyses by Wong, Goodell, and Anthony (1999, p. 806) support the indications of recent radium mobility, but are too imprecise to evaluate the mobility of uranium relative to thorium.

Samples of iron oxide-oxyhydroxide fracture fillings were collected from the PB1 drill core to extend the uranium-series investigations into three dimensions. Long-lived U-series results for the surface fracture-filling materials have been summarized and compared to new U-series analyses of the drill-core fracture-filling materials by Denton et al. (2016). High uranium concentrations in the fracture-fill materials of about 12 to 7700 ppm (Denton et al., 2016, Table 2) indicate uranium mobility and transport from the ore deposit in the past. Uranium concentrations generally decrease with horizontal distance away from the ore deposit. The number of PB1 parent core samples analyzed (3) is insufficient to draw conclusions about trends in uranium concentrations with depth.

Isotopic activity ratios indicate a comlicated geochemical evolution in terms of the timing and extent of actinide mobility. U-Th-Ra-Pa disequilibria and model ages indicate widespread uranium mobility between 0.2 Ma and 1.2 Ma, some uranium mobility but mostly uranium immobility in the last 0.2 Ma, Ra mobility in the last 0.1 to 8 ka, and Th-Pa immobility in the last 185 ka. ^{238}U-^{234}Th-^{232}Th linear age-trend calculations show that fractures sampled at 8.5 m and 191 m were closed to U-Th mobility at 440 ka and 210 ka respectively. The fracture subsamples at 67 m do not form a linear age trend and have recently been an open system for uranium (Denton et al., 2016, p. 23-24). More detailed high-resolution chemical, mineralogical, and isotopic studies may help provide a greater understanding of the open-system processes occurring in some samples.

We also looked for petrographic and geophysical indications that the processes leading to uranium mobilization and sequestration in fractures described by Prikryl, Pickett, and Pearcy (1995) have occurred lower in the stratigraphic section. The hand-held gamma survey of PB1 drill core revealed the existence of "hot spots" where the gamma counts were higher than background values. Most of these were in the Nopal and Coloradas Formations. A majority of the hot spots in the Coloradas Formation were sampled, and many of them are included in the sample descriptions of Table 3. Some of the hot spots correspond to core with iron oxide-oxyhydroxide fracture fillings whose textures suggest pseudomorphous replacement of sulfides. Other hot spots are associated with core containing iron oxide-oxyhydroxide fracture fillings but no obvious sulfide-replacement textures. Hot spots associated with some kind of iron oxide-oxyhydroxide mineralization are the most common, but there are a few high-gamma occurrences that do not obviously share this association. Conversely, not all iron-mineralized fractures are hot spots. On the basis of these observations, it is likely that sulfide-mineralization events and uranium-mobilization processes somewhat similar to those studied on exposed surfaces by Pearcy et al. (1995) and others also occurred deeper in the volcanic section.

Hot spots in the Nopal and Coloradas Formations are present to a depth of about 105 m in PB1 core, whereas the borehole gamma survey suggests that uranium enrichment in those units extends to about 113 m. The deepest workings in the ore body are located equivalent to a depth of about 110 m in PB1 (George-Aniel, Leroy, and Poty, 1985, Figure 3). These relations would seem to indicate that the iron-mineralized fractures with uranium have approximately the same vertical distribution as the ore body. The ambiguity of lateral versus vertical fluid + uranium transport in fractures, recognized by Pearcy et al. (1995), could not be resolved by the PB1 data because the locations of the ore-body boundaries relative to the borehole are not known. In particular, the borehole is not in an optimal location to detect the possible existence of uranium-enriched fracture fillings directly below the ore body, which would provide unambiguous evidence of vertically downward aqueous uranium transport.

Most of the existing evidence indicates low mobility for most of the actinides, especially thorium and protactinium but also uranium, during the most recent history of the ore deposit and unsaturated zone. The results of uranium analyses for both unsaturated-zone and saturated-zone groundwater, including the seepage experiment, confirm that uranium is being dissolved in relatively low amounts from the ore body and from rock near the ore

body under present geochemical and geohydrologic conditions (Goldstein et al., 2016). The mainly closed-system behavior of U-Th-Pa in fracture-filling materials over the past ~200 ka (Murrell, Goldstein, and Dixon, 2002; Denton et al., 2016) provides an indicator of the geochemical immobility of these actinides over long time scales.

Tectonism and Fracture Evolution at Nopal I

The timing, locations, and style of fracturing and brecciation controlled the development of the hydrogeochemical system responsible for initial uranium mineralization. Primary uranium deposition was focused in a vertical zone of broken rock. Much of the subsequent alteration of uranium minerals and other rock constituents, uranium remobilization, and deposition of secondary uranium-bearing minerals has been localized in and around fractures. Information about the three-dimensional fracture characteristics of the entire stratigraphic section is one of the keys to a better understanding of uranium transport through time.

The history of fracture development in response to volcanic processes and the changing tectonic setting remains largely unknown. Rock core from well PB1 provides some information about the relative chronology of fracture development in the deeper subsurface. The entire core was not studied in detail, but a few examples convey a sense of the evolving fracturing style.

The two main types of fractures likely to be present at Nopal I are cooling joints, formed as the tuff contracted upon cooling, and tectonic fractures. Cooling joints usually are the earliest-formed fractures in pyroclastic deposits. Recognition criteria for cooling joints and tectonic fractures were developed by the Yucca Mountain Site Characterization Project based on extensive outcrop and drill-core studies (Buesch et al., 1996). Joints that are very smooth and planar to curviplanar are usually attributable to cooling. The high-temperature mineralogy of fracture coatings confirms cooling-joint origins in some cases. Tectonic fractures tend to be rougher and may merge into breccia zones. These criteria are less applicable to fracture classification at the Nopal cuesta, where some of the most recent tectonic fractures are sub-planar (Pearcy, Prikryl, and Leslie, 1995, p. 689). In addition, the fracture mineralogy at Nopal I is dominated by lower-temperature secondary alteration and any original high-temperature fracture minerals may not have been preserved.

Cooling Joints

No cooling joints could be identified with certainty. The Nopal Formation, as exposed on the Nopal cuesta, contains so many tectonic fractures that cooling fractures could not be identified with confidence. Many of the possible cooling joints in the Coloradas Formation appear incipient – incompletely formed – or have been altered in ways that minimize the fracture aperture.

Possible cooling joints modified by subsequent brecciation are a common feature of the Coloradas Formation and are also present in the Nopal Formation. The best-exposed

examples in the core are breccias bounded by high-angle joints. The attributes of this type of brecciation are difficult to discern in drill core, but are visible in subsurface exposures at Yucca Mountain where brecciated rock is bounded by high-angle cooling joints (Levy et al., 1999). The brecciation occurred in the hanging wall of a block-bounding normal fault formed during Basin and Range extension. Breccia features in PB1 may have a similar origin.

The Pozos Formation contains three intervals of tuff with thicknesses of two to six meters (Dobson et al., 2008, p. 964). These pyroclastic intervals, although thin compared to the Nopal and Coloradas Formations, host planar fractures that resemble cooling joints.

The role of cooling joints as present-day seepage pathways in the shallow subsurface probably is minor. In the deeper subsurface, cooling joints may have served as fluid pathways in the past but appear to have been mostly sealed by rock alteration and secondary-mineral deposition. The permeability of some cooling joints was enhanced by brecciation. Some joints of uncertain origin, surrounded by Liesegang bands in tuff intervals of the Pozos Formation, may have been fluid pathways more recently. This possibility is further discussed in the section on perched water, permeability barriers, and fluid pathways.

Tectonic Fractures

Tectonic fractures, including breccia zones, comprise the majority of fractures in the rocks at Nopal I. Highly fractured intervals are common in all of the geologic units penetrated by PB1 except the Cretaceous limestone penetrated by the borehole. Twenty-three distinct fracture zones were identified in the downhole video log for the Coloradas Formation, and fractured and brecciated zones associated with mineralization were noted in the Pozos Formation (Dobson et al., 2008). The location of the borehole at the margin of the ore body was not optimal to characterize the brecciation thought to have controlled uranium mineralization.

Tectonic fractures exposed on the +00 and +10 mined surfaces (Nopal Formation) of the Nopal I ore deposit were mapped in detail by Reyes-Cortés (1997, pp. 222-224; also reported in Pearcy, 1994, and Pearcy, Prikryl, and Leslie, 1995). Fractures exposed at the surface typically show only minor horizontal offset <5 cm (Pearcy, Prikryl, and Leslie, 1995, p. 693), but some have vertical offsets of up to 20 m (Goodell, 1981, p. 284). The fractures were grouped by Reyes-Cortés (1997) into six major fracture systems corresponding to three regional systems and their complementary subsystems. The intermediate-age system, with faults and fractures oriented N35ºW and N25ºE, was identified with Basin and Range tectonism. Pearcy, Prikryl, and Leslie (1995, p. 693) suggested a sequence of formation based on cross-cutting relations, in which NE-trending fractures are the earliest, NW-trending fractures are of intermediate age, and EW-trending fractures are the youngest.

A prominent EW fracture set traceable for more than 28 m was identified by Pearcy, Prikryl, and Leslie (1995, p. 689, 696-697) as an example of the youngest EW-trending fractures. This fracture set, designated the 13.5 m N fracture by Pearcy, Prikryl, and Leslie (1995, p.693), cuts across the ore body.

Fractures and a fault in the ceiling of an adit eight meters below the +10 surface were documented in relation to the placement of a seepage collection system (Dobson et al., 2012). The fault is oriented N37E and dips 81 degrees to the SE. This orientation is similar to that of the oldest fracture set identified at the surface by Pearcy, Prikryl, and Leslie (1995, p. 693). Continuity of some fractures in the adit ceiling with the surface was inferred from the presence of plant roots in the fractures (Dobson et al, 2012, Figure 15). Many fractures in the adit ceiling shown by Dobson et al (2012, Figure 6) are smooth and planar to curviplanar, with trace lengths up to about eight meters in the horizontal direction. These fractures with common dark reddish fillings dominated by iron oxyhydroxides (Wong, Goodell, and Anthony, 1999, p. 802) retain enough permeability to conduct seepage water, at least in the shallow subsurface (Dobson et al., 2012).

The PB1 core is unoriented and has not been studied sufficiently to identify correlations between structures in the core and local faults, fractures, and breccia zones observed in outcrops and mined surfaces. Most structural features visible in the core are small-scale structures whose significance and representativeness are uncertain. Tectonic fractures were examined in one PB1 core sample from the Pozos Formation with textural features of a scale small enough to reveal a sequence of formation. Sample PB1023995 MTM3 (181.25 m depth) is a fine-grained tuffaceous conglomerate with a faint centimeter-scale network of rough, tight, subvertical fractures with subvertical slickenlines. Much less common are similar fractures of horizontal orientation. There is no macroscopic evidence of offset along these fractures. The fractures have thin, slightly iridescent gray coatings probably of iron oxyhydroxide. A few of these fractures, perhaps those with greater longitudinal continuity, subsequently were dilated. These fractures were filled with kaolinite, and then a smaller subset were further dilated and filled with iron oxyhydroxide and calcite, attaining final filled apertures of three to four millimeters. Similar dilated fractures are present within a 12-m vertical interval including the described sample (Goodell et al., 2003).

The described sequence of fracturing documents an early period of distributed compressional deformation that imparted a fabric to the rock, on at least a local scale. Later extensional deformation occurred along a subset of the original fractures. These observations from one sample represent only a small part of the tectonic deformation at Nopal I, but they convey a sense of the changing stress regimes to which the rocks have been subjected.

SITE GEOHYDROLOGY

Previous studies of the Nopal I uranium deposit postulated that the ore body formed in the saturated zone and that mineralogic alteration and mobilization of uranium began when the deposit was uplifted into the unsaturated zone (e.g., Murphy and Codell, 1999, p. 552). This interpretation is reasonable, considering geochemical principles of uranium solubility and what is known of the local tectonic history. Paleohydrology and present-day geohydrology of the site have not been systematically studied, but some inferences can be made from existing information. Further refinement of the geohydrologic history could lead to a better understanding of uranium migration over time.

Late Cenozoic-Quaternary Topography and Drainage

The existing topography around the cuesta hosting the Nopal I deposit places bounds on possible high stands of the regional static water level at this location. The cuesta is part of the Sierra Peña Blanca horst block and is tilted to the west. The top of the cuesta is a dip slope on the Nopal Formation, which is inclined 25º westward (Goodell, 1981, p. 282, Figure 4). To the west, a structurally controlled low area containing alluvium of unknown thickness separates the cuesta from horst blocks at higher elevation (Goodell, 1981, Figure 3). East of the high-standing cliff edge of the cuesta, alluvial deposits blanket the east-dipping slope.

As a result of uplift, mass wasting, and stream incision, the cuesta is bounded on the north, east, and south by erosional features at elevations of no more than about 1380 to 1400 masl (Instituto Nacional de Estadística Geografía Informática, 2004). A channel in the alluvium on the west side of the west-dipping cuesta occupies elevations of about 1420 to 1440 masl. The regional static water level below the cuesta, measured in borehole PB1, is at an elevation of about 1240 masl (Table 1).

The high point of the cuesta is about 1580 masl. At the PB1 drill site, the uneroded and unexcavated remnant of the uranium deposit extends from the ground surface at 1463 masl to about 1350 masl, with the most highly mineralized portion of the deposit above 1383 masl, These depths are inferred from the gamma log of the borehole (Figure 1). The present-day static water level is about 110 m below the base of the deposit (143 m below the base of the most highly mineralized portion) and 223 m below the exposed remanent top of the deposit. The existing state of erosion around most of the cuesta would preclude the static water level from reaching a position higher than about 1380 to 1400 masl, which is approximately the base of the most highly mineralized portion of the ore deposit.

In the absence of a detailed geomorphological study, it is difficult to quantify the age of the existing topography and drainage patterns. A reconnaissance geologic map of the drainage south of the Nopal 1 cuesta (Stege et al., 1981, Figure 2) shows incision into the pyroclastic bedrock below the level of an earlier alluvium-filled channel. The thickness of the alluvium is about 20 m or less. This information, though minimal, suggests a local multistage history of erosion and deposition around the Sierra Peña Blanca, but

dominated by erosion. A geomorphologic description of the area by Reyes-Cortés (1997, pp. 22 and 24), in which the erosional characteristics of the area are ascribed to a mature geomorphological stage for an arid region with local rejuvenation due to stream piracy, is in general agreement with this assessment.

Local climate, local rates and durations of tectonic activity, and local sedimentation rates typically are the important factors affecting erosion and deposition. Values of these parameters presumably lie within the range of values for internally drained extensional basins of the southeastern Basin and Range Province (Langford et al., 1999; Connell et al., 2005). These basins began to develop their present morphologies around middle Miocene time (about ten million years ago) when rates of Basin-and-Range extension declined. The pattern of streams emptying into internally drained basins, some occupied by permanent or ephemeral lakes, continued to develop through Plio-Pleistocene time along the eastern edge of the Mexican Highland. Some basins have filled with sediment to the extent of burying the lowest lying horst blocks bounding the basin (Langford et al., 1999), but that evidently has not happened to the Sierra Peña Blanca or the Nopal I cuesta.

A general inference from the Cenozoic-Quaternary history of more thoroughly studied sections of the Basin and Range Province is that the present topography and drainages of the Sierra Peña Blanca, and the Nopal I cuesta in particular, began to develop nine to thirteen million years ago and are likely to be at least several million years old. Tectonic rejuvenation of the area has been minimal since the height of Basin and Range extension. The maturity of the dissected landscape around the Nopal cuesta implies that all or most of the Nopal I ore body has been in the unsaturated zone for at least the last several million years.

Perched Water, Permeability Barriers, and Fluid Pathways

Perched water in the unsaturated zone probably has played an important role by contributing to distinctive rock alteration both before and after uranium mineralization occurred. Mineralogic alteration of volcanic tuffs in some cases was localized in low-permeability lithologies. The effectiveness of perched water in mobilizing uranium from the ore body may be inferred from compositions of seepage water collected in an underground adit at Nopal I (Goldstein et al., 2016).

The vitrophyre at the base of the Nopal Formation, as much as 10 to 12 m thick at the Nopal cuesta (Reyes-Cortés, 1997, pp. 219-220, 267-268), is likely to have acted as a permeability barrier throughout the history of the unit. Distinctive smectite ± zeolite alteration of the vitrophyre probably is related to perching of water. The association of low-permeability vitrophyre and alteration is another point of similarity between the Nopal tuff and the Topopah Spring Tuff at Yucca Mountain, where the basal vitrophyre is variably altered to a secondary-mineral assemblage including smectite, zeolites, and silica (Levy, 1984, pp. 961-963). Textural evidence of perched water associated with alteration is preserved as layered fillings in rock pores of altered vitrophyre at Yucca

Mountain (Levy and Valentine, 1993, pp. 146-147). The Topopah Spring vitrophyre, regardless of alteration, continues to maintain a localized perched-water zone within the unsaturated zone (Wu et al., 1999, pp. 161-162).

Electrical resistivity surveys of the Nopal cuesta indicated the possibility of perched water above the basal vitrophyre of the Nopal Formation and above the Pozos conglomerate (Reyes-Cortés, 1997, pp. 274-290). Differences in the results of surveys conducted six months apart, in February and September, 1995, were tentatively interpreted as indications of seasonal perched water. Neutron logs of wells PB1 and PB2, drilled in April, 2003, show indications of higher water content in the vicinity of the vitrophyre (CRWMS M&O, 2004, Figures I-1, I-4).

Samples of perched water were collected in August, 1995, from an unused blast excavation borehole (Pickett and Murphy, 1999, p. 810) extending into or slightly above the basal vitrophyre of the Nopal Formation (inferred from well logs in CRWMS M&O 2004, pp. I-8, I-11). The uranium content of the perched water, up to 5.77 ng/g (recalculated from Pickett and Murphy, 1999, Table II, samples BH12W95-05 and BH12W95-11), is within the range of values for seepage waters from the adit collection system and regional ground waters (Goldstein et al., 2016, Tables 1 and 3). Pickett and Murphy (1999, pp. 811-812) detected haiweeite [$Ca(UO_2)_2(Si_2O_5)_3 \cdot 5H_2O$] in fracture fill in vitrophyre a few meters outside the visible uranium deposit. They speculated that the perched water was close to saturation for haiweeite, so that evaporation of perched water could lead to precipitation of this mineral. The natural gamma log for borehole PB2 shows a small increase in gamma response at the depth of the vitrophyre. No equivalent gamma response is discernible in borehole PB1 at the depth of the vitrophyre because the response is dominated by proximity to the uranium ore body, and a similar pattern was not observed in PB3 (CRWMS M&O, 2004, Figures I-1, I-4, and I-5).

Investigators of the Nopal I ore body generally agree that faults, fractures, and breccia zones played a key role in the genesis of the Nopal I uranium deposit (e.g., Goodell, 1981, p. 284). The role of faults and fractures as permeability barriers or geochemical boundaries limiting the extent of the ore body is a common theme of many site studies. Fayek et al. (2006, p. 57 and Figure 1) identified certain faults and fractures as the bounding features of the deposit. Differences in the elevations of stratigraphic contacts between nearest-neighbor wells at Nopal I are less than 10 meters (Table 1), although contact locations in the two uncored holes are imprecise. Vertical locations of contacts may vary among the wells due to combinations of tectonic tilting, primary depositional differences, erosion, and fault offset. The data indicate possible offset of the Nopal-Coloradas contact between PB1 and PB3 (50 m NE of PB1). Relative to its location in PB1, the contact is about six meters lower at PB3. The Coloradas-Pozos contact is about 4 to 6 m deeper in PB2 and PB3 than in PB1. The configuration of the Pozos-limestone contact diverges from the pattern of the shallower contacts. This contact is about six meters higher in PB3 than in PB1 and four meters higher than in PB2. The difference could represent erosional relief on the limestone surface or the effects of buried faults with offset unlike the faults cutting the overlying units. The contact in PB1 core appears sheared and clayey, with brecciated limestone beneath (Goodell et al., 2003). There is no

indication of orientation or sense of offset on this fault. The existing information for all contacts in the Nopal I wells suggests that elevation differences cannot be attributed to a single, simple structural effect, but proves insufficient to resolve the multiple contributing effects.

The difference in elevation of the Pozos-limestone contact in PB3 compared to PB1 and PB2 is at present the only geologic evidence of a possible flow barrier in the vicinity of the water table and may be related to observed differences in hydrologic behavior and water chemistry. As shown in Table 1, the differences in water-table elevation among the three wells attest to poor connectivity. Differences also were seen in the water-level and recharge responses of the wells to pumping six months after the wells were drilled (Oliver, 2004; Oliver et al., 2005). PB3 experienced less drawdown during pumping, 1.8 m, than the other two wells, even though the largest amount of water (almost 200 gal or 769 L) was pumped from this well. PB1 had drawdowns of at least 3.8 m and PB2 had drawdowns of up to 14 m.

The consistently higher uranium content of PB3 saturated-zone water relative to PB1 and PB2 (Goldstein et al., 2016, Table 2) also demonstrates restricted mixing due to the existence of a flow barrier between the wells. Higher uranium concentrations exist in PB3 water even though this well does not intersect the Nopal I ore deposit, whereas lower concentrations exist in water from PB1, which penetrated the edge of the deposit. This difference may indicate that uranium sources in addition to the ore deposit strongly contribute to the local water chemistry. The existence of a component of preferential lateral transport from the ore deposit toward the water table at PB3 also might help account for the compositional differences. At the very least, the poor connection between PB1/PB2 and PB3 and the distinct water chemistry of PB3 support a conceptual model of limited local mixing and local evolution of fluid composition, but not complete isolation.

Evidence of Changing Redox Conditions

The groundwater beneath the Nopal cuesta contains dissolved oxygen (P. Dobson, written communication, 2009), a good indication of present oxidizing conditions in the shallow saturated zone. Redox conditions in the unsaturated zone presumably are oxidizing, as described below. The evolution of redox conditions beginning at the time of initial uranium mineralization is inferred from the record of uranium-mineral deposition and alteration and from the distribution of sulfide minerals. Textural/mineralogic features related to changing redox conditions are an additional source of information.

The uranium-bearing minerals in the Nopal I ore body provide information about the redox conditions in effect when the minerals formed. Uranium-bearing minerals can be indirect indicators of paleohydrology because the multivalent behavior of the uranium ion is controlled by oxidizing-versus-reducing conditions. Oxidizing conditions are likely to exist in the unsaturated zone, favoring hexavalent uranium in soluble complex ions. In the deeper saturated zone, where reducing conditions are more prevalent, uranium may be reduced to the relatively insoluble tetravalent state and precipitate on rock surfaces

(Osmond and Ivanovich, 1992, p. 260). These are general observations, and the controls on redox conditions in specific settings may be more complex. It is worthwhile to compare what is known about the ages and uranium valence of Nopal I uranium-bearing minerals with other data pertaining to paleohydrology.

Uranium Mineralogy

The uranium minerals of Nopal I have recorded a long, possibly episodic history of varying redox conditions (Fayek et al, 2006, p. 58). Information on uranium mineralization ages and redox conditions inferred from uranium mineralogy was acquired from samples representing the main ore body in the Nopal Formation and uraninite in the Pozos conglomerate. Initial ore-body uraninite precipitation occurred at 32±8 Ma under reducing conditions in the Nopal and Coloradas Formations. A major oxidation event involving the deposition of uranophane occurred at about 3.1 Ma. This event was followed by a reducing event at about 1.6 Ma in which a second generation of uraninite, with a colloform texture, was formed. The ages of schoepite (about 85 ka) and weeksite/boltwoodite (about 41 ka) samples document more recent oxidation conditions in the ore deposit. The older uranium minerals formed during reducing conditions are locally preserved where silicification has restricted fluid access.

Uraninite within the Pozos conglomerate was identified in the PB1 drill core at a depth of 190.8 m, which is about 100 m below the base of the main ore body and 30 m above the water table. The age of this material is less than one million years. Preliminary imaging, spectral, and electron-diffraction studies suggest that anatase (TiO_2) is actively sequestering uranium as uraninite from fluids that have interacted with the conglomerate (Fayek et al., 2006, pp. 57-58). The formation of uraninite as the uranium phase is an indication of reducing conditions. The similarity of ages between the colloform uraninite in the Nopal Formation and the uraninite in the Pozos conglomerate suggests a possible genetic relationship, but additional analyses will be needed to confirm the ages.

Sulfide-Mineral Distribution

As noted above, the observations about sulfide minerals in Table 3 suggest that sulfides formerly existed throughout the stratigraphic section penetrated by borehole PB1. At present, the shallowest occurrences of sulfides include pyrite protected by silicification in the Nopal Formation (Pearcy et al., 1994, p. 717) and sulfides primarily within lithic inclusions in the Coloradas Formation at a depth of 109.62 m in PB1. Sulfides are common only below a depth of about 180 m in the Pozos Formation and Cretaceous limestone.

Iron oxide-oxyhydroxides with textures suggesting pseudomorphous replacement of sulfides are moderately common in the Nopal and Coloradas Formations (Table 3). Direct evidence for incomplete replacement of sulfides is preserved in an oxidized/reduced boundary feature at the 210.29-m depth within silicified micritic siltstone of the Pozos Formation (Goodell et al., 2003; Table 3).

Textural-Mineralogic Features

In addition to the uranium mineralogy and deposition chronology and the sulfide-mineral distribution, there is other textural and mineralogic evidence of changing redox conditions. As noted in Table 5, a tuffaceous layer within the Pozos Formation includes a 30-cm interval between 173.20- and 175.22-m depths in which Liesegang bands are distributed around mostly low-angle fractures. Liesegang bands are distinct bands of mineral that form when coprecipitate ions interdiffuse in a porous rock, leading to discontinuous precipitation bands, usually of iron oxide or oxyhydroxide. The precipitation results from the reaction of oxygenated ground water with soluble ferrous iron (McBride, 2003, p. 729). The iron presumably is derived from dissolution of ferrous iron-bearing minerals such as iron sulfides and siderite (McBride, 2003; Fu, Milliken, and Sharp, 1994). The oxidized/reduced boundary at 210.29-m depth in the Pozos Formation (Table 3), although not a Liesegang band, documents the derivation of at least some iron oxide-oxyhydroxide from iron sulfide.

The ages of the oxidized/reduced boundary and Liesegang bands in the Pozos Formation are not known. Studies of Liesegang-banded rocks in outcrops elsewhere have found the banding only in modern drainages (McBride, 2003, p. 730) or related to fracturing of Recent origin (Shahabpour, 1998, p. 106). At least one reason for this seems to be that older band sets are readily overprinted by new sets aligned with younger fractures so long as the conditions conducive to band formation remain in effect. On the basis of these observations, it is likely that the Liesegang features in the Pozos Formation record conditions in effect during the last few million years.

The combined evidence of uranium mineralogy, sulfide-mineral distribution, and textural-mineralogic features indicates that the rock units are still in the process of equilibrating with oxidizing conditions in the unsaturated zone and the shallow saturated zone. Tectonic information described earlier suggests that the water table began to fall from a higher stand in the volcanic section several million years ago. Local features of very low permeability contribute to the survival of uraninite and some sulfides in the Nopal Formation. The downward transition from rare to common sulfide preservation at around the 180-m depth in the Pozos Formation may mark the approximate stable position of a former water table. However, this depth also corresponds fairly well with a downward transition to lower-permeability rocks (Dobson et al., 2008, Table 1). Both factors could have restricted the interaction of rock sulfides with oxygenated water in what is now the deep unsaturated zone.

URANIUM-SERIES GEOCHEMISTRY OF NOPAL I GROUNDWATERS

Evidence of parent-daughter equilibrium or disequilibrium in the uranium-decay series, taken together with concentration data, can be used to characterize aspects of water-rock interaction and radionuclide transport in the subsurface. Specific applications may include the use of uranium concentration and $^{234}U/^{238}U$ values in groundwater to detect differences in uranium source rocks and seasonal variations in water-rock interaction.

The same data also may help identify mixing of multiple components and act as tracers for fluid-flow rates and flow paths.

Goldstein et al. (2016) studied uranium-series disequilibrium in groundwaters at Nopal I and nearby regional wells. Unsaturated-zone waters were sampled by a seepage-collection system installed in a mine adit about eight meters below the open-pit mine surface. Seepage waters were collected between 2000 and late 2006. The waters were analyzed for various chemical and isotopic suites, including total uranium, $^{234}U/^{238}U$, total thorium, ^{230}Th, and ^{226}Ra. The results and interpretations are briefly described here and examined for their implications about uranium transport to the saturated zone.

Seepage waters from the front of the adit, where the ore body is located, generally have $^{234}U/^{238}U$ activity ratios near unity (0.9 to 1.5) and uranium concentrations between 0.7 and 422 parts per billion (ppb; Goldstein et al., 2016, Table 3). These attributes result from dissolution of rock with a preponderance of uranium in secular equilibrium, as well as longer water-rock interaction times and interaction of water with uranium-rich rock. Spectral gamma-ray analyses of high-grade uranium ore from Nopal I confirm that uranium-series radionuclides high in the decay chain are close to secular equilibrium (French, Anthony, and Goodell, 2006). Samples from the rear of the adit, away from the ore body, have higher $^{234}U/^{238}U$ activity ratios ranging from 2.6 to 5.2 and variable, but mostly lower, uranium concentrations (0.1 to 14.9 ppb). These differences reflect preferential dissolution of recoil-related ^{234}U and uranium concentrations affected by varying fluid flux and/or water-rock interaction times. Seepage-water samples from the middle of the adit have $^{234}U/^{238}U$ activity ratios between 1.0 and 4.9 and uranium concentrations between 0.2 and 85.2 ppb, overlapping the values for the front and back of the adit. Stable-isotope data for seepage water samples show evidence of varying degrees of evaporation (Ghezzehei, 2007). Evaporation would have increased the concentrations of solutions but should not have affected uranium-isotopic systematics.

Uranium concentrations and isotopic ratios for shallow saturated-zone waters from Nopal I and regional wells are presented by Goldstein et al. (2016, Table 2). For most wells, samples were collected from 2003 (when the Nopal wells were drilled) to 2006. In general, uranium concentrations in the Nopal wells have exponentially decreased over time and are now close to undisturbed background values. Uranium concentrations during the last year of sampling (2005-2006) were between 23 and 61 ppb in PB1 and between 370 and 1077 ppb in PB3. Concentrations in the smaller sample set for PB2 are between 11.9 and 137.2 ppb. From 2003 to 2006, uranium varied between 0.1 and 15 ppb in PB4 and between 5.0 and 5.8 ppb at the Pozos Ranch well. Uranium in the well at Peña Blanca Ranch varied from 9.5 to 10.0 ppb between 2003 and 2005.

Activity ratios of $^{234}U/^{238}U$ for all analyzed PB1 and PB2 water samples are between 1.005 and 1.102 (Goldstein et al., 2016, Table 2). Ratios for PB3 are between 1.363 and 1.974. The activity-ratio data, uranium-concentration data, and hydrologic-testing results for the three wells (previously described) all indicate good connectivity between PB1 and PB2 and poor connectivity between these wells and PB3.

The data and implications of $^{234}U/^{238}U$ activity ratios for saturated-zone groundwater transport are discussed in the chapter on regional hydrology (Goodell et al., 2016). Here, we consider the significance of the data with respect to possible conceptual models of uranium transport in the unsaturated zone. Various alternative hypotheses are derived from basic principals of interpretation in Goldstein et al. (2016). The two or three most recent well-water analyses of PB waters, generally with lower uranium contents, are taken as representative of undisturbed conditions.

The near-unity $^{234}U/^{238}U$ activity ratios and uranium concentrations less than 100 ppb in the PB1 and PB2 groundwaters presumably were acquired by percolating water, like the front-adit seepage, that interacted with bedrock containing abundant uranium in secular equilibrium. Waters of this composition in principle could have traveled unmodified from the uraniferous source rock to the shallow saturated zone. However, considerable mixing could occur with minimal effect on the near-unity $^{234}U/^{238}U$ activity ratios if high-uranium waters (e.g., > 100 ppb) mix with low-uranium waters (e.g., < 10 ppb) of any observed activity ratio.

The seepage-composition data from the adit confirm that percolation in the shallow unsaturated zone is highly variable with regard to uranium content and $^{234}U/^{238}U$ activity ratios. Little can be inferred from the existing data about the relative abundances of different water types. On the scale of the cuesta as a whole, shallow percolation is more likely to have relatively low uranium concentrations and activity ratios in the range of about two to five, like seepage from the back of the adit, because the ore body occupies only a small part of the cuesta.

A basic unknown in unsaturated-zone transport at the Nopal cuesta is whether percolation that acquires its uranium-geochemical characteristics from the ore body is sufficient to maintain the distinctive isotopic signature of the shallow saturated-zone water beneath the cuesta. The only direct way to address this issue would be to collect water from the deeper unsaturated zone, which was beyond the scope of the current project. In the absence of direct data, the uraniferous Pozos Formation should be considered as an additional locus of substantial uranium exchange with percolating water. This unit underwent uranium enrichment that predates the uranium mineralization of the Nopal and Coloradas Formations and also contains evidence of uranium mineralization within the last million years. The distance from uranium-rich Pozos rock to the water table is about 30 m versus a minimum of about 95 m between uranium-enriched rock associated with the ore body and the water table. Gamma data for the three boreholes document lateral variability in the uranium content of the Pozos Formation, but it seems likely that much of the unit has some uranium enrichment and could interact with percolating water over a wide area. Comparison of the range in $^{234}U/^{238}U$ activity ratios for unsaturated-zone and saturated-zone ground waters suggest that saturated-zone and unsaturated-zone uranium sources are basically the same. The sources likely are a mixture of uranium from the Nopal ore deposit and uranium from other host rock.

RADIONUCLIDE TRANSPORT IN SOIL AT THE NOPAL CUESTA

The portion of the uranium ore body exposed at the surface of the Nopal cuesta has been subject to physical and chemical weathering for an unknown period of time. The surficial weathering environment has potential importance as a source of uranium transported into the unsaturated zone and as a natural analogue in its own right. Surficial weathering of mineralized rock potentially represents a distinct additional source of uranium introduced into the bedrock that might need to be factored into a fully realized conceptual model of subsurface transport. Certain aspects of this process also could be relevant analogues to extreme nuclear-waste release scenarios involving exposure or deposition of contaminated material on the ground surface. Examples could include volcanic disruption of a repository with pyroclastic deposition of contaminated ash or major erosion at a subsurface disposal site.

Most previous studies of radionuclide transport into soils were driven by dosimetry concerns. These studies generally incorporate conceptual models that surface radiation doses are attenuated as surface-deposited radioactive material moves deeper into the soil profile. Empirical mathematical models have been developed to quantify or at least bound the shielding effect of the soil over time as radionuclides decay and move downward in the soil. The goal of such studies is to estimate averaged values of radiation doses to guide mitigation efforts where doses are high. Results that are particularly relevant to the Nopal locale come from studies of soils around a former uranium mine in Spain (Vera Tomé, Blanco Rodríguez, and Lozano, 2002) and soils in the region of the Chernobyl accident (Likhtarev et al., 2002). A review paper by Anspaugh et al. (2002) provides background for the understanding of radionuclide migration in soils, again from a dosimetry perspective. These studies are discussed below in the context of the Nopal results.

At Nopal I, the original natural soil and substantial amounts of bedrock were removed during the mining operation and are not available for study. Residual evidence for infiltration of uranium from the former ground surface has not been definitively identified. One possible indicator of infiltration is an area on the +00 level where surface gamma intensities above background extend well beyond the area of visible uranium mineralization. This extension is most prominent along a SE-trend that corresponds to the assumed downslope direction of the pre-mining surface where the ore body was naturally exposed on the east-facing scarp of the cuesta. Tuff in the area of the higher gamma intensities is heavily weathered to mainly smectite and minor kaolinite, also suggesting an influence of surface-based chemical weathering (Pearcy, Prikryl, and Leslie, 1995, p. 696). Surficial alteration leading to the formation of uraniferous silica glazes on exposed rock surfaces at the Nopal cuesta is described by Schindler, Fayek, and Hawthorne (2010).

For this project, the concept was developed to study a site close to where blocks of high-grade uranium ore from the Nopal I mine were temporarily stored. The storage site, here called the Prior High Grade Stockpile, is located approximately 250 m west of the Nopal I mine. Blocks of high-grade ore were stockpiled here in the 1980s, while the mine was

active, and later moved to another location in the 1990s. Some of the ore blocks rolled down the gentle slope and were not removed. The ore blocks are located in an area where the soil is not known to have a uranium content above background. One ore block was selected as a site to study the migration of uranium and its daughters from a point source into the underlying soil over a period of about twenty-five years (French, Anthony, and Goodell, 2006). Two graduate students at the University of Texas at El Paso performed most of this research. The description of their studies reported here focuses on information that is not likely to change because some of the research was still in progress when this report was prepared.

In order to analyze the mobility of the radionuclides from the ore block into the soil, the block was removed and soil-samples suites were collected under and adjacent to the original block location. Soil samples of each suite were collected in one- to two-centimeter increments in eight successive intervals downward perpendicular to the ground surface. Three surface-soil samples away from the vicinity of ore blocks were collected to document background radioactivity values. A fragment of the ore block also was collected for analysis.

The samples were analyzed by gamma-ray spectroscopy so that individual radionuclide peaks from the ^{238}U-decay series could be identified. Fragments of ore rock larger than about one centimeter were manually removed from the shallow samples to prevent the ore from overwhelming the isotopic signature of the soil. Peak intensities for the three shallowest intervals of the sample suites were used to calculate daughter/parent activity ratios and evaluate the evidence of equilibrium or disequilibrium for the daughter/parent pairs. The three surface-soil samples collected for background evaluation had gamma intensities below the detection limit of the instrument.

Activities of radionuclides high in the decay series were plotted versus depth in the soil, curves were fitted to the data using the advection-dispersion equation, and values of the field distribution coefficient K_d were calculated. Descriptions of procedures and analyses are given by French, Anthony, and Goodell (2006), French (2006), and Pekar, Walton, and Goodell (2008). These studies did not determine a mass balance for the transfer of radionuclides from the ore block into the soil, and did not account for all surficial redistribution processes. The potential effects of aeolian transport and surface sheetflow were separately considered by Walton et al. (2005) and Velarde et al. (2007).

Gross-gamma counts on two soil-sample suites show the radioactivity generally decreasing with depth, to fairly constant low levels below six to seven centimeters (French, 2006, Figures 9 and 10). Individual samples were analyzed for spectral peaks of ^{234}Th, ^{234}Pa, ^{234}U, ^{230}Th, ^{226}Ra, ^{214}Pb, ^{214}Bi, and ^{210}Pb (French, 2006). The ore-block sample was relatively close to secular equilibrium for daughter/parent pairs ^{230}Th/^{234}U and ^{226}Ra/^{230}Th, with activity ratios of 1.222 and 1.206, respectively (French, 2006, calculated from Tables 14 and 16). A majority of the soil samples have non-equilibrium ^{230}Th/^{234}U activity ratios in the range of 1.80 to 2.18. The two shallowest samples from two soil suites have activity ratios between 1.18 and 1.50 (French, 2006, calculated from Tables 1, 10, and 14). These measurements may have been dominated by ore-block

fragments incorporated into the soil. All soil samples had non-equilibrium $^{226}Ra/^{230}Th$ activity ratios in the range of 1.70 to 2.71 (French, 2006, calculated from Tables 1, 7, and 14).

French (2006) proposed that thorium and uranium were introduced into the soil in particulates from the ore block (mechanical transport). The low solubility of thorium causes it to accumulate in the soil, whereas the more soluble uranium is leached from the soil, resulting in $^{230}Th/^{234}U$ activity ratios above unity in the shallow soil. French (2006) invoked preferential transport of radium from the ore block to the soil, presumably in solution, along with preferential uptake and retention of radium by plants, to account for the $^{226}Ra/^{230}Th$ activity ratios above unity. Data from a similar study at a uranium mine site in Spain also suggest that $^{230}Th/^{234}U$ activity ratios in soil may be affected by differential plant uptake (Vera Tomé, Blanco Rodríguez, and Lozano, 2002).

Gamma counting of the complete eight-interval suite from below the ore block indicates that background radiation levels are reached at depths of about 10 to 15 cm (Pekar, Walton, and Goodell, 2008, Figure 3). There is an exponential decrease in activity with depth for ^{234}Th, ^{234}U, ^{230}Th, and ^{226}Ra (radionuclides lower in the ^{238}U decay chain were measured but not used due to the presumed escape of gaseous ^{222}Rn). The location of the sampling area beneath the ore block protected it from either erosion or deposition during the 22-year residence period of the block.

Pekar, Walton, and Goodell (2008, Figure 3) fitted curves to the depth-activity data based on estimated transport parameters and using a standard advection-dispersion equation with radioactive decay and ingrowth as treated by van Genuchten (1985). The best fits were achieved by setting the advection term (velocity of water flow) to zero. By this means, dispersion coefficients were estimated. The dispersion coefficient ideally accounts for the combined effects of diffusion, physical dispersion, and other transport-related processes that are not explicitly identified. It remains to be seen whether this approach can be further developed. The advection-dispersion equation is based on assumptions of soil homogeneity and steady-state flow (van Genuchten, 1985, p. 129). Pekar, Walton, and Goodell (2008, p. 200-201) identified several conditions at the Nopal cuesta that depart from these assumptions. The arid climate and wet/dry precipitation cycles cause soil conditions to vary from no flow to downward flow following major precipitation to upward flow as the soil dries. Chemical inhomogeneities with depth in the soil may contribute to variable sorption of radionuclides. Bioturbation and plant uptake of radionuclides are additional processes that occur in a non-uniform way within the soil column.

Additional factors potentially relevant to transport in soils have been documented in previous studies. Selected results from two studies of radionuclide migration in soils near Chernobyl, Ukraine, and the Los Ratones uranium mine, Spain, are briefly summarized below. These studies help put the results and interpretations of the Nopal cuesta investigation in a larger context and identify ways in which the present work could be expanded.

Studies of radionuclide penetration into soil associated with the Chernobyl accident suggest that particulate size is an important factor influencing transport rates, although this has not been rigorously investigated (Likhtarev et al., 2002, p. 296-297). Faster vertical migration of ^{137}Cs into the soil was documented at farther distances from the Chernobyl Nuclear Power Plant relative to closer distances. The presumption here is that, other things being equal, finer particles should have traveled farther from the source. Once the particles are deposited on the ground surface, finer particles can more readily penetrate the soil because they are less likely to be blocked by small pores in the soil. A pattern of differential soil penetration with direction from the power plant was observed in a data set that included soil profiles west and south of the plant. Migration into the soil was relatively slower west of the plant, where particles created during the early explosive phase of the release were deposited. Faster migration into the soil occurred south of the plant, where particles formed during the later combustion phase of release were deposited. The differences in relative rates of downward migration would be consistent with larger particulates transported westward and finer particulates transported southward from the power plant.

At the location of the inactive Los Ratones uranium mine in Spain, radioactive material was deposited onto soils principally by the process of surface flow (Vera Tomé, Blanco Rodríguez, and Lozano, 2002, p. 44). Soil-sampling sites included areas that had received deposition of material from the mine and areas that were unaffected by surface flow from the mine. Four separate samples of the top 10 cm of soil were collected at each site. The population of samples from contaminated sites has values of $^{230}Th/^{234}U$ ranging from about 0.69 to 1.16 (estimated from Vera Tomé, Blanco Rodríguez, and Lozano, 2002, Figure 5), but the data collectively define a $^{230}Th/^{234}U$ trend slightly offset from unity in the direction of a relative excess of ^{234}U. Isotopic data for the unaffected soils have large relative uncertainties because of the low radionuclide abundances. The $^{230}Th/^{234}U$ activity ratios show greater departures from unity in both high and low directions. According to the authors, the contrast between contaminated and unaffected sites represents the difference between short-term processes affecting soils known to have received recent radioactive input and long-term processes, including uranium transport in solution, operating on the natural radioactive inventory of the soil.

The Chernobyl soil studies highlight the potential importance of contaminant-particulate size as a factor influencing transport rates into the soils. Particulate matter shed from the ore blocks onto the soil surface at the Nopal cuesta likely has a different and perhaps greater size range than the airborne Chernobyl particulates. Centimeter-size particulates, for example, may be trapped at the surface in the absence of major soil disturbances until they weather by chemical or physical means. Therefore, steady-state conditions may be attained in a manner more complex than by infiltration of fine particulates and solutes.

The $^{230}Th/^{234}U$ values from Los Ratones define statistically distinct daughter/parent trends for contaminated and uncontaminated sites. This is true even though individual samples within each suite might have daughter/parent activity ratios at, above, or below

unity. The relative effects of processes controlling the ratio must vary on a local scale, and this underscores the importance of using multiple measurements to define trends in the isotopic evolution of the soil system.

A review paper by Anspaugh et al. (2002, p. 677) provides a brief assessment and summary of research on vertical migration of radionuclides into soil. Measurements of radionuclides associated with atmospheric nuclear testing indicate soil penetration of at least five centimeters, with very slow transport to deeper levels. These findings are generally consistent with the Nopal cuesta studies reported here. Anspaugh et al. (2002, p. 677) cite studies suggesting that the process of vertical migration into soils is physical rather than chemical. The results of the Nopal study, like those of Vera Tomé, Blanco Rodríguez, and Lozano (2002), confirm that chemical processes are involved in soil transport. The relative importance of physical and chemical transport probably varies with time and the nature of the radioactive particulates deposited on the soil surface.

PERFORMANCE ASSESSMENT MODELING

The Peña Blanca Natural Analogue Project included a task to simulate radionuclide transport in groundwater beneath Nopal I. The simulation would have adapted Yucca Mountain Total System Performance Assessment (TSPA) models for this purpose. This task was not implemented, but a sequence of scoping studies of Nopal I was undertaken by the Yucca Mountain Project.

The concept of simulating radionuclide transport at Nopal I using a modified version of the software employed for Yucca Mountain TSPA was first realized in CRWMS M&O (2000, Appendix C). A numerical model was used to analyze the possible mobilization and groundwater transport of radionuclides potentially released from the Nopal I ore deposit. The goal of the investigation was to estimate whether further field investigations and groundwater sampling at the Nopal I site would provide a basis for a natural-analogue comparison of the Peña Blanca site with the expected performance of the Yucca Mountain site. The analysis would generate only corroborative information and would not provide input to the TSPA.

The numerical analysis was a scoping study utilizing as input a combination of Yucca Mountain process models and Nopal I site-specific data, supplemented by generic information about radionuclide behavior. Yucca Mountain process models, incorporated wholly or in part, included the uranium-oxide dissolution model and infiltration model. Site-specific data included the vertical section of rock units in the unsaturated zone, porosity and permeability data for rock units, the inferred eastward direction of regional groundwater flow, and the generalized dimensions of the ore body. Estimates of the uranium content of the original, preoxidized ore deposit and the inventory of uranium species and some daughter products were based on published studies. The performance-assessment model began with the assumption that the uranium oxide (uraninite) of the

original deposit is analogous to spent nuclear fuel. The primary uranium mineralization was assumed to have occurred about nine million years ago, and the simulation began approximately three million years ago when the deposit was exposed to oxidizing conditions.

The model simulated the processes of meteoric-water infiltration into the unsaturated zone, downward percolation and dissolution of the uraninite, fluid mixing in the unsaturated and saturated zones, and eastward transport in the saturated zone. Radionuclide concentrations were captured for the saturated zone at distances of 150, 600, and 1,300 m downgradient from the Nopal I ore body. The only corroborating data available at the time were water analyses for the mining-camp water-supply well (later renamed PB4) located 1,300 m SE of Nopal I.

A base-case analysis was run, along with sensitivity analyses to investigate the effects of reduced infiltration, variations in the solubility of the ore body, and variations in sorption coefficients. The study concluded that, even with strong sorption, uranium could be transported from the vicinity of Nopal I in amounts that would be detectable in PB4 water. The simulations also projected concentrations of ^{99}Tc in the groundwater derived predominantly from natural fission of ^{238}U (Curtis et al., 1999). Technetium, in the pertechnetate anion, behaves as a conservative non-sorbing species in water, unlike uranium. The model results suggested that ^{99}Tc concentrations would be very low, but analyzable (10^{-8} mg/L).

The model results indicated that uranium concentration at an observation point varies directly with the quantity of infiltration and the solubility of the ore body. In this context, solubility was taken to mean the combined effects of mineral solubility and changes in surface area available for dissolution. The analysis indicated that a groundwater-sampling program could provide data with which to estimate transport parameters for the Peña Blanca site and that, by analogy, these parameters could be useful corroboration for the performance assessment of the Yucca Mountain site. The report proposed an array of vertical boreholes to be drilled to the water table, including one borehole penetrating the ore body and additional boreholes upgradient and downgradient along the hydrologic flow path.

The numerical model was updated as the Peña Blanca Natural Analogue Model (PBNAM; Saulnier and Statham, 2006). The PBNAM adapted a Yucca Mountain performance-assessment model to simulate the release and transport of radionuclides from the Nopal I ore deposit. The results were calibrated to uranium concentrations reported for water samples from the shallow saturated zone in boreholes PB1, PB2, and PB3. The concentration data represent water samples collected in 2003 about six months after the wells were drilled.

Examples of model results presented in Saulnier and Statham (2006, p. 233) include a base-case simulation for ^{238}U transport for 100 realizations of the uncertain dissolution parameters, but not including sorption. The observed uranium concentrations in the well waters beneath the ore body are bracketed by the range of results obtained in the

simulations and within the uncertainty of the source-dissolution parameters. This result remains generally valid even with the trend of gradually diminishing uranium content, presumably to natural pre-drilling values, shown by more recent Nopal saturated-zone water samples (Goldstein et al., 2016, Figure 5). Recalibration of the model to the lower uranium values would improve the results. The updated PBNAM predicted a ^{99}Tc concentration of 2.8×10^{-5} mg/L in groundwater directly beneath the ore body (Saulnier and Statham, 2006, p. 233).

Useful lessons were learned in the process of collecting data specifically to support radionuclide-transport modeling. Most of these lessons led to better understanding of the limits on our ability to collect certain kinds of data. They are briefly summarized here.

Due to budgetary limitations, no dedicated wells were drilled to monitor water chemistry downgradient of Nopal I and planned tracer tests were not performed. The existence of additional monitoring wells close to Nopal I would have afforded us a greater likelihood of detecting a tracer plume and projecting its direction of travel in the subsurface. The very slight decrease in elevation of the static water level between Nopal I and PB4 (1240 masl at PB1 versus 1236 masl at PB4; Goodell et al., 2016) compounds the difficulty of predicting downgradient flow paths from beneath the ore body without close-in monitoring wells. Consequently, it was not possible to verify that the existing downgradient well PB-4 is in an optimal location to intersect a solute-tracer plume originating in groundwater passing beneath Nopal I.

After the PB wells were drilled at Nopal I, water from all three wells had elevated uranium concentrations that decreased with time (Goldstein et al., 2016). This provided an opportunity for an informal tracer test in which higher uranium concentrations might be detected in well PB4. However, the three-year record of water chemistry for PB4 contains no clear evidence for passage of water with elevated uranium content. Goldstein et al. (2016) used the record of declining uranium content at the Nopal I wells to calculate bounds on the rate of water movement. They estimated that the groundwater flow velocities in the Pozos Formation beneath the Nopal cuesta are in the range of 5 to 15 m/y. Flow velocities probably are low in the Cretaceous limestone that comprises most of the saturated-zone flow path to the east, so that a tracer plume could take hundreds of years to reach PB4.

PB4 also was not an optimal monitoring well because it experienced undocumented, but probably irregular, use during the study period. This was unavoidable because project personnel could not control access to the well. This situation, along with other unknown factors, contributed to the temporal variability of uranium concentrations measured in PB4 water samples. The variability in this well was notably higher than in the Pozos Ranch well (Goldstein et al., 2016, Figure 5). Therefore, it likely would have been difficult to conduct a formal tracer test using this well as the closest downgradient monitoring site even if the expected travel time were practical for such a test.

The results of the scoping simulation with respect to predicted ^{99}Tc concentrations suggested that it would be worthwhile to have Peña Blanca well waters analyzed for this radionuclide. Water samples from PB3 and the Pozos Ranch well were submitted for analysis by liquid scintillation counting. Aliquots from the two sources were analyzed at the Idaho State University Environmental Monitoring Laboratory and at the U.S. Department of Energy, Idaho Operations Office. Analytical results from the Environmental Monitoring Laboratory were inconclusive, possibly due to the presence of uranium, uranium progeny, or other alpha- and beta-emitting interferences. Attempts to remove the uranium using URAEX™ extractive solvent were unsuccessful because the solvent appeared to have an affinity for ^{99}Tc as well as for uranium (Dunker, 2006).

Initial analyses at the Idaho Operations Office appeared to detect ^{99}Tc in the PB3 water sample. Additional sets of water samples from the same sources were prepared in a variety of ways. The use of a hydrochloric-acid rinse to remove excessive molybdenum interference that had been observed during the initial analyses caused different interferences for analyses by liquid scintillation counting. The acid rinse caused residual amounts of ^{238}U and ^{234}U to remain in the anion exchange resin used to collect ^{99}Tc. Detectable ^{210}Po also was retained, verifying the presence of unwanted uranium progeny. No ^{99}Tc was observed above a detection limit of about 0.00006 parts per billion in optimally prepared water samples (Backstrom, 2006). As a result of these findings, no effort was made to incorporate *in-situ* generation and transport of ^{99}Tc into the performance assessment model.

DISCUSSION

The Peña Blanca Natural Analogue Project was conceived with the understanding that the natural-analogue site would not be characterized as fully as a potential waste-repository site. However, there was an underlying assumption that the analogue-site attributes were sufficiently simple and adequately documented to support the present study. Project results would be used to develop a conceptual model and numerical simulation of radionuclide transport from an ore body in the unsaturated zone as an analogue to transport from radioactive-waste packages in a geologic repository at Yucca Mountain.

The scaled-back studies reported here and in accompanying articles provide key information about the Nopal site. Three boreholes were drilled to the water table, and geophysical logs were collected. A seepage-collection system was installed in the shallow unsaturated zone. Variations in saturated- and unsaturated-zone water compositions were recorded over a period of several years. Geochronologic studies established the age of primary uranium mineralization in the volcanic section and provided preliminary indications about the timing, locations, and geochemical conditions of subsequent uranium-mineral deposition. We have used all these contributions to refine the conceptual model of uranium transport at the analogue site. The model itself is not complete, but the new data helped us identify the most important information still to be collected.

At the beginning of this study, the prevailing conceptual model for the onset of uranium migration at Peña Blanca was that the Nopal I uranium deposit remained largely intact under reducing conditions in the saturated zone until about three million years ago. The site then was uplifted into the unsaturated zone, and uranium began to be transported away from the primary deposit under oxidizing conditions. Our results, and the results of other studies, generally are compatible with this concept. However, our mineralogic and geochronologic studies indicate that, after three million years, the rock units have not fully equilibrated with the mostly oxidizing environment. Sulfide minerals and primary uraninite survive in less permeable rocks. Secondary uraninite up to about 1.6 million years old is present in both the deep and shallow unsaturated zone, attesting to the persistence of local reducing conditions. These results show that the time spent in geochemical transition is not negligible compared to time spans of regulatory interest for nuclear-waste repositories. A fully developed numerical simulation of radionuclide migration at Nopal I during the last three million years would have to incorporate the gradual transition from reducing to oxidizing conditions.

The starting conceptual model of uranium migration, supported by preliminary numerical modeling, begins with the dissolution of uranium in the Nopal I ore body by downward-percolating water. The uranium experiences some sorption in the unsaturated zone, but a sufficient amount arrives at the water table to form a detectable plume in the shallow saturated zone. This model is based on an assumption that no other significant uranium sources exist along the flow paths. Our preliminary observations of high uranium content and the presence of uraninite less than one million years old in parts of the Pozos Formation suggest that this unit may play a more complex role in water-rock interaction in the deep unsaturated zone. Additional work will be required to document the history of uranium transport. Important alteration processes in the Pozos Formation could include the incorporation of uranium during early diagenesis, gain or loss of uranium during the mineralization event that created the Nopal I ore body, gain or loss of uranium during subsequent mineralization, and gain or loss of uranium during the transition from saturated reducing conditions to unsaturated oxidizing conditions. Has the Pozos formation served as both a sink for aqueous uranium derived from the ore body and as a source of uranium for downward-percolating water? What are the relative contributions of the Pozos Formation and the Nopal I ore body to the radionuclide composition of the shallow saturated-zone water beneath the Nopal cuesta?

This project provided compositional data for shallow unsaturated-zone infiltration close to the ore body and shallow saturated-zone groundwater. Collection of core throughout the unsaturated zone for water extraction is the only way to document direct evidence of water-rock interaction in the Pozos and other subsurface formations, but it would be a very expensive operation. Useful information could be obtained by sampling and analyzing the Pozos Formation in outcrop and small-scale cores. The analyses would document variations in uranium content and isotopic systematics supporting an assessment of the potential contributions from this formation to the uranium budget of the unsaturated zone. Laboratory experiments could place bounds on the amount of leachable uranium in Pozos rocks. Detailed chemical and mineralogical studies of the Pozos rocks might identify additional geochemical signatures of this unit that are

different from the ore body and that could be detected in the saturated-zone water. Studies of this kind might lead to a narrowing of hypotheses sufficient to formulate conceptual and numerical models that address the identified issues.

This project attempted to cross the research divide between earlier surface-derived sample studies centered on the ore deposit and studies that would interrogate the hydrologic and geochemical systems in the subsurface beneath and beyond the Nopal cuesta. Some success was achieved toward this goal, as described above. We were unable to conduct tracer studies between the Nopal wells and PB-4. Scaled-back funding was the direct reason for this, but our experiences showed that logistics and infrastructure issues would have made field-testing very difficult. Neither we nor any other research entity had physical control of the site, and we were unable to control or monitor access to the wells by non-researchers. These issues would have to be addressed should opportunities for hydrologic testing arise in the future.

Information gained in this project and answers to the questions posed above will help determine the best use of the Nopal I site as a natural analogue for subsurface transport of nuclear waste or other radioactive byproducts. The preliminary performance-assessment modeling of UZ transport could be confirmed or modified based on additional research. A more comprehensive characterization of the alteration history holds promise for other natural-analogue applications. In particular, it would be worthwhile to more thoroughly document the early history of the ore body as an analogue to nuclear-waste emplacement in the saturated zone. Alteration research already accomplished would then form the foundation for studies of the potential effects of a declining water table on a repository originally in the saturated zone.

CONCLUSIONS

The Peña Blanca Natural Analogue Project supported the drilling of three boreholes – PB1, PB2, and PB3 – to the water table and the installation of a seepage-collection system at the Nopal I uranium ore body in Chihuahua, México. Water, core, outcrop, and soil samples from the site have been collected and studied. Our studies have reached the stage of allowing us to express potential alternative hypotheses about the roles of the Nopal I uranium ore body and the uraniferous Pozos Formation in unsaturated-zone uranium transport. This information provides the basis for the conceptual model of Nopal I as a natural analogue for subsurface uranium transport from an underground radioactive-waste repository in the unsaturated zone. The project originally was conceived as a natural analogue for Yucca Mountain, Nevada.

The first direct dating of uranium minerals from the Nopal I ore body and underlying Pozos Formation established an age of 32±8 million years for the primary uranium mineralization. Alteration and uranium-mineral deposition at 3.1±0.5 million years may mark the beginning of a transition from a reducing environment under saturated

conditions to an oxidizing environment under unsaturated conditions. The presence of residual sulfides within the uranium ore body and in the lower Pozos Formation, as well as the occurrence of 1.6±0.5 ma uraninite in the ore body, indicates that the transition from reducing to oxidizing conditions has been a long process that still is not complete.

Borehole gamma logs and fluorescence studies define highly uraniferous zones in the Nopal-Coloradas ore body and in parts of the Pozos Formation. The timing of initial uranium enrichment in the Pozos may date from a period of early diagenesis. Authigenic uraninite less than one million years old in the Pozos documents more recent water-rock interaction involving the redistribution of uranium. Most of the uranium redistribution in the UZ appears to have diminished prior to about 200 ka. The possibility that the Pozos Formation has served as both a sink and source for uranium complicates the original conceptual model of uranium transport downward from the Nopal ore body through the unsaturated zone to the water table.

Water samples were collected from a shallow underground seepage-collection system and from the wells in the shallow saturated zone. In the unsaturated zone, seasonal and lateral variations in the uranium content and $^{234}U/^{238}U$ activity ratios result from differences in uranium content of the rock, fluid flux, and water-rock interaction times. Activity ratios near unity result from dissolution of rock with a preponderance of uranium in secular equilibrium, as well as longer water-rock interaction times and interaction of water with uranium-rich rock. Seepage waters from less uranium-rich rock have activity ratios from 2.6 to 5.2, which may be more representative of shallow unsaturated-zone waters at the Nopal cuesta.

Uranium-concentration data and the results of pump tests both indicate that shallow saturated-zone waters at PB3 are somewhat isolated from the waters at PB1 and PB2. All shallow saturated-zone waters have activity ratios close to unity. Derivation of the saturated-zone uranium predominantly from the Nopal ore body could occur if highly uraniferous waters from the ore body, with near-unity activity ratios, mix only with waters of much lower uranium content in the unsaturated zone. An alternate hypothesis, that uranium in the shallow saturated zone is derived in part from the Pozos Formation below the ore body, could be evaluated only with additional study. These two hypotheses have very different implications for the conceptual model of uranium transport in the unsaturated zone.

Studies were conducted of uranium-series radionuclide migration from a block of high-grade uranium ore into underlying undisturbed soil. The block had been in place for a period of about twenty-two years. Radionuclides were found to have penetrated to depths of about 10 to 15 cm. The finding of non-equilibrium parent-daughter radioisotope activity ratios suggests that preferential aqueous transport of uranium and radium has occurred.

Numerical simulations of aqueous uranium transport from the Nopal I ore body downward through the unsaturated zone and eastward within the shallow saturated zone were conducted as scoping studies early in the project. The study concluded that, even

with strong sorption, uranium could be transported from the vicinity of Nopal I in amounts that would be detectable at well PB4 1,300 m downgradient from the assumed source. Recommended tracer tests could not be performed under the later reduced scope of the project. There was a possibility that the artificially high uranium concentrations generated during the Nopal drilling operations might serve as natural tracers, but so far nothing unusual has been detected at PB4. The utility of PB4 as a monitoring well was less than optimal because the project could not control access to the well.

Information from this study and other sources indicates that the ore-body host rock and underlying uraniferous units had a long and complex alteration history in the saturated zone before beginning the hydrologic and geochemical transition to unsaturated conditions perhaps three million years ago. In this sense, the Nopal I site may be a relevant analogue for nuclear-waste disposal in the saturated zone and for multi-million-year changes culminating in unsaturated, oxidizing conditions. These studies should be relevant as well for other environmental issues of subsurface radionuclide transport.

ACKNOWLEDGMENTS

We would like to thank our colleagues at the Autonomous University of Chihuahua, particularly Professors Victor Reyes and Lourdes Villalba. Our thanks also to Mabel Amador for Spanish translation and facilitating communication with our colleagues in México. John Dinsmoor led the field effort for our main 2006 site visit, and Alan Mitchell helped with the planning of earlier site visits. Frances Knudson was instrumental in the final assembly and submission of this report.

Abraham van Luik of the United States Department of Energy, Office of Civilian Radioactive Waste Management (U.S. DOE, OCRWM), provided oversight and review of this project. Ardyth Simmons guided the project through its important early stages, including the drilling at Nopal I. Kenneth Rehfeldt found ways to help us bring the project to completion. This project was funded by the U.S. DOE, OCRWM under contract DE-AC02-05CH11231. The views expressed in this article are those of the authors and do not necessarily reflect the views or policies of the U.S. DOE or OCRWM.

REFERENCES

A. Abdel-Fattah, S. Goldstein, S. Tarimala, and S. Levy, “Colloid-Size Characterization for the Peña Blanca Natural Analogue Project,” in “Final Report for the Peña Blanca Natural Analogue Project,” S. Levy, compiler, Los Alamos National Laboratory report XXXXX (2016).

L. Alba and R. Chavez, “K-Ar ages of volcanic rocks from central Sierra Peña Blanca, Chihuahua, Mexico,” *Isochron West* **10**, 21-23 (1974).

T. Allard and J.-P. Muller, “Kaolinite as an *in situ* dosimeter for past radionuclide migration at the Earth’s surface,” *Applied Geochemistry* **13**, 751-765 (1998).

L. R. Anspaugh, S. L. Simon, K. I. Gordeev, I. A. Likhtarev, R. M. Maxwell, and S. M. Shinkarev, "Movement of Radionuclides in Terrestrial Ecosystems by Physical Processes," *Health Physics* **82**, 669-679 (2002).

G. Backstrom, U.S. Department of Energy, Idaho Operations Office, personal communication, December 2006.

D. C. Buesch, R. W. Spengler, T. C. Moyer, and J. K. Geslin, "Proposed Stratigraphic Nomenclature and Macroscopic Identification of Lithostratigraphic Units of the Paintbrush Group Exposed at Yucca Mountain, Nevada," U.S. Geological Survey Open-File Report 94-469 (1996).

G. L. Booman and J. E. Rein, "Uranium," in *Treatise on Analytical Chemistry*, I. M. Kolthoff and P. J. Elving, Eds., (John Wiley & Sons, New York, New York, 1962), Part II, Volume 9, Section A, pp. 1-188.

G. Calas, P. Agrinier, T. Allard, and P. Ildefonse, "Alteration geochemistry of the Nopal I uranium deposit (Sierra Peña Blanca, Mexico), a natural analogue for a radioactive waste repository in volcanic tuffs," *Terra Nova* **20**, 206-212 (2008).

S. Connell, J. Hawley, and D. Love, "Late Cenozoic Drainage Development in the Southeastern Basin and Range of New Mexico, Southeasternmost Arizona, and Western Texas," in *New Mexico's Ice Ages*, S. Lucas, G. Morgan, and K. Ziegler, Eds., New Mexico Museum of Natural History and Science Bulletin No. 28, pp. 125-150 (available URL: http://econtent.unm.edu/cdm4/document.php?CISOROOT=/bulletins&CISOPTR=493&REC=8), 2005.

D. L. Cowan, V. Priest, and S. S. Levy, "ESR Dating of Quartz From Exile Hill, Nevada," *Applied Radiation and Isotopes* **44**, 1035-1039 (1993).

Civilian Radioactive Waste Management System Management & Operating Contractor (CRWMS M&O), "Total System Performance Assessment for the Site Recommendation," CRWMS M&O report TDR-WIS-PA-000001 REV 00 ICN 01 (available URL: https://www.researchgate.net/publication/263542706_Total_System_Performance_Assessment_for_the_Site_Recommendation), 2000.

CRWMS M&O, "Natural Analogue Synthesis Report," CRWMS M&O report TDR-NBS-GS-000027 REV01 (available URL: www.osti.gov/scitech/servlets/purl/883016), 2004.

D. Curtis, J. Fabryka-Martin, P. Dixon, and J. Cramer, "Nature's uncommon elements: Plutonium and technetium," *Geochimica et Cosmochimica Acta* **63**, 275-285 (1999).

J.S. Denton, S.J. Goldstein, P. Paviet, A.J. Nunn, R.S. Amato, and K.A. Hinrichs, "A record of uranium-series transport at Nopal I, Sierra Peña Blanca, Mexico: Implications for natural uranium deposits and radioactive waste repositories," *Chemical Geology* **434**, 12-27 (2016).

P. F. Dobson, M. Fayek, P. C. Goodell, T. A. Ghezzehei, F. Melchor, M. T. Murrell, R. Oliver, I. A. Reyes-Cortés, R. de la Garza, and A. Simmons, "Stratigraphy of the PB-1 Well, Nopal I Uranium Deposit, Sierra Peña Blanca, Chihuahua, Mexico," *International Geology Review* **50**, 959-974 (2008b).

P. F. Dobson, T. A. Ghezzehei, P. J. Cook, J. A. Rodríguez-Pineda, L. Villalba, and R. De la Garza, "Heterogeneous seepage at the Nopal I natural analogue site, Chihuahua, Mexico," *Hydrogeology Journal* **20**, 155-166 (2012).

R. E. Dunker, "Idaho State University Environmental Monitoring Laboratory, Case Narrative, Technetium-99" in Notebook OSTI-LBNL-PD-1, pp. 120-122 (available URL: https://adamspublic.nrc.gov/navigator/, LSN accession number DN2002462778), 2006.

M. Fayek, M. Ren, P. Goodell, P. Dobson, A. Saucedo, A. Kelts, S. Utsunomiya, R. Ewing, L. Riciputi, and I. Reyes, "Paragenesis and Geochronology of the Nopal I Uranium Deposit, Mexico," *Proceedings of the 11th International High-Level Radioactive Waste Management Conference, April 30-May 4, 2006, Las Vegas, Nevada* (American Nuclear Society, La Grange Park, Illinois, 2006), pp. 55-62.

Fluorescent Mineral Society, "Fluorescent Minerals," (available URL: http://www.uvminerals.org/minerals.htm), 1992-2004.

D. C. French, "Gamma-Ray Characterization of the U-Series Intermediate Daughters from Soil Samples at the Peña Blanca Natural Analog, Chihuahua, Mexico," M. Sc. thesis, Department of Geological Sciences, The University of Texas at El Paso (2006).

D. French, E. Anthony, and P. Goodell, "U-Series Disequilibrium in Soils, Peña Blanca Natural Analog, Chihuahua, Mexico," *Proceedings of the 11th International High-Level Radioactive Waste Management Conference, April 30-May 4, 2006, Las Vegas, Nevada*, (American Nuclear Society, La Grange Park, Illinois, 2006), pp. 63-69.

L. Fu, K. L. Milliken, and J. M. Sharp, Jr., "Porosity and permeability variations in fractured and liesegang-banded Breathitt sandstones (Middle Pennsylvanian), eastern Kentucky: diagenetic controls and implications for modeling dual-porosity systems," *Journal of Hydrology* **154**, 351-381 (1994).

F. Garay Jiménez, "Registro Geofísico Pozo UCMX-NA-PB1; Registro Geofisico Pozo UCMX-NA-PB2; Registro Geofisico Pozo UCMX-NA-PB3; Registro Geofisico Pozo UCMX-NA-PB4," Compamento El Nopal, para la Universidad de Chihuahua (Geophysical Logs inWells PB1, PB2, PB3, and PB4 located in the Nopal Field, for the University of Chihuahua)," Comision Federal de Electricidad, in Binder YMP-LBNL-

PD-2A, pp. 121-274 (available URL: https://adamspublic.nrc.gov/navigator/, LSN accession number DN2001644400), 2003.

J. E. García Ramírez, "Present Issues in the National Waste Management Program for Mexico," in *Geological Challenges in Radioactive Waste Isolation: Fourth Worldwide Review*, Lawrence Berkeley National Laboratory report LBNL-59808 (2006), pp. 155-158.

B. George-Aniel, J. Leroy, and B. Poty, "Uranium Deposits of the Sierra Peña Blanca," in *Uranium Deposits in Volcanic Rocks, Proceedings of a Technical Committee Meeting on Uranium Deposits in Volcanic Rocks Organized by the International Atomic Energy Agency and Held in El Paso, Texas, 2-5 April 1984* (International Atomic Energy Agency, Vienna, Austria, 1985), pp. 175-186.

T. A. Ghezzehei, Lawrence Berkeley National Laboratory, personal communication, May 2007.

T. A. Ghezzehei, P. F. Dobson, J. A. Rodriguez, and P. J. Cook, "Infiltration and Seepage through Fractured Welded Tuff," in *Proceedings of the 11th International High-Level Radioactive Waste Management Conference, Las Vegas, Nevada, April 30-May 4, 2006* (American Nuclear Society, La Grange Park, Illinois, 2006), pp. 105-110.

S. J. Goldstein, A. I. Abdel-Fattah, M. T. Murrell, P. F. Dobson, D. E. Norman, R. S. Amato, and A. J. Nunn, "Uranium-Series Constraints on Radionuclide Transport and Groundwater Flow at the Nopal I Uranium Deposit, Sierra Peña Blanca, Mexico," *Environmental Science and Technology* **44**, 1579-1586 (2010).

S. J. Goldstein, A. I. Abdel-Fattah, M. T. Murrell, P. F. Dobson, D. E. Norman, R. S. Amato, and A. J. Nunn, "Uranium-Series Constraints on Radionuclide Transport and Groundwater Flow at the Nopal I Uranium Deposit, Sierra Peña Blanca, México," in "Final Report for the Peña Blanca Natural Analogue Project," S. Levy, compiler, Los Alamos National Laboratory report XXXXX (2016).

P. Goodell, "Geology of the Peña Blanca Uranium Deposits, Chihuahua, Mexico," in *Uranium In Volcanic and Volcaniclastic Rocks, AAPG Studies In Geology No. 13, Papers from the symposium on Uranium in volcaniclastic rocks, conducted at the Annual Meeting of the Southwest Section of The American Association of Petroleum Geologists, El Paso, Texas* (American Association of Petroleum Geologists, Tulsa, Oklahoma, 1981), pp. 275-291.

P. C. Goodell, "Chihuahua City Uranium Province, Chihuahua, Mexico," in *Uranium Deposits in Volcanic Rocks, Proceedings of a Technical Committee Meeting on Uranium Deposits in Volcanic Rocks Organized by the International Atomic Energy Agency and Held in El Paso, Texas, 2-5 April 1984* (International Atomic Energy Agency, Vienna, Austria, 1985), pp. 97-124.

P. Goodell, M. Fayek, M. Murrell, P. Dobson, and R. Oliver, "Descriptions of core samples from PB-1 well (based on transcribed notes)," in Binder YMP-LBNL-PD-2A, pp. 18-81, P. Dobson, compiler (available URL: https://adamspublic.nrc.gov/navigator, LSN accession number DN200164400) 2003.

P. Goodell, J. A. Rodríguez Pineda, P. Dobson, S. Harder, and S. Levy, "Regional Hydrology and Uranium Occurrences around Nopal I," in "Final Report for the Peña Blanca Natural Analogue Project," S. Levy, compiler, Los Alamos National Laboratory report------ (2016).

J. W. Handschy and R. Dyer, "Polyphase deformation in Sierra del Cuervo, Chihuahua, Mexico: Evidence for Ancestral Rocky Mountain tectonics in the Ouachita foreland of northern Mexico," *Geological Society of America Bulletin* **99**, 618-632 (1987).

S. Harder, "Differential GPS results," in Notebook OSTI-LBNL-PD-1, p. 23 (available URL: https://adamspublic.nrc.gov/navigator/, LSN accession number MOL200708100045), 2006.

C. Henry and J. Aranda-Gomez, "Plate interactions control middle-late Miocene, proto-Gulf and Basin and Range extension in the southern Basin and Range," *Tectonophysics* **318**, 1-26 (2000).

Instituto Nacional de Estadística Geografía Informática, *Carta Topográfica 1:50 000 El Sauz, H13C46, Chihuahua* (2004).

T.-L. Ku and S. Luo, "Natural Analogue Studies at Peña Blanca, México: Uranium-Series Radioisotope Measurements," in "Final Report for the Peña Blanca Natural Analogue Project," S. Levy, compiler, Los Alamos National Laboratory report xxxx (2016).

T. L. Ku, S. Luo, S. J. Goldstein, M. T. Murrell, W. L. Chu, and P. F. Dobson, "Modeling non-steady state radioisotope transport in the vadose zone – A case study using uranium isotopes at Peña Blanca, Mexico," *Geochimica et Cosmochimica Acta* **73**, 6052-6064 (2009).

R. Langford, M. Jackson, and M. Whitelaw, "The Miocene to Pleistocene filling of a mature extensional basin in Trans-Pecos Texas: geomorphic and hydrologic controls on deposition," *Sedimentary Geology* **128**, 131-153 (1999).

S. Levy, "Studies of Altered Vitrophyre for the Prediction of Nuclear Waste Repository-Induced Thermal Alteration at Yucca Mountain, Nevada," in *Scientific Basis for Nuclear Waste Management VII, Materials Research Society Symposia Proceedings* (Materials Research Society, Pittsburgh, Pennsylvania, 1984), Vol. 26, pp. 959-966.

S. Levy, and G. Valentine, "Natural Alteration in the Cooling Topopah Spring Tuff, Yucca Mountain, Nevada, as an Analog to a Waste-Repository Hydrothermal Regime,"

in *Proceedings of the Topical Meeting on Site Characterization and Model Validation, Focus '93, September 26-29, 1993, Las Vegas, Nevada* (American Nuclear Society, Inc, La Grange Park, Illinois, 1993), pp.145-149.

S. Levy, S. Chipera, G. WoldeGabriel, J. Fabryka-Martin, and D. Sweetkind, "Flow-Path Textures and Mineralogy in Tuffs of the Unsaturated Zone," in *Faults and Subsurface Fluid Flow in the Shallow Crust* (American Geophysical Union, Washington, DC, 1999) Geophysical Monograph 113, pp. 159-184.

I. A. Likhtarev, L. N. Kovgan, P. Jacob, and L. R. Anspaugh, "Chernobyl Accident: Retrospective and Prospective Estimates of External Dose of the Population of Ukraine," *Health Physics* **82**, 290-303 (2002).

J. Luhr, C. Henry, T. Housh, J. Aranda-Gómez, and W. McIntosh, "Early extension and associated mafic alkalic volcanism from the southern Basin and Range Province: Geology and petrology of the Rodeo and Nazas volcanic fields, Durango, México," *Geological Society of America Bulletin* **113**, 760-773 (2001).

M. Machette, S. Personius, K. Kelson, R. Dart, and K. Haller, "Map and data for Quaternary faults and folds in New Mexico," U.S. Geological Survey Open-File Report 98-521 (2000).

E. F. McBride, "Pseudofaults resulting from compartmentalized Liesegang bands: update," *Sedimentology* **50**, 725-730 (2003).

F. McDowell, "Timing of Intense Magmatic Episodes in the Northern Sierra Madre Occidental, Mexico," *Geological Society of America Abstracts with Programs* **39**(6), 391 (2007).

F. McDowell, and R. Mauger, "K-Ar and U-Pb zircon chronology of Late Cretaceous and Tertiary magmatism in central Chihuahua State, Mexico," *Geological Society of America Bulletin* **106**, 118-132 (1994).

F. A. Melchor Pérez, "Petrographic Analysis," in Binder YMP-LBNL-PD-2A, pp. 369-467, P. Dobson, compiler (available URL: https://adamspublic.nrc.gov/navigator, LSN accession number DN2001644400), 2003-2004.

P. Michard, E. Guibal, T. Vincent, and P. Le Cloirec, "Sorption and desorption of uranyl ions by silica gel: pH, particle size and porosity effects," *Microporous Materials* **5**, 309-324 (1996).

J.-P. Muller, P. Ildefonse, and G. Calas, "Paramagnetic Defect Centers in Hydrothermal Kaolinite from an Altered Tuff in the Nopal Uranium Deposit, Chihuahua, Mexico," *Clays and Clay Minerals* **38**, 600-608 (1990).

W. M. Murphy, and R. B. Codell, "Alternate Source Term Models for Yucca Mountain Performance Assessment based on Natural Analog Data and Secondary Mineral Solubility," in *Scientific Basis for Nuclear Waste Management XXII, Materials Research Society Symposium Proceedings* (Materials Research Society, Pittsburgh, Pennsylvania, 1999), Vol. 556, pp. 551-559.

M. T. Murrell, S. J. Goldstein, and P. R. Dixon, "Uranium Decay Series Mobility at Peña Blanca, Mexico: Implications for Nuclear Repository Stability," in *Eighth EC Natural Analogue Working Group Meeting, Proceedings of an International Workshop held in Strasbourg, France, from 23 to 25 March 1999*, H. von Maravic and W. R. Alexander, Eds. (Office for Official Publications of the European Communities, Luxembourg, Luxembourg, 2002), pp. 339-347.

L. A. Neymark, Y. Amelin, J. B. Paces, and Z. E. Peterman, "U-Pb ages of secondary silica at Yucca Mountain, Nevada: implications for the paleohydrology of the unsaturated zone," *Applied Geochemistry* **17**, 709-734 (2002).

R. Oliver, "PB Well Conditioning – Draft Field Notes" (available URL: https://adamspublic.nrc.gov/navigator/, LSN accession number DN2000515697, 2004.

R. D. Oliver, J. C. Dinsmoor, S. J. Goldstein, I. A. Reyes-Cortés, and R. De La Garza, "Initial Test Well Conditioning at Nopal I Uranium Deposit, Sierra Peña Blanca, Chihuahua, Mexico," *Geological Society of America Annual Meeting & Exposition Abstracts with Programs* **37** (7), 197 (2005).

J. Osmond and M. Ivanovich, "Uranium-Series Mobilization and Surface Hydrology," in *Uranium-Series Disequilibrium: Applications to Earth, Marine, and Environmental Sciences, second edition*, M Ivanovich and R. Harmon, Eds. (Oxford University Press, New York, New York, 1992), pp. 259-289.

J. B. Paces, L. A. Neymark, B. D. Marshall, J. F. Whelan, and Z. E. Peterman, "Ages and Origins of Calcite and Opal in the Exploratory Studies Facility Tunnel, Yucca Mountain, Nevada," U.S. Geological Survey Water-Resources Investigations Report 01-4049 (2001).

E. C. Pearcy, "Fracture Transport of Uranium at the Nopal I Natural Analog Site," Center for Nuclear Waste Regulatory Analyses Report CNWRA 94-011 (1994).

E. C. Pearcy, J. D. Prikryl, W. M. Murphy, and B. W. Leslie, "Uranium Mineralogy of the Nopal I Natural Analog Site, Chihuahua, Mexico," Center for Nuclear Waste Regulatory Analyses report CNWRA 93-012 (1993).

E. C. Pearcy, J. D. Prikryl, and B. W. Leslie, "Uranium transport through fractured silicic tuff and relative retention in areas with distinct fracture characteristics," *Applied Geochemistry* **10**, 685-704 (1995).

E. C. Pearcy, J. D. Prikryl, W. M. Murphy, and B. W. Leslie, "Alteration of uraninite from the Nopal I deposit, Peña Blanca District, Chihuahua, Mexico, compared to degradation of spent nuclear fuel in the proposed U.S. high-level nuclear waste repository at Yucca Mountain, Nevada," *Applied Geochemistry* **9**, 713-732 (1994).

K. Pekar, J. Walton, and P. Goodell, "Modeling of Transport Rates Through Unsaturated Soil at Peña Blanca," in *Proceedings of the 12th International High-Level Radioactive Waste Management Conference, September 7-11, 2008, Las Vegas, Nevada* (American Nuclear Society, La Grange Park, Illinois, 2008), pp. 196-203.

D. A. Pickett and W. M. Murphy, "Unsaturated Zone Waters from the Nopal I Natural Analog, Chihuahua, Mexico – Implications for Radionuclide Mobility at Yucca Mountain," in *Scientific Basis for Nuclear Waste Management XXII, Materials Research Society Symposium Proceedings* (Materials Research Society, Pittsburgh, Pennsylvania, 1999), Vol. 556, pp. 809-816.

D. A. Pickett, J. D. Prikryl, B. W. Leslie, and E. C. Pearcy, "Radionuclide Mobility at the Nopal I Natural Analog," prepared for U.S. Nuclear Regulatory Commission Contract No. NRC-02-07-006 (available URL: adams.nrc.gov/wba, ADAMS accession number ML112720140), 2011.

D. A. Pickett, J. D. Prikryl, and E. C. Pearcy, "Geochemical Natural Analog Research," in "NRC High-Level Radioactive Waste Research at CNWRA July-December 1995," Center for Nuclear Waste Regulatory Analyses Report CNWRA 95-02S, pp. 2-1 to 2-21 (available URL: http://www.nrc.gov/reading-rm/adams.html, ADAMS accession number ML040230584), 1996.

J. Price and C. Henry, "Stress orientations during Oligocene volcanism in Trans-Pecos Texas: Timing the transition from Laramide compression to Basin and Range tension," *Geology* **12**, 238-241 (1984).

J. D. Prikryl, D. A. Pickett, and E. C. Pearcy, "Geochemical Natural Analog Research," in "NRC High-Level Radioactive Waste Research at CNWRA January-June 1995," Center for Nuclear Waste Regulatory Analyses report CNWRA 95-01S, pp. 2-1 to 2-26 (available URL: http://www.nrc.gov/reading-rm/adams.html, ADAMS accession number ML040220368), 1995.

J. D. Prikryl, D. A. Pickett, W. M. Murphy, and E. C. Pearcy, "Migration behavior of naturally occurring radionuclides at the Nopal I uranium deposit, Chihuahua, Mexico," *Journal of Contaminant Hydrology* **26**, 61-69 (1997).

M. Rearick, P. Dobson, S. Goldstein, J. Rodríguez, and S. Levy, "Groundwater Analyses for Nopal I and the Peña Blanca Region, Chihuahua, México," in "Final Report for the Peña Blanca Natural Analogue Project," S. Levy, compiler, Los Alamos National Laboratory report LAxxxxxxx (2016).

I. Reyes-Cortés, "Geologic Studies in the Sierra de Peña Blanca, Chihuahua, México," Ph.D. Thesis, Department of Geological Sciences, The University of Texas at El Paso (1997).

I. Reyes-Cortés, "Geologic Setting and Mineralisation: Sierra Peña Blanca, Chihuahua, México," in *Eighth EC Natural Analogue Working Group Meeting, Proceedings of an International Workshop held in Strasbourg, France from 23 to 25 March 1999*, H. von Maravic and W. Alexander, Eds. (Office for Official Publications of the European Communities, Luxembourg, Luxembourg, 2002), pp. 321-331.

R. Rodriguez Torres, R. Yza Dominguez, R. Chavez Aguirre, and S. Constantino, "Rocas Volcanicas Acidas y su Potencial como Objectivos para Prospectar Uranio," in *Exploration for Uranium Ore Deposits, Proceedings of a Symposium on Exploration of Uranium Ore Deposits Organized by the International Atomic Energy Agency and the OECD Nuclear Energy Agency and held in Vienna, 29 March-2 April 1976.* (International Atomic Energy Agency, Vienna, Austria, 1976) pp. 601-623.

G. J. Saulnier, Jr and W. Statham, "The Peña Blanca Natural Analogue Performance Assessment Model," in *Proceedings of the 11th International High-Level Radioactive Waste Management Conference, April 30-May 4, 2006, Las Vegas, Nevada*. (American Nuclear Society, La Grange Park, Illinois, 2006), pp. 228-235.

M. Schindler, M. Fayek, and F. C. Hawthorne, "Uranium-rich opal from the Nopal I uranium deposit, Peña Blanca, Mexico: Evidence for the uptake and retardation of radionuclides," *Geochimica et Cosmochimica Acta* **74**, 187-202 (2010).

J. Shahabpour, "Liesegang blocks from sandstone beds of the Hojedk Formation, Kerman, Iran," *Geomorphology* **22**, 93-106 (1998).

B. Stege, N. Pingitore, P. Goodell, and D. LeMone, "Limestone Bedrock as a Barrier to Uranium Migration, Sierra Peña Blanca, Chihuahua, Mexico," in *Uranium In Volcanic and Volcaniclastic Rocks, AAPG Studies In Geology No. 13, Papers from the symposium on Uranium in volcaniclastic rocks, conducted at the Annual Meeting of the Southwest Section of The American Association of Petroleum Geologists, El Paso, Texas*, P. Goodell, and A. Waters, Eds. (American Association of Petroleum Geologists, Tulsa, Oklahoma, 1981), pp. 265-274.

R. H. Steiger, and E. Jäger, "Subcommission on Geochronology: Convention on the use of decay constants in geo- and cosmochronology," *Earth and Planetary Science Letters* **36**, 359-362 (1977).

M. Th. van Genuchten, "Convective-Dispersive Transport of Solutes Involved in Sequential First-Order Decay Reactions," *Computers & Geosciences* **11**, 129-147 (1985).

R. Velarde, P. Goodell, T. Gill, and R. Arimoto, "Wind Transport of Radionuclide-Bearing Dust, Peña Blanca, Chihuahua, Mexico," *Eos, Transactions, American Geophysical Union* **88** (3), Abstract GS22A-05 (2007).

F. Vera Tomé, P. Blanco Rodríguez, and J. C. Lozano, "Distribution and mobilization of U, Th and ^{226}Ra in the plant-soil compartments of a mineralized uranium area in south-west Spain," *Journal of Environmental Radioactivity* **59**, 41-60 (2002).

J. Walton, P. Goodell, C. Beshears, D. French, and A. Kelts, "Radionuclide Dispersion Rates by Aeolian, Fluvial, and Porous Media Transport," *Geological Society of America Abstracts with Programs* **37** (7), 268 (2005).

V. Wong, P. C. Goodell, and E. Y. Anthony, "Characterization of U-Series Disequilibria at the Peña Blanca Natural Analogue Site, Chihuahua, Mexico," in *Scientific Basis for Nuclear Waste Management XXII, Materials Research Society Symposium Proceedings* (Materials Research Society, Pittsburgh, Pennsylvania, 1999), Vol. 556, pp. 801-808.

Y. S. Wu, A. C. Ritcey, and G. S. Bodvarsson, "A modeling study of perched water phenomena in the unsaturated zone at Yucca Mountain," *Journal of Contaminant Hydrology* **38**, 157-184 (1999).

R. A. Zielinski, "Uranium in Secondary Silica: A Possible Exploration Guide," *Economic Geology* **75**, 592-602 (1980).

R. A. Zielinski, "Uraniferous Opal, Virgin Valley, Nevada: Conditions of Formation and Implications for Uranium Exploration," *Journal of Geochemical Exploration* **16**, 197-216 (1982).

REGIONAL HYDROLOGY AND URANIUM OCCURRENCES AROUND NOPAL I

Philip C. Goodell, José Alfredo Rodríguez Pineda, Patrick Dobson, Steven H. Harder, and Schön S. Levy

INTRODUCTION

Regional saturated-zone hydrology is important to studies of subsurface uranium transport in arid lands because groundwater is the predominant medium for long-range transport of radionuclides released from an underground source. The Nopal I uranium ore deposit in Chihuahua, México, was studied as a natural analogue for a nuclear waste repository in the unsaturated zone of an arid region. One aspect of the natural-analogue concept concerns aqueous migration of uranium from the ore body (representing a nuclear waste form) downward into the saturated zone. The ore deposit, hosted by tuffaceous rocks, was formed about 32 million years ago (Fayek et al., 2006) and now lies about 220 to 110 meters above the water table. Some fraction of the uranium dissolved from the ore deposit by percolating water presumably has reached the water table and entered the saturated zone. Interpretation of the geochemistry of locally mixed groundwater below the ore deposit benefits from information about the sources and pathways of regional groundwater passing beneath the ore body. The existence of uranium-enriched rock other than the Nopal I ore body could complicate the detection of Nopal-derived radionuclides in the groundwater. In addition, the potential to trace radionuclides in the saturated zone downgradient from Nopal I would be improved by documentation of the regional potentiometric surface and uranium-isotopic characteristics of regional ground water.

The synthesis of regional hydrology presented here reflects the paucity of information about the groundwater system. There are very few wells in the area around Nopal I. With the exception of the four PB wells drilled or reconditioned for the Peña Blanca Natural Analogue Project by the U.S. Department of Energy, Office of Civilian Radioactive Waste Management (U.S. DOE, OCRWM) the existing wells are not optimally located to document the potentiometric surface or flow paths in areas most relevant to the project. These are serious limitations, considering that the Sierra Peña Blanca region is an area of considerable topographic relief, faulting, and permeability contrasts, which may present hydrologic complications in trying to visualize the groundwater system.

In general, the hydrogeologic setting may have similarities to the conceptual model of Mahlknecht et al. (2008, Figure 1). This conceptual model emphasizes the importance of aquifers in alluvial basins that are major aquifers for the city of Chihuahua. The regional flow model is based on data from wells in alluvium. Groundwater flows from higher elevations in the west to lower elevations in the east, exploiting connections between alluvial basins. The main groundwater flow path from west to east takes a large bend southward to follow contiguous alluvial aquifers.

A conceptual model of regional groundwater flow more focused on the Sierra Peña Blanca, including the Nopal I uranium deposit, must incorporate flow through bedrock. The small number of wells drilled in bedrock here undoubtedly reflects the higher cost of drilling and the low productivity of bedrock aquifers compared to alluvial aquifers. Bedrock wells have been adequate to support cattle ranching and uranium-mining camps. The wells drilled at Nopal I are unique in this area for having been drilled at a topographic high area and penetrating a very thick unsaturated zone before reaching the water table.

REGIONAL PHYSIOGRAPHY, GEOLOGY, AND STRUCTURE

The Nopal 1 uranium deposit is located on the southeast side of a west dipping cuesta, or tilted structural block, composed of felsic tuffaceous rocks. This cuesta is at the southeastern edge of the Peña Blanca mountain range, also known as the Sierra Peña Blanca or northern Sierra del Cuervo. The range is oriented north-south and is approximately 8 km wide at this location.

The following features can be seen in Figure 1 from west to east. The Sacramento-Encinillas Basin, also known as the Valle El Sauz Encinillas, is an elongated N-S graben. It has a broad flat surface at approximately 1550 m elevation and contains as much as 600 m of alluvial fill (Villalobos-Aragón et al., 2007). This feature will be referred to as the Encinillas Basin in the remainder of this report. To the west of the Encinillas Basin is the high volcanic plateau known as the Sierra del Nido (not shown in Figure 1), with elevations up to 2200 m.

East of the Encinillas Basin and separated from it by a range of hills up to 180 m high is another elongated N-S valley that hosts several lakes, including Laguna El Diablo. This valley is the western half of the Sierra Peña Blanca structural block. It consists of a broad synclinal structure with the lake in the center of the syncline (Figures 1 and 2). Most of the valley floor lies between the elevations of 1560 and 1580 m. Surface elevations east of the valley reach the highest in the Sierra Peña Blanca, approximately 1980 m. At this highest part of the range, the rocks are ash flow tuffs of the Mesa, escuadra, and Nopal Formations (younger to older), dipping slightly to moderately westward. The Nopal Formation rests on a 20-m section of Pozos conglomerate, which in turn rests unconformably on the very thick and massive carbonate reef of Cretaceous age. The highest part of the range is bounded on the east by a normal fault zone dipping steeply to the east, with downward offset on the eastern side (Figure 2; also shown in Stege et al., 1981, Figure 2). Vertical offsets along these faults range from about 40 to 200 m (reyes-Cortés, 1997, p. 174-175).

Fault displacement has locally exposed Cretaceous reef rock at the surface along and adjacent to the fault scarp. Reef limestone underlies the Tertiary volcanic and clastic rocks throughout the study area. That this reef acts as a hydrologic barrier was first proposed by Stege et al. (1981). The rock has very low matrix porosity and permeability and generallly may act as an aquitard, even though it is the aquifer for the PB4 well. The six-meter section of limestone penetrated at the bottom of well PB1 contain macroscopic

fractures and breccia (Goodell et al., 2003), but the intact-matrix permeability is ≤ 0.001 millidarcy (Dobson et al., 2008, Table 1).

The graben east of the fault is informally referred to as the Margaritas zone (Figure 2). This zone is an irregular topographic low area one to two kilometers wide, oriented approximately N-S. The low area is called the Boquilla Colorada microbasin by Reyes-Cortés (1997, p. 151). the graben is bounded on the east by telted horsts of the Sierra Peña Blanca, including the Nopal cuesta. Potential groundwater-flow connectivity might be provided by southeast extensions of the Margaritas graben fault system into the drainages bordering the cuesta.

To the east of the Peña Blanca range is the large Aldama-El Cuervo Basin or playa lake, with the playa surface at an elevation of about 1230 m. The basin is elongate in a N-S direction. Laguna El Cuervo is the present-day playa lake. Alluvial sediments in the basin are up to 1500 m thick (Rodriguez et al., 1999). This feature is called el Cuervo Basin in the rest of this report.

An initial assumption, inferred from the overall regional slope to the east is that regional hydrologic flow generally proceeds from west to east, from the Sierra del Nido to the Encinillas and then to the El Cuervo basin. The existence of considerable topographic variability, structural complexity, and lithologic heterogeneity supports an additional assumption that local groundwater flow systems have developed as well (Domenico and Schwartz, 1998, p. 79-80).

SURVEY OF REGIONAL WELLS, SURFACE WATER, AND SPRINGS

A reconnaissance groundwater survey was carried out in 2005 within a broad east-west band, including Nopal I, to document the general configuration of the regional water table (Table 1). The main objective was to look for indications of hydrologic connectivity or isolation through the Sierra Peña Blanca between the Encinillas and the El Cuervo basins. A differential Global Positioning System survey was used to measure the locations and ground-level elevations, as well as elevations of wellheads, of the water wells along this transect. Depth to the water table in wells was measured with a Solinst® Model 101 water-level meter. For each measured well, the depth-to-water was subtracted from the ground-level or wellhead elevation to determine the elevation of the water table. The synthesis of groundwater configuration also relies on anecdotal information.

REGIONAL HYDROLOGY SYNTHESIS

Figure 1 shows the locations of the water wells and shaft where the water-table elevations were measured, and the location of the El Penol (A on Figure 3)-Rancho los Pozos (B on Figure 3) transect. Figure 3 shows the topography and water-table elevations along the transect defined by water-level data selected from Table 1. Water-table data not included in the transect are consistent with levels shown in Figure 3. For transect locations where multiple wells with similar water levels are very close together, an average water-level value from Table 1 was plotted.

Table 1. Wells Used to Define the Regional Water Table

Identifier	Location (UTM northing, easting in meters; latitude, longitude)	Casing/Ground Elevation, meters above sea level	Water Level Elevation, meters above sea level
El Peñol (well)	3224220, 380684; 29°8'26.7"N, 106°13'34.1"W	1552	1534
Nuevo Delicias2 (well)	3216526, 378000; 29°4'15.8"N, 106°15'10.3"W	1560	1528
San Isidro (well)	3215723, 378666; 29°3'49.9"N, 106°14'45.4"W	1559	1528
Laguna El Diablo (well)	3223899, 387717; 29°8'19.2"N, 106°9'15.5"W	1559	1542
Rancho la Parrita (well)	3224063, 392731; 29°8'26.1"N, 106°6'10.0"W	1565	1559
Peña Blanca-1 (well)	3224715, 397207; 29°8'48.6"N, 106°3'24.6"W	1407	1346
Peña Blanca-2 (well)	3224577, 397178; 29°8'44.1"N, 106°3'25.6"W	1420	1344
Average, Peña Blanca wells	—	—	1345
El Nopal III (shaft)	3221414, 397991; 29°7'1.6"N, 106°2'54.5"W*	~1410*	~1370*
PB1 (well)	3220793, 399275; 29°6'41.1"N, 106°2'5.0"W	1464	1240
PB3 (well)	3220801, 399325; 29°6'41.4"N, 106°2'3.2"W	1453	1238
Average, PB1 and PB3	—	—	1239
PB4 (well)	3220061, 400374; 29°6'17.7"N, 106°1'24.1"W	1337	1236
Los Pozos (well)	3219928, 402591; 29°6'14.2"N, 106°0'2.1"W	1259	1196
Rancho los Pozos (well)	3217833, 405853; 29°5'6.7"N, 105°58'0.8"W	1203	1183
La Peña (well)	3233846, 403624; 29°13'46.4"N, 105°59'28.2"W	1250	1179
Rancho Martinez (well)	3227498, 406298; 29°10'20.9"N, 105°57'47.2"W	1206	1185

*Location estimated from Rodriguez Torres et al. (1976, Figure 9) and George-Aniel, Leroy, and Poty (1991, Figure 2). Ground elevation estimated from El Sauz 1:50 000 topographic map (INEGI, 2004). See text for explanation of estimated water level.

On the NW (left)side of the diagram is the Encinillas basin at approximately 1550 meters elevation. The static water levels in September 2005 stood at 1530 meters. The numerous water wells provide for extensive irrigated agriculture, and static water levels are affected by pumping. Drainage patterns visible on the Landsat Thematic Mapper image (Figure 1)and the slight northward inclination of the topographic surface of the Encinillas basin in the region of interest both suggest dominant surface-water flow from south to north toward intermittent Laguna Encinillas. At present, the Encinillas basin is a closed basin. The water-table data in Table 1 indicate that the potentiometric surface is approximately horizontal, and this is supported by data from Mahlknecht et al. (2008, Figure 1).

During wetter climates in the past, this lake had an outflow to the east, near the northern boundary of Figure 1, that conveyed surface discharge from ancient Laguna Encinillas toward ancient Laguna El Cuervo. The nature of present-day ground water flow between these basins, other than through alluvial aquifers to the south, is not well known. The existence of some interbasin flow through bedrock is suggested by the fact that in 1985 a ranch at the northern end of the Sierra Peña Blanca had a functioning artesian well (star in Figure 1) at 1325 meters elevation (Goodell, 1985, Figure 1) in the La Mesa Formation, the uppermost unit in the local volcanic sequence. The intermittent artesian-well behavior attests to the presence of a confined aquifer that is periodically recharged more than usual. The Encinillas Basin may supply the necessary hydrologic head for this artesian system. Reyes-Cortés (1997, p. 24, 127) also mentions, without giving specific locations, the presence of artesian wells in the El Cuervo basin.

Water-table elevations in the Laguna El Diablo valley and highlands to the east are defined by a well in the valley and a well at Rancho la Parrita. As shown in Figure 3, these data define a water table rising slightly eastward from the Encinillas basin, reaching a maximum elevation of about 1559 m.

Water-table elevations in the Margaritas structural graben immediately to the east are inferred from measurements at the Peña Blanca wells (not to be confused with the PB prefixed wells at Nopal I) and from the presence of groundwater that is occasionally present in the 40-m-deep Nopal III shaft (location taken from Rodriguez Torres et al., 1976, Figure 9, and George-Aniel, Leroy, and Poty, 1991, Figure 2). One measurement of 15 m from the ground surface to the top of the water in the shaft has been made, but this probably represents perched water. For the purposes of this study, the water-table elevation at this location is assumed to be approximately at the bottom of the shaft.

There appears to be a steep gradient in water-table elevations between the Sierra Peña Blanca highlands, represented by Laguna El Diablo and Rancho la Parrita wells, and the Peña Blanca wells (Figure 3). This may reflect lower transmissivity of the carbonate reef rock or the fault zone.

The Peña Blanca wells are located within an area that was studied by Reyes-Cortés (1997) as a potential disposal site for uranium-mine tailings. the water table in the wells is at an elevation of about 1345 m, about 65 m below ground surface. Reyes-Cortés (1997, p. 173) determined from electrical resistivity surveys that the thickness of alluvium, talus, and conglomerate in this area varies from a few meters to more than 30 meters. Therefore, the wells may be sited in alluvium with the water table located several tens of meters into the underlying volcanic/volcaniclastic section.

The Nopal III shaft is located along the Arroyo el Tigre about 0.3 km east of where the arroyo intersects the Margaritas graben (Figure 2), probably within the Nopal or Coloradas Formation (Reyes-Cortés, 1997, Plate 2). This location puts the shaft in a different surface-drainage basin than the Peña Blanca wells, which are within La Boquilla Colorada drainage. The two water locations may represent different aquifers as well. For

the purpose of this description, Nopal III is grouped with the Peña Blanca wells because the water-table levels are similar and there is insufficient hydrologic information to define an additional aquifer. Surface-drainage topography around Nopal III, described below, suggests this could be a separate aquifer.

East of the Margaritas graben are the west-dipping cuestas that constitute the eastern-most portion of the Sierra Peña Blanca in this region (Figure 2). The Nopal I ore deposit is at the southeastern end of the southernmost cuesta. The average groundwater table in wells PB1 and PB3 at Nopal I in November, 2005, was at approximately 1239 meters elevation. The well designated PB4 is about 1.3 km SE of Nopal I. The elevation of the water table in PB4 is about 1236 m. All PB wells are tapping the Cretaceous limestone aquifer.

The difference in elevation of the water table between the Margaritas zone and the PB wells at Nopal cuesta is in the range of 106 to 131 m, and the elevation drop may occur over a distance of as little as two kilometers or less (the distance between Nopal III and Nopal I). Beside the elevation difference in water table between the Margaritas and Nopal zones, the aquifer changes from Tertiaryvolcanic rocks in Margaritas to Cretaceous limestone at Nopal. These differences suggest that little or no flow occurs within the volcanic section between the two zones.

Stepping out from the Sierra Peña Blanca into the El Cuervo Basin are alluvial fans that extend into the basin, as shown by the surface-elevation profile in Figure 3. The well at Los Pozos, with a water-table elevation of about 1196 m, is representative of the aquifer in the alluvial-fan deposits. At Rancho Los Pozos, the water-table elevation is about 1183 m. Water-table elevations in the central El Cuervo basin are below 1200 m (Mahlknecht et al., 2008). These observations define an eastward decline in water-table elevations, following topography. The water-table data are too sparse to indicate whether there could be a small but abrupt change in elevation at the transition between limestone-bedrock (e.g., PB4) and alluvial aquifers.

LOCAL DRAINAGE BASINS

The three local drainage basins including and surrounding the Nopal cuesta are shown in Figure 4. The southernmost drainage, designated the Nogales drainage, surrounds the Arroyo los Nogales and includes the southern slope of the Nopal cuesta. The arroyo hosts an intermittent stream and its tributaries. Inclination of the drainage surface and direction of flow are eastward toward the regional El Cuervo basin. The southern and eastern portions of the drainage are directly underlain by Cretaceous limestone. In the northern and northwest portions of the drainage, limestone is covered by Tertiary pyroclastic and volcaniclastic deposits with a maximum pre-mining thickness of about 300 m at the Nopal cuesta. The thickness of alluvium in the Arroyo los Nogales is about 20 m or less (Stege et al., 1981). All of the PB wells are located within this drainage.

North of the Nogales drainage basin is the El Tigre drainage defined by Arroyo el Tigre (Figure 4). Surface-water transport is eastward to the El Cuervo basin. The El Tigre

drainage and most of its tributaries are developed within the Tertiary volcanic rocks. An east-west-trending tributary or extension of the Arroyo el Tigre appears to have developed along a prominent fracture corssing the Margaritas graben and extending into the massive limestone reef. Faults of various orientations extend from the Margaritas graben into this area (Reyes-Cortés, 1997, Plate 2). No water wells are present in this drainage.

The largest drainage in Figure 4 includes the Margaritas zone and its intersection with the east-trending drainage that includes the Peña Blanca wells and the Boquilla Colorada. Surface water in the valley of the Margaritas graben flows north to the Boquilla Colorada microbasin, previously described, and joins the larger drainage that extends from the Sierra Peña Blanca highlands to the El Cuervo basin.

Almost all of the bedrock within the drainage belongs to the Tertiary pyroclastic-volcaniclastic section (Reyes-Cortés, 1997, Plate 2). Cretaceous limestone lies within the western wall of the Margaritas graben (Figure 2). As described above, the combination of alluvium, talus, and conglomerate is as thick as 30 m in the Boquilla Colorada microbasin.

GROUNDWATER INTERACTION WITH URANIUM-ENRICHED ROCK

Information about known or estimated uranium-rich rocks along flow paths that may pass beneath the Nopal cuesta was taken from reconnaissance studies and documentation of developed mines or prospects. The reconnaissance information relates to surface or near-surface uranium occurrences. Uranium content and isotopic systematics have been measured in groundwaters from the PB wells and two nearby wells for this project, and a few published data are available for regional alluvial aquifers and surface waters.

Airborne Radiometric Anomalies and Stream-Sediment Survey

A semi-quantitative airborne radiometric survey in the 1960s identified 104 radiation anomalies at the ground surface in the Peña Blanca region. The anomalies were investigated first by surface surveys and later by excavations, including trenches, tunnels, shafts, and drill holes.

A stream-sediment geochemistry study was carried out before extensive ground disturbance began in preparation for mining (Carraway and Goodell, 1983; Goodell, 1985). The original objective of the stream-sediment survey was to identify areas of uranium-enriched sediments that could be traced upslope or upstream to uranium deposits. Figure 5 shows uranium-concentration ranges for 171 stream-sediment samples taken from the Peña Blanca region. The highest measured values were about 26 ppm (Goodell, 1985, Table II). The data were re-examined within the context of the natural-analogue study to test for the presence of areas containing uranium mineralization or concentrations of uraniferous sediments within the drainages near the Nopal cuesta. Either type of material could contribute to an elevated uranium content of groundwater beneath the Nopal I site.

The Nopal I deposit was the only excavation within the Nogales drainage basin; and no other airborne radiometric anomalies are known. This suggests that there were no significant uranium deposits elsewhere within the basin. It should be noted that the mine symbol on the map in Figure 4 located about half a kilometer north of PB3 is in error; a drill site exists, but no excavation or mine is located there. Five stream-sediment samples collected downslope or down drainage from the Nopal I deposit, including a sample close to the PB4 well, have uranium contents greater than 7 ppm. Three of the high-uranium samples were collected within about 0.5 km of Nopal I and almost certainly contain detritus from the deposit (Figure 5).

Nopal III was the only significant airborne uranium anomaly and excavation in the El Tigre basin. The prospect consisted of a 40-m-deep shaft and a short exploration tunnel. Stream-sediment uranium concentrations in the El Tigre drainage north of Nopal I show widespread elevated values from 4.9 ppm to more than 7 ppm uranium (Figure 5).

Numerous airborne radiometric anomalies were identified in the Margaritas area. These were explored by drilling from 1977 to 1983. Open-pit and underground mines were developed at Margaritas (Goodell, 1981, p. 287). In 1983, this activity terminated and has not been resumed. At the time of deactivation, the Margaritas open pit had not yet reached the subsurface ore zone. No stream-sediment samples were collected in the streambeds immediately adjacent to the Margaritas deposits or within about two kilometers in the downstream direction. A few uranium values greater than 7 ppm were detected in stream sediments near the Peña Blanca wells and further downstream (Figure 5), but are not spatially attributable to the Margaritas deposits.

Uranium in Groundwater

The small number of groundwater uranium analyses is insufficient to quantify regional variations in uranium concentration or isotopic composition, but the data do provide some information about possible sources of variability. The Peña Blanca Natural Analogue Project analyzed water samples from the shallow saturated zones of the PB, Peña Blanca, and Pozos Ranch wells. Data also are available for surface water from the Chuvíscar River near Aldama, about 40 km south of Nopal I (Villalba et al., 2006) and groundwater from the Chihuahua-Sacramento Valley, the southern part of the Encinillas basin (Rentería Villalobos et al., 2007)

Goldstein et al. (this report) present and discuss the data in terms of uranium concentration and $^{234}U/^{238}U$ activity ratios. The waters are mixtures of multiple components. One type of component has a relatively high U content with $^{234}U/^{238}U$ activity ratios near unity, as would result from bulk dissolution of a rock in secular equilibrium. The PB well waters from around Nopal I may be predominantly composed of this component. A second type of component has variable U content and $^{234}U/^{238}U$ activity ratios much higher than unity. The high $^{234}U/^{238}U$ activity ratios indicate a relatively high content of ^{234}U derived from several possible mechanisms, including alpha recoil (Paces et al., 2002, p. 752). Variability of uranium content may be due to

numerous processes including dissolution, precipitation, evaporation, and mixing. Large temporal variations in uranium content of water from a single well may be caused by anthropogenic factors rather than natural variations in aquifer characteristics. The $^{234}U/^{238}U$ activity-ratio values tend to be less sensitive to borehole conditions (Paces et al., 2002, pp. 755, 759).

Groundwaters from Peña Blanca and the Chuvíscar River (average) have high $^{234}U/^{238}U$ and U contents that overlap the lower part of the concentration range for Nopal PB well waters. A third water type has intermediate $^{234}U/^{238}U$ activity ratios and variable U concentration. The PB4 and Pozos Ranch well waters may be examples of this water type.

Unsaturated-zone water samples were collected from an adit at Nopal I located about 8 m below the mined surface. Variations in uranium isotopic ratios of these samples help define the factors that influence isotopic composition (Goldstein et al., 2016). The data confirm that the most distinctive compositions are those with $^{234}U/^{238}U$ activity ratios close to unity and that percolating water acquires such compositions through interaction with uranium-rich rock in secular equilibrium.

Saturated-zone waters from the PB wells at the Nopal cuesta have $^{234}U/^{238}U$ activity ratios in the range of 1.005 to 1.974 (Goldstein et al., 2016). The PB4 well, about 1.3 km SE and presumably downgradient from Nopal I within the same carbonate aquifer, has $^{234}U/^{238}U$ activity ratios between 1.422 and 2.066. The Los Pozos well, about 2.3 km due east of PB4 and sited at least partly in alluvium, has $^{234}U/^{238}U$ activity ratios between 2.108 and 2.159. A simple, qualitative interpretation of these data is that the $^{234}U/^{238}U$ activity-ratio signature of values near unity is acquired by groundwater passing beneath and through the uranium-rich bedrock of Nopal I. This signature dominates the uranium isotopic composition of groundwater for at least several kilometers downgradient from Nopal I as the uranium-rich water from Nopal gradually mixes with water of variable uranium content that contains excess ^{234}U.

The Peña Blanca wells have $^{234}U/^{238}U$ activity ratios in the range of 4.603 to 4.616 (Goldstein et al., 2016, Table 1). Activity ratios in water samples from the Chuvíscar River are in the range of 4.0 to 4.5 (Villalba et al., 2006, Table 1). Water samples from two wells in the Chihuahua-Sacramento Valley have activity ratios of 3.49 and 4.0 (Rentería Villalobos, 2007, Table IV). The isotopic systematics of these waters are dominated by processes, such as alpha recoil, and water-rock interactions that preferentially transfer ^{234}U to the water. The stream sediments and their local source rocks upgradient from the Peña Blanca wells are slightly enriched in uranium, and some of the water flowing from the Margaritas mine areas toward Peña Blanca may have interacted with uranium-mineralized rock in secular equilibrium. By the time water reaches the Peña Blanca wells, however, it has acquired a fairly consistent $^{234}U/^{238}U$ activity ratio well above unity.

DISCUSSION

General regional groundwater flow through the Sierra Peña Blanca is from west to east, but the combination of regional slope, topographic variability, permeability contrasts between geologic units, and structural complexity has led to the development of local groundwater systems. Most significant for the natural analogue study is that groundwater in the Nopal zone appears to be isolated from groundwater in the Margaritas zone and perhaps the groundwater beneath the El Tigre drainage. The isolation reflects more than simply the existence of three topographically separate drainage basins. Apart from the differences in water-table elevation is the difference in hydrostratigraphy. The Margaritas zone and El Tigre aquifers both have upper water-producing layers within the Tertiary volcanic section and presumably have lower aquifers in the Cretaceous limestone. The Nopal zone (Nogales drainage) has a thin aquifer of about 20 m within the volcanic section at PB1 (Levy et al., 2016) and a carbonate aquifer at greater depth.

Patterns of mineralogic alteration in the PB1 drill core (Fayek et al., 2006; Levy et al., 2016) seem to indicate that a higher water table within the volcanic section of the Nopal cuesta existed in the past. Also, the presence of secondary-minerals with ages less than one million years in the volcanic rocks (e.g., Murrell et al., 1999; Pickett et al., 2000; Fayek et al., 2006) documents that at least some infiltration and percolation have occurred in the recent geologic past. Infiltration, under either natural or post-mining disturbed conditions, may produce ephemeral perched-water zones (Reyes-Cortés, 1997, pp. 274-290) but is insufficient to maintain an aquifer in the volcanic rocks.

Exact reasons for the low water table below the Nopal cuesta have not been identified. The approximate latitude of the cuesta corresponds to a north-to-south transition in surficial geology from Tertiary volcanic rocks to Cretaceous limestone (Reyes-Cortés, 1997, Plate 2). These rock types differ with respect to hydrologic properties such as porosity and permeability (Dobson et al., 2008, Table 1) that may affect patterns of infiltration and percolation. Structural complexity associated with the Margaritas graben may channel groundwater away from the Nopal zone. Geomorphological evolution also could be a contributing factor. The Nopal cuesta, as the southernmost cuesta of the Sierra Peña Blanca, has been preferentially reduced in height and area by erosion and is becoming topographically isolated from the rest of the range. A consequent reduction of local surface area available for rainwater infiltration into the volcanic rocks may have reduced the potential for local recharge. A general geomorphological description of the area by Reyes-Cortés (1997, pp. 22 and 24) mentions local rejuvenation due to stream piracy without specifying locations. The low topographic saddle west of the Nopal cuesta may be a location where minor topographic modifications could have redirected stream flow from the Nogales drainage into the Margaritas basin, with possible consequences for local recharge.

CONCLUSIONS

The orientation of the regional potentiometric surface indicates groundwater flow generally from the Encinillas basin in the west to the El Cuervo basin in the east.

Structural geology, surface-drainage patterns, water-table levels, and groundwater geochemistry all indicate that local groundwater flow systems have developed within the regional flow pattern.

Based on airborne radiometric surveys, stream-sediment studies, and groundwater uranium-isotopic analyses, it is likely that the vicinity of Nopal I is the only source of high-uranium groundwater with $^{234}U/^{238}U$ activity ratios close to secular equilibrium in the Nogales drainage basin. The aquifer in this basin seems to be sufficiently isolated that no uranium-enriched groundwater with the distinctive $^{234}U/^{238}U$ activity ratios is entering from adjacent basins. Groundwaters throughout the region most commonly have $^{234}U/^{238}U$ activity ratios well above unity.

The distinctive uranium isotopic composition acquired by groundwater passing beneath the Nopal I site acts as a recognizable tracer moving downgradient from the site. Combined with the relative isolation of the Nogales basin with respect to groundwater flow from upgradient basins, this attribute provides a basis to study uranium transport away from the Nopal cuesta. Existing downgradient wells are not optimally located or maintained for sampling to characterize the uranium plume, but they provide qualitative evidence of downgradient transport.

ACKNOWLEDGMENTS

This project was funded by the U.S. DOE, OCRWM under contract DE-AC02-05CH11231. The views expressed in this article are those of the authors and do not necessarily reflect the views or policies of the U.S. DOE or OCRWM.

REFERENCES

K. Carraway and P. C. Goodell, "Stream sediment geochemical survey of the Pena Blanca uranium district, Chihuahua, Mexico," in *Geology and Mineral Resources of North-Central Chihuahua, Guidebook for the 1983 Field Conference*, K. F. Clark and P. C. Goodell, Eds. (El Paso Geological Society, El Paso, Texas, 1983), pp. 353-362.

P. F. Dobson, M. Fayek, P. C. Goodell, T. A. Ghezzehei, F. Melchor, M. T. Murrell, R. Oliver, I. A. Reyes-Cortés, R. de la Garza, and A. Simmons, "Stratigraphy of the PB-1 Well, Nopal I Uranium Deposit, Sierra Peña Blanca, Chihuahua, Mexico," *International Geology Review* **50**, 959-974 (2008).

P. A. Domenico and F. W. Schwartz, *Physical and Chemical Hydrogeology*, second ed. (John Wiley & Sons, Inc., New York, 1998) 506 pp.

M. Fayek, M. Ren, P. Goodell, P. Dobson, A. Saucedo, A. Kelts, S. Utsunomiya, R. Ewing, L. Riciputi, and I. Reyes, "Paragenesis and Geochronology of the Nopal I Uranium Deposit, Mexico," *Proceedings of the 11th International High-Level*

Radioactive Waste Management Conference, April 30-May 4, 2006, Las Vegas, Nevada (American Nuclear Society, La Grange Park, Illinois, 2006), pp. 55-62.

B. George-Aniel, J. L. Leroy, and B. Poty, "Volcanogenic Uranium Mineralizations in the Sierra Pena Blanca District, Chihuahua, Mexico: Three Genetic Models," *Economic Geology* **86**, 233-248 (1991).

S. J. Goldstein, A. Abdel Fattah, M. T. Murrell, P. F. Dobson, D. E. Norman, R. S. Amato, and A. J. Nunn, "Uranium-Series Constraints on Radionuclide Transport and Groundwater Flow at the Nopal I Uranium Deposit, Sierra Peña Blanca, México," in "Final Report for the Peña Blanca Natural Analogue Project," S. S. Levy, compiler, Los Alamos National Laboratory report XXXXXX (2016).

P. Goodell, "Geology of the Peña Blanca Uranium Deposits, Chihuahua, Mexico," in *Uranium In Volcanic and Volcaniclastic Rocks, AAPG Studies In Geology No. 13, Papers from the symposium on Uranium in volcaniclastic rocks, conducted at the Annual Meeting of the Southwest Section of The American Association of Petroleum Geologists, El Paso, Texas* (American Association of Petroleum Geologists, Tulsa, Oklahoma, 1981), pp. 275-291.

P. C. Goodell, "Chihuahua City Uranium Province, Chihuahua, Mexico," in *Uranium Deposits in Volcanic Rocks, Proceedings of a Technical Committee Meeting on Uranium Deposits in Volcanic Rocks Organized by the International Atomic Energy Agency and Held in El Paso, Texas, 2-5 April 1984* (International Atomic Energy Agency, Vienna, Austria, 1985), pp. 97-124.

P. Goodell, M. Fayek, M. Murrell, P. Dobson, and R. Oliver, "Descriptions of core samples from PB-1 well (based on transcribed notes)," in "Core Description for PB-1. Data Tracking Number LB0402PBCORELG.001," P. F. Dobson, compiler (available URL: http://www.lsnnet.gov/, Licensing Support Network accession number DN2001644400) 2003.

Instituto Nacional de Estadística Geografía Informática (INEGI), *Carta Topográfica 1:50 000 El Sauz H13C46, Chihuahua* (2004).

S. Levy et al, "Foundations of the Conceptual Model for Uranium Transport at the Nopal I Natural Analogue Site," in "Final Report for the Peña Blanca Natural Analogue Project," S. S. Levy, compiler, Los Alamos National Laboratory report ------ (2016).

J. Mahlknecht, A. Horst, G. Hernández-Limón, and R. Aravena, "Groundwater geochemistry of the Chihuahua City region in the Rio Conchos Basin (northern Mexico) and implications for water resources management," *Hydrological Processes* **22**, 4736-4751 (2008).

M. T. Murrell, P. Paviet-Hartmann, S. J. Goldstein, A. J. Nunn, R. C. Roback, P. A. Dixon, and A. Simmons, "U-Series Natural Analog Studies at Pena Blanca, Mexico:

How Mobile is Uranium?" *EOS, Transactions, American Geophysical Union* **80** (46), F1205 (1999).

J. B. Paces, K. R. Ludwig, Z. E. Peterman, and L. A. Neymark, "$^{234}U/^{238}U$ evidence for local recharge and patterns of ground-water flow in the vicinity of Yucca Mountain, Nevada, USA," *Applied Geochemistry* **17**, 751-779 (2002).

D. Pickett, B. Leslie, W. Murphy, and M. Nugent, "Estimating Radionuclide Release from a Uranium Deposit Through Uranium-Series Systematics in Carbonates and Opal," *Journal of Conference Abstracts* **5**, 797 (2000).

M. Rentería Villalobos, M. E. Montero Cabrera, M. Reyes Cortés, E. F. Herrera Peraza, A. Rodríguez Pineda, G. Manjón Collado, R. García Tenorio, T. Crespo, and M. Valenzuela Hernández, "Characterization of source rocks and groundwater radioactivity at the Chihuahua valley," *Revista Mexicana de Física*, S53 (3), 16-22 (2007).

I. Reyes-Cortés, "Geologic Studies in the Sierra de Peña Blanca, Chihuahua, México," Ph.D. Thesis, Department of Geological Sciences, The University of Texas at El Paso (1997).

J. A. Rodríguez, N. E. Pingitore, G. R. Keller, and A. Pérez, "An Integrated Gravity and Remote Sensing Assessment of Ground Water Resources in Central Chihuahua, Mexico" *Environmental & Engineering Geosciences* **V**, 73-85 (1999).

R. Rodriguez Torres, R. Yza Dominguez, R. Chavez Aguirre, and S. Constantino, "Rocas Volcanicas Acidas y su Potencial como Objectivos para Prospectar Uranio," in *Exploration for Uranium Ore Deposits, Proceedings of a Symposium on Exploration of Uranium Ore Deposits Organized by the International Atomic Energy Agency and the OECD Nuclear Energy Agency and held in Vienna, 29 March-2 April 1976.* (International Atomic Energy Agency, Vienna, Austria, 1976) pp. 601-623.

B. Stege, N. Pingitore, P. Goodell, and D. LeMone, "Limestone Bedrock as a Barrier to Uranium Migration, Sierra Peña Blanca, Chihuahua, Mexico," in *Uranium In Volcanic and Volcaniclastic Rocks, AAPG Studies In Geology No. 13, Papers from the symposium on Uranium in volcaniclastic rocks, conducted at the Annual Meeting of the Southwest Section of The American Association of Petroleum Geologists, El Paso, Texas*, P. Goodell, and A. Waters, Eds. (American Association of Petroleum Geologists, Tulsa, Oklahoma, 1981), pp. 265-274.

M. L. Villalba, L. H. Colmenero-Sujo, M. E. Montero-Cabrera, G. Manjón, R. Chávez-Aguirre, M. Royo-Ochoa, and A. Pinales-Munguía, "Presencia de Uranio en el río Chuvíscar, Estado de Chihuahua, México," *GEOS* **25**, 363-367 (2006).

A. Villalobos-Aragón, R. Cháves-Aguirre, A. Osuna-Viscarra, and V. V. Espejel-Garcia, "Geophysical and Hydrological Characterization of Alluvial Fans in the Valle El Sauz

Encinillas, Chihuahua, México," Eos, *Transactions, American Geophysical Union* **88** (23), Joint Assembly Supplement, Abstract H53E-05 (2007).

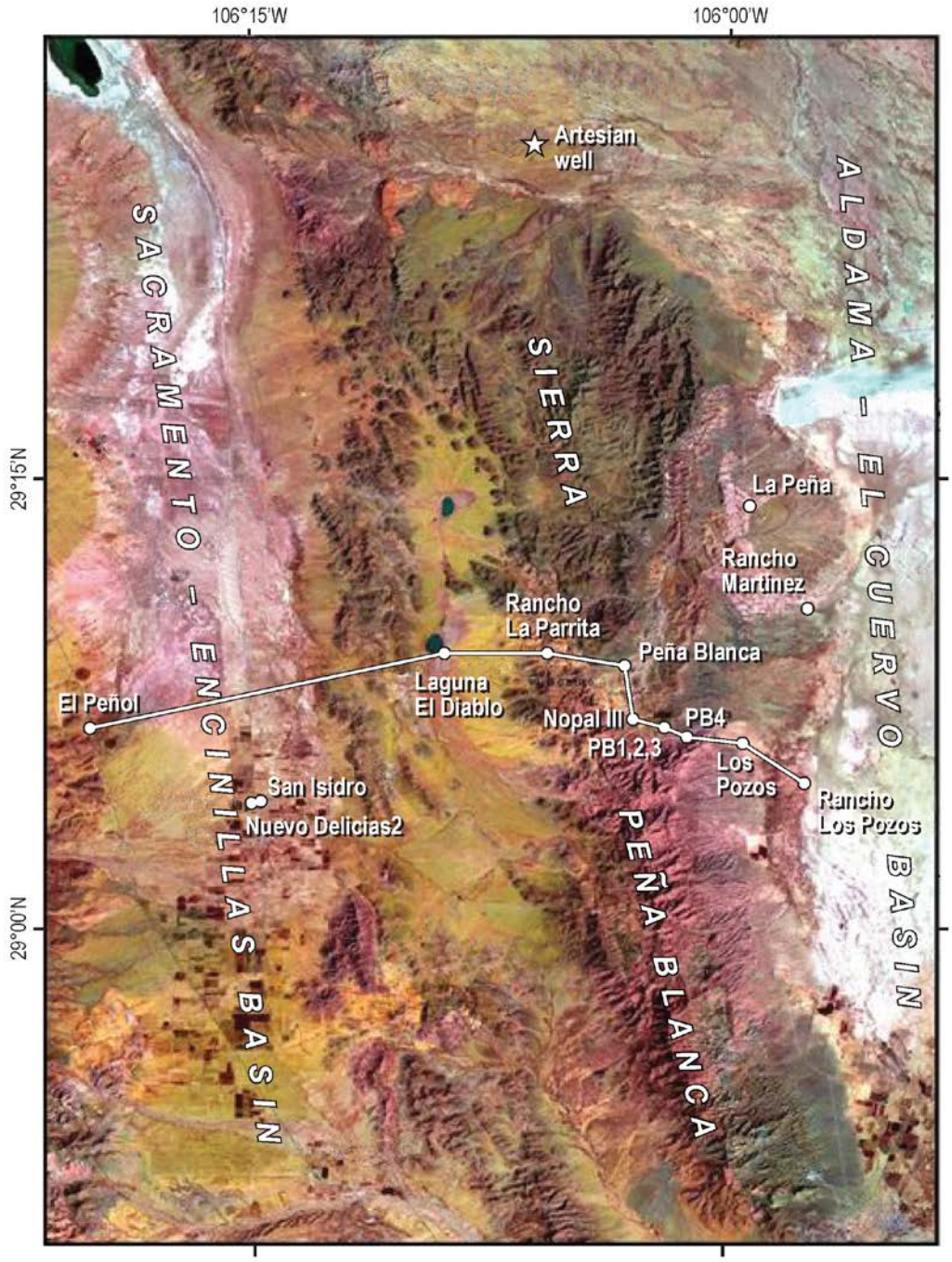

Figure 1. Physiographic and hydrologic features of the Peña Blanca region, showing transect and locations of wells plotted in Figure 3.

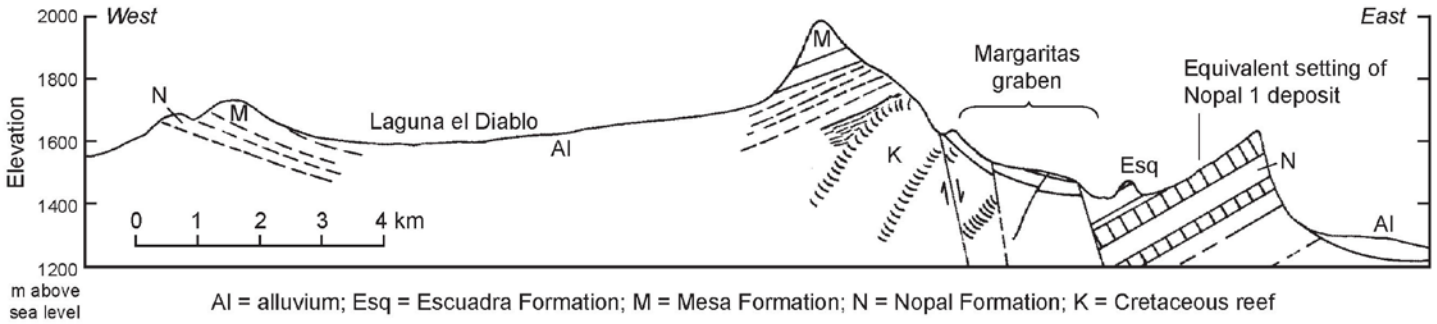

Figure 2. Geologic profile of the Sierra Peña Blanca.

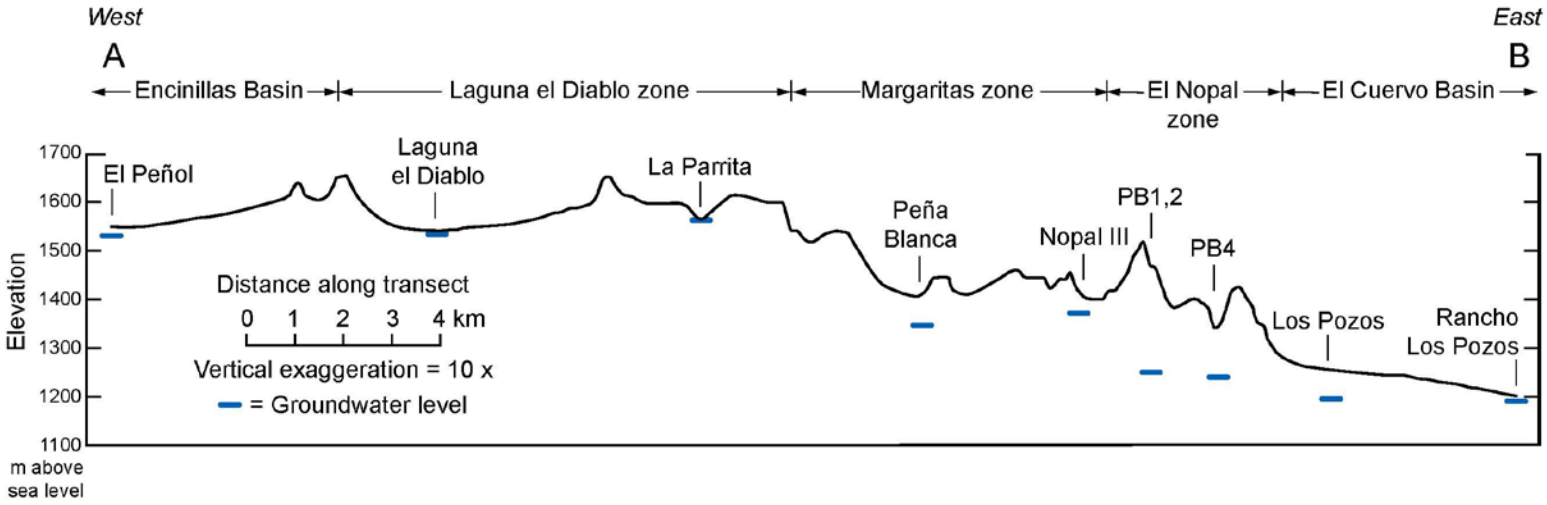

Figure 3. West to East vertical profile of surface and water-table elevations. Groundwater levels are from wells shown in Figure 1 and listed in Table 1.

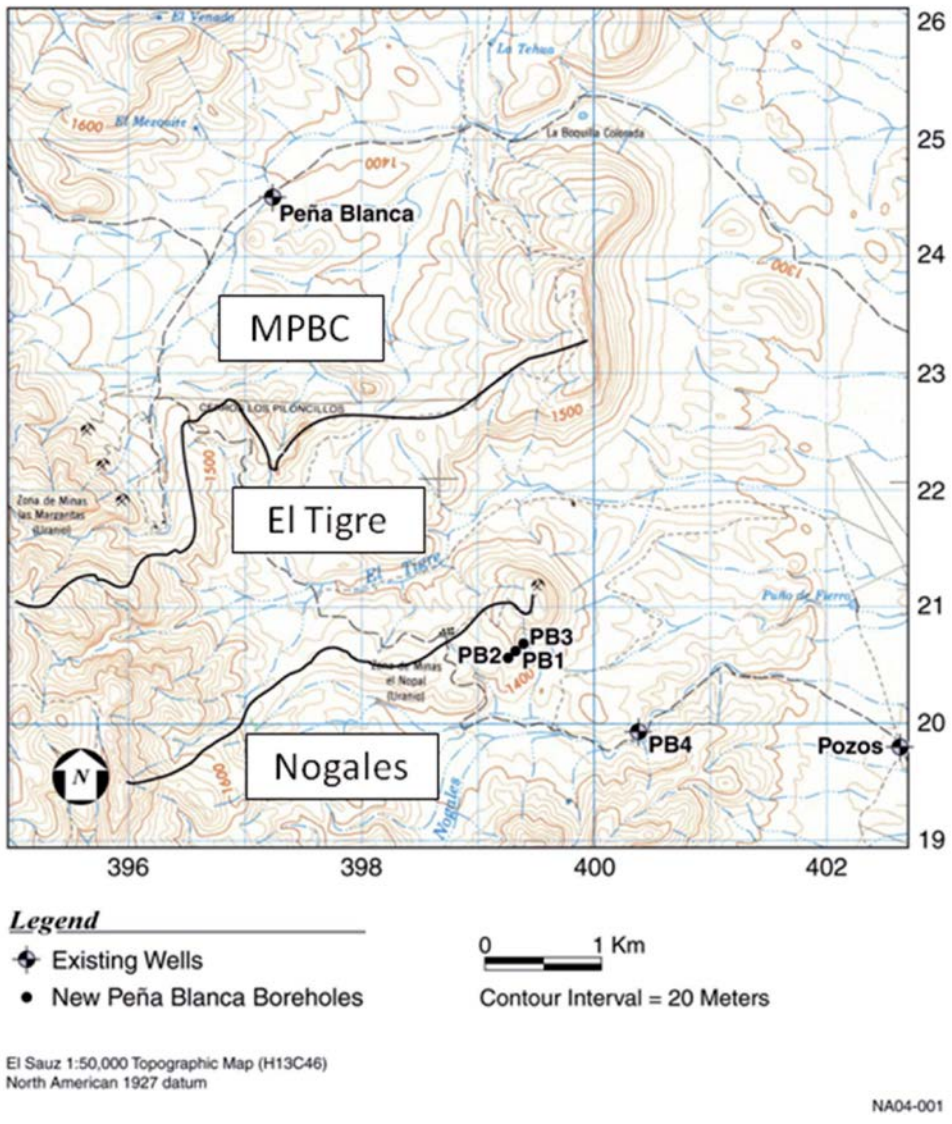

Figure 4. Local drainage basins. Numbers along the border of the figure are Universal Transverse Mercator coordinates in hundreds of thousands of meters east and 32xx000 m north.

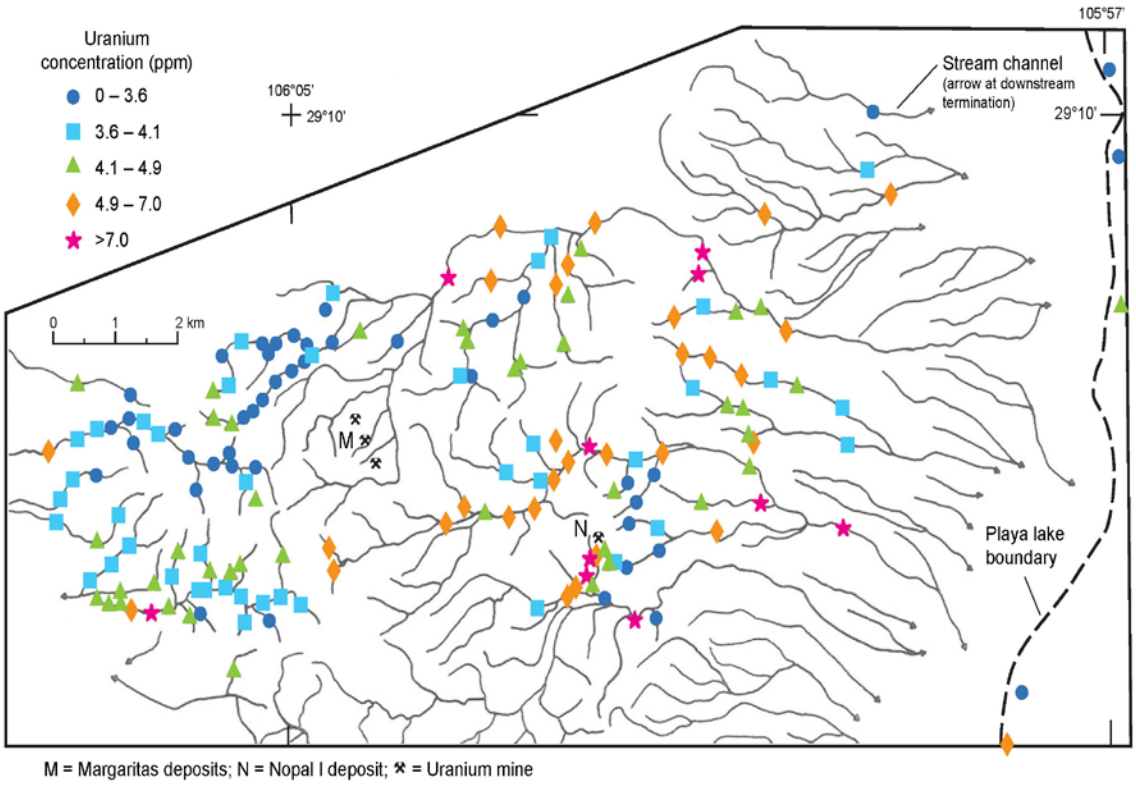

Figure 5. Uranium in stream-sediment samples.

URANIUM-SERIES CONSTRAINTS ON RADIONUCLIDE TRANSPORT AND GROUNDWATER FLOW AT THE NOPAL I URANIUM DEPOSIT, SIERRA PEÑA BLANCA, MEXICO

Steven J. Goldstein, Amr I. Abdel-Fattah, Michael T. Murrell, Patrick F. Dobson, Deborah E. Norman, Ronald S. Amato and Andrew J. Nunn

INTRODUCTION

Geological barriers are an important possible mechanism for isolation of radioactive contaminants from the biosphere. One measure of the effectiveness of such barriers is determination of retardation factors, i.e. the transport rate of contaminants relative to groundwater. Uranium-series techniques are an important method for determining in-situ retardation factors in groundwater (e.g. Krishnaswami et al., 1982; Luo et al., 2000; Porcelli and Swarzenski, 2003). In a geochemical system that is closed for greater than five daughter half-lives, the activity of each U-series daughter will be equivalent to that of its parent nuclide. This is true for rocks that have been closed systems for approximately one million years. However, as U-series nuclides are dissolved in groundwater during water-rock interaction, chemical fractionations may occur between different elements, resulting in disequilibria among U-series nuclides. For long-lived U-series daughters where decay in groundwater is negligible, the magnitude of U-series disequilibria is proportional to the relative mobility of each U-series nuclide in groundwater. As an approximation, the extent of U-series disequilibria also is inversely related to relative retardation factors. Hence, measurement of long-lived daughters such as ^{234}U, ^{230}Th, ^{226}Ra, and ^{239}Pu can be used to directly determine their relative mobility or retardation in groundwater.

We have applied these techniques to study groundwater flow and radionuclide transport near the Nopal I uranium deposit located in the Peña Blanca region, Chihuahua, México (Figures 1 and 2). This area, approximately 50 km north of Chihuahua City, was a major target of uranium exploration and mining by the Mexican government in the 1970s. More recently, this deposit has been extensively studied as an analogue for evaluating the fate of spent nuclear fuel, associated actinides, and fission products at a geologic repository in fractured, unsaturated volcanic tuff. Briefly, the deposit represents an environment similar to the once-proposed U.S. Yucca Mountain high-level radioactive waste repository in the following ways, 1) climatologically, both are located in semi-arid to arid regions, 2) structurally, both are parts of a basin-and-range horst structure composed of Tertiary rhyolitic tuffs overlying carbonate rocks, 3) hydrologically, both are located in a chemically oxidizing environment within an unsaturated zone, 200 m or more above the water table, and have broadly similar water chemistries, and 4) chemically, because the alteration of primary uraninite to secondary uranium minerals at Nopal I (Pearcy et al., 1994) may be similar to the eventual fate of uranium fuel rods in a geologic repository according to results of spent-fuel alteration experiments (Wronkiewicz et al., 1996). In this study, we measured long-lived U-series nuclide abundances in groundwater from this site by sensitive mass spectrometric methods. U-series measurements, including our measurements of ^{238}U-^{239}Pu disequilibrium, are used to constrain recent radionuclide transport and groundwater hydrologic processes at this location. This provides a unique opportunity to follow transport of

U-series nuclides in three dimensions from a well-defined source term, namely the ore body. Our study may add to the conceptual understanding of similar processes at waste-disposal or remediation sites in semi-arid, unsaturated zone settings.

SAMPLES AND METHODS

Saturated zone (SZ) waters were collected from six wells near the Nopal I uranium deposit, and seepage waters from the unsaturated zone (UZ) were obtained from an adit at the Nopal I mine (Figures 2 and 3). SZ intervals of the PB1, PB2, and PB3 wells, located immediately adjacent to the Nopal I ore deposit, occur mostly within Pozos conglomerate, with the lowest section of each well in Cretaceous limestone (Dobson et al., 2008). SZ intervals for two wells located SE of the Nopal I deposit, PB4 and Pozos Ranch, are totally within Cretaceous limestone. The subsurface geology at Peña Blanca Ranch is not constrained near the water table.

UZ water sample locations from the mine adit are shown in Figure 3. The mine adit is located at the +00 level of the deposit near PB1. UZ rocks near the mine adit consist of rhyolitic welded ash-flow tuffs (Nopal and Coloradas Formations) that host the ore deposit (Dobson et al., 2008). Groundwater samples from the adit and regional wells were collected during 2000-2006, whereas samples from the PB1, PB2, and PB3 wells have been collected from 2003-2006.

Most SZ water samples were collected by bailer, but in two instances (December 2003 and August 2006) they were collected by pumping. UZ water samples were collected from the mine adit via two seepage-collection systems (Figure 3), initially a drip collection system consisting of plastic sheeting and later a rigid plastic grid that funneled water into plastic bottles (Figure 4). Water samples for U-series analyses were filtered (0.20 μm or 0.45 μm filters) after collection and acidified to a pH of 1-2 with high-purity nitric acid for long-term storage. Samples from the PB1 and PB4 wells collected specifically for colloid analysis were stored in coolers immediately after collection and refrigerated until analysis. These samples were ultrafiltered in the laboratory using separate sterile ultrafiltration stirred cells (Millipore, USA), equipped with both 300 kDa (kilodalton) membrane filters and 20-nm in-line syringe filters. U concentrations of unfiltered and filtered splits were measured to determine how much of the U is associated with colloids.

Uranium, thorium, radium, and plutonium were analyzed in separate aliquots, each spiked with ^{233}U, ^{229}Th, ^{228}Ra, or ^{244}Pu tracer. After tracer equilibration, uranium was purified using anion exchange columns and loaded onto single or triple Re filaments (Goldstein, Murrell, and Janecky, 1989). Uranium isotopes (^{238}U, ^{235}U, ^{234}U) were measured multi-statically using a GV Sector 54 mass spectrometer equipped with multiple Faraday cups and a Daly ion counting detector. Calibration between Daly and Faraday detectors was determined by switching the ^{235}U beam between these collectors, and instrumental mass fractionation was corrected by normalization to the natural $^{238}U/^{235}U$ ratio of 137.88.

Radium was purified using cation exchange columns for the major element separation, EDTA-cation columns for Ra-Ba separation, and a final cation exchange column to rid the samples of EDTA. Radium was loaded onto Pt filaments using a silica gel enhancer and analyzed dynamically on a NBS 12-90 sector mass spectrometer equipped with a SEM ion counting detection system (Volpe, Olivares, and Murrell, 1991).

Thorium was purified using an HCl anion column for Th-U separation and a nitric acid anion column for major element separation (Goldstein, Murrell, and Janecky, 1989). Thorium was analyzed using the Isoprobe-P MC-ICPMS with multistatic collection of ^{232}Th and ^{229}Th on Faraday cups and ^{229}Th and ^{230}Th on a Daly detector. Samples were bracketed with gravimetric thorium standard solutions of known ^{232}Th/^{229}Th ratio to correct for instrumental mass fractionation and calibrate the gains between Daly and Faraday detectors.

Plutonium was purified using coprecipitations followed by anion exchange columns. The purified plutonium was then loaded onto a single resin bead that was placed in a single Re canoe carburized filament. Plutonium isotopes were measured dynamically on a GV Sector 54 mass spectrometer equipped with a Daly ion counting detector.

Measurement accuracy for both U concentration and ^{234}U/^{238}U ratio was verified by measurement of NBS U-960 and NIST 4321C natural uranium standard reference materials. For uranium and radium, filtration and process blanks are negligible in comparison to sample size. A ^{232}Th blank correction of ~ 43 pg was applied to the data, corresponding to less than one-third of the ^{232}Th signals measured. For ^{239}Pu, an isobaric interference corresponding to the equivalent of 35 atoms ^{239}Pu/g sample was subtracted from the data and is similar in size to the total ^{239}Pu signal for each sample. Hence, no ^{239}Pu was detected in the samples, with an upper limit of ~50 atoms ^{239}Pu/g sample.

RESULTS AND DISCUSSION

Long-lived uranium-series results (^{238}U, ^{234}U, ^{230}Th, ^{226}Ra) for samples collected in 2000-2001 are shown in Table 1. Uranium concentrations and ^{234}U/^{238}U ratios for SZ and UZ samples collected in 2003-2006 are given in Tables 2 and 3. Uranium concentrations and ^{234}U/^{238}U ratios for unfiltered, filtered, and ultrafiltered samples are given in Table 4.

Uranium Constraints on Groundwater Flow in the Saturated Zone

In 2003, three groundwater wells were drilled directly adjacent to (PB1) and ~50 m on either side of the Nopal I uranium deposit (PB2 and PB3). After drilling, U concentrations were elevated in all three wells (0.1-18 mg U/kg) due to drilling activities. The pH values were as high as 11.3 from detergents in the drilling fluids, and interaction of these high pH fluids with surrounding rock led to the high U concentrations. The pH decreased in a matter of a few months (by July 2003) to more typical groundwater values (pH = 7 to 9). Well productivity and SZ permeability obtained from pump tests (Oliver et al., 2005) decrease in the order PB3>PB1>PB2, and this correlates with initial U concentrations. This suggests that wells with higher permeability had greater water-rock interaction. PB1 and PB2 wells have very low productivities and permeabilities (Oliver et al., 2005). As shown in Figure 5, U concentrations for the new wells have exponentially decreased over time, although well pumping and conditioning in December 2003 and August 2006 disturbed this general trend.

Uranium isotopic and concentration data for the SZ are shown in Figure 6, in which conservative mixing between components results in linear trends. $^{234}U/^{238}U$ activity ratios are similar for PB1and PB2 (1.005-1.090) but higher for PB3 (1.36-1.97) over the 2003-2006 time period. These data, along with results of pumping (Oliver et al., 2005) which found drawdown of PB1 during PB2 pumping and vice versa, suggest interconnectivity between the PB1 and PB2 wells. However, PB1 and PB2 waters are distinct from PB3 in both [U] and $^{234}U/^{238}U$. Regional groundwater wells located several km from the deposit also have distinct U isotopic characteristics, indicative of multiple components of uranium. The average of results for 11 water samples collected from the Chuviscar River, located near Aldama, about 50 km south of the Nopal I mine, also is given in Figure 6 (average $^{234}U/^{238}U$ activity ratio = 4.3 ± 0.2 (1σ); Villalba et al, 2006). The river drains alluvial fans and volcanic rocks of Sierra la Gloria that are similar to those in the Peña Blanca uranium district. Multiple hypothetical components shown in Figure 6 consist of 1) a high U component with $^{234}U/^{238}U$ activity ratios near unity, as would result from bulk dissolution of a rock in secular equilibrium, 2) a high U, high $^{234}U/^{238}U$ component, which reflects a greater recoil-related $^{234}U/^{238}U$ signature, and 3) a component with $^{234}U/^{238}U$ activity ratio near unity and low U concentration. Varying uranium concentrations of the components may be generated by any number of processes including dissolution/precipitation/sorption and evaporation/dilution.

Decreasing uranium concentrations in the new wells (Figure 5) can be modeled in a variety of ways, including physical and chemical models or combinations thereof. Here we present a simple physical model that places order-of-magnitude constraints on groundwater flow velocity. We use a one-dimensional tank model, where the tank consists of the SZ well volume that is continuously flushed with groundwater (Drost et al., 1968). We assume that uranium is introduced as a slug to each of the wells and transported as a conservative tracer by groundwater flow. Hence, U concentration, *C*, is a simple function of groundwater flow velocity or specific discharge. Since background U in groundwater is negligibly small compared to the U defined by the initial slug, we obtain the following relations derived for this study:

$$dC/dt = -2qhrC/V \qquad (1)$$

$$q = \frac{V}{2hr(t_2 - t_1)} \ln\left(C_1 / C_2\right) \qquad (2)$$

where q is the groundwater specific discharge, V is the saturated zone well volume (163-208 L), h is the casing perforation height (9.15 to 12.20 m), C_1 is the U concentration at time t_1 and C_2 that at t_2, and r is the well casing internal radius (4.825 cm). The model is only approximate, and additional factors are often included to account for flow distortion or skin effects from drilling, which can modify flow through the borehole relative to the surrounding formation (e.g., Drost et al., 1968). If the most likely chemical effects – U sorption and precipitation – were added to this model, it would reduce the flow required to decrease U concentrations with time, hence the physical model above may provide an upper limit on groundwater flow rates.

The most reliable velocity data are likely obtained from the initial decrease in U concentration in 2003, when the model is relatively unaffected by the background U in groundwater. Using 2003 data for all three wells, the model yields specific discharge of 0.7 to 2.3 m/y. Using a porosity value of 15% for the Pozos conglomerate (Dobson et al., 2008), this corresponds to groundwater

flow velocities, *v*, ranging from 5 to 15 m/y, where $v = q/n$, and n = porosity. The slow flow velocities obtained are not inconsistent with the evidence of interconnectivity observed between PB1 and PB2 during field tests (Oliver et al., 2005), as much higher flow rates would be expected during active pumping. ^{222}Rn measurements taken before and after pumping PB1 in August 2006 also indicate a relatively low specific discharge of ~ 2 m/y (Luo et al., 2007). Consequently, the uranium concentration and isotopic results, low well productivities, and ^{222}Rn constraints suggest slow saturated-zone groundwater flow with little or no regional-scale mixing at this location.

Uranium Constraints on Dissolution Inputs and Residence Times in the Shallow Unsaturated Zone

Uranium isotopic systematics for all adit waters collected from 1995-2006, including results obtained independently by Pickett and Murphy (1999) are shown in Figure 5 and appear to show a spatial dependence. In general, the overall range of ^{234}U/^{238}U activity ratios for the UZ (1-6) and SZ (1-5) are similar (Figures 6 and 7). The front adit generally has ^{234}U/^{238}U activity ratios near unity and higher U concentrations, as would result from dissolution of a rock in secular equilibrium. The rear adit is characterized by high ^{234}U/^{238}U activity ratios from 2-5 and variable U concentration, indicating a high recoil-related component and U concentration affected by varying U dissolution fluxes and/or rock-water interaction times. Finally, the middle adit appears to be a mixture of these two end members. There also may be a seasonal dependence, with samples collected in the wet monsoon season (July-December) tending to have higher ^{234}U/^{238}U and greater recoil signature than those collected in the January-June dry season (Ku et al., 2009). Here we discuss the stronger spatial dependence only.

These results can be evaluated using a model simulating a non-steady state situation for uranium isotope transport in groundwater, which provides constraints on in-situ radioisotope migration in dissolved and colloidal phases in terms of retardation factor and water-rock interaction time (Luo et al., 2000; Ku et al., 2009). For uranium, the model is based on the fact that water passing through the UZ has its U concentration and ^{234}U/^{238}U ratio modified by U dissolution from rocks and α-recoil input of ^{234}U from rock surfaces. The model predicts that intermittent UZ flushing gives rise to waters having a linear relationship between 1/[U] and ^{234}U/^{238}U (Figure 7).

The isotope mixing relations seen in Figure 7 appear scattered, and a linear model can only approximate the results. Similar range and scatter for the U isotopic systematics of UZ water near Yucca Mountain, Nevada, were observed by Paces et al. (2002). Scatter in both of these studies may be due to imperfect or insufficient sampling of the full range of natural conditions. However, the intercept and slope of the linear approximation reveals consistent results in terms of uranium dissolution inputs and/or water-rock interaction times. Samples from the front and middle adit correspond to low intercept (near secular equilibrium), reflecting increased U dissolution inputs toward the front adit, where the ore deposit is located. Their generally high U concentration and slope reflect longer rock-water interaction times. High intercept, low slope, and generally lower U concentration for samples from the back adit suggest that these samples have experienced decreased U dissolution inputs and variable but generally shorter water-rock interaction times. More detailed modeling of these results is presented in Ku et al. (2009).

Consistent with these results, shorter seepage times have been observed for the back adit relative to the front, based on rainfall measurements along with seepage results from transducer-monitored adit collector columns. Measured matrix permeabilities of the Nopal tuff are low (<0.1 millidarcy), thus flow through the altered tuff is predominantly controlled by fracture flow (Dobson et al., 2008). Although there are fractures throughout the adit, the back adit is characterized by greater and more rapid fracture flow than the front adit where the deposit is located. Evaporation during rapid fracture flow in the back adit in the summer monsoon season is expected to be quite limited. However, considerable evaporation can take place during the longer seepage times at the front, and seepage from the front adit generally has higher salinity and lower volume. Similar hydrogen and oxygen isotopic compositions of seepage water from the back adit and summer rainfall, and heavier hydrogen and oxygen compositions for seepage water from the front adit also support these conclusions.

Our preliminary results suggest that uranium dissolution inputs for the back adit for fractures with water-rock interaction times of ~0.5 days are ~1 ppb dissolved U/day. It may also be possible to determine dissolution fluxes for a wide range of elements in the UZ in the back adit, where complicating effects of evaporation and mineral precipitation on seepage water elemental abundance are relatively minor. Although we are aware of no other field measurements of this type, the U dissolution rate above can be compared to laboratory experiments that indicate rapid initial dissolution (~200 to 4000 ppb dissolved U/day) of soluble uranyl phases present in the suspended sediment of the Upper Puerco River, New Mexico (deLemos et al., 2008). Our estimate is two to three orders of magnitude lower, presumably due to differences in water/rock ratio and uranium characteristics of solid phases.

Uranium-Series Constraints on Radionuclide Mobility

Our ^{238}U-^{234}U-^{230}Th-^{226}Ra disequilibria measurements for groundwater samples located primarily in the UZ (Table 1) indicate that $^{230}Th/^{238}U$ activity ratios range from 0.005 to 0.48, and $^{226}Ra/^{238}U$ activity ratios range from 0.006 to 113. Following equations (7-9 or also 4,10) in Krishnaswami et al. (1982), for groundwater in contact with a solid matrix in secular equilibrium, activity ratios of long-lived U-series nuclides are inversely related to relative retardation factors. The rocks and some of the uranium minerals at Nopal I have ages >1 Ma, (Dobson et al., 2008; Fayek et al., 2006) and should be near secular U-series equilibrium. In addition, some of the younger secondary minerals deposited in fractures also are near secular equilibrium, with activity ratios ranging from 0.9 to 1.5 for $^{234}U/^{238}U$, 1.0 to 1.5 for $^{230}Th/^{238}U$, and 0.7 to 1.2 for $^{226}Ra/^{230}Th$ (Murrell, Goldstein, and Dixon, 2002). Consequently, $R_f(^{230}Th)/R_f(^{238}U)$ ranges from ~2-200, and $R_f(^{226}Ra)/R_f(^{238}U)$ ranges from ~0.009-170, where R_f is the retardation factor. Because $^{226}Ra/^{238}U$ ratios are highest in the UZ and lowest in the SZ, radium appears to have enhanced mobility in UZ waters near the deposit. This observation is similar to results obtained from U-series studies of surface fractures near the deposit, which indicate relatively recent mobility for ^{226}Ra (Murrell, Goldstein, and Dixon, 2002). It is also similar to results obtained for vegetation near the deposit (Leslie, Pickett, and Pearcy, 1999), which also show high levels of ^{226}Ra relative to ^{230}Th and ^{238}U. In the absence of significant Ra/U fractionation upon plant uptake, this would also indicate greater mobility of Ra in the UZ.

We also have studied the ^{238}U-^{239}Pu disequilibrium systematics for four SZ groundwater samples (PB1, PB2, PB3, and PB4) collected in December 2003. We did not measure any ^{239}Pu in any of the filtered samples, with the corresponding upper limit $^{239}Pu < 50$ atoms/g (see above). Uranium systematics for samples collected at this time are quite reproducible (Table 2), with sample PB3 having the highest U concentration of 966 ppb. Assuming that the Pu in sample PB3 would be naturally derived from neutron reactions with ^{238}U, comparison of the measured upper limit Pu/U ratio (2×10^{-14}; based on $^{239}Pu < 50$ atoms/g and U = 966 ppb) with the secular equilibrium ratio (based on the average Pu/U in old uranium ores of $\sim 2 \times 10^{-11}$ (Curtis et al., 1999) provides constraints on the relative mobility of Pu and U in the SZ. These results indicate that Pu mobility in the SZ at Peña Blanca is at least 3 orders of magnitude lower than the U mobility. Hence, $R_f(^{239}Pu)/R_f(^{238}U)$ is calculated to be ≥ 1000.

By combining long-lived nuclide data from this study with short-lived nuclide data (Luo et al., 2007), we estimate that $R_f(^{238}U)$ varies from ~30 to 7200, with an average value of 1300 (Table 5; Figure 8). Estimates of $R_f(^{238}U)$ are obtained from equations 5 and 9 in Luo et al. (2000), which in general at Peña Blanca reduce to $R_f(^{238}U) \approx A(^{222}Rn)/A(^{238}U)$, where A denotes activity. Estimated retardation factors for short-lived U-series nuclides also are obtained by comparing their activities with the ^{222}Rn activities, indicative of the supply rate of short-lived nuclides in the ^{238}U decay series due to recoil related effects (Krishnaswami et al., 1982). In addition, some samples in the UZ have values of $R_f(^{226}Ra)/R_f(^{238}U)$ near 0.01, indicating that for these samples $R_f(^{238}U) \geq 100$, since $R_f(^{226}Ra)$ must be ≥ 1.

Ranges of retardation factors for the SZ are ~10 to 10,000 for ^{238}U and ^{226}Ra, ~1000 to 10,000,000 for ^{230}Th, and >34,000 for ^{239}Pu. However, using the average value of 1300 for $R_f(^{238}U)$ in the SZ, the retardation factor for ^{239}Pu in the SZ is likely to be >1,000,000. Based on the data in Table 5 and Figure 8, average values of SZ retardation factors range from 10^3 to 10^7, and decrease in the order $^{239}Pu \approx ^{210}Po \approx ^{230}Th > ^{210}Pb > ^{238}U \approx ^{226}Ra$.

Using the average value of 1300 for $R_f(^{238}U)$ in the SZ, absolute retardation factors for U-series daughter nuclides in the UZ range from ~10 to 230 for ^{226}Ra and from ~1300 to 260,000 for ^{230}Th based on samples from the mine adit. Both ^{226}Ra and ^{230}Th have greater mobility in the UZ near the ore deposit than in the SZ. Greater UZ mobility for these nuclides is an unusual characteristic that may be related to higher sulfate concentrations for the UZ and near-field SZ relative to the far-field SZ (Civilian Radioactive Waste Management System Management & Operating Contractor, 2004). Greater mobility does not persist into the SZ, where retardation factors return to high values more typical of groundwater systems in general (e.g. Krishnaswami et al., 1982; Luo et al., 2000; Porcelli and Swarzenski, 2003).

Our results on U-series nuclide mobility at Peña Blanca can be compared to sorption data for Yucca Mountain tuff obtained from laboratory experiments (Sandia National Laboratories, 2007). In general, K_d values for U = 2-20 mL/g, for Ra and Th = 100-10,000 mL/g, and for Pu = 10-10,000 mL/g. Based on the porosity and bulk density of the Yucca Mountain tuffs, retardation factors are a factor of ~10 larger than the K_d values. Results presented here are consistent with some of these trends, but not all of them. Most notably, Yucca Mountain sorption data indicate that Ra should be retarded much more strongly than U. Since Ra mobility in the SZ at Peña Blanca is typical of groundwater in general, the major difference in the data

sets for the SZ appears to be related to U mobility. Specifically, U mobility appears to be a factor of 10-100 higher in the sorption data set relative to in-situ U-series measurements performed at Peña Blanca and other sites (Luo et al., 2000).

In order to define the uranium colloidal contribution, two SZ samples (PB1 and PB4) were ultrafiltered in the laboratory. Uranium concentration measurements (Table 4) indicate that ~93-97% of uranium present is truly dissolved. Similar $^{234}U/^{238}U$ for unfiltered, filtered (<200-nm), and ultrafiltered (<20-nm) aliquots also support this conclusion. These results are similar to studies for other uranium deposits such as Koongarra (Payne, Edis, and Seo, 1992), which indicate that as much as 6.5% of the uranium in groundwater is associated with colloids (<1 μm). These results also agree with results for groundwater from the Nevada Test Site (Abdel-Fattah et al., 2005). However, the small fraction of colloidal uranium could have environmental implications in some cases, as it can migrate in subsurface media much faster and can travel much greater distances than dissolved uranium (e.g., Kersting et al., 1999). This may be due to the presence of small quantities of highly mobile colloids within the colloid population (Robinson et al., 2007).

CONCLUSIONS

Our U-series results provide initial field data on uranium dissolution inputs (~1 ppb dissolved U/day) in the UZ. At Nopal I, our U concentration data suggest that SZ groundwater flow rates are slow (~10 m/y). We also obtained initial constraints on ^{238}U-^{239}Pu disequilibrium in the SZ, with Pu mobility >1000 times lower than the U mobility. Radionuclide transport rates in the SZ are, on average, factors of 10^3 to 10^7 lower than the groundwater flow rate and decrease in the order $^{226}Ra \approx ^{238}U > ^{239}Pu \approx ^{230}Th$. Both Ra and Th appear to have on average greater mobility (~×10) in the UZ than the SZ.

ACKNOWLEDGMENTS

We thank Ignacio Reyes and Rodrigo de la Garza (Universidad Autónoma de Chihuahua), José Alfredo Rodríguez Pineda (World Wildlife Fund), Paul Cook and Teamrat Ghezzehei (LBNL), and Paul Reimus, John Dinsmoor, and Ron Oliver (LANL) for valuable discussions and assistance in the field. We also thank Ardyth Simmons and Schön Levy (LANL) for project guidance.

This work was supported by the United States Department of Energy (U.S. DOE), Office of Civilian Radioactive Waste Management (OCRWM), under contract DE-AC02-05CH11231. The views expressed in this article are those of the authors and do not necessarily reflect the views or policies of the U.S. DOE or OCRWM.

REFERENCES

A. I. Abdel-Fattah, D. Smith, M. Murrell, S. Goldstein, A. Nunn, R. Gritzo, B. Martinez, and P. Reimus, "Colloid Characterization and Radionuclide Associations with Colloids in Source-Term Waters at the Nevada Test Site," Los Alamos National Laboratory report LA-UR-05-5312 (2005).

Civilian Radioactive Waste Management System Management & Operating Contractor (CRWMS M&O), "Natural Analogue Synthesis Report," CRWMS M&O Report TDR-NBS-GS-000027 REV01 (available URL: www.osti.gov/scitech/servlets/purl/883016), 2004.

D. Curtis, J. Fabryka-Martin, P. Dixon, and J. Cramer, "Nature's uncommon elements: plutonium and technetium," *Geochimica et Cosmochimica Acta* **63**, 275-285 (1999).

J. L. deLemos, B. C. Bostick, A. N. Quicksall, J. D. Landis, C. C. George, N. L. Slagowski, T. Rock, D. Brugge, J. Lewis, and J. L. Durant, "Rapid Dissolution of Soluble Uranyl Phases in Arid, Mine-Impacted Catchments near Church Rock, NM," *Environmental Science and Technology* **42**, 3951-3957 (2008).

P. F. Dobson, M. Fayek, P. C. Goodell, T. A. Ghezzehei, F. Melchor, M. T. Murrell, R. Oliver, I. A. Reyes-Cortés, R. de la Garza, and A. Simmons, "Stratigraphy of the PB-1 Well, Nopal I Uranium Deposit, Sierra Peña Blanca, Chihuahua, Mexico," *International Geology Review* **50**, 959-974 (2008).

W. Drost, D. Klotz, A. Koch, H. Moser, F. Neumaier, and W. Rauert, "Point Dilution Methods of Investigating Ground Water Flow by Means of Radioisotopes," *Water Resources Research* **4**, 125-146 (1968).

M. Fayek, M. Ren, P. Goodell, P. Dobson, A. Saucedo, A. Kelts, S. Utsunomiya, R. Ewing, L. Riciputi, and I. Reyes, "Paragenesis and Geochronology of the Nopal I Uranium Deposit, Mexico," *Proceedings of the 11th International High-Level Radioactive Waste Management Conference, April 30-May 4, 2006, Las Vegas, Nevada* (American Nuclear Society, La Grange Park, Illinois, 2006), pp. 55-62.

P. Goodell, J. A. Rodríguez Pineda, P. Dobson, S. Harder, and S. Levy, "Regional Hydrology and Uranium Occurrences around Nopal I," in "Final Report for the Peña Blanca Natural Analogue Project," S. Levy, compiler, Los Alamos National Laboratory report------ (2016).

S. J. Goldstein, M. T. Murrell, and D. R. Janecky, "Th and U isotopic systematic of basalts from the Juan de Fuca and Gorda Ridges by mass spectrometry," *Earth and Planetary Science Letters* **96**, 134-146 (1989).

Kersting, A.B.; Efurd, D.W.; Finnegan, D.L.; Rokop, D.J.; Smith, D.K.; Thompson, J.L. Migration of plutonium in groundwater at the Nevada Test Site, *Nature* **397**, 56-59 (1999).

S. Krishnaswami, W. C. Graustein, K. K. Turekian, and J. F. Dowd, "Radium, Thorium and Radioactive Lead Isotopes in Groundwaters: Application to the in Situ Determination of Adsorption-Desorption Rate Constants and Retardation Factors," *Water Resources Research* **6**, 1663-1675 (1982).

T. L. Ku, S. Luo, S. J. Goldstein, M. T. Murrell, W. L. Chu, and P. F. Dobson, "Modeling non-steady state radioisotope transport in the vadose zone – A case study using uranium isotopes at Peña Blanca, Mexico," *Geochimica et Cosmochimica Acta* **73**, 6052-6064 (2009).

B. W. Leslie, D. A. Pickett, and E. C. Pearcy, "Vegetation-derived insights on the mobilization and potential transport of radionuclides from the Nopal I natural analog site, Mexico," in *Scientific Basis for Nuclear Waste Management XXII, Materials Research Society Symposium Proceedings* (Materials Research Society, Pittsburgh, Pennsylvania, 1999), Vol. 556, pp. 833-842.

S. Luo, T. L. Ku, R. Roback, M. Murrell, and T. L. McLing, "In-situ radionuclide transport and preferential groundwater flows at INEEL (Idaho): decay-series disequilibrium studies," *Geochimica et Cosmochimica Acta* **64**, 867-881 (2000).

S. Luo, T. Ku, V. Todd, M. T. Murrell, and J. C. Dinsmoor, "Increased concentrations of short-lived decay-series radionuclides in groundwaters underneath the Nopal I uranium deposit at Pena Blanca, Mexico," *Eos Transactions, American Geophysical Union **88*** (23) Joint Assembly Supplement, Abstract GS22A-03 (2007).

M. T. Murrell, S. J. Goldstein, and P. R. Dixon, "Uranium Decay Series Mobility at Peña Blanca, Mexico: Implications for Nuclear Repository Stability," in *Eighth EC Natural Analogue Working Group Meeting, Proceedings of an International Workshop held in Strasbourg, France, from 23 to 25 March 1999*, H. von Maravic and W. R. Alexander, Eds. (Office for Official Publications of the European Communities, Luxembourg, Luxembourg, 2002), pp. 339-347.

R. D. Oliver, J. C. Dinsmoor, S. J. Goldstein, I. A. Reyes-Cortés, and R. De La Garza, "Initial Test Well Conditioning at Nopal I Uranium Deposit, Sierra Peña Blanca, Chihuahua, Mexico," *Geological Society of America Annual Meeting & Exposition Abstracts with Programs* **37** (7), 197 (2005).

J. B. Paces, K. R. Ludwig, Z. E. Peterman, and L. A. Neymark, "$^{234}U/^{238}U$ evidence for local recharge and patterns of groundwater flow in the vicinity of Yucca Mountain, Nevada, USA," *Applied Geochemistry* **17**, 751-779 (2002).

T. E. Payne, R. Edis, and T. Seo, "Radionuclide Transport by Groundwater Colloids at the Koongarra Uranium Deposit," in *Scientific Basis for Nuclear Waste Management XV, Materials Research Society Symposium Proceedings* (Materials Research Society, Pittsburgh, Pennsylvania, 1992), Vol. 257, pp. 481-488.

E. C. Pearcy, J. D. Prikryl, and B. W. Leslie, "Uranium transport through fractured silicic tuff and relative retention in areas with distinct fracture characteristics," *Applied Geochemistry* **10**, 685-704 (1995).

E. C. Pearcy, J. D. Prikryl, W. M. Murphy, and B. W. Leslie, "Alteration of uraninite from the Nopal I deposit, Peña Blanca district, Chihuahua, Mexico, compared to degradation of spent

nuclear fuel in the proposed US high-level nuclear waste repository at Yucca Mountain, Nevada," *Applied Geochemistry* **9**, 713-732 (1994).

D. A. Pickett and W. M. Murphy, "Unsaturated Zone Waters from the Nopal I Natural Analog, Chihuahua, Mexico – Implications for Radionuclide Mobility at Yucca Mountain," in *Scientific Basis for Nuclear Waste Management XXII, Materials Research Society Symposium Proceedings* (Materials Research Society, Pittsburgh, Pennsylvania, 1999), Vol. 556, pp. 809-816.

D. Porcelli and P. W. Swarzenski, "The behavior of U- and Th-series nuclides in groundwater," *Review of Mineralogy and Geochemistry* **52**, 317-361 (2003).

M. Rearick, P. Dobson, S. Goldstein, A. Rodríguez, and S. Levy, "Groundwater Analyses for Nopal I and the Peña Blanca Region, Chihuahua, México," in "Final Report for the Peña Blanca Natural Analogue Project," S. Levy, compiler, Los Alamos National Laboratory report xxxxx (2016).

Robinson, B.A.; Wolfsberg, A.V.; Viswanathan, H.S.; Reimus, P.W. A colloid-facilitated transport model with variable colloid transport properties. *Geophysical Research Letters* **34** 2007, L09401.

Sandia National Laboratories, "Site-scale Saturated Zone Transport;" Report MDL-NBS-HS-000010 REV03; Sandia National Laboratories: Albuquerque, New Mexico (available URL: www.lsnnet.gov/, Licensing Support Network accession number DEN001573977), 2007.

M. L. Villalba, L. H. Colmenero-Sujo, M. E. Montero-Cabrera, G. Manjón, R. Chávez-Aguirre, M. Royo-Ochoa, and A. Pinales-Munguía, "Presencia de Uranio en el río Chuvíscar, Estado de Chihuahua, México," *GEOS* **25**, 363-367 (2006).

A. M. Volpe, J. A. Olivares, and M. T. Murrell, "Determination of radium isotope ratios and abundances in geologic samples by thermal ionization mass spectrometry," *Analytical Chemistry* **63**, 913-916 (1991).

D. J. Wronkiewicz, J. K. Bates, S. F. Wolf, and E. C. Buck, "Ten-year results from unsaturated drip tests with UO_2 at 90°C: implications for the corrosion of spent nuclear fuel," *Journal of Nuclear Materials* **238**, 78-95 (1996).

Table 1. U-Th-Ra disequilibria systematics for unsaturated and saturated zone water samples collected in 2000-2001 measured by isotope dilution mass spectrometry.

Location	Sample ID	Date Collected	[U] (ng/g)	$^{234}U/^{238}U$ (activity ratio)	[Th] (pg/g)	[^{230}Th] (fg/g)	$^{230}Th/^{234}U$ (activity ratio)	[^{226}Ra] (fg/g)	$^{226}Ra/^{230}Th$ (activity ratio)	$^{226}Ra/^{238}U$ (activity ratio)
Unsaturated Zone:										
Perched water from borehole at +10 level	AS-5	25-Feb-00	5.734 ± 0.011	2.856 ± 0.003	136.7 ± 0.4	3.11 ± 0.03	0.0116 ± 0.0001			
Perched water from borehole at +10 level	030701-01	7-Mar-01	10.40 ± 0.002	2.051 ± 0.002				0.022 ± 0.001		0.0062 ± 0.0002
Front of Adit near UACH 1a	030701-05	7-Mar-01	13.01 ± 0.03	1.023 ± 0.002	17.13 ± 0.13	76.1 ± 0.2	0.349 ± 0.002	54.3 ± 0.3	34.4 ± 0.2	12.4 ± 0.1
Front of Adit near UACH 3	AS-1	25-Feb-00	68.46 ± 0.13	1.060 ± 0.001	8.76 ± 0.06	87.7 ± 0.5	0.0737 ± 0.0005	194 ± 5	106 ± 2	8.38 ± 0.19
Front of Adit near UACH 5	AS-2	25-Feb-00	36.92 ± 0.07	0.939 ± 0.002	6.72 ± 0.04	5.29 ± 0.03	0.00930 ± 0.00006	202 ± 1	1840 ± 10	16.2 ± 0.1
Front of Adit near UACH 5	030701-04	7-Mar-01	16.49 ± 0.05	0.920 ± 0.004	0.725 ± 0.003	42.8 ± 0.1	0.172 ± 0.001	>20	>20	>3
Middle of Adit near UACH 7	AS-3	25-Feb-00	4.035 ± 0.008	1.177 ± 0.002	0.73 ± 0.07	0.59 ± 0.02	0.0075 ± 0.0003	76 ± 6	6200 ± 600	56 ± 4
Middle of Adit near UACH 7	030701-03	7-Mar-01	26.96 ± 0.05	1.173 ± 0.001	0.66 ± 0.03	2.23 ± 0.01	0.00429 ± 0.00003	>470	>10000	>50
Back of Adit near UACH 9	AS-4	25-Feb-00	2.872 ± 0.009	2.207 ± 0.006	1.47 ± 0.03	1.57 ± 0.01	0.0151 ± 0.0001	5.51 ± 0.04	169 ± 2	5.68 ± 0.05
Back of Adit near UACH 9	030701-02	7-Mar-01	1.201 ± 0.003	2.588 ± 0.005	19.0 ± 0.5	18.8 ± 0.2	0.370 ± 0.003	46.0 ± 0.6	117 ± 2	113 ± 2
Saturated Zone:										
PB4	AS-6	25-Feb-00	2.528 ± 0.006	1.183 ± 0.003	604 ± 2	19.7 ± 0.1	0.402 ± 0.003			
Pozos Ranch	030701-06	7-Mar-01	5.711 ± 0.011	2.035 ± 0.002	<0.07			0.124 ± 0.003		0.0641 ± 0.0014

Errors are 2σ. Half-lives used are 4.468×10^9 yr for ^{238}U, 245250 yr for ^{234}U, 75690 yr for ^{230}Th, and 1600 yr for ^{226}Ra.

Table 2. Groundwater well uranium concentrations and $^{234}U/^{238}U$ activity ratios for samples collected in 2003-2006 measured by isotope dilution mass spectrometry.

Well	Sample ID	Date Collected	[U] (ng/g)	$^{234}U/^{238}U$ (activity ratio)
PB1	SPC1025028	1-Jul-03	802.3	1.029
	SPC1025022	6-Aug-03	328.0	1.058
	SPC1025029	29-Aug-03	166.5	1.021
	SPC1025044	9-Dec-03	241.4	1.011
	SPC1025047	9-Dec-03	194.9	1.028
	SPC1025049	9-Dec-03	77.69	1.050
	SPC1025058	5-Feb-04	92.96	1.006
	SPC1031344	17-Nov-04	43.88	1.044
	SPC1038245	11-Nov-05	32.82	1.010
	SPC2041865	21-Jun-06	22.91	1.040
	SPC1025068	23-Aug-06	60.68	1.102
PB2	SPC1025017	6-May-03	137.2	1.005
	SPC1025026	1-Jul-03	87.28	1.019
	SPC1025023	6-Aug-03	12.67	1.025
	SPC1025030	29-Aug-03	16.94	1.019
	SPC1025043	8-Dec-03	123.9	1.079
	SPC1025050	8-Dec-03	123.4	1.065
	SPC1025059	5-Feb-04	79.16	1.039
	SPC1031341	17-Nov-04	11.91	1.090
PB3	SPC1025019	7-May-03	18200	1.794
	SPC1025027	1-Jul-03	3596	1.363
	SPC1025024	6-Aug-03	5343	1.516
	SPC1025046	10-Dec-03	966.5	1.835
	SPC1025051	10-Dec-03	966.2	1.837
	SPC1025060	5-Feb-04	820.6	1.974
	SPC1031350	17-Nov-04	540.6	1.969
	SPC1038246	11-Nov-05	369.9	1.966
	SPC2041885	22-Jun-06	397.6	1.973
	SPC1025069	24-Aug-06	658.6	1.966
	SPC1025070	24-Aug-06	1077	1.862
PB4	032703-1	27-Mar-03	0.162	1.422
	SPC1025020	7-May-03	0.482	1.712
	SPC1025025	6-Aug-03	2.388	1.494
	SPC1025031	29-Aug-03	1.110	1.631
	SPC1025048	12-Dec-03	0.091	1.470
	SPC1025052	12-Dec-03	0.209	1.431
	SPC1025061	5-Feb-04	15.41	1.048
	SPC1031127	8-Apr-05	3.197	2.012
	SPC1040200	21-Mar-06	5.793	2.066
	SPC2041867	21-Jun-06	5.229	2.066
Pozos Ranch	020403-1	4-Feb-03	5.024	2.156
	SPC1025021	7-May-03	5.291	2.149
	SPC1025039	26-Sep-03	5.097	2.150
	SPC1031348	17-Nov-04	5.773	2.108
	SPC1031118	6-Apr-05	5.135	2.159
	SPC1038249	11-Nov-05	5.189	2.152
	SPC2041876	22-Jun-06	5.264	2.152

Table 2. Groundwater well uranium concentrations and $^{234}U/^{238}U$ activity ratios for samples collected in 2003-2006 measured by isotope dilution mass spectrometry (continued).

Well	Sample ID	Date Collected	[U] (ng/g)	$^{234}U/^{238}U$ (activity ratio)
Peña Blanca Ranch	020403-3	4-Feb-03	10.02	4.603
	SPC1025037	26-Sep-03	9.945	4.603
	SPC1031114	6-Apr-05	9.538	4.616

Typical errors (2σ) are <0.5% for [U] and <0.2% for $^{234}U/^{238}U$. Half-lives used are 4.468E9 yr for ^{238}U and 245250 yr for ^{234}U.

Table 3. Uranium concentrations and $^{234}U/^{238}U$ activity ratios for unsaturated zone samples collected from the mine adit in 2003-2006 measured by isotope dilution mass spectrometry.

Location	Sample ID	Date Collected	[U] (ng/g)	$^{234}U/^{238}U$ (activity ratio)
Front of Adit UACH 4	SPC1025062	11-Apr-05	6.034	0.999
Front of Adit UACH 5	SPC1025063	11-Apr-05	3.350	1.326
Front of Adit LBNL 39B	SPC1038735	11-Jan-06	90.76	1.186
Front of Adit LBNL 39B	SPC1040975	13-Dec-06	0.698	1.465
Front of Adit LBNL 47E	SPC1038778	11-Jan-06	422.4	0.817
Front of Adit LBNL 47E	SPC1041416	13-Dec-06	8.819	0.854
Middle of Adit UACH 6	SPC1025066	11-Apr-05	0.424	1.278
Middle of Adit UACH 6	SPC1038243	10-Nov-05	0.043	1.207
Middle of Adit UACH 7/7a	SPC1025056	29-Jan-04	17.97	1.313
Middle of Adit UACH 7/7a	SPC1025057	29-Jan-04	85.15	0.999
Middle of Adit UACH 8	SPC1025034	1-Jul-03	0.249	4.879
Middle of Adit UACH 8	SPC1025035	26-Sep-03	4.495	1.504
Middle of Adit UACH 8	SPC1025042	15-Oct-03	29.41	2.291
Middle of Adit UACH 8	SPC1025055	29-Jan-04	2.050	1.804
Middle of Adit UACH 8	SPC1025064	11-Apr-05	1.650	1.581
Middle of Adit LBNL 23B	SPC1038263	10-Jan-06	22.42	1.242
Middle of Adit LBNL 27C	SPC1038227	9-Nov-05	6.254	1.237
Middle of Adit LBNL 27C	SPC1040246	22-Mar-06	0.689	1.340
Middle of Adit LBNL 32A	SPC1040259	22-Mar-06	0.431	1.730
Middle of Adit LBNL 34E	SPC1040953	12-Dec-06	1.000	2.731
Back of Adit UACH 9	SPC1025033	1-Jul-03	0.357	2.570
Back of Adit UACH 9	SPC1025036	26-Sep-03	2.817	4.197
Back of Adit UACH 9	SPC1025041	15-Oct-03	0.443	5.181
Back of Adit UACH 9	SPC1025054	29-Jan-04	0.571	4.399
Back of Adit UACH 10	SPC1025032	1-Jul-03	2.838	3.625
Back of Adit UACH 10	SPC1025040	15-Oct-03	4.517	4.431
Back of Adit UACH 10	SPC1025053	29-Jan-04	3.349	2.573
Back of Adit UACH 10	SPC1025065	11-Apr-05	14.93	4.315
Back of Adit LBNL 4D	SPC1038005	8-Nov-05	12.03	4.785
Back of Adit LBNL 8B	SPC1037917	8-Nov-05	12.56	4.392
Back of Adit LBNL 11A	SPC1037936	8-Nov-05	1.439	5.526
Back of Adit LBNL 18A	SPC1037978	10-Nov-05	0.233	4.489
Back of Adit LBNL 18A	SPC1038255	10-Jan-06	0.088	2.966
Back of Adit LBNL 18A	SPC1040296	23-Mar-06	1.385	2.528
Back of Adit LBNL 18A	SPC2041957	26-Aug-06	0.518	3.697

Typical errors (2σ) are <0.5% for [U] and <0.2% for $^{234}U/^{238}U$. Half-lives used are 4.468E9 yr for ^{238}U and 245250 yr for ^{234}U.

Table 4. Comparison of uranium concentrations and $^{234}U/^{238}U$ ratios for unfiltered samples, samples filtered in the field, and ultrafiltered samples.

Location - Filtration	Sample ID	Date Collected	[U] (ng/g)	$^{234}U/^{238}U$ (activity ratio)
PB1 - unfiltered	SPC1031345	17-Nov-04	48.58 ± 0.11	0.995 ± 0.002
PB1 - <0.20 μm in field	SPC1031344	17-Nov-04	43.88 ± 0.09	1.044 ± 0.003
PB1 - ultrafiltered in lab	SPC1031345	17-Nov-04	45.64 ± 0.10	1.000 ± 0.002
PB4 – unfiltered	SPC1031127	8-Apr-05	3.237 ± 0.007	2.002 ± 0.003
PB4 - <0.20 μm in field	SPC1031127	8-Apr-05	3.197 ± 0.007	2.012 ± 0.003
PB4 – ultrafiltered in lab	SPC1031127	8-Apr-05	3.152 ± 0.007	2.009 ± 0.003

Errors are 2σ. Half-lives used are 4.468E9 yr for ^{238}U and 245250 yr for ^{234}U.

Table 5. Estimated retardation factors for various U-series nuclides for saturated and unsaturated zone samples. Data from this study and Luo et al. (2007).

Location	Sample ID	Date Collected	R_f-^{238}U	R_f-^{230}Th	R_f-^{226}Ra	R_f-^{239}Pu[1]
Saturated Zone:						
PB1	SPC1025068	23-Aug-06	370	900000	1500	
PB2	SPC1025072	25-Aug-06	7140	250000	420	
PB3	SPC1025069	24-Aug-06	34	7400	79	
PB3	SPC1025051	10-Dec-03				>34000
PB4	SPC1031127	8-Apr-05	240	95000	780	
Pozos Ranch	SPC1031118	6-Apr-05	130	5800000	2500	
Peña Blanca Ranch	SPC1031114	6-Apr-05	26	500000	690	
Average SZ			1300	1300000	1000	>1000000
Unsaturated Zone[2]:						
Range UZ				1300-260000	11-230	
Average UZ				73000	100	

[1]Value of R_f for ^{239}Pu determined from upper limit of $^{239}Pu/^{238}U$ for PB3 and value of R_f-^{238}U = 34. Based on the average SZ value of R_f-^{238}U = 1300, R_f-^{239}Pu would be greater than 1000000.
[2]Values of R_f for unsaturated zone samples determined from range and average of $^{230}Th/^{238}U$ and $^{226}Ra/^{238}U$ ratios from the mine adit and an average SZ value of R_f-^{238}U = 1300.

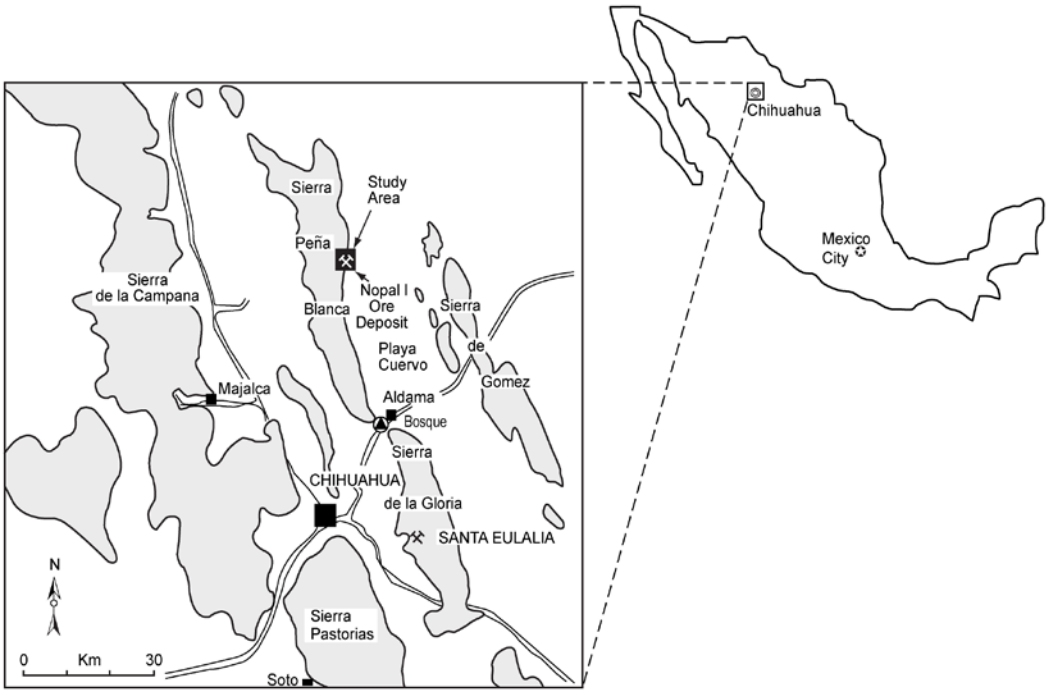

Figure 1. Location of study area. Assumed direction of groundwater flow is from the west to the east from the Sierra Peña Blanca toward the Playa Cuervo (Goodell et al., 2016). Bosque near Aldama is the location of sampling of the Chuviscar River by Villalba et al (2006).

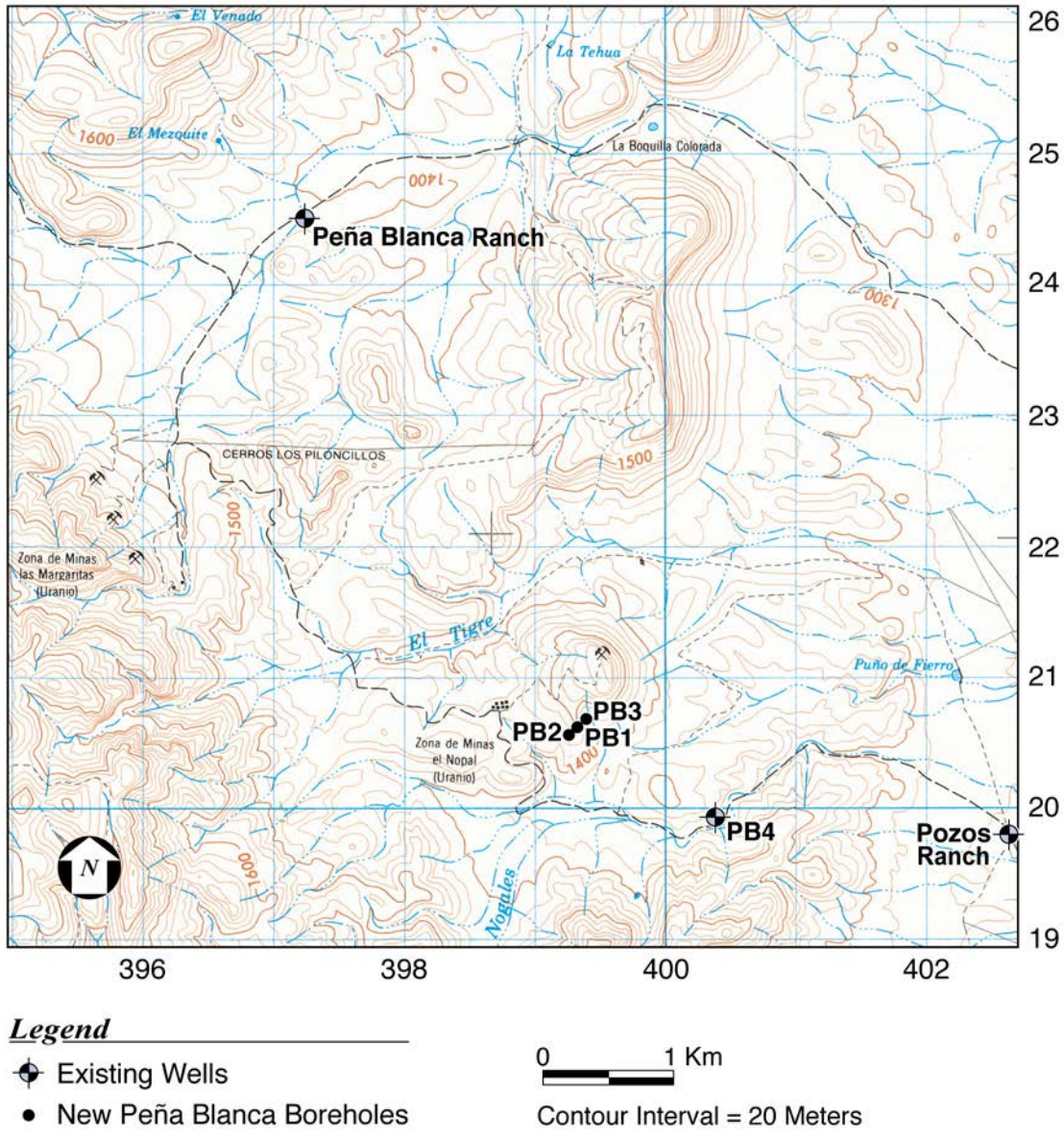

Figure 2. Location of wells in this study. Base map taken from Instituto de Estadística, Geografía e Informática 1:50,000 El Sauz topographic map (H13C46). Numbers along the border of the figure are Universal Transverse Mercator coordinates in hundreds of thousands of meters east and 32xx000 m north.

Figure 3. Schematic map of the UACH (Universidad Autónoma de Chihuahua) and LBNL (Lawrence Berkeley National Laboratory) unsaturated-zone sample-collection sites from the mine adit located on the +00 level. The collectors consisted of plastic sheeting designed to funnel seepage water into plastic bottles (blue boxes; UACH), or a fine grid of hard plastic collectors and bottles (red outlined boxes; LBNL). The LBNL collectors replaced the UACH collectors in 2005. Locations of the UACH collectors are approximate only. A fracture map of the mined ground surface (+00 at lower right, +10 in the rest of the figure), the extent of the uranium orebody (in gray), and orthogonal coordinate system in meters are from Pearcy, Prikryl, and Leslie (1995).

Figure 4. An array of LBNL seepage collectors along with a column equipped with transducers to measure the timing and volume of seepage events.

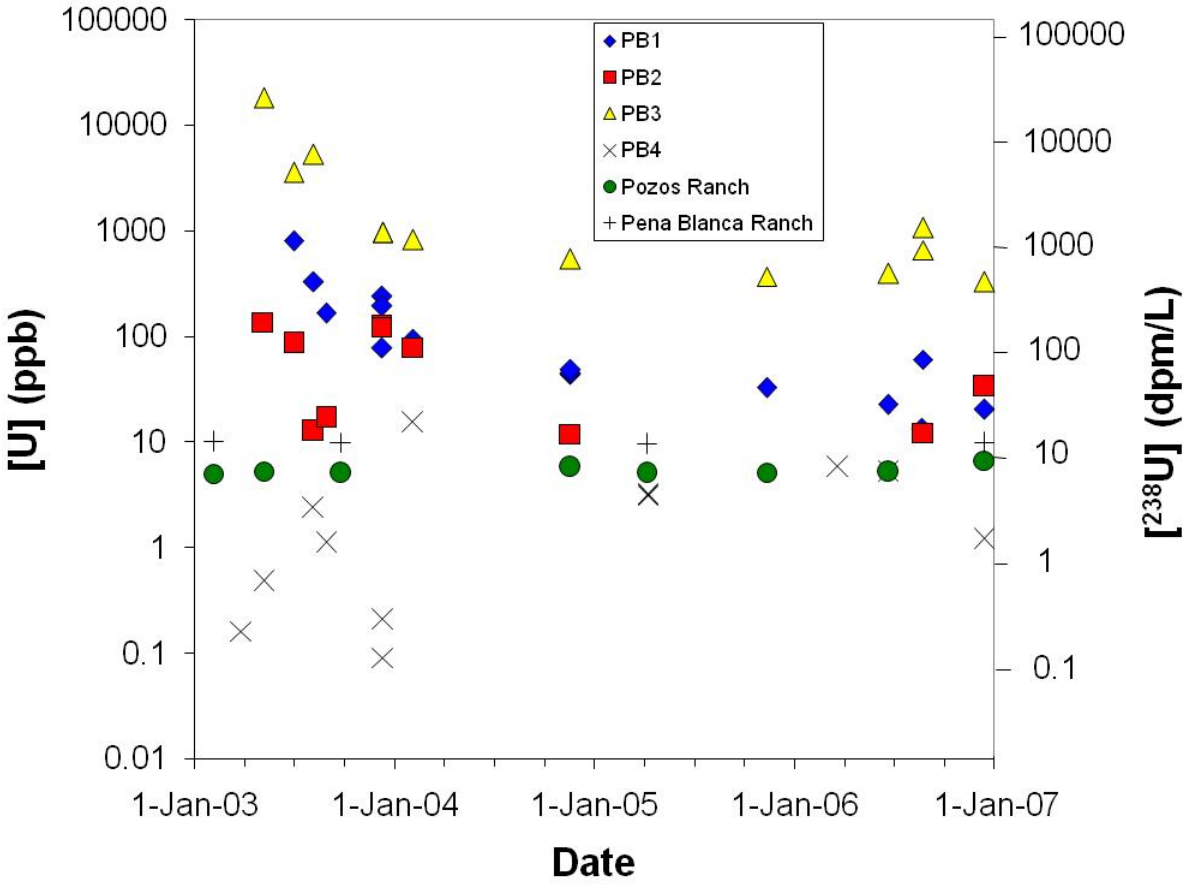

Figure 5. Time-series of uranium concentrations in saturated-zone groundwater samples near Peña Blanca. Uranium concentrations in Nopal wells drilled in 2003 (PB1, PB2, PB3) have generally exponentially decreased over time, although well pumping and conditioning in December 2003 and August 2006 disturbed the trend. Results for PB4, Peña Blanca Ranch, and Pozos Ranch have remained low over this time period. Results for December 2006 are from Rearick et al. (2016).

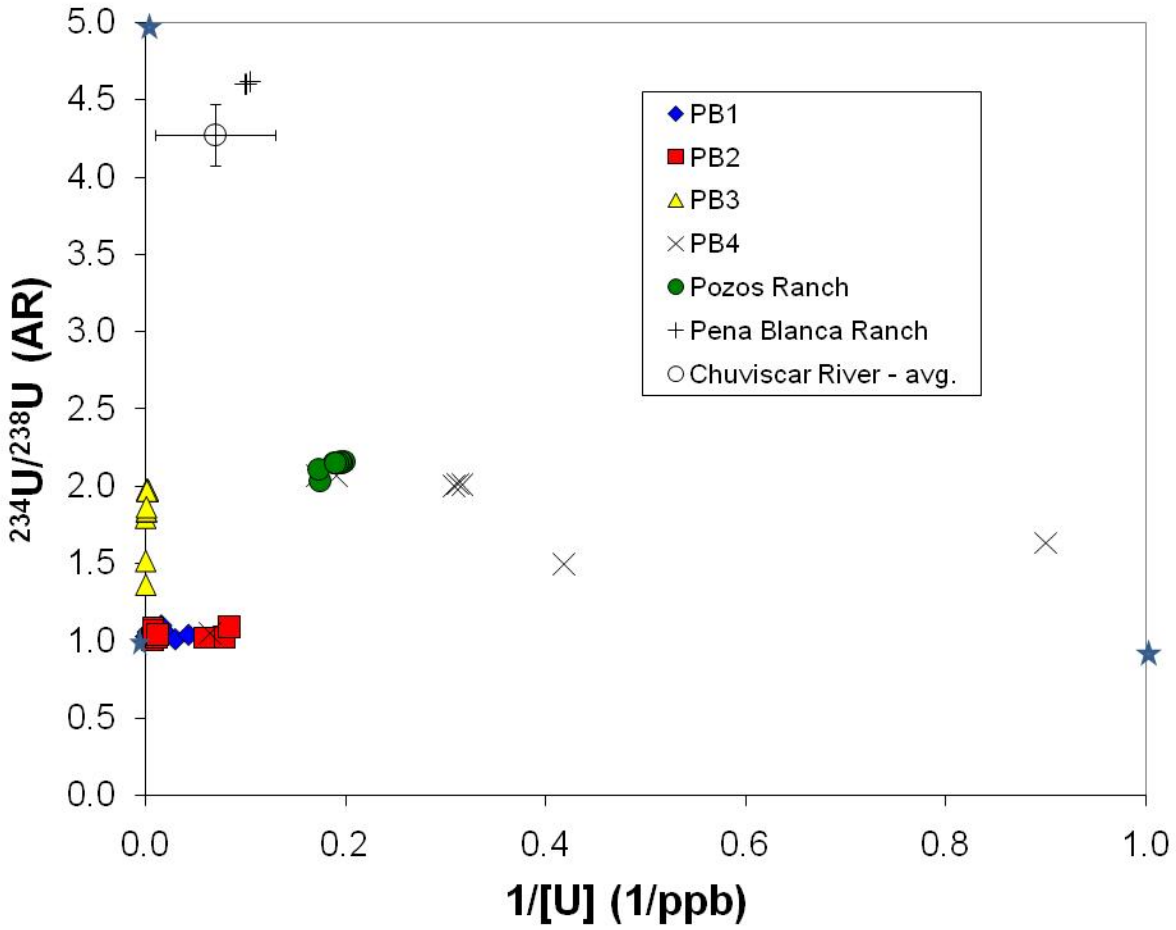

Figure 6. Uranium-isotope mixing diagram for groundwater samples from the saturated zone. Data with 1/[U] >1 not shown. At least three components for uranium (denoted by stars), with limited mixing between these components, are indicated. The values for PB1 and PB2 are an exception to this mixing scheme. Well pumping and conditioning results suggest interconnectivity of the groundwater in these two wells. See text for further discussion. Average values for Chuvíscar River calculated from data of Villalba et al. (2006).

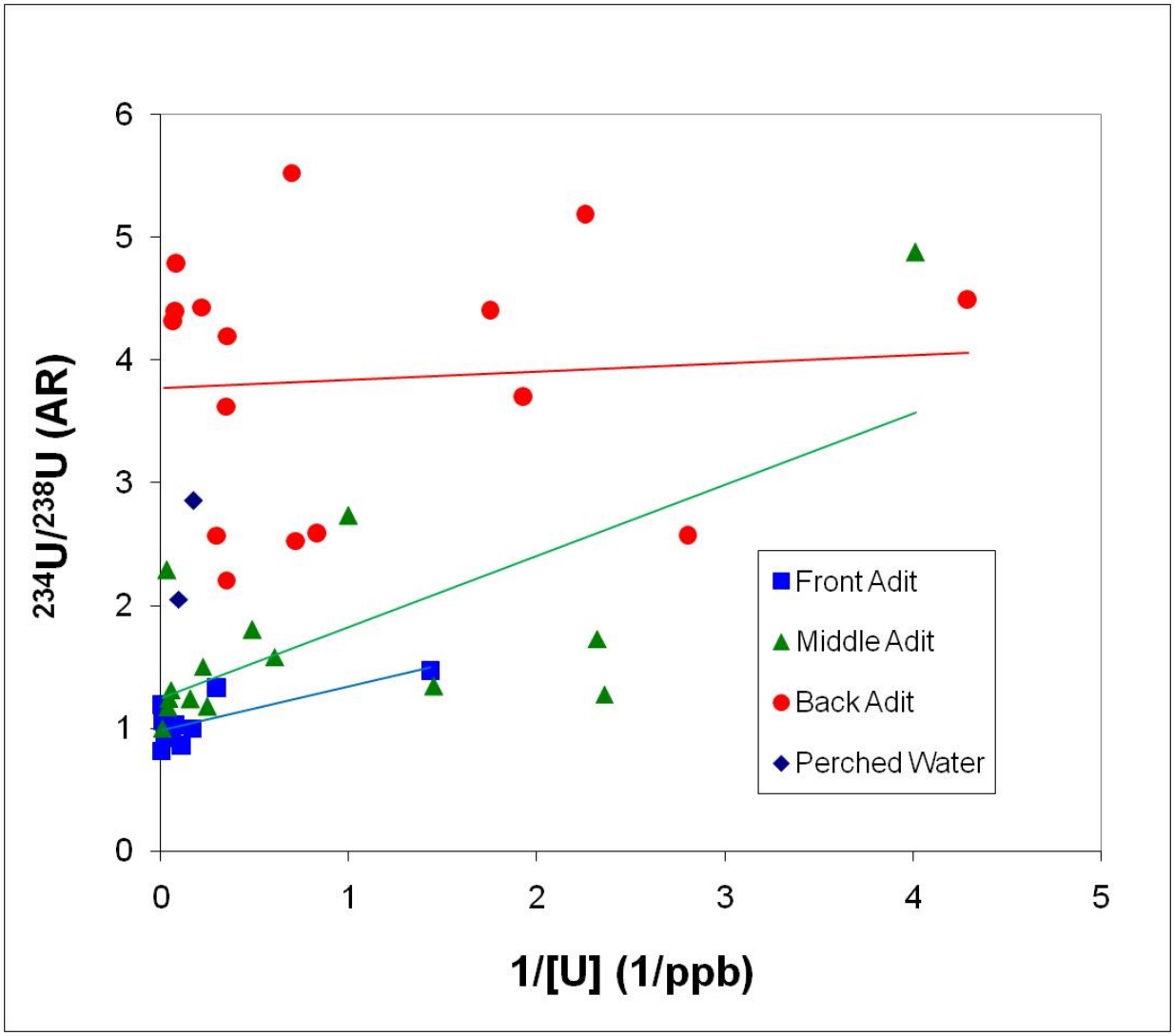

Figure 7. Uranium isotope mixing diagram for the adit water samples from the unsaturated zone. Data are from this study and Pickett and Murphy (1999). Data with 1/[U] > 5 not shown. A spatial dependence for the uranium isotopic systematics is indicated, and a weak seasonal dependence may also be present (Ku et al., 2009).

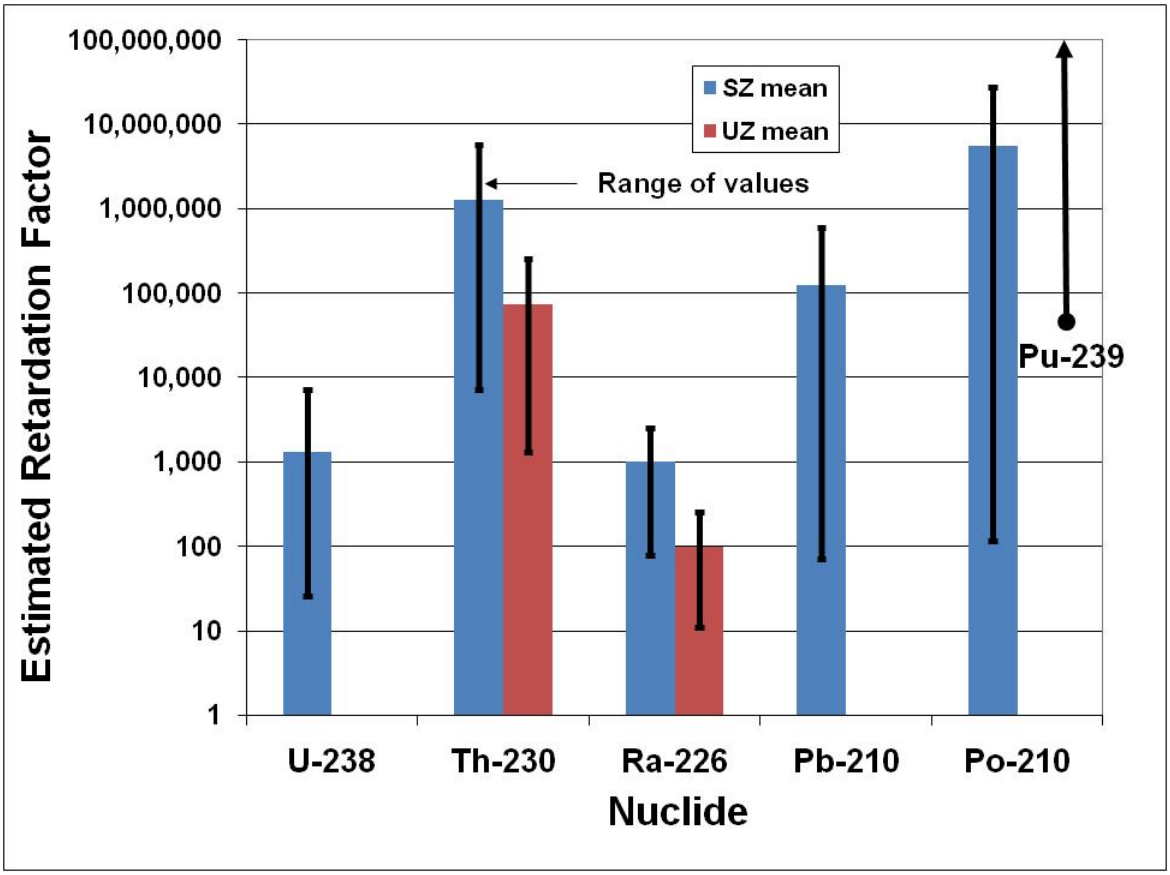

Figure 8. Graphical representation of the average and range of estimated retardation factors determined from U-series disequilibria for various U-series nuclides in the SZ and UZ. Average values of SZ retardation factors range from 10^3 to 10^7, and decrease in the order ^{239}Pu~^{210}Po~^{230}Th>^{210}Pb>^{238}U~^{226}Ra. Both ^{230}Th and ^{226}Ra appear to have greater mobility in the UZ than the SZ. Results are based on data from this study and from Luo et al. (2007).

NATURAL ANALOGUE STUDIES AT PEÑA BLANCA, MÉXICO: URANIUM-SERIES RADIOISOTOPE MEASUREMENTS

Teh-Lung Ku and Shangde Luo

INTRODUCTION

In managing nuclear waste disposal, an important mechanism in keeping the waste constituents away from human environments is their isolation by geological barriers. One measure of the effectiveness of such barriers is the transport rate of a radionuclide relative to that of groundwater, which can be bounded by parameters such as the retardation factor.

As part of a project entitled "Building Confidence in Yucca Mountain Performance through the Peña Blanca Natural Analogue," a study was conducted using naturally occurring decay-series radioisotopes as analogs for radioactive wastes. The study site was an abandoned uranium mine in Chihuahua, México (Figure 1). This site was considered to be a suitable analogue for Yucca Mountain, Nevada, that was characterized as a potential high-level nuclear-waste repository (Murphy, 1995). By studying the distribution of the U- and Th-series nuclides in groundwater of the mine area, we could evaluate in-situ transport rates of the different radioactive nuclides over a range of time scales following the methodologies of Ku et al. (1992,1998), Murrell et al. (2002), and Luo et al. (2000a,b). The evaluation involves modeling the radioactive disequilibria observed from the measurements. Such an evaluation could provide qualitative, corroborative information on radionuclide transport for performance-assessment models of geologic nuclear-waste disposal.

The abandoned uranium mine, Nopal I, is a uranium deposit in the Peña Blanca region approximately 50 km north of Chihuahua, México. This site that was investigated by the U. S. Department of Energy as a natural analog for spent fuel and its associated actinides and fission products at the potential high-level waste repository at Yucca Mountain, as the two sites have similar semi-arid to arid climates and thick, oxidizing unsaturated zones. The silicic tuffs of the host rock at both sites also are similar (Goodell, 1981; Murphy, 1995). The studies at Nopal I also are relevant to general issues of subsurface radionuclide migration in arid regions.

METHODS

Groundwater sampling was done during two field trips. The first trip took place in April 2005 to collect samples from the Peña Blanca, Pozos Ranch, and PB4 wells. The second trip, in September 2006, accomplished the sampling for the PB1, PB2, and PB3 wells drilled in 2003 through and adjacent to the Nopal I uranium deposit. Figure 1 shows the well locations in the study area.

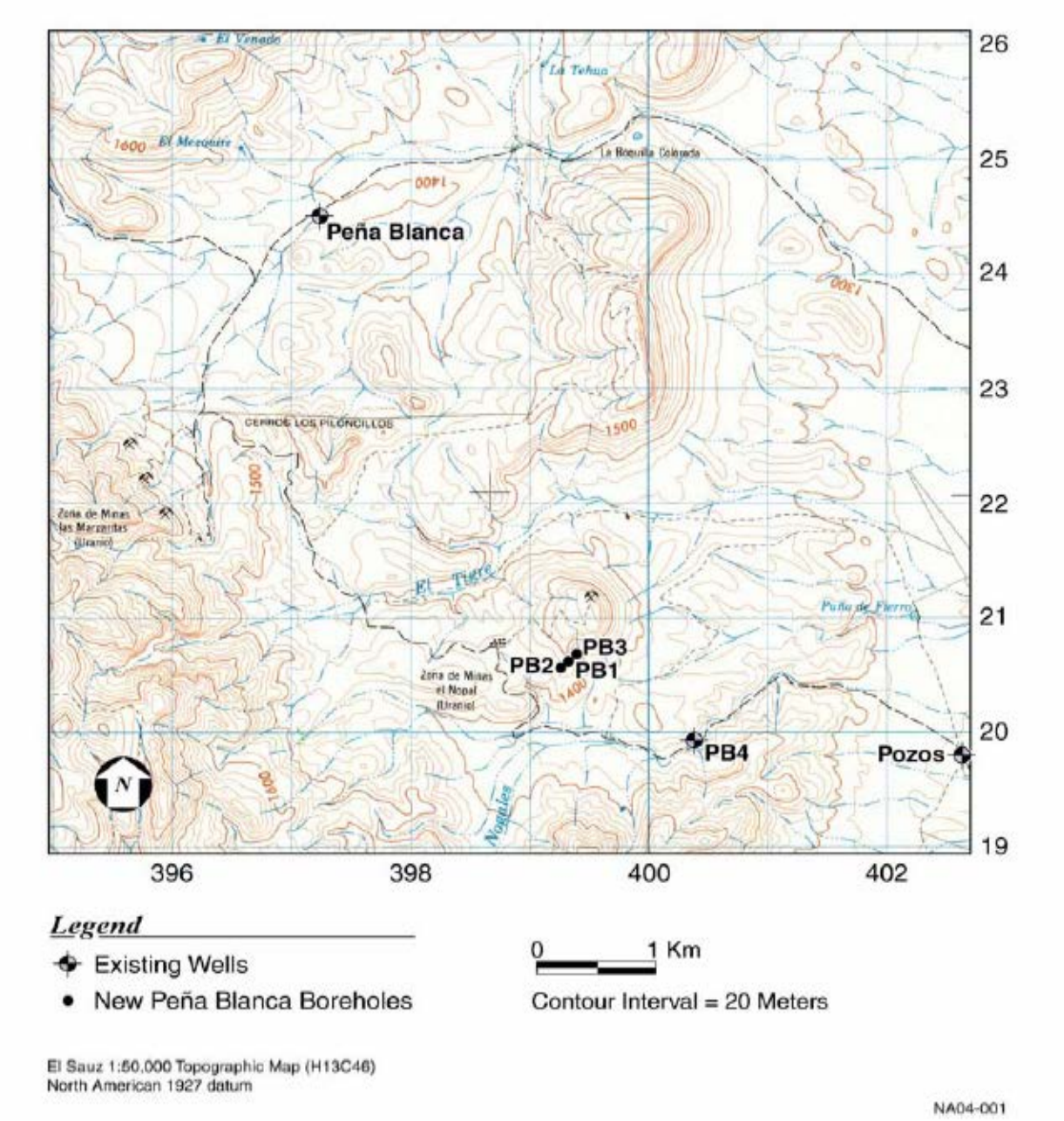

Fig. 1. Locations of the sampled wells in the Sierra Peña Blanca region, México. Numbers along the border of the figure are Universal Transverse Mercator coordinates in hundreds of thousands of meters east and 32xx000 m north.

Collection of Groundwaters for Isotope Analysis

We carried out two sampling trips in the field during this project, which took place in April 2005 and September 2006. The 2005 trip enabled us to sample the Peña Blanca ,

Pozos Ranch, and PB4 wells by the large-volume sampling method via in-situ MnO_2 fiber cartridge filtration for the analyses of a suite of decay-series nuclides. We also collected small-volume samples for radon analysis at these wells. Our second field trip in 2006 allowed us to complete the similar samplings for wells PB1, PB2, and PB3. During this trip, extra small-volume samples were collected at the start and end of the large-volume sampling to evaluate the changes in U, Pb and Rn isotope concentrations during the sampling.

Methods for groundwater collection and analysis followed those of Luo et al. (2000a). For analyses of ^{210}Po, ^{210}Pb and short-lived isotopes of Th and Ra, large volumes (from ~500 to mostly >1000 liters) of groundwater were pumped from each well using submersible pumps. The water was passed through a pre-filter cartridge (housing for polypropylene filter with a nominal pore size of 0.45 μm) to remove particles before passing through two serially connected in-line MnO_2-fiber cartridge filtration systems (Figure 2) that adsorb the nuclides. The difference in the adsorbed activities of a given isotope by these two MnO_2-fiber cartridges allowed the determination of the collection efficiency for the isotope.

Before sampling, each well was purged of about three times the well volume. Pumping rates were held to less than 10 liters/minute. A downhole probe was used to monitor pH, dissolved oxygen, temperature, and water level during the pumping.

After the large-volume sampling, groundwater samples were also collected from the wells in a sealed ~2 L glass bottle for analysis of ^{222}Rn by alpha-scintillation counting. The small-volume samples from wells PB1, PB2, and PB3 also were used for U and Po isotope analysis by alpha spectrometry.

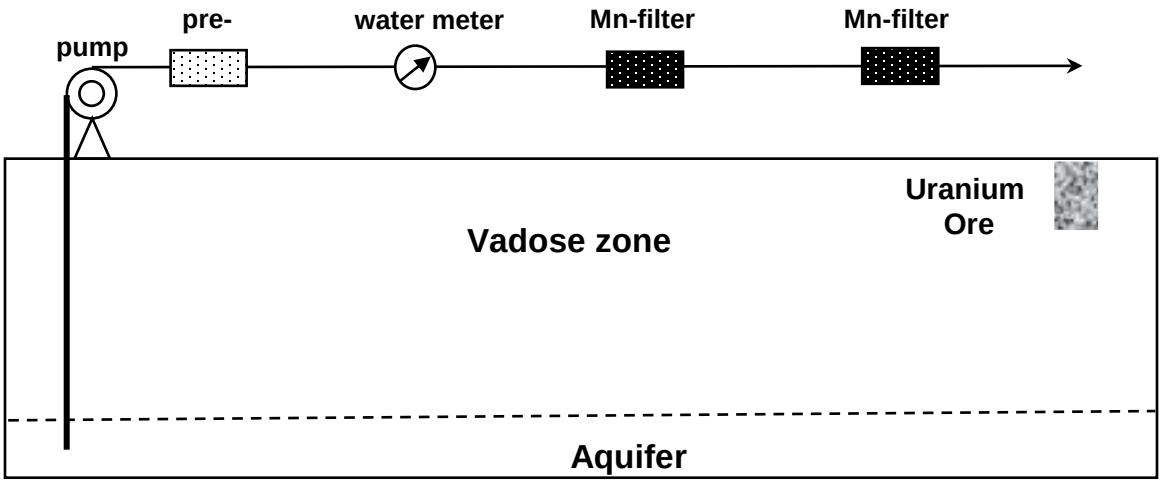

Fig. 2. Schematic drawing showing the in-line MnO_2-filber cartridge filtration system for in-situ large-volume sampling.

Radiochemical Analysis

Removal of Radionuclides from the MnO_2-fiber Cartridges

Each MnO_2-fiber cartridge was cut into small strips and immerged in about 200 mL of 4 M HCl in the presence of ^{236}U, ^{229}Th, ^{209}Po, Pb^{2+}, Ba^{2+}, and Fe^{3+} as yield tracers or carriers. Hydroxylamine hydrochloride ($NH_2OH \cdot HCl$) was added to the solution to facilitate the dissolution of MnO_2. When the fiber turned completely whitish, it was rinsed with de-ionized water, squeezed dry, and removed from the solution.

Co-precipitation of U, Th, Pb, and Po with $Fe(OH)_3$ and Ra with $BaSO_4$

The sample solution was adjusted to pH~7 by adding NH_4OH to precipitate $Fe(OH)_3$. The precipitate, which adsorbed isotopes of U, Th, Po, and Pb, was separated from the solution by 0.45-µm membrane filtration. The solution was then acidified to pH ~2 with nitrate acid. To the solution was added H_2SO_4 and Ra and Ba, which remained soluble in the solution during the $Fe(OH)_3$ precipitation, were co-precipitated out of the solution as $Ba(Ra)SO_4$. The precipitate was collected by 0.45-µm membrane filtration and burned in a Pt crucible to remove the polyethylene membrane.

Measurement of Ra Isotopes

The dry $BaSO_4$ precipitate was weighed and packed into a gamma-counting vial. The vial was immediately counted for short-lived ^{228}Ra, ^{224}Ra and ^{223}Ra in a well-type gamma spectrometer equipped with an ORTEC EG&G intrinsic Ge detector. After about three weeks, the counting vial was gamma-counted again for ^{226}Ra via the counting rate of the in-grown daughter nuclides of ^{214}Pb.

Measurement of ^{238}U, ^{210}Pb and ^{234}Th

The $Fe(OH)_3$ precipitate was dissolved with HCl and the solution was transferred into a gamma counting vial. The activities of ^{210}Pb and ^{234}Th were determined by counting the gamma photons with energies of 46.5 keV (for ^{210}Pb) and 63.3 keV (for ^{234}Th). ^{238}U activities were estimated by gamma-counting the ^{235}U activities (assuming that $^{235}U/^{238}U$ activity ratio = 0.046).

Measurement of ^{210}Po

After gamma counting for ^{210}Pb and ^{234}Th, the sample solution was transferred to a Teflon beaker and dried. The residue was dissolved with 1 M HCl. Ascorbic acid was then added to the solution until the yellow color of the solution turned clear. Polonium-210 and tracer ^{209}Po were self-plated onto a silver planchet at 80ºC for 4 hours and counted in an alpha spectrometer.

Measurement of U and Th Isotopes

After the ^{210}Po plating, concentrated nitrate acid was added to the sample solution to decompose the ascorbic acid and the solution was dried up on a hot plate. The residue was dissolved with 8 M HCl. Uranium and thorium isotopes in the solution were separated and purified by anion exchange. They were extracted separately into TTA-benzene solutions and plated onto stainless steel planchets for alpha spectrometric measurements.

Measurement of Radon in Small-Volume Samples

About 100-mL of the small volume groundwater sample was transferred to a glass vessel. The radon gas in the solution was purged out using He as a carrier gas and introduced into a pre-vacuumed radon-counting cell. After the cell stands for about two hours to allow radioactive equilibrium between radon and its daughter nuclides, the ^{222}Rn activity in the cell was counted in an alpha-scintillation counter. The counting efficiency of the cell was calibrated with an NIST ^{226}Ra standard.

Measurement of U and Pb Isotopes in Small-Volume Samples

About 2 to 10 ml of groundwater samples from wells PB1, PB2 and PB3 was each weighed for measurement of U isotopes by alpha spectrometry. The same samples were also analyzed for ^{210}Pb by alpha-counting techniques through the in-growth of its daughter isotope (^{210}Po). The samples were acidified and dried in the presence of ^{232}U and ^{209}Po spikes. The methods used for the Po and U isotope analysis were similar to those described above for the large-volume samples collected with MnO_2 fiber cartridges.

RESULTS AND DISCUSSION

Isotope activities are reported in Tables 1 through 8. The ^{222}radon isotopic activities in Table 1, ^{210}Pb isotopic activities in Table 5, ^{238}U activities in Table 6, and ^{234}Th activities in Table 7 are reported in disintegrations per minute per liter (dpm/L). Radium isotopic activities in Table 2, ^{210}Pb and ^{210}Po activities in Table 4, and $^{230, 232, 228}$Th activities in Table 7 are reported in disintegrations per minute per cubic meter (dpm/m^3). All uncertainties listed in the tables are one standard deviation (1σ) based on counting statistics. Preliminary results also have been reported by Luo et al. (2005, 2007).

^{222}Radon

Table 1 lists the ^{222}Rn activities in groundwater from Peña Blanca wells. Note that samples for these measurements were collected at the end of large-volume samplings except for well PB1 where water samples PB1(I) and PB1(II) were collected respectively before the beginning and after the completion of the large-volume groundwater sampling.

^{222}Rn activities were higher in PB1, PB2 and PB3 than in other wells in the area, providing evidence for the enrichment of uranium-series radionuclides in groundwater underneath the uranium ore body, the base of which is located in the vadose zone about 110 m above the water table (Levy et al., 2016). The enrichment indicates a local abundant supply of parent uranium or, alternatively, rapid transport of uranium and/or radium from the vadose zone to the saturated zone.

^{222}Rn activities at PB1 were significantly lower at the start of pumping, indicating that a long residence time of groundwater in wells could have caused a significant loss of ^{222}Rn to radioactive decay (the half-life of ^{222}Rn is 3.8 days; Ivanovich, 1992). If so, ^{222}Rn could provide a useful tracer for quantifying the groundwater residence time and transport velocity.

Table 1. ^{222}Rn activities in wells.

Well Identifier	^{222}Rn (dpm/L)
Peña Blanca	1831 ± 80
Pozos Ranch	1421 ± 67
PB4	595 ± 37
PB1(I)	9629 ± 135
PB1(II)	34966 ± 238
PB2	38238 ± 247
PB3	27146 ± 243

Radium Isotopes

Four radium isotopes (^{226}Ra, ^{228}Ra, ^{224}Ra, and ^{223}Ra) from large-volume groundwater samples were measured by gamma spectrometry. Their concentrations and activity ratios are shown in Table 2 and Table 3, respectively. In Table 3, ^{222}Rn/^{224}Ra activity ratios, estimated based on the ^{222}Rn activities in samples collected at the end of the large-volume sampling, are also listed for comparison.

Wells PB1, PB2, and PB3 show a very large variation in their dissolved radium activities, even though they are located within about one hundred meters of each other. The variation may reflect poor hydraulic connectivity among the wells.

The PB1, PB2, and PB3 waters from beneath the uranium ore deposits exhibit radium-isotope signals significantly different from those from the other three wells in the area. The waters from PB1, PB2, and PB3 have highly elevated activities in all four Ra

Table 2. Radium isotope activities in wells.

Well Identifier	^{226}Ra (dpm/m^3)	^{228}Ra (dpm/m^3)	^{224}Ra (dpm/m^3)	^{223}Ra (dpm/m^3)
Peña Blanca	268.2 ± 4.5	2614 ± 69	4984 ± 64	96 ± 52
Pozos Ranch	191.9 ± 4.5	622 ± 19	997 ± 16	29 ± 17
PB4	716.4 ± 7.0	540 ± 14	589 ± 10	29 ± 20
PB1	21246 ± 224	3501 ± 122	5781 ± 74	544 ± 95
PB2	85994 ± 535	4729 ± 165	10791 ± 92	1136 ± 366
PB3	339238 ± 1330	1028 ± 511	5537 ± 41	2611 ± 999

isotopes relative to those found in the Peña Blanca, Pozos Ranch, and PB4 wells, and are at the high end of the range for groundwater in general (e.g., Chapman, 1988; Clark and Turekian, 1990; King, Michel, and Moore, 1982; Krishnaswami et al., 1982; Luo et al., 2000a; Szabo et al., 2005; Scott and Barker, 1962, for semi-quantitative data).

Compared to the regional wells, the Nopal wells have very high and variable ^{226}Ra/^{228}Ra ratios (in contrast to the more consistent ^{224}Ra/^{228}Ra ratios), and much higher ratios of ^{222}Rn/^{224}Ra and ^{226}Ra/^{228}Ra. They have values of ^{223}Ra/^{224}Ra that range from slightly higher to one order of magnitude higher than values for regional wells. These results indicate that ^{226}Ra and ^{223}Ra are enriched in the aquifer rocks underneath the Nopal I uranium ore deposit, caused by rapid migration of uranium and/or radium from the uranium ore body in the vadose zone down to the underlying ground waters.

Table 3. Radium isotope ratios in wells.

Well Identifier	^{222}Rn/^{224}Ra	^{226}Ra/^{228}Ra	^{224}Ra/^{228}Ra	^{223}Ra/^{224}Ra
Peña Blanca	367 ± 17	0.103 ± 0.003	1.907 ± 0.056	0.019 ± 0.010
Pozos Ranch	1426 ± 71	0.309 ± 0.012	1.604 ± 0.056	0.029 ± 0.017
PB4	1011 ± 65	1.326 ± 0.036	1.090 ± 0.033	0.050 ± 0.034
PB1	6048 ± 88	6.07 ± 0.22	1.651 ± 0.061	0.094 ± 0.017
PB2	3544 ± 38	18.19 ± 0.65	2.282 ± 0.082	0.105 ± 0.034
PB3	4903 ± 57	330 ± 164	5.4 ± 2.7	0.472 ± 0.180

Lead and Polonium Isotopes

Table 4 presents the results for Pb and Po isotopes in groundwater obtained by large-volume sampling of wells at Peña Blanca. The results show that in wells away from the Nopal I uranium ore deposits (Peña Blanca, Pozos Ranch, and PB4), both ^{210}Pb and ^{210}Po activities are very low, reflecting the high affinity of these nuclides to the aquifer solids. In contrast, we find that these two nuclides show much higher and more variable activities in the wells PB1, PB2, and PB3 underneath the Peña Blanca uranium ore deposit. The highest values (281±0.8 dpm/L for ^{210}Pb and 230 ±17 dpm/L for ^{210}Po) were found in PB3, whereas the activities of ^{222}Rn in PB3 are comparable to those in PB1 or PB2.

In contrast to the large variability of the activities of ^{210}Pb and ^{210}Po, the activity ratio of ^{210}Po/^{210}Pb varies within one order of magnitude: from ~0.1 at Peña Blanca to ~1.0 at PB4. It shows no significant differences among the wells underneath the Nopal I uranium ore deposit (PB1, PB2, and PB3) and those wells far from the uranium deposit (Peña Blanca, Pozos Ranch, and PB4).

Table 5 shows a comparison of ^{210}Pb activities (dpm/m^3) obtained by small-volume sampling versus those by large-volume sampling (via in-situ MnO_2 fiber cartridge filtration) of the Peña Blanca wells. The small-volume sampling was done just before as well as just after the large-volume sampling. It is noteworthy that while there existed significantly higher ^{210}Pb activities in the wells prior to the large-volume sampling, the measured ^{210}Pb activities by large-volume sampling are more or less consistent with those measured through small-volume sampling at the end of large-volume sampling, and that the large variations in ^{210}Pb activities between PB1, PB2, and PB3 by large-volume sampling are also reflected by those through the small-volume sampling at the end of large-volume sampling. Whether the elevated ^{210}Pb activities in wells PB1 and/or PB3 prior to the large-volume sampling reflect a reduced retardation of radioisotopes in the wells remains unclear.

Table 4. ^{210}Pb and ^{210}Po activities in large-volume samples of regional groundwaters.

Well Identifier	^{210}Pb (dpm/m^3)	^{210}Po (dpm/m^3)	^{210}Po/^{210}Pb
Peña Blanca	45.5 ± 1.4	4.9 ± 0.3	0.108 ± 0.007
Pozos Ranch	3.2 ± 1.2	0.69 ± 0.07	0.216 ± 0.084
PB4	94.1 ± 4.3	95.3 ± 3.7	1.013 ± 0.061
PB1	(0.57 ± 0.04)×10^3	(0.43 ± 0.01)×10^3	0.750 ± 0.062
PB2	(18.2 ± 0.2)×10^3	(6.3 ± 0.6)×10^3	0.347 ± 0.033
PB3	(381 ± 0.8)×10^3	(230 ± 17)×10^3	0.605 ± 0.045

Table 5. ^{210}Pb activities in groundwater collected by small-volume and large-volume sampling.

Well Identifier	^{210}Pb (I), (dpm/L)	^{210}Pb (II), (dpm/L)	^{210}Pb (L), (dpm/L)
PB1	1.7 ± 0.3	1.0 ± 0.3	0.57 ± 0.04
PB2	not sampled	6.6 ± 0.5	18.2 ± 0.2
PB3	970 ± 48	256 ± 10	281 ± 0.8

Notes:
I: small samples collected prior to large-volume sampling; II: small samples collected after large-volume sampling; L: large-volume sampling.

In its report, *Technical Evaluation Report on the Content of the U.S. Department of Energy's Yucca Mountain Repository License Application; Postclosure Volume: Repository Safety After Permanent Closure*, the U.S. Nuclear Regulatory Commission (NRC; 2011) identified only one specific further information need: additional data on the abundance and behavior of ^{210}Po. According to the report, "A source of uncertainty is the potential contribution to dose from Po-210, a daughter of Pb-210 in the U-238 decay chain. There are some observations to indicate that Po-210 may not be removed by sorption from natural waters as readily as its immediate parent, Pb-210…At two locations in the United States, Po-210 has been measured in groundwater at concentrations greater than would be expected based on measured Pb-210 concentrations." The NRC concluded that DOE assumptions that short-lived daughters (half-life less than 180 days) are in secular equilibrium with their parent primary radionuclide and that deviations from secular equilibrium would not significantly affect dose calculations for the groundwater exposure scenario in the biosphere model required further confirmation.

An NRC literature review suggested that excess ^{210}Po is more likely to be found in reducing, alkaline groundwaters with organic content and microbial-mediated sulfur cycling. NRC conceded that, in the Yucca Mountain saturated zone system, groundwater near the boundary with the accessible environment is characterized by oxidizing waters of neutral pH (6.8 to 8.5 with a median of 7.85, low organic content, and no measurable sulfide. Therefore, a recommendation was made that DOE should provide groundwater data for the flow path away from Yucca Mountain to support the absence of geochemical conditions associated with excess polonium in other locations.

The activity ratios of ^{210}Po/^{210}Pb given in Table 4 indicate little or no excess of ^{210}Po relative to ^{210}Pb in the oxidizing, near-neutral-pH (Rearick et al., 2016) saturated-zone groundwaters of the Peña Blanca region. These results suggest only minor differences in sorption behavior between parent and daughter radioisotopes. The NRC (2011) posited that the difference in sorption of the much longer-lived parents at the head of the ^{238}U decay chain relative to ^{210}Po is more significant than the relative sorption of the immediate parent, ^{210}Pb. Activity ratios of ^{210}Po/^{238}U, calculated from data in Table 4 and mean ^{238}U activities from Table 6, range from 7.0 to 1,340.4 for the Nopal wells.

These values indicate excesses of ^{210}Po by the NRC standard in the groundwater below the Nopal uranium deposit. Analytical values are not available to calculate this ratio for the regional wells, and the question remains whether any of these wells are within flow paths downgradient of the Nopal cuesta and therefore suitable sources of analogue far-field data. The issue raised by the NRC (2011) therefore is not completely addressed by the Peña Blanca data, although the data for regional wells in Table 4 do indicate ^{210}Po activities reduced by about one to five orders of magnitude relative to its activities in the Nopal wells.

Uranium Isotopes

Table 6 shows the measurements of U isotopes in ground waters from the wells at Nopal I by the different sampling methods. The ^{238}U activities in waters obtained by large-volume sampling agree within the uncertainties with those in water collected by small-volume sampling just after the large-volume sampling, although there are variations of ^{238}U activities in the latter water collected prior to and after the large-volume sampling. The table also shows ^{238}U activities converted to parts per million (ppm; e.g., Ivanovich and Murray, 1992) for ease of comparison with the results of Goldstein et al. (2016).

The highest ^{238}U activity occurs in PB3 where high activities for other isotopes are also found. It should be noted that the ^{238}U activity is so high that MnO_2-fiber cartridges A and B used in the large-volume sampling both became saturated with respect to uranium, rendering the ^{238}U concentration of the PB3 well undeterminable by our methodology. Therefore, the ^{238}U/^{232}Th ratio was estimated based on the ^{238}U concentration in the small-volume sample collected at the end of large-volume sampling.

The large differences in concentrations of uranium and other radioisotopes among wells PB1, and PB2, and PB3 support the concept of poor hydraulic connections, despite the 50- to 100-m mutual proximity of the wells (Oliver et al., 2005). The differences may reflect the existence of preferential pathways, probably fractures, for transport of groundwater and radioisotopes from the vadose zone to the aquifer as well as transport within the aquifer.

The ^{234}U/^{238}U ratios vary in the order of PB1<PB2<PB3. This order differs from the PB2<PB1<PB3 pattern of ^{238}U activity among the wells, suggesting that there could be different mechanisms controlling the geochemical behavior of U isotopes in ground waters among these three wells.

The data in Table 6 make interesting comparisons to the larger data set of Goldstein et al. (2010, 2014) from mostly bailed water samples. For PB3, our data fall within the trend of very high ^{238}U concentration (approximately equivalent to total uranium) and variable ^{234}U/^{238}U values found by Goldstein et al. (2010, 2016). Our PB1 ^{238}U concentration values are within the range of total-uranium values in the larger data set, although one of our samples has a slightly higher ^{234}U/^{238}U value. Our PB2 analyses have ^{238}U contents substantially lower than any other saturated-zone water sample from the PB wells at Nopal I (Goldstein et al., 2016, Table 2). The uranium concentrations are similar to the

highest values for saturated-zone water samples from the PB4 well, which have quite variable uranium content (Goldstein et al., 2016, Table 2). The single PB2 $^{234}U/^{238}U$ ratio from our study is within the range of values for PB4 (Goldstein et al., 2016, Table 2). Our PB2 uranium-concentration data also are within the ranges of values for shallow unsaturated-zone waters around Nopal I (Goldstein et al., 2016, Table 3; Rearick et al., 2016, Table 2).

One possible explanation of our PB2 data could be the existence of a hydrologically productive zone within the limestone that is present about 13 m below the water table. This same limestone constitutes the entire section of the PB4 well. The extensive pumping of PB2, even at a relatively low pumping rate, may have exhausted the local supply of water interacting with uraniferous rocks in the very shallow saturated zone or derived from downward percolation through the volcanic rocks that host the uranium ore. As pumping continued, an increasing proportion of water from the low-uranium limestone may have entered the filtration and sampling system. Gross-gamma geophysical logging in PB2 did not extend into the limestone, so we have no direct indication of low uranium content. However, the gamma log for PB1 does indicate low counts in the limestone (Dobson et al., 2008).

The correlation suggests that the enrichment of uranium in the aquifer rocks comes from secondary minerals, not from the primary uranium ore deposits that should have a $^{234}U/^{238}U$ ratio close to unity. If so, the enrichment could have occurred within the last several hundreds of thousands of years.

Table 6. Uranium isotopes in large- and small-volume samples.

Well Identifier	Sample type	^{238}U (dpm/L)	^{238}U (ppm)	$^{234}U/^{238}U$
PB1	Small-volume (I)	20.5 ± 1.2	27.5	1.01 ± 0.08
	Small-volume (II)	78.3 ± 5.6	104.9	1.24 ± 0.09
	Large-volume	85.8 ± 0.4	114.1	
PB2	Small-volume (II)	4.3 ± 0.7	5.8	1.64 ± 0.33
	Large-volume	5.0 ± 0.2	6.7	
PB3	Small-volume (I)	1037 ± 40	1390	1.85 ± 0.06
	Small-volume (II)	701 ± 38	939	1.89 ± 0.04
	Large-volume	n.d.*	n.d.*	n.d.*

Notes:
Roman numerals for small-volume samples indicate samples collected at the beginning (I) or end (II) of large-volume sampling. For PB2, the small-volume sampling took place only at the end of large-volume sampling.
*The high ^{238}U concentration in PB3 caused MnO_2-fiber cartridges A and B to be saturated with respect to uranium, so that no ^{238}U concentration could be determined (n.d.).

Thorium Isotopes

Measurements of the activities and activity ratios of thorium isotopes (^{234}Th, ^{230}Th, ^{232}Th, and ^{228}Th) are listed in Tables 7 and 8, respectively. Table 7 shows low ^{232}Th concentrations at Peña Blanca and Pozos Ranch, typical for groundwater and consistent with the low solubility of thorium in natural waters. However, abnormally high concentrations of ^{232}Th are present in other wells of the area, particularly at PB3 where the concentration is about 3 orders of magnitude higher than that at Pozos Ranch. This elevated thorium concentration may be attributed to an occurrence of colloids in the groundwater.

The thorium-isotope measurements also show higher ^{230}Th concentrations and/or higher ^{230}Th/^{232}Th activity ratios (Table 8) in the groundwater at Nopal I. ^{230}Th is a product of the ^{238}U decay series, whereas ^{232}Th is the parent of a separate decay series (e.g., Ivanovich, 1992). The high ^{230}Th/^{232}Th ratios suggest that there is a local source of uranium in the aquifer rocks, based on an assumption that most of the ^{230}Th is produced *in situ* rather than being transported from the Nopal I ore body. This is consistent with observations of uranyl-activated ultraviolet fluorescence in the Pozos Formation within about four meters of the static water level (Levy et al., 2016). Fayek et al. (2006) reported a uranium content of about 475 parts per million for the uranium-rich portion of the Pozos Formation about 25 m above the saturated zone.

Measurements of the ^{228}Th/^{232}Th ratio (Table 8) show no significant differences between the wells affected by the Nopal I uranium ore deposit (PB1, PB2, and PB3) and those unaffected by the deposit (Peña Blanca, Pozos Ranch, and PB4). These observations suggest that the geochemical behavior of thorium-series radioisotopes shows no significant differences among these wells except for the concentrations of long-lived thorium isotopes (^{232}Th and ^{230}Th) that are much higher in the ground waters from PB1, PB2, PB3 and PB4 and may imply the occurrence of high concentrations of colloids in these wells. The measured activities of ^{228}Th in all wells are about two orders of magnitude higher than those of ^{232}Th. They are little affected by the occurrence of colloids in the groundwater owing to the fact that they are mainly supported by the radioactive decay of the soluble ^{228}Ra in groundwater, as is seen by their general correlation with the activities of ^{228}Ra (cf. Tables 2 and 7).

Similarly, the activities of the short-lived ^{234}Th are supported mainly from the radioactive decay of the soluble uranium parent (^{238}U). For instance, high ^{234}Th activities are found in the PB1 and PB3 wells where high ^{238}U activities are present (Table 7).

Table 7. Th isotope activities in large-volume samples.

Well Identifier	^{234}Th (dpm/L)	^{230}Th (dpm/m^3)	^{232}Th (dpm/m^3)	^{228}Th (dpm/m^3)
Peña Blanca	0.055 ± 0.018	0.375 ± 0.026	0.098 ± 0.012	11.75 ± 0.39
Pozos Ranch	0.069 ± 0.028	0.083 ± 0.008	0.024 ± 0.004	4.61 ± 0.12
PB4	0.112 ± 0.057	5.86 ± 0.24	2.14 ± 0.10	8.67 ± 0.34
PB1	4.81 ± 0.05	35.31 ± 0.87	0.76 ± 0.04	54.5 ± 1.3
PB2	1.65 ± 0.10	144.5 ± 7.2	8.03 ± 0.48	53.4 ± 2.7
PB3	39.64 ± 0.49	3646 ± 149	34.6 ± 1.5	54.0 ± 2.3

Table 8. Thorium isotope ratios in groundwater collected by large-volume sampling

Well Identifier	^{238}U/^{232}Th (10^3)	^{230}Th/^{232}Th	^{228}Th/^{232}Th	^{228}Th/^{228}Ra
Peña Blanca	—	3.84 ± 0.54	120 ± 15	0.0045 ± 0.0002
Pozos Ranch	—	3.40 ± 0.66	190 ± 32	0.0074 ± 0.0003
PB4	—	2.74 ± 0.17	4.1 ± 0.2	0.0161 ± 0.0008
PB1	112.5 ± 5.9	46.3 ± 2.7	71.4 ± 4.1	0.0156 ± 0.0007
PB2	0.63 ± 0.04	18.0 ± 1.4	6.7 ± 0.5	0.0113 ± 0.0007
PB3	20.3 ± 1.4	105.5 ± 6.4	1.6 ± 0.1	0.053 ± 0.026

SUMMARY OF MAJOR FINDINGS

- Elevated concentrations of radioisotopes, both long- and short-lived, were found in ground waters (in particular in PB3) underneath the Peña Blanca uranium ore deposit, suggesting a rapid transport of uranium and radium from the vadose zone, where the ore deposit is located, to the underlying groundwater.

- Very different radioisotope concentrations were observed from the wells PB1, and PB2, and PB3, although all these wells are located close to each other within only about one or two hundreds of yards. This provides evidence for the

- poor hydraulic connection of groundwater in the aquifer at the site. They also provide evidence for the occurrence of preferential pathways (likely the large rock fractures) for transport of groundwater and radioisotopes from the vadose zone to the aquifer as well as the transport within aquifer.

- There exists an elevated concentration of colloids in the ground waters in PB1 through PB4, which may facilitate the transport of many particle-reactive radioisotopes

- A preliminary U-series modeling suggests that:

    A. The groundwater discharge rate is about $(1.93\pm0.03)\times10^3$ L m^{-2} yr^{-1} at PB1 and for a porosity of (0.197±0.029), this rate can be translated to a groundwater transport velocity of (9.8±1.4) m yr^{-1}.
    B. The mean fracture width is estimated to vary from ~0.2 to ~4.0 μm in the region, with the larger mean fracture width occurring mostly wells PB1 through PB4.
    C. The apparent retardation factors of Ra in PB1, PB2, and PB3 are very similar and show no significant difference with those of $\sim10^3$ in other regional wells. The effective transport velocity of Ra is estimated to be ~10 m kyr^{-1}, assuming the groundwater discharge rate to be about $(1.93\pm0.03)\times10^3$ L m^{-2} yr^{-1} in the aquifer at the site.
    D. The apparent retardation factors of Th are smaller than those of Ra by about two to three orders of magnitude, and they decrease with increasing concentrations of colloids in wells PB1 through PB4.
    E. High apparent retardation factors, comparable to those of Th, were also found for Po and Pb in wells with low concentrations of colloids. For wells PB1 through PB4 (PB3 in particular), the increased concentrations of colloids can significantly reduce the apparent retardation factors of Po and Pb.

REFERENCES

J. B. Chapman, "Chemical and Radiochemical Characteristics of Groundwater in the Culebra Dolomite, Southeastern New Mexico," New Mexico Health and Environment Department, Environmental Improvement Division, Environmental Evaluation Group report EEG-39 (March 1988).

J. F. Clark and K. K. Turekian, "Time scale of hydrothermal water-rock reactions in Yellowstone National Park based on radium isotopes and radon," *Journal of Volcanology and Geothermal Research* **40**, 169-180 (1990).

P. F. Dobson, M. Fayek, P. C. Goodell, T. A. Ghezzehei, F. Melchor, M. T. Murrell, R. Oliver, I. A. Reyes-Cortés, R. de la Garza, and A. Simmons, "Stratigraphy of the PB-1 Well, Nopal I Uranium Deposit, Sierra Peña Blanca, Chihuahua, Mexico," *International Geology Review* **50**, 959-974 (2008).

M. Fayek, M. Ren, P. Goodell, P. Dobson, A. Saucedo, A. Kelts, S. Utsunomiya, R. Ewing, L. Riciputi, and I. Reyes, "Paragenesis and Geochronology of the Nopal I Uranium Deposit, Mexico," *Proceedings of the 11th International High-Level Radioactive Waste Management Conference, April 30-May 4, 2006, Las Vegas, Nevada* (American Nuclear Society, La Grange Park, Illinois, 2006), pp. 55-62.

S. J. Goldstein, A. I. Abdel-Fattah, M. T. Murrell, P. F. Dobson, D. E. Norman, R. S. Amato, and A. J. Nunn, "Uranium-Series Constraints on Radionuclide Transport and Groundwater Flow at the Nopal I Uranium Deposit, Sierra Peña Blanca, Mexico," *Environmental Science and Technology* **44**, 1579-1586 (2010).

S. J. Goldstein, A. I. Abdel-Fattah, M. T. Murrell, P. F. Dobson, D. E. Norman, R. S. Amato, and A. J. Nunn, "Uranium-Series Constraints on Radionuclide Transport and Groundwater Flow at the Nopal I Uranium Deposit, Sierra Peña Blanca, México," in "Final Report for the Peña Blanca Natural Analogue Project," S. Levy, compiler, Los Alamos National Laboratory report XXXXX (2016).

P. Goodell, "Geology of the Peña Blanca Uranium Deposits, Chihuahua, Mexico," in *Uranium In Volcanic and Volcaniclastic Rocks, AAPG Studies In Geology No. 13, Papers from the symposium on Uranium in volcaniclastic rocks, conducted at the Annual Meeting of the Southwest Section of The American Association of Petroleum Geologists, El Paso, Texas* (American Association of Petroleum Geologists, Tulsa, Oklahoma, 1981), pp. 275-291.

M. Ivanovich, "The phenomenon of radioactivity," in *Uranium-Series Disequilibrium: Applications to Earth, Marine, and Environmental Sciences*, Second Edition, M. Ivanovich and R. S. Harmon, Eds., (Oxford Univ. Press, New York, 1992), pp. 1-33.

M. Ivanovich and A. Murray, "Spectroscopic Methods," in *Uranium-Series Disequilibrium: Applications to Earth, Marine, and Environmental Sciences*, Second Edition, M. Ivanovich and R. S. Harmon, Eds., (Oxford Univ. Press, New York, 1992), pp.127-173.

P. T. King, J. Michel, and W. S. Moore, "Ground water geochemistry of ^{228}Ra, ^{226}Ra and ^{222}Rn," *Geochimica et Cosmochimica Acta* **46**, 1173-1182 (1982).

S. Krishnaswami, W. C. Graustein, K. K. Turekian, and J. F. Dowd, "Radium, Thorium and Radioactive Lead Isotopes in Groundwaters: Application to the in Situ Determination of Adsorption-Desorption Rate Constants and Retardation Factors," *Water Resources Research* **6**, 1663-1675 (1982).

T.-L. Ku, S. Luo, B. W. Leslie, and D. E. Hammond, "Decay-series disequilibrium applied to the study of rock-water interaction and geothermal systems," in *Uranium-Series Disequilibrium: Applications to Earth, Marine, and Environmental Sciences,*

Second Edition, M. Ivanovich and R. S. Harmon, Eds., (Oxford Univ. Press, New York, 1992), pp. 631-668.

T.-L. Ku, S. Luo, B. W. Leslie, and D. E. Hammond, "Assessing *in situ* Radionuclide Migration from Natural Analog Studies: Response to McKinley and Alexander (1996)," *Radiochimica Acta* **80**, 219-223 (1998).

S. Levy et al, "Foundations of the Conceptual Model for Uranium Transport at the Nopal I Natural Analogue Site," in "Final Report for the Peña Blanca Natural Analogue Project," S. S. Levy, compiler, Los Alamos National Laboratory report ------ (2016).

S. Luo, T. L. Ku, R. Roback, M. Murrell, and T. L. McLing, "In-situ radionuclide transport and preferential groundwater flows at INEEL (Idaho): decay-series disequilibrium studies," *Geochimica et Cosmochimica Acta* **64**, 867-881 (2000a).

S. Luo, T. L. Ku, R. Roback, M. Murrell, and T. McLing, "Decay-Series Disequilibrium Study of In-Situ, Long-Term Radionuclide Transport in Water-Rock Systems," in *Scientific Basis for Nuclear Waste Management XXIII, Materials Research Society Symposium Proceedings* (Materials Research Society, Pittsburgh, Pennsylvania, 2000b), Vol. 608, pp. 217-223.

S. Luo, T.-L. Ku, V. Todd, M. T. Murrell, J. A. Rodríguez, J. C. Dinsmoor, and A. J. Mitchell, "In-situ radionuclide transport near the Nopal I uranium deposit at Peña Blanca, Mexico: Constraints from short-lived decay series radionuclides," *Geological Society of America Annual Meeting & Exposition Abstracts with Programs* **37** (7), 198 (2005).

S. Luo, T.-L. Ku, V. Todd, M. T. Murrell, J. A. Rodríguez, and J. C. Dinsmoor, "Increased concentrations of short-lived decay-series radionuclides in groundwaters underneath the Nopal I uranium deposit at Peña Blanca, Mexico," *Eos Transactions AGU* **88** (23), Joint Assembly Supplement, Abstract GS22A-03 (2007).

W. M. Murphy, "Natural Analogs for Yucca Mountain," *Radwaste Magazine* **2**(6), 44-50 (1995).

M. T. Murrell, S. J. Goldstein, and P. R. Dixon, "Uranium Decay Series Mobility at Peña Blanca, Mexico: Implications for Nuclear Repository Stability," in *Eighth EC Natural Analogue Working Group Meeting, Proceedings of an International Workshop held in Strasbourg, France, from 23 to 25 March 1999*, H. von Maravic and W. R. Alexander, Eds. (Office for Official Publications of the European Communities, Luxembourg, Luxembourg, 2002), pp. 339-347.

R. D. Oliver, J. C. Dinsmoor, S. J. Goldstein, I. A. Reyes-Cortés, and R. De La Garza, "Initial Test Well Conditioning at Nopal I Uranium Deposit, Sierra Peña Blanca, Chihuahua, Mexico," *Geological Society of America Annual Meeting & Exposition Abstracts with Programs* **37** (7), 197 (2005).

M. Rearick, P. Dobson, S. Goldstein, J. Rodríguez, and S. Levy, "Groundwater Analyses for Nopal I and the Peña Blanca Region, Chihuahua, México," in "Final Report for the Peña Blanca Natural Analogue Project," S. Levy, compiler, Los Alamos National Laboratory report LAxxxxxxx (2016).

R. C. Scott and F. B. Barker, "Data on Uranium and Radium in Ground Water in the United States, 1954 to 1957," U.S. Geological Survey Professional Paper 426 (1962).

Z. Szabo, V. T. dePaul, T. F. Kraemer, and B. Parsa, "Occurrence of Radium-224, Radium-226, and Radium-228 in Water of the Unconfined Kirkwood-Cohansey Aquifer System, Southern New Jersey," U.S. Geological Survey Scientific Investigations report 2004-5224 (2005).

U.S. Nuclear Regulatory Commission, "Technical Evaluation Report on the Content of the U.S. Department of Energy's Yucca Mountain Repository License Application; Postclosure Volume: Repository Safety After Permanent Closure." Available URL: http://pbadupws.nrc.gov/docs/ML1119/ML111990436.pdf.

GROUNDWATER COLLOIDS AT NOPAL I

Amr Abdel-Fattah, Steven Goldstein, Sowmitri Tarimala, and Schön S. Levy

INTRODUCTION

The Peña Blanca Natural Analogue Project is a set of integrated studies of radionuclide transport at Nopal I, an abandoned uranium mine in the Sierra Peña Blanca region, approximately 50 km north of Chihuahua City, México. Many of the studies pertain to aspects of subsurface aqueous transport of radionuclides. Although most radionuclides are transported primarily as dissolved species in groundwater, it has long been recognized that some radionuclides are more likely to transport in association with colloids (suspended solid particles typically less than 1 μm diameter) because of their low solubilities in groundwater or strong sorption to mineral surfaces or both (Kersting et al., 1999). Groundwater samples were collected from recently drilled wells and a seepage-collection system in the unsaturated zone at Nopal I and from existing regional wells for a preliminary assessment of colloid size-distributions and concentrations.

SAMPLE COLLECTION AND ANALYSIS

Locations of the sampled wells are shown in Figures 1 and 2 of Goldstein et al. (2016). The samples were collected during three sampling trips between 2004 and 2006. Table 1 lists the samples and indicates whether they were collected by bailing, pumping, or other methods. Water samples from the wells proximal to Nopal I (PB1, PB2, and PB3), drilled in 2003, and the ~25-year-old mine-supply well (PB4) were collected *in situ* from below the water table. The seepage-water sample UACH 4 was collected on plastic sheeting installed below the ceiling in a mine adit about 10 m beneath the surface of open-pit workings (Dobson et al., 2012). Natural seepage was conducted from the surface to the adit primarily through the fracture system. The location of the seepage sample is described in Table 3 and Figure 3 of Goldstein et al. (2016). Samples collected from PB1 and PB4 for ultrafiltration and colloid analysis were divided in the field into unfiltered and 0.2-μm filtered aliquots, stored in coolers immediately after collection, and refrigerated until analysis to prevent bacterial growth.

Groundwater samples were analyzed for colloid concentrations and size distributions using a high-sensitivity liquid in-situ particle spectrometer, model HSLIS-S50 (Particle Measuring Systems, Inc., Boulder, CO). The HSLIS-S50 provides a colloid count per unit volume and size distribution information for all colloids within a size range of 50- to 1000-nm diameter (particles larger than 1000 nm are recorded as 1000-nm colloids). The measurement is made by first diluting the sample with ultrafiltered deionized water and then running the diluted sample through a laser light beam and light detection system that records each light scattering event as a colloid and uses the intensity and direction of the scattered light to calculate an equivalent spherical particle diameter. Samples must be diluted sufficiently to avoid coincident light scattering events from separate colloids. This dilution is performed internally by the instrument, with the user adjusting the relative flow rates of the sample and the water used for dilution until colloid count rates

are low enough to ensure no coincident counting. Instrument verifications were performed with NIST size standards #1691 (0.3 μm) and #1963 (0.1 μm). The verification procedure was performed prior to each episode of measurements. Sample dilution factor, injection rate, and injection dilution factor are given for each sample run in Tables 2 through 14.

Colloid analyses were re-run for some Nopal I water samples over periods of a year or more. Measured particle concentrations tended to remain constant or to decrease by as much as an order of magnitude. These results are consistent with the findings of Kung (2000) for colloids in water from a well in rhyolitic tuff near Yucca Mountain, Nevada. Data from these later runs of Nopal I waters are not included in this report.

Aliquots of the filtered water samples collected from PB1 and PB4 specifically to investigate proportions of uranium in true solution and in association with colloids were ultrafiltered in the laboratory using separate sterile ultrafiltration stirred cells (Millipore, USA), equipped with both 300 kDa (kilodalton; molecular weight cut-off of 3×10^5 unified atomic mass units but actual filtration characteristics not evaluated for PB colloid compositions) membrane filters and 20-nm in-line syringe filters. The results of these experiments, combined with chemical analyses of the unfiltered waters and filtrates, were interpreted by Goldstein et al. (2016) and are summarized below.

Mass concentrations of colloids in unfiltered water samples from the Nopal wells were estimated following the methodology of McCarthy and Degueldre (1993), in which the mass of colloids is related to the number of particles as a function of particle density and diameter. The estimate is imprecise because all particles in a size class are assumed to

Table 1. Summary of Sample Collection and Analysis

Water Source	Sample ID	Collection Date	Aliquots	Analysis Date(s)	Notes
PB1 well	SPC 1031345	11/17/2004	unfiltered	9/20/2005	bailed sample
			ultrafiltered	9/20/2005	
	SPC 1025068	8/23/2006	unfiltered	8/31/2006	pumped sample
PB2 well	SPC 1031342	11/17/2004	unfiltered	9/8/2006	bailed sample
	SPC 1025072	8/25/2006	unfiltered	8/31/2006	pumped sample
PB3 well	SPC 1031351	11/17/2004	unfiltered	5/12/2005	bailed sample
	SPC 1025070	8/24/2006	unfiltered	8/31/2006	pumped sample
PB4 well	SPC 1031127	4/8/2005	unfiltered	9/20/2005	bailed sample
			ultrafiltered	9/20/2005	
Peña Blanca well	SPC 1031114	4/6/2005	unfiltered	5/12/2005	bailed sample from tank
Pozos Ranch well	SPC 1031118	4/6/2005	unfiltered	5/12/2005	bailed sample from tank
Adit seepage UACH 4	SPC 1025062	4/11/2005	unfiltered	5/12/2005	sample from plastic sheet collector

have the diameter of the upper size limit of the class. In addition, all colloids are assumed to have a density of 2 g/cm^3, taken as an average for clay, hydrated silica, and iron hydroxide (McCarthy and Degueldre, 1993). The mass concentrations were calculated from single analyses or from the mean values of duplicate analyses of particle concentrations.

RESULTS

Colloid-particle concentrations and size distributions for Nopal I well and seepage waters and for regional wells are presented in Tables 2 through 14

Col1oid Mass Concentrations

Mass concentrations of ≤1000 nm colloids in water samples from wells PB1, PB2, and PB3, collected and analyzed in 2006, are presented in Table 15. The similarity of values for wells PB1 and PB2 is consistent with data indicating good hydraulic connectivity between these two wells (Oliver et al., 2005). A relatively higher colloid-mass concentration in PB3 may correlate with a higher degree of rock alteration at the sampling depth. We have no direct evidence to support this, but the gross gamma counts in the relevant depth intervals may be taken as a proxy for some of the alteration experienced by the rock units. There is a very strong gamma anomaly in PB3 within and slightly above the top of the colloid sample depth range (Levy et al., 2016). Alternatively, the high colloid concentrations in PB3 may be related to the increased use of high-pH drilling fluids due to lost circulation during drilling. The fluids may have leached rock constituents, including uranium, into solution and released particulates as well.

No quantitative significance is ascribed to the colloid concentration of the adit-seepage sample because of the likelihood that the seepage-water particulate content was modified by evaporation (Ghezzehei, 2007), dust settling, and mass wasting from the ceiling. The remoteness of the site and the unpredictability of seepage arrival made it too difficult to collect seepage samples immediately after they accumulated.

The colloid-mass concentration of PB4 water is about a factor of 5 lower than concentrations in the well waters of Nopal I. This value may be more representative of the colloid content of water collected directly from the production zone of a decades-old well. Direct comparisons are complicated by the differences in lithology – limestone at PB4 versus a combination of pyroclastic rock, volcaniclastic and calciclastic rock, and limestone at Nopal I.

Table 2. Colloid Size Distribution and Concentrations, PB1 (SPC 1031345), Unfiltered and Ultrafiltered, 11/17/2004 Sample, 9/20/2005 Measurements

Size (nm)	Measured concentration (particles/mL)			Actual concentration (particles/mL)		
	Unfiltered	Ultrafiltered		Unfiltered	Ultrafiltered	
		Run 1	Run 2		Run 1	Run 2
50	8475	4686.7	9578.1	1.70E+07	9.37E+05	9.58E+05
60	8081.3	4469.5	9331.7	1.62E+07	8.94E+05	9.33E+05
70	6460.4	3237.3	7289.1	1.29E+07	6.47E+05	7.29E+05
80	4916.7	2535.5	5584.8	9.83E+06	5.07E+05	5.58E+05
90	5218.8	2673.4	6177.9	1.04E+07	5.35E+05	6.18E+05
100	2245.8	981.6	2226.4	4.49E+06	1.96E+05	2.23E+05
110	1575	568.1	1507.9	3.15E+06	1.14E+05	1.51E+05
120	1102.1	401	998.3	2.20E+06	8.02E+04	9.98E+04
130	795.8	309.1	797.8	1.59E+06	6.18E+04	7.98E+04
140	783.3	300.8	618.2	1.57E+06	6.02E+04	6.18E+04
150	550	380.1	789.5	1.10E+06	7.60E+04	7.90E+04
160	535.4	296.6	593.1	1.07E+06	5.93E+04	5.93E+04
170	454.2	238.1	584.8	9.08E+05	4.76E+04	5.85E+04
180	410.4	208.9	455.3	8.21E+05	4.18E+04	4.55E+04
190	354.2	188	413.5	7.08E+05	3.76E+04	4.14E+04
200	264.3	174.4	383.4	5.29E+05	3.49E+04	3.83E+04
220	127.6	72.4	170.6	2.55E+05	1.45E+04	1.71E+04
240	93.9	54.8	115.2	1.88E+05	1.10E+04	1.15E+04
260	63.9	33.1	85.4	1.28E+05	6.62E+03	8.54E+03
280	34.6	17.4	50.3	6.92E+04	3.48E+03	5.03E+03
300	89	50.4	113.8	1.78E+05	1.01E+04	1.14E+04
400	22.7	11.2	29	4.54E+04	2.24E+03	2.90E+03
500	29.9	13.7	32.5	5.98E+04	2.74E+03	3.25E+03
600	58.4	17.8	49.3	1.17E+05	3.56E+03	4.93E+03
800	23.7	4	13.1	4.74E+04	8.00E+02	1.31E+03
1000	63.1	3.9	12.8	1.26E+05	7.80E+02	1.28E+03
Total Actual Particle Concentration (particles/mL)				8.57E+07	4.39E+06	4.80E+06

Sediments in bottom of original sample.
Unfiltered sample dilution factor = 1; injection rate = 5 min/mL; injection dilution factor = 2000.
Ultrafiltered Run 1 dilution factor = 1; injection rate = 0.5 min/mL; injection dilution factor = 200.
Ultrafiltered Run 2 dilution factor = 1; injection rate = 0.25 min/mL; injection dilution factor = 100.

Table 3. Colloid Size Distribution and Concentrations, PB1 (SPC 1025068), 8/23/2006 Sample, 8/31/2006 Measurements

Size (nm)	Measured concentration (particles/mL)		Actual concentration (particles/mL)	
	Run 1	Run 2	Run 1	Run 2
50	5270.6	5183.6	1.05E+06	1.04E+06
60	6756.9	6848.9	1.35E+06	1.37E+06
70	5945	5972.5	1.19E+06	1.19E+06
80	4433.8	4757.9	8.87E+05	9.52E+05
90	3072.4	3092.7	6.14E+05	6.19E+05
100	2610.3	2541.7	5.22E+05	5.08E+05
110	3109.9	2879.8	6.22E+05	5.76E+05
120	2198.2	1778	4.40E+05	3.56E+05
130	1423.8	1389.8	2.85E+05	2.78E+05
140	1411.3	1427.4	2.82E+05	2.85E+05
150	1698.6	1527.5	3.40E+05	3.06E+05
160	2060.8	1965.8	4.12E+05	3.93E+05
170	1836	1953.3	3.67E+05	3.91E+05
180	1748.5	2015.9	3.50E+05	4.03E+05
190	2398	2053.4	4.80E+05	4.11E+05
200	2192.6	2158.8	4.39E+05	4.32E+05
220	1447.4	1437.3	2.89E+05	2.87E+05
240	1208.7	1224.7	2.42E+05	2.45E+05
260	995.9	978.5	1.99E+05	1.96E+05
280	638.2	615.9	1.28E+05	1.23E+05
300	2219.3	2213.3	4.44E+05	4.43E+05
400	720.3	764.7	1.44E+05	1.53E+05
500	1064.2	1005.5	2.13E+05	2.01E+05
600	2121.3	2138.7	4.24E+05	4.28E+05
800	771.8	780.6	1.54E+05	1.56E+05
1000	852.7	880.4	1.71E+05	1.76E+05
Total Actual Particle Concentration (particles/mL)			1.20E+07	1.19E+07
Runs 1 and 2 sample dilution factor = 1; injection rate (min/mL) = 0.5; injection dilution factor = 200				

Table 4. Colloid Size Distribution and Concentrations, PB2 (SPC 1031342), 11/17/2004 Sample, 9/8/2006 Measurements

Size (nm)	Measured concentration (particles/mL)		Actual concentration (particles/mL)	
	Run 1	Run 2	Run 1	Run 2
50	5998.8	6110	2.40E+06	2.44E+06
60	6479.4	6572.3	2.59E+06	2.63E+06
70	5536.8	5222.8	2.21E+06	2.09E+06
80	4363.3	4248.2	1.75E+06	1.70E+06
90	3508.1	4273.2	1.40E+06	1.71E+06
100	2521.8	2530.2	1.01E+06	1.01E+06
110	2259.7	2417.7	9.04E+05	9.67E+05
120	2047.4	2092.9	8.19E+05	8.37E+05
130	2103.6	1980.4	8.41E+05	7.92E+05
140	2103.6	2199.1	8.41E+05	8.80E+05
150	2628	2467.7	1.05E+06	9.87E+05
160	2253.4	2486.5	9.01E+05	9.95E+05
170	2453.2	2480.2	9.81E+05	9.92E+05
180	2272.2	2055.4	9.09E+05	8.22E+05
190	1554.3	1561.8	6.22E+05	6.25E+05
200	2557.7	2575.4	1.02E+06	1.03E+06
220	1220.2	1206.3	4.88E+05	4.83E+05
240	781.4	750.6	3.13E+05	3.00E+05
260	421	421	1.68E+05	1.68E+05
280	222.3	220.2	8.89E+04	8.81E+04
300	436.7	421	1.75E+05	1.68E+05
400	70.1	68.4	2.80E+04	2.74E+04
500	69.1	57.9	2.76E+04	2.32E+04
600	67.6	57.6	2.70E+04	2.30E+04
800	5.1	6.7	2.04E+03	2.68E+03
1000	18.3	13.4	7.32E+03	5.36E+03
Total Actual Particle Concentration (particles/mL)			2.16E+07	2.18E+07
Sediments in bottom of original sample. Runs 1 and 2 sample dilution factor = 1; injection rate = 1 min/mL; injection dilution factor = 400.				

Table 5. Colloid Size Distribution and Concentrations, PB2 (SPC 1025072), 8/25/2006 Sample, 8/31/2006 Measurements

Size (nm)	Measured concentration (particles/mL)		Actual concentration (particles/mL)	
	Run 1	Run 2	Run 1	Run 2
50	4432.4	4230.4	8.86E+05	8.46E+05
60	5133.6	5316.1	1.03E+06	1.06E+06
70	4232.1	3968.4	8.46E+05	7.94E+05
80	3280.5	3331.9	6.56E+05	6.66E+05
90	1903.2	2271.2	3.81E+05	4.54E+05
100	1828	2233.8	3.66E+05	4.47E+05
110	2128.5	2071.5	4.26E+05	4.14E+05
120	1627.7	1784.5	3.26E+05	3.57E+05
130	1051.8	948.4	2.10E+05	1.90E+05
140	1177	1123.1	2.35E+05	2.25E+05
150	1189.5	1085.7	2.38E+05	2.17E+05
160	1051.8	1372.7	2.10E+05	2.75E+05
170	1126.9	998.3	2.25E+05	2.00E+05
180	1202	1123.1	2.40E+05	2.25E+05
190	1302.2	1360.2	2.60E+05	2.72E+05
200	1428	1512.7	2.86E+05	3.03E+05
220	974.5	969.3	1.95E+05	1.94E+05
240	829.8	886.7	1.66E+05	1.77E+05
260	664.8	681.4	1.33E+05	1.36E+05
280	454.1	464.6	9.08E+04	9.29E+04
300	1448.3	1481	2.90E+05	2.96E+05
400	501	511.3	1.00E+05	1.02E+05
500	755.2	746.3	1.51E+05	1.49E+05
600	1598.9	1603.1	3.20E+05	3.21E+05
800	603	614.9	1.21E+05	1.23E+05
1000	920.5	928.9	1.84E+05	1.86E+05
Total Actual Particle Concentration (particles/mL)			8.57E+06	8.72E+06
Runs 1 and 2 sample dilution factor = 1000; injection rate = 0.5 min/mL; injection dilution factor = 2000				

Table 6. Colloid Size Distribution and Concentrations, PB3 (SPC 1031351) Unfiltered, 11/17/2004 Sample, 5/12/2005 Measurements

Size (nm)	Measured concentration (particles/mL)	Actual concentration (particles/mL)
50	4137.5	3.31E+06
60	3900	3.12E+06
70	3008.3	2.41E+06
80	2558.3	2.05E+06
90	2758.3	2.21E+06
100	1375	1.10E+06
110	1083.3	8.67E+05
120	658.3	5.27E+05
130	508.3	4.07E+05
140	479.2	3.83E+05
150	341.7	2.73E+05
160	320.8	2.57E+05
170	279.2	2.23E+05
180	220.8	1.77E+05
190	212.5	1.70E+05
200	178.1	1.42E+05
220	80.4	6.43E+04
240	58.5	4.68E+04
260	40.9	3.27E+04
280	24.1	1.93E+04
300	63.5	5.08E+04
400	19.7	1.58E+04
500	24.9	1.99E+04
600	43.5	3.48E+04
800	20.5	1.64E+04
1000	58.7	4.70E+04
Total Actual Particle Concentration (particles/mL)		1.80E+07
Foamy and sediments in bottom of original sample. Sample dilution factor = 1; Injection rate (min/mL) = 2; Injection dilution factor = 800.		

Table 7. Colloid Size Distribution and Concentrations, PB3 (SPC 1025070), 8/24/2006 Sample, 8/31/2006 Measurements

Size (nm)	Measured concentration (particles/mL)		Actual concentration (particles/mL)	
	Run 1	Run 2	Run 1	Run 2
50	4868.9	4662.5	3.90E+06	3.73E+06
60	5461.9	5531.3	4.37E+06	4.43E+06
70	4943.8	5362.5	3.96E+06	4.29E+06
80	4369.5	4325	3.50E+06	3.46E+06
90	2671.7	2906.3	2.14E+06	2.33E+06
100	3264.7	3243.8	2.61E+06	2.60E+06
110	4151.1	4193.7	3.32E+06	3.35E+06
120	2740.3	2575	2.19E+06	2.06E+06
130	1872.7	1850	1.50E+06	1.48E+06
140	1729.1	1812.5	1.38E+06	1.45E+06
150	1679.2	1531.3	1.34E+06	1.23E+06
160	1473.2	1562.5	1.18E+06	1.25E+06
170	1367	1481.3	1.09E+06	1.19E+06
180	1329.6	1343.8	1.06E+06	1.08E+06
190	1392	1331.2	1.11E+06	1.06E+06
200	1107.4	1110.1	8.86E+05	8.88E+05
220	621	615	4.97E+05	4.92E+05
240	498.7	502	3.99E+05	4.02E+05
260	363.9	388.5	2.91E+05	3.11E+05
280	229.3	249.7	1.83E+05	2.00E+05
300	737.6	746.7	5.90E+05	5.97E+05
400	230.5	238.1	1.84E+05	1.90E+05
500	331.5	324.3	2.65E+05	2.59E+05
600	781	770	6.25E+05	6.16E+05
800	401.6	410.5	3.21E+05	3.28E+05
1000	1773.5	1711.5	1.42E+06	1.37E+06
Total Actual Particle Concentration (particles/mL)			4.03E+07	4.06E+07
Runs 1 and 2 sample dilution factor = 1; injection rate = 2 min/mL; injection dilution factor = 800				

Table 8. Colloid Size Distribution and Concentrations, PB4 (SPC 1031127), Unfiltered, 4/8/2005 Sample, 9/20/2005 Measurements

Size (nm)	Measured concentration (particles/mL)		Actual concentration (particles/mL)	
	Run 1	Run 2	Run 1	Run 2
50	4808	8945.8	1.92E+06	1.79E+06
60	4549.5	8404.2	1.82E+06	1.68E+06
70	3806.3	7025	1.52E+06	1.41E+06
80	2975.8	5620.8	1.19E+06	1.12E+06
90	3384.8	6379.2	1.35E+06	1.28E+06
100	1861.4	3608.3	7.45E+05	7.22E+05
110	1477.5	2895.8	5.91E+05	5.79E+05
120	1110.2	2087.5	4.44E+05	4.18E+05
130	863.9	1570.8	3.46E+05	3.14E+05
140	914	1516.7	3.66E+05	3.03E+05
150	726.2	1370.8	2.90E+05	2.74E+05
160	588.5	1095.8	2.35E+05	2.19E+05
170	496.7	1087.5	1.99E+05	2.18E+05
180	446.6	804.2	1.79E+05	1.61E+05
190	388.1	795.8	1.55E+05	1.59E+05
200	270.9	543.9	1.08E+05	1.09E+05
220	129.2	267.4	5.17E+04	5.35E+04
240	88.4	188.2	3.54E+04	3.76E+04
260	64.3	129.2	2.57E+04	2.58E+04
280	33.9	71.7	1.36E+04	1.43E+04
300	87.2	188	3.49E+04	3.76E+04
400	25.6	45.8	1.02E+04	9.16E+03
500	30.3	60.6	1.21E+04	1.21E+04
600	65.9	126.4	2.64E+04	2.53E+04
800	32.8	63.2	1.31E+04	1.26E+04
1000	101.8	204.7	4.07E+04	4.09E+04
Total Actual Particle Concentration (particles/mL)			1.17E+07	1.10E+07

Sediments in bottom of original sample.
First run sample dilution factor = 1; injection rate = 1 min/mL; injection dilution factor = 400.
Second run sample dilution factor = 1; injection rate = 0.5 min/mL; injection dilution factor = 200

Table 9. Colloid Size Distribution and Concentrations, PB4 (SPC 1031127) Ultrafiltered, 4/8/2005 Sample, 9/20/05 Measurements

Size (nm)	Measured concentration (particles/mL)		Actual concentration (particles/mL)	
	Run 1	Run 2	Run 1	Run 2
50	1041.7	2433.3	2.08E+05	2.43E+05
60	1250	2441.7	2.50E+05	2.44E+05
70	1266.7	2420.8	2.53E+05	2.42E+05
80	1104.2	2116.7	2.21E+05	2.12E+05
90	1683.3	3429.2	3.37E+05	3.43E+05
100	620.8	1441.7	1.24E+05	1.44E+05
110	483.3	995.8	9.67E+04	9.96E+04
120	425	795.8	8.50E+04	7.96E+04
130	283.3	587.5	5.67E+04	5.88E+04
140	275	637.5	5.50E+04	6.38E+04
150	233.3	433.3	4.67E+04	4.33E+04
160	158.3	333.3	3.17E+04	3.33E+04
170	158.3	329.2	3.17E+04	3.29E+04
180	112.5	212.5	2.25E+04	2.13E+04
190	54.2	145.8	1.08E+04	1.46E+04
200	41.4	82.4	8.28E+03	8.24E+03
220	11.7	26.1	2.34E+03	2.61E+03
240	6.7	15.1	1.34E+03	1.51E+03
260	4.7	8.5	9.40E+02	8.50E+02
280	2.3	6.7	4.60E+02	6.70E+02
300	5.7	14.6	1.14E+03	1.46E+03
400	2.4	3.5	4.80E+02	3.50E+02
500	2	4.6	4.00E+02	4.60E+02
600	5.9	12	1.18E+03	1.20E+03
800	1.1	3.6	2.20E+02	3.60E+02
1000	1.2	2.4	2.40E+02	2.40E+02
Total Actual Particle Concentration (particles/mL)			1.85E+06	1.89E+06

Sediments in bottom of original sample.
Run 1 sample dilution factor = 1; injection rate = 0.5 min/mL; injection dilution factor = 200.
Run 2 sample dilution factor = 1; injection rate = 0.25 min/mL; injection dilution factor = 100.

Table 10. Colloid Size Distribution and Concentrations, Adit Seepage UACH 4 (SPC 1025062), 4/11/2005 Sample, 5/12/2005 Measurements

Size (nm)	Measured concentration (particles/mL)	Actual concentration (particles/mL)
50	6720.4	2.69E+07
60	5013.5	2.01E+07
70	3235.8	1.29E+07
80	2046.2	8.18E+06
90	1640.3	6.56E+06
100	883.6	3.53E+06
110	712.9	2.85E+06
120	470.4	1.88E+06
130	344.5	1.38E+06
140	301.8	1.21E+06
150	250.8	1.00E+06
160	211.3	8.45E+05
170	209.2	8.37E+05
180	187.3	7.49E+05
190	158.2	6.33E+05
200	116.2	4.65E+05
220	57	2.28E+05
240	39.5	1.58E+05
260	24.5	9.80E+04
280	14.2	5.68E+04
300	36.8	1.47E+05
400	11.2	4.48E+04
500	14.3	5.72E+04
600	36	1.44E+05
800	21.2	8.48E+04
1000	73.5	2.94E+05
Total Actual Particle Concentration (particles/mL)		9.13E+07
Sediments in bottom of original sample. Sample dilution factor = 1; injection rate (min/mL) = 10; injection dilution factor = 4000		

Table 11. Colloid Size Distribution and Concentrations, Peña Blanca Well (SPC 1031114), 4/6/2005 Sample, 5/12/2005 Measurements

Size (nm)	Measured concentration (particles/mL)	Actual concentration (particles/mL)
50	22241.2	1.78E+07
60	17583.5	1.41E+07
70	12504.2	1.00E+07
80	8568.4	6.85E+06
90	8785.5	7.03E+06
100	2783.8	2.23E+06
110	1874	1.50E+06
120	1306.3	1.05E+06
130	901.5	7.21E+05
140	801.3	6.41E+05
150	722	5.78E+05
160	584.3	4.67E+05
170	379.8	3.04E+05
180	438.2	3.51E+05
190	261.1	2.09E+05
200	211.8	1.69E+05
220	63.1	5.05E+04
240	32.1	2.57E+04
260	16.1	1.29E+04
280	9.1	7.28E+03
300	21.1	1.69E+04
400	4.6	3.68E+03
500	3.6	2.88E+03
600	6	4.80E+03
800	1.3	1.04E+03
1000	6	4.80E+03
Total Actual Particle Concentration (particles/mL)		6.41E+07
Sample dilution factor = 1; injection rate = 2 min/mL; injection dilution factor = 800.		

Table 12. Colloid Size Distribution and Concentrations, Peña Blanca Well (SPC 1031114), 4/6/2005 Sample, 5/12/2005 Measurements

Size (nm)	Measured concentration (particles/mL)		Actual concentration (particles/mL)	
	Run 1	Run 2	Run 1	Run 2
50	11766.9	11932.4	1.18E+06	1.19E+06
60	12117.8	12696.2	1.21E+06	1.27E+06
70	10062.7	9879	1.01E+06	9.88E+05
80	6967.4	7287.1	6.97E+05	7.29E+05
90	5338.3	5446.6	5.34E+05	5.45E+05
100	1792	2003.3	1.79E+05	2.00E+05
110	1629.1	1615.2	1.63E+05	1.62E+05
120	990	1039.2	9.90E+04	1.04E+05
130	814.5	788.8	8.15E+04	7.89E+04
140	990	901.5	9.90E+04	9.02E+04
150	639.1	688.6	6.39E+04	6.89E+04
160	576.4	475.8	5.76E+04	4.76E+04
170	463.7	488.3	4.64E+04	4.88E+04
180	488.7	463.3	4.89E+04	4.63E+04
190	250.6	237.9	2.51E+04	2.38E+04
200	666.2	649.6	6.66E+04	6.50E+04
220	197.3	199.4	1.97E+04	1.99E+04
240	119.8	111.4	1.20E+04	1.11E+04
260	66.4	65.6	6.64E+03	6.56E+03
280	35.1	39.8	3.51E+03	3.98E+03
300	87.7	81.7	8.77E+03	8.17E+03
400	15.6	12.9	1.56E+03	1.29E+03
500	13.5	16.8	1.35E+03	1.68E+03
600	12.3	13.8	1.23E+03	1.38E+03
800	3.6	3	3.60E+02	3.00E+02
1000	15	14.4	1.50E+03	1.44E+03
Total Actual Particle Concentration (particles/mL)			5.61E+06	5.72E+06
Notes: sample dilution factor = 1; injection rate (min/mL) = 0.25; injection dilution factor = 100.				

Table 13. Colloid Size Distribution and Concentrations, Pozos Ranch Well (SPC 1031118), 4/6/2005 Sample, 5/12/2005 Measurements

Size (nm)	Measured concentration (particles/mL)		Actual concentration (particles/mL)	
	Run 1	Run 2	Run 1	Run 2
50	162.8	225.2	1.63E+04	2.25E+04
60	313	275.2	3.13E+04	2.75E+04
70	162.8	287.7	1.63E+04	2.88E+04
80	212.9	237.7	2.13E+04	2.38E+04
90	100.2	212.7	1.00E+04	2.13E+04
100	62.6	112.6	6.26E+03	1.13E+04
110	62.6	37.5	6.26E+03	3.75E+03
120	25	25	2.50E+03	2.50E+03
130	25	12.5	2.50E+03	1.25E+03
140	25	75.1	2.50E+03	7.51E+03
150	37.6	37.5	3.76E+03	3.75E+03
160	37.6	37.5	3.76E+03	3.75E+03
170	37.6	37.5	3.76E+03	3.75E+03
180	87.6	50	8.76E+03	5.00E+03
190	137.7	50	1.38E+04	5.00E+03
200	66.7	59.1	6.67E+03	5.91E+03
220	33.5	32.3	3.35E+03	3.23E+03
240	32.6	26.6	3.26E+03	2.66E+03
260	18.2	16.4	1.82E+03	1.64E+03
280	6	10.2	6.00E+02	1.02E+03
300	19.7	18.5	1.97E+03	1.85E+03
400	4.2	4.2	4.20E+02	4.20E+02
500	3.9	3.6	3.90E+02	3.60E+02
600	3.9	5.1	3.90E+02	5.10E+02
800	0.6	0.3	6.00E+01	3.00E+01
1000	6.6	4.2	6.60E+02	4.20E+02
Total Actual Particle Concentration (particles/mL)			1.69E+05	1.89E+05
Runs 1 and 2 sample dilution factor = 1; injection rate = 0.25 min/mL; injection dilution factor = 100.				

Table 14. Colloid Size Distribution and Concentrations, Pozos Ranch Well (SPC 1031118), 4/6/2005 Sample, 5/12/2005 Measurements

Size (nm)	Measured concentration (particles/mL)	Actual concentration (particles/mL)
50	950.8	3.80E+05
60	608.8	2.44E+05
70	487.9	1.95E+05
80	346.1	1.38E+05
90	346.1	1.38E+05
100	171	6.84E+04
110	87.6	3.50E+04
120	54.2	2.17E+04
130	62.6	2.50E+04
140	45.9	1.84E+04
150	66.7	2.67E+04
160	45.9	1.84E+04
170	58.4	2.34E+04
180	58.4	2.34E+04
190	41.7	1.67E+04
200	43.1	1.72E+04
220	16.2	6.48E+03
240	15.6	6.24E+03
260	9.1	3.64E+03
280	2.9	1.16E+03
300	5.8	2.32E+03
400	1.5	6.00E+02
500	1.1	4.40E+02
600	1.3	5.20E+02
800	0.4	1.60E+02
1000	0.6	2.40E+02
Total Actual Particle Concentration (particles/mL)		1.41E+06
Notes: sample dilution factor = 1; injection rate (min/mL) = 1; injection dilution factor = 400.		

Table 15. Colloid-Mass Concentrations in Nopal and Regional Wells

Well and Sample Number	Source Table	Sample Depth Range (m)	Colloid Size Fraction (nm)	Colloid Mass (mg/L)
PB1, SPC 1025068	3	223-255	50-1000	0.44
PB2, SPC 1025072	5	229-254	50-1000	0.39
PB3, SPC 1025070	7	214-243	50-1000	1.93
PB4 SPC 1031127	9	92-124	50-1000	0.089
Adit UACH 4 SPC 1025062	10	fracture seepage, plastic sheet collector	50-1000	0.473
Peña Blanca Ranch, SPC 1031114	12	water tank	50-1000	0.008
Pozos Ranch, SPC 1031118	13	water tank	50-1000	0.001

Data on colloid-mass abundances in groundwaters worldwide compiled by McCarthy and Degueldre (1993, Table 6) provide a basis for comparison with the range of colloid-mass concentrations in the Sierra Peña Blanca region. Sample sites include rhyolitic welded tuffs of southern Nevada, the Alligator River (Australia) sandstone-hosted uranium-ore

body, and the Cigar Lake (Canada) sandstone-hosted uranium-ore body. Colloid-mass concentrations range from 0.005 to 106 mg/L, with the majority of values between about 0.1 and 3 mg/L. The colloid concentrations in the Nopal wells and in regional wells are within the range of common values that McCarthy and Degueldre (1993) associate with mid-level aquifer systems that are not experiencing extremes of tectonic, hydrothermal, or hydrogeochemical perturbation.

Colloid Compositions

Concentrations of colloids in the water samples from the PB wells were deemed insufficient for chemical or mineralogical analysis. Nevertheless, a few inferences about radionuclides associated with colloids may be drawn from water analyses. Goldstein et al. (2016) concluded from analysis of the PB1 and PB4 unfiltered, filtered, and ultrafiltered water samples that ~93-97% of the uranium present is truly dissolved and therefore not associated with colloids. Plutonium, a low-solubility radionuclide, has been detected in association with colloids in groundwater at the Nevada National Security Site, formerly the Nevada Test Site (Kersting et al., 1999). The dominant source of this plutonium was underground nuclear testing. Plutonium-239 also is produced naturally in uranium ores by neutron irradiation of U^{238} (Clark et al., 2008), and therefore could be present among the groundwater colloids beneath Nopal I. However, no plutonium was detected in PB well waters. The water samples were analyzed by mass spectrometry for ^{239}Pu with a detection limit of ~50 atoms ^{239}Pu/g sample (Goldstein et al., 2016).

Comparisons of unfiltered and 0.45-μm filtered aliquots of well waters by Rearick et al. (2016) identified reduced Al concentrations in the filtered aliquots, a likely indication of very fine clay particles. Other elements possibly associated with colloids include Mo, As, Cr, V, and B. The content of Th is below the detection limit of 0.001 ppm in all water samples. Data from earlier analyses, some with lower detection limits, confirm the generally low Th content of groundwater and suggest that observed concentration variability may be attributable to differences in colloid abundance (CRWMS M&O, 2004).

DISCUSSION

There are difficulties in comparing the calculated values of total colloid mass among the Nopal wells and for all sampled regional wells. The three Nopal wells (PB1, PB2, and PB3) were drilled in 2003, and the local groundwater may not have returned to background colloid concentrations. Well PB4 dates to the 1980s, and the other regional wells probably predate the Nopal drilling project by many years, increasing the likelihood of recovery from drilling disturbance. The Pozos Ranch and Peña Blanca well waters could be sampled only from holding tanks rather than from the wellbore, with uncertain consequences for the measured colloid population.

The documentation of a trend in the colloid content of Nopal I wells during the three years after they were drilled is complicated by differences in sampling methods (bailed versus pumped) and, possibly, analytical conditions such as injection dilution factor. The

2004 samples from Nopal wells were bailed, whereas the 2006 samples were pumped. McCarthy and Degueldre (1993) consider slowly pumped samples to be more representative of *in situ* colloid concentrations because bailing tends to resuspend settled particles. The 2004 and 2006 samples from PB1 (Tables 2 and 3) and PB2 (Tables 4 and 5) appear to show decreasing total particle concentration over time, but this trend could be partly due to the differences in sampling methodology. The 2006 measurements of pumped water may be the best approximations of natural abundances because of the sample-collection method and the greater elapsed time since drilling.

As described above, no quantitative significance is ascribed to the colloid concentration of the adit-seepage sample because of the likelihood that the seepage-water particulate content was modified by evaporation, dust settling, and mass wasting from the ceiling. The potential value of this type of sample would be as an indication of colloids acquired by recharge water passing through the uranium-ore deposit. Chemical analyses of the unfiltered and ultrafiltered PB1 waters indicate that very little uranium exists in colloidal form in saturated-zone waters below the deposit (Goldstein et al., 2016). Equivalent information for recharge water interacting with the ore deposit would help elucidate the fate and transport of radionuclide-bearing colloids in the unsaturated zone.

The low colloid contents of the Pozos Ranch and Peña Blanca wells may be attributable to the greater ages of these wells relative to the Nopal I wells and to their presumed long-term, regular pumping. Additional processes of unknown effect could include particle settling and adhesion in the holding tanks and input of rainfall and airborne particulates.

CONCLUSIONS

The colloid-mass concentrations in the Nopal I wells are within the range of common values for mid-level aquifer systems, but probably remain elevated relative to undisturbed ambient concentrations. Unsaturated-zone seepage from a mine adit at Nopal I contains colloids, but the significance of the measured colloid abundance is complicated by uncertainties about the seepage-collection conditions.

Colloid concentrations in the mine-supply well PB4 are about five times lower than in the Nopal I wells. Of the samples analyzed for this study, PB4 water may be most representative of natural conditions in regional groundwater. Two regional wells have colloid-mass concentrations an order of magnitude lower than the PB4 value, but the water for the analyses came from storage tanks rather than from the wellbore.

REFERENCES

D. L. Clark, S. S. Hecker, G. D. Jarvinen, and M. P. Neu, “Plutonium,” in *The Chemistry of the Actinide and Transactinide Elements, Third Edition*, L. R. Morss, N. M. Edelstein, and J. Fuger, Eds. (Springer, Dordrecht, The Netherlands, 2008), Vol. 1, Chapter 7, pp. 813-1264.

Civilian Radioactive Waste Management System Management & Operating Contractor (CRWMS M&O), "Natural Analogue Synthesis Report," CRWMS M&O report TDR-NBS-GS-000027 REV01 (available URL: www.osti.gov/scitech/servlets/purl/883016), 2004.

P. F. Dobson, T. A. Ghezzehei, P. J. Cook, J. A. Rodríguez-Pineda, L. Villalba, and R. De la Garza, "Heterogeneous seepage at the Nopal I natural analogue site, Chihuahua, Mexico," *Hydrogeology Journal* **20**, 155-166 (2012).

T. A. Ghezzehei, Lawrence Berkeley National Laboratory, electronic communication, May 2007.

S. Goldstein, A. Abdel-Fattah, M. Murrell, P. Dobson, D. Norman, R. Amato, and A. Nunn, "Uranium-Series Constraints on Radionuclide Transport and Groundwater Flow at the Nopal I Uranium Deposit, Sierra Peña Blanca, México," in "Final Report for the Peña Blanca Natural Analogue Project," S. Levy, compiler, Los Alamos National Laboratory report ------ (2016)

A. B. Kersting, D. W. Efurd, D. L. Finnegan, D. J. Rokop, D. K. Smith, and J. L. Thompson, "Migration of plutonium in ground water at the Nevada Test Site," *Science* **397**, 56-59 (1999).

K. S. Kung, "Colloid Characterization and Quantification in Groundwater Samples," Los Alamos National Laboratory report LA-13727-MS (2000).

S. Levy et al, "Foundations of the Conceptual Model for Uranium Transport at the Nopal I Natural Analogue Site," in "Final Report for the Peña Blanca Natural Analogue Project," S. Levy, compiler, Los Alamos National Laboratory report ------ (2016).

J. F. McCarthy and C. Degueldre, "Sampling and Characterization of Colloids and Particles in Groundwater for Studying Their Role in Contaminant Transport," in *Environmental Particles*, J. Buffle and H. P. van Leeuwen, eds., (Lewis Publishers, Boca Raton, Florida, 1993), Vol. 2, pp. 247-315.

R. D. Oliver, J. C. Dinsmoor, S. J. Goldstein, I. A. Reyes-Cortés, and R. De La Garza, "Initial Test Well Conditioning at Nopal I Uranium Deposit, Sierra Peña Blanca, Chihuahua, Mexico," *Geological Society of America Annual Meeting & Exposition Abstracts with Programs* **37** (7), 197 (2005).

M. Rearick, P. Dobson, S. Goldstein, J. A. Rodríguez, and S. Levy, "Groundwater Analyses for Nopal I and the Peña Blanca Region, Chihuahua, México," in "Final Report for the Peña Blanca Natural Analogue Project," S. Levy, compiler, Los Alamos National Laboratory report --------- (2016).

GROUNDWATER ANALYSES FOR NOPAL I AND THE PEÑA BLANCA REGION, CHIHUAHUA, MÉXICO

Michael Rearick, Patrick Dobson, Steve Goldstein, José Alfredo Rodríguez Pineda, and Schön S. Levy

INRODUCTION

Characterization of water chemistry from an abandoned mine at Nopal I (saturated zone and unsaturated zone) and in regional wells (saturated zone) was undertaken to provide baseline information on variations in water composition. One objective of this study was to support planned tracer studies that ultimately were dropped from the project due to budget cutbacks. A second objective was to document chemical changes along the flow path of the groundwaters downgradient from Nopal I. The scope of work for this objective also had to be scaled back. This report includes the chemical analyses performed in 2007 for a subset of samples collected in 2005 and 2006.

SAMPLE COLLECTION

All water samples received a unique alphanumeric identifier of the form SPCxxxxxxxx, in which the identifier is completed by eight digits, e.g., SPC01041433. Well-water samples also are identified in the data tables below by the source well, such as PB1. The system for naming seepage-water samples is described below.

Saturated-zone water samples were bailed from the wells drilled in 2003 at Nopal I – PB1, PB2, and PB3 – and from the reconditioned mine-supply well called PB4. Additional samples were collected from the storage tanks of wells at Peña Blanca and Pozos Ranch. Locations of all the wells are shown in Figures 1 and 2 of Goldstein et al. (2016), and geographic coordinates of the wells are listed in Goodell et al. (2016). One or more aliquot of each sample was filtered through a 0.45-μm filter at the time of collection, and aliquots of water for cation analysis were acidified with high-purity nitric acid.

The original and replacement seepage-collection systems installed in an adit located about eight meters below the mined surface at Nopal I are described by Goldstein et al. (2016). The location for the seepage sample labeled “Left adit” is shown as blue box “6” in Figure 3 of Goldstein et al. (2016). This sample was collected from water accumulated on plastic sheeting in the original collection system.

The sample names for seepage samples from the replacement collection system are keyed to their locations in the collection arrays shown in Figure 3 of Goldstein et al. (2016). Each location is uniquely specified by a number and letter combination, in which the number represents the row from the collection system (48 rows in all) and the letter denotes one of the five collectors per row (A through E, from left to right to an observer facing into the mine). Roman numerals appended to a sample name indicate the position of that sample in the sequence of samples retrieved from the same collector. After the

first suite of samples was collected (November, 2005), six of the sites were reconfigured from collection bottles to columns with pressure transducers where the rate of seepage was monitored every two hours. Collection histories from the instrumented columns are presented graphically by Dobson (2008). Two column samples are included in the analyses reported here.

A sample of condensate was collected from a special collector with a "roof" cover to prevent direct seepage of water into the collector. A tray channeled condensate into a collection bottle. The condensate-collection station was located adjacent to the 25A collector site where condensation previously had been observed.

All seepage samples submitted for chemical analysis were filtered with a 0.2-μm filter. Aliquots of water for cation analysis were acidified with high-purity nitric acid. No pH measurements were made at the time of collection.

ANALYTICAL METHODS

Major cations and trace metals were analyzed by inductively coupled plasma optical emission spectrometry and by inductively coupled plasma mass spectrometry utilizing U.S. Environmental Protection Agency (EPA) Methods 200.7 and 200.8 (Creed, Brockhoff, and Martin, 1994a, 1994b). The systems used for these analyses were the Perkin Elmer Optima 2100 DV and the Elan 6100. Ultra high-purity nitric acid (Fisher Trace Metal Grade) was used in sample and calibration preparation prior to sample analysis. Internal standards (Sc, Ge, Bi, and In) were added to both samples and standards to correct for matrix effects that can result from differing sample-introduction rates. Some samples were diluted prior to analysis to minimize matrix effects as well as allow the analytes of interest to remain within the linear dynamic range of the calibration. Standard Reference Material® 1640 (National Institute of Standards and Technology, 2010) was used to check the accuracy of the multi-element calibrations. Typical parameters for both methods were 1300 W forward power, 15 mL/min cooling gas, 0.2 mL/min auxiliary flow, 0.8 mL/min nebulizer flow, and 1.5 mL/min sample uptake.

Alkalinity measurements were mad following EPA Method 310.1 (U.S. Environmental Protection Agency, 1978), which is a titrimetric analysis with an endpoint of pH = 4.5. Inorganic anion samples were analyzed by ion chromatography following EPA Method 300.0 (Pfaff, 1993) on a Dionex DX-600 system.

For one of the seepage samples, 47E-II, there was insufficient water to allow for analysis of the complete chemical suite. In this case, bicarbonate was not analyzed.

RESULTS AND DISCUSSION

Table 1 presents analytical results for saturated-zone waters from PB1, PB2, PB3, and PB4 in the vicinity of Nopal I. Table 2 presents analytical results for saturated-zone

waters from ranch- and domestic-supply wells in the Sierra Peña Blanca region. Table 3 presents analytical results for unsaturated-zone seepage samples from a seepage collection system installed in an adit about eight meters below the mined surface.

Uranium data for the well waters are discussed by Goldstein et al. (2016) as the most recent values in a data series that began in 2003, when the Nopal I wells were drilled. The values reported here confirm that uranium concentrations in the new wells have gradually returned to natural, undisturbed levels.

Bats were observed in the adit where the seepage collection system was installed, and there was evidence that some seepage collectors had been disturbed by animals seeking water. Samples that appeared to contain defecation products were excluded from analysis. However, some of the analyzed samples may contain lesser amounts that were not detected by visual examination. This probably explains the high nitrate and phosphate contents in some of the seepage samples.

Comparisons of unfiltered and 0.45-μm filtered aliquots of well waters provide a very qualitative sense of the presence and composition of colloids. All the water samples have reduced concentrations of Al in the filtered aliquots, a likely indication of very fine clay particles. Uranium shows a similar pattern for all sample pairs, although more rigorous studies by Goldstein et al. (2016) indicate that ~93 to 97% of the U in PB1 and PB4 waters truly is dissolved. Other elements possibly associated with colloids include Mo, As, Cr, V, and B. The content of Th is below the detection limit of 0.001 ppm in all water samples; consequently, nothing can be inferred about the presence of Th-bearing colloids. In this discussion, no distinction is made between true colloids and elements adsorbed onto mineral or organic colloids.

REFERENCES

J. T. Creed, C. A. Brockhoff, and T. D. Martin, "Determination of Metals and Trace Elements in Water and Wastes by Inductively Coupled Plasma-Atomic Emission Spectrometry, Revision 4.4," U.S. Environmental Protection Agency Method 200.7 (available URL: http://www.epa.gov/waterscience/methods/method/), 1994a.

J. T. Creed, C. A. Brockhoff, and T. D. Martin, "Determination of Trace Elements in Water and Wastes by Inductively Coupled Plasma-Mass Spectrometry, Revision 4.4," U.S. Environmental Protection Agency Method 200.8 (available URL: http://www.epa.gov/waterscience/methods/method/), 1994b.

P. F. Dobson, P. J. Cook, T. Ghezzehei, J. A. Rodríguez, and R. de la Garza, "Heterogeneous Seepage at the Nopal I Uranium Mine, Chihuahua, Mexico," Lawrence Berkeley National Laboratory Paper LBNL-34E (available URL: http://repositories.cdlib.org/lbnl/LBNL-34E), 2008.

S. J. Goldstein, A.I. Abdel-Fattah, M. T. Murrell, P. F. Dobson, D.E. Norman, R. S. Amato, and A. J. Nunn, "Uranium-Series Constraints on Radionuclide Transport and

Groundwater Flow at the Nopal I Uranium Deposit, Sierra Peña Blanca, México," S. Levy, compiler, Los Alamos National Laboratory report XXXXX (2016).

P. C. Goodell, J. A. Rodríguez Pineda, P. Dobson, S. H. Harder, and S. S. Levy, "Regional Hydrology and Uranium Occurrences around Nopal I," S. Levy, compiler, Los Alamos National Laboratory report XXXXX (2016).

National Institute of Standards and Technology, "Certificate of Analysis, Standard Reference Material® 1640, Trace Elements in Water," (available URL: https:/www-s.nist.gov/srmors/view_cert.cfm?srm=1640), 2010.

J. D. Pfaff, "Determination of Inorganic Anions by Ion Chromatography," U.S. Environmental Protection Agency Method 300.0 (available URL: http://www.epa.gov/waterscience/methods/method/), 1993.

U.S. Environmental Protection Agency, "Alkalinity (Titrimetric, pH 4.5)," U.S. Environmental Protection Agency Method 310.1 (available URL: http://www.nemi.gov/apex/f?p=237:12:3791234004469181), 1978.

Table 1. Water Chemistry of Samples from Nopal 1 Wells.

	PB1, filtered	PB1, unfiltered	PB2, filtered	PB2, unfiltered	PB3, filtered	PB3, unfiltered	PB4, filtered	PB4, unfiltered
Sample ID	SPC01041433 SPC01041431	SPC01041434	SPC01041437 SPC01041435	SPC01041438	SPC01041441 SPC01041439	SPC01041442	SPC01041430 SPC01041425	SPC01041429
Collection date	12/14/06	12/14/06	12/14/06	12/14/06	12/14/06	12/14/06	12/13/06	12/13/06
Analysis date	02/01/07 03/13/07	02/01/07	02/01/07 03/13/07	02/01/07	02/01/07 03/13/07	02/01/07	02/01/07 03/13/07	02/01/07
Ag, ppm	<0.001	<0.001	<0.001	<0.001	<0.001	<0.001	<0.001	<0.001
Al, ppm	0.008±0.000	0.014±0.000	0.004±0.000	0.011±0.000	0.003±0.000	0.013±0.000	0.002±0.000	0.005±0.000
Total alkalinity, ppm $CaCO_3$	331	—	277	—	207	—	73.4	—
As, ppm	0.0464±0.0006	0.0590±0.0020	0.0105±0.0000	0.0127±0.0009	0.0478±0.0001	0.0603±0.0014	0.0003±0.0000	0.0003±0.0000
B, ppm	0.181±0.000	0.167±0.001	0.153±0.002	0.154±0.001	0.134±0.001	0.185±0.004	0.048±0.001	0.077±0.002
Ba, ppm	0.078±0.001	0.073±0.001	0.051±0.001	0.059±0.000	0.063±0.001	0.051±0.000	0.029±0.000	0.010±0.000
Be, ppm	<0.001	<0.001	<0.001	<0.001	<0.001	<0.001	<0.001	<0.001
Br, ppm	0.25	—	0.19	—	0.23	—	0.11	—
Ca, ppm	35.5±0.2	37.2±0.2	50.8±0.4	54.1±1.4	78.4±1.2	78.6±1.2	22.8±0.3	22.8±0.5
Cd, ppm	<0.001	<0.001	<0.001	<0.001	<0.001	<0.001	<0.001	<0.001
Cl, ppm	14.8	—	12.6	—	12.8	—	8.39	—
Co, ppm	<0.001	<0.001	<0.001	<0.001	<0.001	<0.001	<0.001	<0.001
CO_3, ppm	16.5	—	9.17	—	0.0	—	0.0	—
Cr, ppm	0.002±0.000	0.013±0.000	0.0.001±0.000	0.012±0.000	0.001±0.000	0.010±0.001	<0.001	0.003±0.000
Cs, ppm	0.006±0.000	0.007±0.000	0.012±0.000	0.013±0.001	0.007±0.000	0.008±0.000	0.002±0.000	0.002±0.000
Cu, ppm	0.013±0.000	0.014±0.001	0.004±0.000	0.010±0.001	0.005±0.000	0.005±0.000	0.004±0.000	0.002±0.001
F, ppm	3.69	—	2.37	—	2.66	—	1.85	—
Fe, ppm	0.04±0.00	0.06±0.00	0.03±0.00	0.02±0.00	0.04±0.00	0.03±0.00	0.02±0.00	0.02±0.00
HCO_3, ppm	370	—	320	—	252	—	89.6	—
Hg, ppm	0.00007±0.00001	0.000014±0.00000	<0.00005	0.00002±0.00000	<0.00005	<0.00005	<0.00005	<0.00005
K, ppm	4.69±0.02	4.64±0.04	10.9±0.1	11.0±0.0	3.21±0.02	3.14±0.08	2.04±0.02	2.08±0.03
Li, ppm	0.206±0.001	0.203±0.002	0.224±0.002	0.214±0.019	0.112±0.001	0.108±0.002	0.033±0.000	0.034±0.000
	PB1, filtered	PB1, unfiltered	PB2, filtered	PB2, unfiltered	PB3, filtered	PB3, unfiltered	PB4, filtered	PB4, unfiltered

	PB1, filtered	PB1, unfiltered	PB2, filtered	PB2, unfiltered	PB3, filtered	PB3, unfiltered	PB4, filtered	PB4, unfiltered
Mg, ppm	11.8±0.0	11.7±0.1	27.0±0.2	27.4±0.0	11.6±0.0	11.3±0.0	8.12±0.10	8.17±0.05
Mn, ppm	0.086±0.001	0.095±0.001	0.049±0.000	0.002±0.000	0.243±0.002	0.095±0.001	0.017±0.000	<0.001
Mo, ppm	0.032±0.001	0.047±0.000	0.020±0.000	0.033±0.000	0.124±0.004	0.172±0.000	0.001±0.000	0.002±0.000
Na, ppm	110±0	109±1	101±2	102±0	62.3±1.7	60.9±0.6	25.3±0.1	25.3±0.2
Ni, ppm	0.003±0.000	0.003±0.000	0.003±0.000	0.003±0.000	0.004±0.000	0.006±0.000	0.002±0.000	0.002±0.000
NO_2, ppm	<0.01	—	<0.01	—	<0.01	—	<0.01	—
NO_3, ppm	<0.01	—	0.03	—	0.03	—	2.06	—
C_2O_4, ppm	<0.01	—	<0.01	—	<0.01	—	<0.01	—
Pb, ppm	0.0128±0.0001	0.0375±0.0010	0.0030±0.0000	0.0019±0.0001	0.0008±0.0000	0.0009±0.0000	<0.0002	<0.0002
PO_4, ppm	<0.01	—	<0.01	—	0.04	—	<0.01	—
Rb, ppm	0.017±0.000	0.018±0.000	0.033±0.000	0.035±0.002	0.013±0.000	0.014±0.000	0.007±0.000	0.007±0.000
Sb, ppm	<0.001	<0.001	<0.001	<0.001	<0.001	<0.001	<0.001	<0.001
Se, ppm	<0.001	<0.001	<0.001	<0.001	<0.001	<0.001	<0.001	<0.001
Si, ppm	9.9±0.0	10.0±0.1	12.5±0.1	12.9±0.0	10.7±0.0	10.5±0.1	5.80±0.04	5.80±0.04
SiO_2, calculated ppm	21.1	21.4	26.8	27.7	22.9	22.4	12.4	12.4
SO_4, ppm	81.4	—	195	—	156	—	79.5	—
Sn, ppm	<0.001	<0.001	<0.001	<0.001	<0.001	<0.001	<0.001	<0.001
Sr, ppm	0.81±0.00	0.83±0.01	1.09±0.01	1.15±0.01	1.01±0.01	1.00±0.01	0.47±0.00	0.48±0.00
Th, ppm	<0.001	<0.001	<0.001	<0.001	<0.001	<0.001	<0.001	<0.001
Ti, ppm	<0.002	<0.002	<0.002	<0.002	<0.002	<0.002	<0.002	<0.002
Tl, ppm	<0.001	<0.001	<0.001	<0.001	<0.001	<0.001	<0.001	<0.001
U, ppm	0.0205±0.0002	0.0247±0.0004	0.0338±0.0002	0.0393±0.0016	0.3274±0.0099	0.3650±0.0026	0.0012±0.0000	0.0014±0.0000
V, ppm	<0.001	0.004±0.000	<0.001	0.003±0.000	<0.001	0.003±0.000	<0.001	0.001±0.000
Zn, ppm	0.017±0.000	0.028±0.000	0.008±0.000	0.012±0.000	0.024±0.000	0.014±0.000	0.013±0.000	0.001±0.001
pH, field	7.1	7.1	7.4	7.4	7.1	7.1	7.1	7.1
pH, laboratory	8.24	—	8.03	—	7.76	—	8.00	—
Total dissolved solids, ppm	671	—	757	—	605	—	253	—

	PB1, filtered	PB1, unfiltered	PB2, filtered	PB2, unfiltered	PB3, filtered	PB3, unfiltered	PB4, filtered	PB4, unfiltered
Cation sum, meq/l	7.688	—	9.469	—	7.703	—	2.977	—
Anion sum, meq/l	8.933	—	10.080	—	7.892	—	3.493	—
Cation/anion balance, %	−7.49	—	−3.12	—	−1.21	—	−7.97	—

Table 2. Water Chemistry of Samples from Peña Blanca Regional Wells

	Peña Blanca, filtered	Peña Blanca, unfiltered	Pozos Ranch tank, filtered	Pozos Ranch tank, unfiltered
Sample ID	SPC01041428 SPC01041423	SPC01041427	SPC01041450 SPC01041448	SPC01041451
Collection date	12/13/06	12/13/06	12/14/06	12/14/06
Analysis date	02/01/07, 03/13/07	02/01/07	02/01/07, 03/13/07	02/01/07
Ag, ppm	<0.001	<0.001	<0.001	<0.001
Al, ppm	0.002±0.000	0.007±0.000	0.010±0.001	0.011±0.000
Total alkalinity, ppm $CaCO_3$	233	—	164	—
As, ppm	0.0407±0.0008	0.0463±0.0006	0.0226±0.0061	0.0179±0.0003
B, ppm	0.153±0.001	0.170±0.002	0.050±0.003	0.069±0.002
Ba, ppm	0.009±0.000	0.008±0.000	0.032±0.001	0.028±0.000
Be, ppm	<0.001	<0.001	<0.001	<0.001
Br, ppm	0.15	—	0.09	—
Ca, ppm	39.5±0.8	38.9±1.5	66.4±2.8	63.8±1.6
Cd, ppm	<0.001	<0.001	<0.001	<0.001
Cl, ppm	12.7	—	8.96	—
Co, ppm	<0.001	<0.001	<0.001	<0.001
CO_3, ppm	13.9	—	0.0	—
Cr, ppm	<0.001	0.008±0.000	0.002±0.001	<0.001
Cs, ppm	0.010±0.000	0.011±0.000	0.006±0.001	0.005±0.000
Cu, ppm	0.004±0.000	0.004±0.000	0.002±0.000	0.001±0.000
F, ppm	2.45	—	1.94	—
Fe, ppm	<0.01	<0.01	<0.01	<0.01
HCO_3, ppm	256	—	200	—
Hg, ppm	<0.0005	<0.0005	<0.0005	<0.0005
K, ppm	4.42±0.02	4.24±0.15	2.04±0.07	1.96±0.02
Li, ppm	0.042±0.000	0.041±0.001	0.033±0.002	0.033±0.001
Mg, ppm	4.89±0.05	4.82±0.04	8.59±0.30	8.39±0.03
Mn, ppm	<0.001	<0.001	<0.001	<0.001
Mo, ppm	0.004±0.000	0.005±0.000	0.004±0.000	0.005±0.000
Na, ppm	49.8±0.4	47.9±0.4	25.8±0.9	24.9±0.1

	Peña Blanca, filtered	Peña Blanca, unfiltered	Pozos Ranch tank, filtered	Pozos Ranch tank, unfiltered
Sample ID	SPC01041428 SPC01041423	SPC01041427	SPC01041450 SPC01041448	SPC01041451
Ni, ppm	0.002±0.000	0.002±0.000	0.004±0.001	0.003±0.000
NO_2, ppm	<0.01	—	<0.01	—
NO_3, ppm	8.81	—	7.84	—
C_2O_4, ppm	<0.01	—	<0.01	—
Pb, ppm	0.0003±0.0000	0.0003±0.0000	0.0004±0.0001	0.0005±0.0000
PO_4, ppm	<0.01	—	<0.01	—
Rb, ppm	0.017±0.000	0.018±0.000	0.011±0.003	0.008±0.000
Sb, ppm	<0.001	<0.001	<0.001	<0.001
Se, ppm	<0.001	0.001±0.000	0.001±0.001	<0.001
Si, ppm	26.1±0.4	25.3±0.4	11.0±0.3	10.6±0.1
SiO_2, calculated ppm	55.9	54.2	23.6	22.7
SO_4, ppm	20.8	—	78.8	—
Sn, ppm	<0.001	<0.001	<0.001	<0.001
Sr, ppm	0.35±0.01	0.35±0.00	0.66±0.02	0.65±0.00
Th, ppm	<0.001	<0.001	<0.001	<0.001
Ti, ppm	<0.002	<0.002	<0.002	<0.002
Tl, ppm	<0.0001	<0.0001	<0.0001	<0.0001
U, ppm	0.0098±0.0003	0.0105±0.0001	0.0067±0.0013	0.0051±0.0000
V, ppm	0.020±0.000	0.022±0.000	0.007±0.002	0.005±0.000
Zn, ppm	0.016±0.000	0.017±0.000	0.007±0.001	0.006±0.001
pH, field	6.8	6.8	7.1	7.1
pH, laboratory	8.41	—	7.99	—
Total dissolved solids, ppm	470	—	425	—
Cation sum, meq/l	4.667	—	5.213	—
Anion sum, meq/l	5.724	—	5.410	—
Cation/anion balance, %	−10.17	—	−1.86	—

Table 3. Water Chemistry of Seepage from Nopal I.

	8B	18A	Left adit	18A column	Condensate	34E column	39B-III	47E-II
Sample ID	SPC 01037918	SPC 01037979	SPC 01038241	SPC 02041957	SPC 01040904	SPC 01040953	SPC 01040975	SPC 01041416
Collect-ion date	11/08/05	11/08/05	11/10/05	08/26/06	12/12/06	12/12/06	12/13/06	12/13/06
Anal-ysis date	06/05/07	06/05/07	06/05/07	06/05/07	06/05/07	06/05/07	06/05/07	06/05/07
Ag, ppm	<0.001	<0.001	<0.001	<0.001	<0.001	0.0017± 0.0000	<0.001	<0.001
Al, ppm	0.015± 0.001	<0.002	0.004± 0.000	0.016± 0.000	0.072± 0.002	0.006± 0.000	0.040± 0.001	0.078± 0.002
Total alka-linity, ppm $CaCO_3$	70.9	22.2	0.0	6.35	17.3	24.4	17.6	—
As, ppm	0.0215± 0.0015	0.0567± 0.0088	0.0716± 0.0006	0.0540± 0.0015	0.0091± 0.0002	0.0103± 0.0003	0.3553± 0.0079	0.4150± 0.0111
B, ppm	0.012± 0.001	<0.002	0.082± 0.001	<0.002	0.006± 0.001	<0.002	<0.002	<0.002
Ba, ppm	<0.001	<0.001	0.042± 0.001	0.005± 0.000	0.066± 0.004	0.020± 0.000	0.074± 0.015	0.055± 0.002
Be, ppm	<0.001	<0.001	<0.001	<0.001	<0.001	<0.001	<0.001	<0.001
Br, ppm	<0.01	<0.01	<0.01	0.05	0.44	0.59	<0.01	<0.01
Ca, ppm	22.4±0.2	8.09±0.04	84.0±0.9	10.1±0.1	9.53±0.07	13.0±0.0	248±1	442±8
Cd, ppm	<0.001	<0.001	0.012±0.000	<0.001	<0.001	<0.001	0.035±0.001	0.013±0.000
Cl, ppm	0.94	1.07	18.7	4.37	10.4	13.1	225	31.4
Co, ppm	<0.001	<0.001	0.005± 0.000	<0.001	0.001± 0.000	<0.001	0.019± 0.001	0.018± 0.001
CO_3, ppm	0.0	0.0	0.0	0.0	0.0	0.0	0.0	0.0
Cr, ppm	<0.001	<0.001	<0.001	<0.001	0.005± 0.000	0.003± 0.000	<0.001	0.004± 0.000
Cs, ppm	0.003± 0.000	0.003± 0.000	0.004± 0.000	0.002± 0.000	<0.001	0.001± 0.000	0.007± 0.000	0.009± 0.000
Cu, ppm	0.001± 0.000	0.002± 0.000	0.003± 0.000	0.003± 0.000	0.005± 0.000	0.004± 0.000	0.012± 0.000	0.045± 0.003
F, ppm	0.50	1.07	0.57	1.02	0.15	0.19	5.22	7.16
Fe, ppm	<0.01	<0.01	<0.01	<0.01	0.01±0.00	0.02±0.00	<0.01	<0.01
HCO_3, ppm	86.5	27.0	<0.8	7.75	21.1	29.8	21.5	—
Hg, ppm	<0.00005	<0.00005	<0.00005	<0.00005	<0.00005	<0.00005	0.00011± 0.00001	0.00014± 0.00000
K, ppm	1.02±0.01	1.15±0.01	6.93±0.10	3.6±0.0	11.4±0.0	9.00±0.07	16.1±0.1	24.5±0.1

	8B	18A	Left adit	18A column	Condensate	34E column	39B-III	47E-II
Sample ID	SPC 01037918	SPC 01037979	SPC 01038241	SPC 02041957	SPC 01040904	SPC 01040953	SPC 01040975	SPC 01041416
Li, ppm	0.004± 0.000	0.002± 0.000	0.080± 0.001	0.001± 0.000	0.007± 0.000	0.001± 0.000	0.52±0.00	0.14±0.00
Mg, ppm	0.54±0.01	0.36±0.00	6.39±0.08	0.39±0.00	1.06±0.00	0.52±0.00	29.3±0.2	20.8±0.1
Mn, ppm	<0.001	<0.001	0.25±0.00	0.021±0.000	0.029±0.000	0.16±0.00	0.31±0.00	0.17±0.00
Mo, ppm	0.059± 0.000	0.066± 0.002	0.049± 0.000	0.068± 0.001	0.012± 0.000	0.007± 0.000	0.118± 0.000	0.319± 0.003
Na, ppm	4.32±0.05	3.26±0.02	66.7±0.9	3.07±0.02	3.99±0.01	3.55±0.01	485±1	1150±2
Ni, ppm	<0.001	<0.001	0.004± 0.000	0.001± 0.000	0.007± 0.000	0.005± 0.000	0.025± 0.001	0.040± 0.002
NO_2, ppm	<0.01	<0.01	<0.01	<0.01	<0.01	<0.01	<0.01	<0.01
NO_3, ppm	2.21	0.12	117	19.0	6.77	2.06	891	254
C_2O_4, ppm	<0.01	<0.01	<0.01	<0.01	<0.01	<0.01	<0.01	<0.01
Pb, ppm	<0.0002	<0.0002	0.0003± 0.0000	0.0002± 0.0000	0.0020± 0.0000	0.0003± 0.0000	0.0012± 0.0000	0.0014± 0.0001
PO_4, ppm	<0.01	<0.01	1.22	2.31	1.09	0.05	1.01	<0.01
Rb, ppm	0.007± 0.000	0.009± 0.001	0.032± 0.001	0.012± 0.000	0.016± 0.001	0.013± 0.000	0.041± 0.002	0.082± 0.002
Sb, ppm	<0.001	<0.001	<0.001	<0.001	0.25±0.00	<0.001	<0.001	0.004± 0.000
Se, ppm	<0.001	<0.001	0.007± 0.000	<0.001	<0.001	<0.001	0.067± 0.004	0.196± 0.003
Si, ppm	7.31±0.07	6.63±0.05	23.0±0.2	5.53±0.03	0.69±0.00	1.76±0.02	22.85±0.10	11.44±0.03
SiO_2, calcul-ated ppm	15.6±0.2	14.2±0.1	49.2±0.5	11.8±0.1	1.5±0.0	3.8±0.0	48.9±0.2	24.5±0.1
SO_4, ppm	4.47	10.4	295	10.5	18.1	13.9	515	3285
Sn, ppm	<0.001	<0.001	<0.001	<0.001	<0.001	<0.001	<0.001	<0.001
Sr, ppm	0.05±0.00	0.04±0.01	0.39±0.01	0.03±0.00	0.03±0.00	0.05±0.00	1.36±0.00	2.39±0.01
Th, ppm	<0.001	<0.001	<0.001	<0.001	<0.001	<0.001	<0.001	<0.001
Ti, ppm	<0.002	<0.002	<0.002	<0.002	<0.002	<0.002	<0.002	<0.002
Tl, ppm	<0.001	<0.001	<0.001	<0.001	<0.001	<0.001	<0.001	0.001± 0.000
U, ppm	0.0141± 0.0011	0.0002± 0.0000	<0.0002±	0.0006± 0.0000	0.0014± 0.0000	0.0013± 0.0001	0.0008± 0.0001	0.0147± 0.0004
V, ppm	0.014± 0.001	0.013± 0.002	0.002± 0.000	0.008± 0.000	0.002± 0.000	0.002± 0.000	0.007± 0.000	0.006± 0.000

	8B	18A	Left adit	18A column	Condensate	34E column	39B-III	47E-II
Sample ID	SPC 01037918	SPC 01037979	SPC 01038241	SPC 02041957	SPC 01040904	SPC 01040953	SPC 01040975	SPC 01041416
Zn, ppm	0.002± 0.000	0.010± 0.001	1.46± 0.01	0.098± 0.000	0.076± 0.001	0.033± 0.000	9.98±0.08	1.60±0.02
pH, labora-tory	7.93	7.01	5.71	6.40	6.81	7.29	5.16	6.99
Total dissolved solids, ppm	139	67.0	648	74.4	85.8	90.0	2498	5242
Cation sum, meq/l	1.379	0.606	7.869	0.770	1.034	1.086	36.595	74.188
Anion sum, meq/l	1.600	0.751	8.595	0.859	1.154	1.201	31.996	73.262
Cation/ anion balance, %	–7.42	–10.72	–4.41	–5.46	–5.47	–5.04	6.70	0.63